The role of mRNA cap methyltransferase PCIF1 in Acute Myeloid Leukemia

Felice Wallner

University of Oxford

St Catherine's College





A thesis presented for the degree of

Doctor of Philosophy

Supervised by Professor Yang Shi and Professor Rob Klose

Michaelmas Term

11th October 2025

Abstract

Acute Myeloid Leukemia (AML) is characterized by an uncontrolled expansion of immature blasts in the bone marrow. While treatment strategies have improved patient prognoses, about 50% of patients treated with standard induction chemotherapy still relapse within the first 5 years post treatment, underscoring an unmet clinical need for finding novel targets and treatments. Recent clinical advances have reported sensitivity of AML to the depletion of specific epitranscriptomic players, creating a scope for exploration of other RNA epigenetic writers, readers and erasers in cancer. Phosphorylated CTD-interacting Factor 1 (PCIF1) is the sole enzyme responsible for catalyzing N6,2'-O-methylation (m6Am) on cap-adjacent adenosine of mRNA. A lack of consensus remains regarding the impact of m6Am on transcription, mRNA stability, and translation efficiency, and various studies have described PCIF1's influence on cancer, the immune system, and viral infections, revealing context-dependent effects. Leukemia has yet to be investigated in the context of this enzyme.

This thesis investigates whether the underexplored epitranscriptomic writer PCIF1 is a potential therapeutic vulnerability in acute myeloid leukemia. In this work, we establish and characterize the effects of PCIF1 loss in AML cell lines and show that knockdown in MOLM-13 and SKNO-1, but not Kasumi-1, THP-1, and U-937 cell lines, decreases cell proliferation and colony-forming capacity, as well as increases apoptosis, differentiation, and markers of monocyte maturation. Loss of PCIF1 does not synergize with common cancer therapeutics venetoclax, azacitidine or sorafenib. Bulk-RNA sequencing revealed that common differentially regulated genes in sensitive cell lines are involved in poly-unsaturated

fatty acid (PUFA) synthesis, oxidative stress processes and mTORC1 signaling cascades. Measurements of intracellular ROS show mild upregulation in PCIF1 KD cells. Fatty acid desaturase 1 and 2 (*FADS1*/2) mRNA is consistently downregulated in the sensitive, but not resistant cell lines. Supplementation of fatty acids in cell culture media does not rescue the growth defect seen upon PCIF1 knockdown. shRNA knockdown of FADS1/2 in AML WT cell lines indicates that PCIF1 sensitive cells are dependent on FADS1/2 for proliferation. We show that PCIF1 has an impact on acute myeloid leukemia and may regulate important metabolic pathways, possibly through FADS1/2, that drive leukemia cell line proliferation, differentiation and chemoresistance.

Declaration

This thesis has not been submitted, either partially or in full, for another qualification at this University, or for a qualification at any other institution. The work presented in this thesis is entirely my own, and except when otherwise stated in figure captions or listed below describe my own research, experimentation and analysis.

Public data:

1. **Chapter 4.1: Figure 4.1 (A-B)** RNA-seq profiles of cell lines generated by the HPA and the Cancer Cell Line Encyclopedia were downloaded form The Human Protein Atlas **(C-E)** Data using cell line RNA-seq profiles and proteomics were downloaded from the DepMap Portal, version: DepMap Public 25Q2.

2. **Chapter 4.1: Figure 4.2 and appendix A.4** TCGA and GTEx data was visualized using GEPIA2.

3. **Chapter 4.1: Figure 4.3 and appendix A.5** Data from the Beat-AML trial were downloaded from vizome.org (Beat-AML 2.0).

4. **Chapter 4.1: Figure 4.4** Data from the TARGET and TCGA Pancancer trials were downloaded from the UCSC Xenabrowser.

Data generated in this work:

Chapter 4.3: Illumina sequencing results were run in the NF-core pipeline by Dr. Qianpeng Li. Downstream analysis (from raw counts) was performed by myself.

Note on illustrations: Illustrations in this thesis were created with Biorender, using a subscription kindly provided by the Shi lab and Ludwig Institute funding. Illustrations were designed using images published in referenced publications as a guidance and otherwise represent my own work.

Acknowledgments

This work would not have been possible without the generous funding support from the Ludwig Institute for Cancer Research. I am truly grateful to have been part of such an inspiring community of scientists, without whom I would not be the researcher I am today.

First and foremost, I would like to thank my supervisors, Professor Yang Shi and Professor Rob Klose. I have been immensely privileged to work under the guidance of such a kind, patient, enthusiastic, and intellectually generous mentor as Yang, who has shaped my scientific path in countless ways. I am grateful not only for your guidance throughout these four years, but also for the opportunity to complete my undergraduate internship in your lab, back when doing my PhD in Oxford was still a dream I didn't realize I had.

In a similar spirit, I want to thank Dr Alan Jiao, who first introduced me to the joys and excitement of academic research and fueled my wish of doing a PhD. I could not have been luckier to have had you as my first supervisor. Your encouragement, listening ear, as well as thoughtful advice during my most uncertain moments in those first DPhil years meant more than you know. I know no one who is better equipped to be a scientist and teacher than you.

Many postdocs in the Shi Lab, past and present, have left a lasting imprint on my journey. I am grateful to have worked with Dr Amir Hosseini - thank you for warmly welcoming me onto the PCIF1 project and trusting me to carry it forward. My heartfelt thanks goes to Dr Damayanti Chakraborty for taking me under her wing and providing unwavering guidance, giving me the tools for the first successful experiment on this project. I will forever be envious of your future PhD students, who will thrive under your mentorship in your own lab in Texas. Thank you to Dr

Berna Bou-Tayeh for your steady advice on flow cytometry, and to Dr Ines Kaltheuner for many stimulating conversations about PCIF1, help with the LC-MS, and quiet moments of encouragement that helped rebuild my self-belief. Thank you for having my back, encouraging me to stand up for myself and believing in me. I also deeply appreciate everyone who took the time to give me feedback and whose thoughtful questioning of thesis drafts (especially Dr Michael McClellan) strengthened both my writing and reasoning.

My appreciation goes to all the Ludwig Institute students whose lunchtime conversations (equal parts insightful and insane) kept me going when things got tough. My mental health is especially grateful for Emelie, Lucy, Tom, Alex, Alina N and Alina M, who convinced me (although it did not take much) to go on a hiking trip in the Dolomites just before I retreated to Austria to begin writing up. I thank Nandini for sharing long cell culture sessions one TC Hood over and inspiring me to try a little harder, no matter how bad it gets. Thank you also to Matthew, Yunyi, Chenyu, Cherubin, and Yuhua for being such wonderful labmates. Special thanks also to Sabina Sprincean, who endured my supervision of her bachelor project while I was wrapping up the project and whose excitement about science made me remember what it was like when I first started.

To the friends I made beyond the lab: I could not possibly name everyone who walked beside me on this road. Thank you to Laurence, Kim, Sam, and Arunima, my steadfast non-lab support. It means the world to me that you were there when the imposter got too loud. I am truly lucky to call you my friends. My thanks also to my fellow Junior Deans at Catz, for your care and good humor in these final weeks.

Counterintuitively, much of this thesis was written in the Institute for New Economic Thinking,

whose members kindly tolerated my long-term occupation of one of the hot desks. Thank you for the endless tea, coffee, late-night chats, takeaways, life advice, and for granting me mock honorary membership.

I would not be here without the love and support of my friends and family back home. Thank you to my home friends, who never begrudged me for not calling and visiting enough. None of this would have been possible without my parents, who have supported me from the very beginning, who taught me that I could do hard things, and who reminded me of that truth many times. Thank you to my sisters, who always made coming home feel as though I had never left. Moving to Oxford has meant missing birthdays, anniversaries, holidays and life milestones, but I hope you know how deeply grateful I am that you are always only a call away.

Last, but certainly not least, thank you to my partner, Ben, who has been by my side since the very first day when we met at St Catherine's College registration. Thank you for cooking countless dinners, for your patience when I arrived an hour past when I said I would be done in the lab (again), and most importantly for celebrating every success while quietly carrying me through the low points. I truly could not have done this without you.

It sounds ridiculous, but it has taken me until today, the day of submission, to believe that I might be able to do this. I wish I had had the courage to believe it earlier. In many ways, my DPhil journey has mirrored my near-daily cycle up the hill to the Old Road Campus labs. Some days were easier, others were grueling, sometimes I thought I might have to get off and push my bike up the hill. Over time, the climb became second nature. Most days left me breathless, sweaty, and occasionally envious of those with electric bikes. But every ascent brought me a little closer to

the top, and every struggle taught me something about myself. Now, I think I'm finally ready to pause, take a deep breath, and enjoy the view.

Table of Contents

1 Introduction **1**

1.1 Epigenetics and epitranscriptomics as cancer hallmarks 1

1.1.1 mRNA modifications, transcription, translation and the mRNA cap 3

1.1.2 The multifaceted roles of m6Am on transcription, mRNA stability, and translation 6

1.1.3 PCIF1: oncogene or tumor suppressor? 11

1.2 Introduction to Acute Myeloid Leukemia (AML) 18

1.2.1 AML Subtypes 18

1.2.2 Epigenetics and Leukemia 22

2 Rationale, aims and objectives **24**

3 Materials and Methods **25**

3.1 Methods 25

3.1.1 Cell culture and maintenance 25

3.1.2 Lentivirus production and transduction of AML cell lines 25

3.1.3 Proliferation assays 27

3.1.4 EC50/IC50 treatment protocol with chemotherapeutic compounds 28

3.1.5 May-Grünwald Giemsa staining 29

3.1.6 Immunofluorescence staining and confocal microscopy 30

3.1.7 Flow cytometry 31

3.1.8 Methylcellulose colony forming unit (CFU) assay 33

3.1.9 RNA isolation 34

3.1.10 HPLC-QQQ sample preparation and m6Am quantification 35

3.1.11 Quantitative real-time PCR (qPCR) . . . 36
3.1.12 Western Blotting . . . 36
3.1.13 Cloning of plasmids and gene constructs . . . 37
3.1.14 mRNA sequencing and analysis . . . 38
3.1.15 Quantification of PCIF1 expression and patient survival in public datasets . . . 39
3.1.16 Statistical analysis and replicates . . . 39
3.2 Materials . . . 40

4 Results **43**

4.1 Exploring *PCIF1* gene expression in human tissue, cell lines and cancer . . . 44
4.1.1 *PCIF1* expression in human tissues and gene/cancer essentiality scores . . . 44
4.1.2 *PCIF1* TCGA pan-cancer expression . . . 48
4.1.3 *PCIF1* expression and patient survival in the Beat-AML trial . . . 49
4.1.4 *PCIF1* in TARGET vs TCGA pan-cancer patient cohorts . . . 53
4.2 The effect of PCIF1 depletion on AML cell lines . . . 57
4.2.1 Background and aims . . . 57
4.2.2 Selection of AML cell lines used for protein depletion studies . . . 58
4.2.3 Establishing and optimizing a protein depletion strategy . . . 61
4.2.3.1 siRNA-mediated knockdown of PCIF1 . . . 61
4.2.3.2 CRISPR/Cas9 mediated knockout of PCIF1 . . . 62
4.2.3.3 pLKO.1 shRNA-mediated stable knockdown of PCIF1 . . . 66
4.2.4 Effect of PCIF1 depletion on proliferation, apoptosis and cell cycle . . . 72
4.2.4.1 MOLM-13 and SKNO-1 AML cell lines show decreased proliferation and viability upon loss of PCIF1 . . . 73
4.2.4.2 PCIF1 sensitive knockdown cells show increased levels of apoptosis . . . 75

4.2.5 Effect on differentiation 83
4.2.5.1 AML cells sensitive to PCIF1 loss show morphological signs of monocyte/macrophage differentiation 84
4.2.5.2 Sensitive cell lines produce fewer and smaller colonies in methylcellulose medium conditions upon loss of PCIF1 89
4.2.5.3 Loss of PCIF1 induces the expression of monocytic surface markers CD11b, CD14 and CD86 90
4.2.6 PCIF1 depleted AML cells respond differently to chemotherapeutics 94
4.2.6.1 Choice of therapeutic drugs 94
4.2.6.2 PCIF1 depletion does not confer sensitivity to venetoclax treatment . . . 95
4.2.7 Chapter summary, discussion and limitations 96
4.3 Changes in the transcriptomic landscape upon loss of PCIF1 101
4.3.1 Bulk RNA-sequencing reveals differential expression of fatty acid metabolism and oxidative stress genes 101
4.3.1.1 Gene ontology and gene set enrichment analysis of DEGs in *PCIF1* KD AML cells reveal downregulation of mTORC1 signaling, bile acid and cholesterol homeostasis pathway players 104
4.3.1.2 Differential transcript isoform expression analysis of common dysregulated sensitive genes 108
4.3.1.3 Chapter summary and discussion 111
4.3.2 Preliminary investigations of reactive oxygen species and poly-unsaturated fatty acid biosynthesis pathways in *PCIF1* KD AML cell lines 123
4.3.2.1 Chapter summary and discussion 134

5 Discussion, limitations and future directions **136**

5.1 Summary of key findings and discussion 136

5.1.1 Implications for cancer therapy 139

5.1.2 Limitations 142

5.1.3 Remaining questions and future directions 144

Appendix A Appendix **172**

List of Figures

1.1 mRNA cap methylation 4

1.2 Multifaceted roles of m6Am 16

4.1 PCIF1 expression and sensitivity across tissues and cancers 46

4.2 Pan-cancer expression of *PCIF1* queried in GEPIA2 49

4.3 *PCIF1* expression and patient survival in the Beat-AML trial 51

4.4 *PCIF1* expression and patient survival across TARGET and TCGA cancer tissues 54

4.5 AML cell lines transfected with predesigned siRNA against *PCIF1* using Lipofectamine RNAiMAX. 62

4.6 Optimizing polyclonal and single clone PCIF1 knockouts in AML cells. 65

4.7 AML cell lines infected with lentiviral particles containing pLKO.1 against *PCIF1* mRNA or a scrambled control. 68

4.8 Ratio of m6Am / A measured with LCMS. 70

4.9 Proliferation and viability of all AML cell lines infected with scramble shRNA or *PCIF1* shRNA. 74

4.10 Annexin-V apoptosis staining. 77

4.11 Caspase analysis in resistant and sensitive AML cell lines. 79

4.12 Cell cycle analysis of AML cell lines infected with shRNA for scramble control or PCIF1. 81

4.13 Stages of hematological differentiation (myeloid lineage) with histological samples. 85

4.14 May Grünwald Giemsa staining for hematological differentiation. 87

4.15 Analysis of colony forming capabilities of AML cells upon PCIF1 knockdown. 90

4.16 Expression of monocytic surface markers in PCIF1 depleted AML cell lines. 93

4.17 Viability of AML cell lines treated with Venetoclax (BCL2i) and Sorafenib (Ras-pathway inhibitor). 97
4.18 Differential Gene Expression analysis of *PCIF1* KD AML cell lines. 103
4.19 Gene Ontology (gProfiler) pathways in *PCIF1* KD cells. 105
4.20 Transcription factor motif and Gene Set Enrichment Analysis (GSEA) 107
4.21 Transcription start nucleotide (TSN) analysis 109
4.22 Overview of fatty acid desaturation process 121
4.23 Reactive oxygen species are elevated in *PCIF1* KD cells 124
4.24 Fatty Acid Desaturase 1 and 2 (*FADS1* and *FADS2*) expression in AML cell lines and viability upon inhibition. 126
4.25 shRNA mediated knockdown of FADS1, FADS2, and ELOVL6. 130
4.26 Proliferation analysis of fatty acid desaturase pathway intermediate metabolites supplementation in media. 132

A.1 Appendix: PCIF1 expression in DepMap 173
A.2 Appendix: Statistics Table: t-test and FDR p.adj for HPA Cancer cell lines 174
A.3 Appendix: Statistics Table: t-test and FDR p.adj for DepMap Cancer cell lines 175
A.4 Appendix: PCIF1 expression and survival in GEPIA2 176
A.5 Appendix: PCIF1 expression and patient survival in the BEAT-AML trial 177
A.6 Appendix: PCIF1 patient survival in the TARGET AML and TARGET AML-IF subgroup 178
A.7 Appendix: PCIF1 shRNA mediated knockdown measurements. 179
A.8 Appendix: LCMS acquired measurements of m6Am, m6A and A nucleotides from poly A+ enriched mRNA. 180
A.9 Appendix: Gating strategy Annexin-V and single stained controls 181
A.10 Appendix: Representative snapshots from MGG staining of wildtype AML cell line cultures 182

A.11 Appendix: Gating strategy and representative plots for SKNO-1 cell line of flow cytometry measurements of monocytic differentiation markers. 183
A.12 Appendix: Gating strategy and representative plots for Kasumi-1 cell line of flow cytometry measurements of monocytic differentiation markers. 184
A.13 Appendix: qPCR and flow cytometry based measurement of monocytic differentiation markers and therapeutic resistant markers. 185
A.14 Appendix: Principle Component Analysis of RNA-seq samples 186
A.15 Appendix: Gene Set Enrichment Analysis (GSEA) - extended 187
A.16 Appendix: TSN analysis 188
A.17 Appendix: DEG expression association with PCIF1 expression in WT AML and blood lineage cells 189
A.18 Appendix: ROS and Fatty acid supplementation experiment appendix 190

List of Tables

1.1 Major ICC categories of myeloid neoplasms and acute leukemias 20

1.2 2022 ELN genetic risk classification at initial diagnosis 21

3.1 R packages used 40

3.2 List of primers, guide oligos, and siRNAs used in this work 41

3.3 List of antibodies used in this work 42

3.4 List of small molecules and chemotherapeutics 42

4.1 Overview of AML cell lines used for experiments 58

4.2 Immunophenotypic marker expression of wildtype AML cell lines from cell line repository 93

List of Abbreviations

A . . . . . Adenosine

ALL . . . . . Acute Lymphoblastic Leukemia

allo-HSCT . . . . . Allogeneic Hematopoietic Stem Cell Transplantation

AML . . . . . Acute Myeloid Leukemia

Am . . . . . 2'-O-Methyladenosine

APL . . . . . Acute Promyelocytic Leukemia

Aza . . . . . Azacitidine

BCL2 . . . . . B-Cell Lymphoma 2

CEBPA . . . . . CCAAT/Enhancer Binding Protein Alpha

CML . . . . . Chronic Myeloid Leukemia

CRISPR . . . . . Clustered Regularly Interspaced Short Palindromic Repeats

DepMap . . . . . Cancer Dependency Map

DNA . . . . . Deoxyribonucleic Acid

ESCA . . . . . Esophageal Carcinoma

FLT3 . . . . . FMS-like Tyrosine Kinase 3

GTEx . . . . . Genotype-Tissue Expression (Project)

HNSC . . . . . Head and Neck Squamous Cell Carcinoma

HPA . . . . . Human Protein Atlas

ICC . . . . . International Consensus Classification

inv . . . . . Inversion

KD . . . . . Knockdown

KIRP . . . . . Kidney Renal Papillary Cell Carcinoma

KMT2A . . . . . Lysine Methyltransferase 2A (formerly MLL)

KO . . . . . Knockout

LIHC . . . . . Liver Hepatocellular Carcinoma

LSC . . . . . Leukemic Stem Cell

MAPK . . . . . Mitogen-Activated Protein Kinase

m6A N6-Methyladenosine

m6Am . . . . . N6,2'-O-Dimethyladenosine

MDS . . . . . Myelodysplastic Syndrome

MPN . . . . . Myeloproliferative Neoplasm

mTOR . . . . . Mechanistic Target of Rapamycin

mTORC . . . . . mTOR Complex

Mtase . . . . . Methyltransferase

OXPHOS . . . . . Oxidative Phosphorylation

PCIF1 . . . . . Phosphorylated-CTD Interacting Factor 1

READ . . . . . Rectum Adenocarcinoma

RNA . . . . . Ribonucleic Acid

RUNX1 . . . . . Runt-related Transcription Factor 1

TARGET . . . . . Therapeutically Applicable Research to Generate Effective Treatments

TCGA . . . . . The Cancer Genome Atlas

TSN . . . . . Transcription Start Nucleotide

TSS . . . . . Transcription Start Site

Ven . . . . . Venetoclax

WHO . . . . . World Health Organization

WT . . . . . Wildtype

mut . . . . . Mutant

1 | Introduction

One interpretation of the central dogma of molecular biology describes that the flow of genetic information occurs from DNA, to RNA, then to protein and a physiological function [1, 2, 3]. Advances in genetics have evolved our understanding on the roles of ribonucleic and deoxyribonucleic acid from the traditional role of information intermediates to the independent dynamic nature of DNA and RNA that shape cell function. Past decades of research revealing extensive modification of chromatin and RNA have taught us that our genetic information is even more dynamic than originally assumed. Deciphering the information encoded in our (epi)genomes has revealed a multi-faceted contribution in development and disease. The following introductory chapter covers three main subject areas, which intersect to form the background for this thesis, in which the contribution of epitranscriptomic methyltransferase protein, PCIF1 (Phosphorylated CTD-interacting Factor 1), to acute myeloid leukemia (AML) was investigated. The first section will provide a brief introduction to epigenetics, epitranscriptomics and other cancer hallmarks, a subsection of which is dedicated to fundamentals on the mRNA cap structure to provide the background for a more in depth summary of the current knowledge of PCIF1 in various contexts. Lastly, a brief overview on acute myeloid leukemia and the heterogeneous subtypes as well as treatment options will be outlined in the last section.

1.1 Epigenetics and epitranscriptomics as cancer hallmarks

The hallmarks of cancer were first coined by Hanahan and Weinberg at the beginning of the twenty-first century [4]. The original six core hallmarks have been revised over the last 25 years to

incorporate eight additional aspects as overarching characteristics of the cancer phenotype [5, 6]. The cancer hallmarks are defined as sustaining proliferative signaling, evading growth suppressors, resisting cell death, enabling replicative immortality, inducing/accessing vasculature, activating invasion and metastasis, deregulating cellular metabolism, and avoiding immune destruction, as well as prospective new hallmarks, such as unlocking phenotypic plasticity, non mutational epigenetic reprogramming, polymorphic microbiomes, and senescent cells.

The hallmark "nonmutational epigenetic reprogramming" includes modifications made to DNA, histones, and RNA and plays a driving role in the heterogeneity of many cancer types [6]. Changes to the methylation state on DNA and histones can influence gene transcription by affecting binding of transcriptional machinery and chromatin compaction. RNA epigenetics, also known as epitranscriptomics, affects RNA species by modulating their transcription, stability, translation, association and interaction with binding partners [7, 8]. Epigentic reprogramming of the cancer genome influences other cancer hallmarks as well, for example by shaping cellular metabolism during hypoxia to induce vascularization or impacting the conformation and stability of DNA, which can induce genome instability and malignant genetic lesions [6]. The frequency of dysregulated epigenetic modulators as well as the plasticity of cancer cell epigenomes offer opportunities for therapeutic intervention [9]. In hematopoietic malignancies, which have been found to be especially affected by epigenetic reprogramming, agents such as azacytidine, a nucleoside analog imparting hypomethylation consequences through DNA-methyltransferase inhibition, leads to a derepression of tumor suppressors [10]. However, only around 50% of AML/MDS patients respond to this treatment, and intrinsic as well as secondary resistance are challenges still faced in the clinic, underscoring the necessity to better understand the steps leading to refractory responses

and study novel putative leukemia vulnerabilities [10, 11].

1.1.1 mRNA modifications, transcription, translation and the mRNA cap

RNA species are abundantly decorated with an assortment of epitranscriptomic marks that impart transcriptional and translational functions. Although their biological significance cannot be understated, this thesis focuses on PCIF1, an mRNA cap-specific methyltransferase, and the following section is therefore dedicated to the process of mRNA cap formation, methylation and its putative effects on transcription, mRNA stability and translation.

The mRNA cap consists of a methylguanosine molecule added to the 5' end of the transcript via a triphosphate bridge in a cotranscriptional manner. RNGTT (RNA guanylyltransferase and 5' phosphatase) is recruited to the emerging end of the transcript via binding to the phosphorylated Serine-5 of the C-terminal domain (CTD) of RNA polymerase II (RNAPII) to form the basic cap structure [12, 13]. A methyl group is then added by the RNA guanine-7 methyltransferase (RNMT), in coordination with RNMT-activating miniprotein (RAM), which enables efficient substrate binding and methyltransferase activity of RNMT using SAM (S-adenosylmethionine) as a methyl donor [12, 13]. CMTR1 (Cap methyltransferase 1) binds to RNAPII and methylates the ribose ring of the first transcribed nucleotide after the cap, creating cap1 m7G-ppp-Am [14]. PCIF1 (Phosphorylated CTD-interacting factor 1) lastly binds to Ser5 of RNAPII and SAM to catalyze the formation of m6A, creating cap-adjacent N6,2'-O-dimethyladenosine on the previously Am methylated transcription start nucleotide (TSN) (cap2: m7G-ppp-m6Am) (Figure 1.1).

mRNA capping and methylation at the transcription start site (TSS) occurs cotranscriptionally. Capping enzymes are recruited to RNAPII during the promoter-proximal pausing step of RNAPII,

suggesting a quality control checkpoint for correct assembly of transcriptional factors and before release into productive elongation [12, 15, 16, 17].

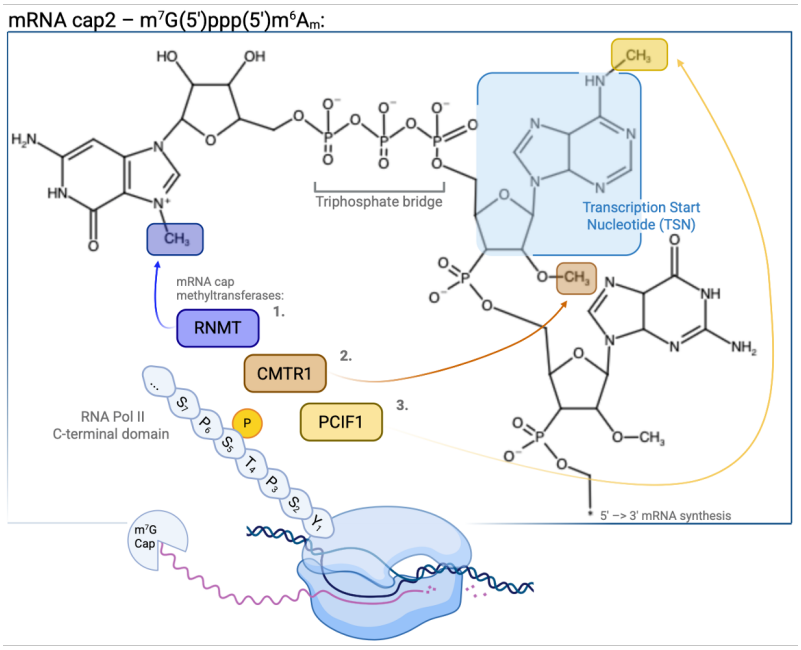

Figure 1.1. mRNA cap methylation. The basic cap is generated by RNGTT (not shown here) and then undergoes further emthylaitons steps by RNMT (activated by RAM), which catalyzes the methylation on guanosine (m7G), CMTR1, which catalyzes ribose methylation (Am) of the first transcribed nucleotide, and PCIF1, which catalyzes N6 methylation of the first transcribed nucleotide (m6A), resulting in m6Am. RNMT, CMTR1, PCIF1 bind to phosphorylated serine on RNAPII CTD. Figure created with Biorender.

The mRNA cap has a diverse set of roles in the mammalian genome. Most prominently, the cap serves to stabilize transcripts for export into the cytoplasm and initiate translation [12, 17]. mRNA stability can be enhanced by the cap through protecting the 5' end from exoribonucleic decay. Decapping enzymes act on transcripts int he cytoplasm and show varying substrate preferences depending on RNA features, such as sequence motifs and structural confirmation, as well as association with RNA-binding proteins and cellular context [18]. Eukaryotic initiation factor 4F (eIF4F) associates with the cap and enables recruitment of tRNA and the 40S ribosomal subunit for translation. Methylation of cap nucleotides can further promote binding of cap-associated pro-

teins, as well as inhibit binding of decapping enzymes, thus the methylated cap can upregulate the translation of target genes [12, 17, 19].

Dysregulation of mRNA capping, methylation, and decapping directly impacts viral infection pathways, differentiation, and cancer. RNMT has been shown to have roles in upregulating translational capacity by directly promoting ribosome biogenesis to drive metabolic reprogramming and enhance T-cell activation [20]. CMTR1 promotes RNAPII binding to certain TSS sites and seems to be elevated during neural developmental processes [21]. Importantly, eIF4E can regulate the capping efficiency of oncogenic ncRNAs in AML [22].

The catalytic methyltransferase domain of PCIF1 is conserved in vertebrates and deposits m6Am in the nucleus, and while the Pcif1 ortholog in *Drosophila melanogaster* retains its WW domain, which binds the RNAPII pCTD, it is catalytic-dead and m6Am is not detectable on fly mRNA [23, 24]. Curiously, mutations in the nuclear localization sequence of fly Pcif1 results in a markedly decreased fertility, especially in females, suggesting that a nuclear RNAPII-binding function of Pcif1 is vital in regulating transcription [25]. In mammals, research efforts have thus far focused on the implications of the PCIF1 methyltransferase activity on mRNA. Recently, studies have been published showing a significant role of the RNAPII CTD-interacting WW domain in glioma tumorigenesis, where overexpression of the WW domain inhibited proliferation of glioma cell lines in vitro and in xenograft mouse models [26, 27]. This observation sheds light on possible mechanisms by which PCIF1 could influence transcription and which have been neglected so far.

PCIF1 is the only cap-adjacent methyltransferase, as knockout of PCIF1 has been shown to deplete levels to background level amounts in LC-MS (liquid chromatography tandem mass spectrome-

try) [24]. PCIF1 and the effects of m6Am on transcription, translation and mRNA stability have recently been the focus of numerous studies, which have yielded partially contradicting results, likely due to various cellular contexts and mapping techniques employed. Although its specific location on the first transcribed nucleotide limits m6Am abundance in the total mRNA pool to one single specific nucleotide in the entire mRNA transcript, it is proposed to adorn a high proportion of transcript isoforms encoding adenosine (short: A, from here on) as the TSN. An overview of the current opinions on the effect of m6Am on gene expression is detailed below.

1.1.2 The multifaceted roles of m6Am on transcription, mRNA stability, and translation

N6,2'-O-dimethyladenosine was described as a novel nucleotide modification downstream of the m7G-cap in mammalian cells in 1975 and, due to its proximity to the mRNA cap, was suggested to play a role in transcription and translation [28]. A few decades later, in 2003, Fan and colleagues identify a novel protein, Phosphorylated CTD-interacting factor 1 (PCIF1), and its eponymous ability to bind to the phosphorylated Ser-5 residue on RNAPII via its WW domain [29]. The group drew similarities between the WW domain of PCIF1 and Pin1, which exerts transcriptionally repressive functions on RNAPII and inhibits cell cycling through its PPIase (peptidyl-prolyl cis-trans isomerase) activity [29, 30]. PCIF1 does not have a PPIase domain, and thus it was hypothesized that effects on protein synthesis are likely mediated through a separate mechanism. Indeed, in 2008, the same group described a negative regulation of PCIF1 on RNAPII transcription by inhibiting transcriptional elongation [23]. Moreover, a putative MTase function for PCIF1 was proposed in 2015 on the basis of phylogenetic similarity to prokrayotic DNA m6A MTases

M.EcoKI and M.TaqI [31].

In 2019, four groups independently identified PCIF1 to be the sole enzyme responsible for catalyzing cap-adjacent m6Am [24, 32, 33, 34]. The domain responsible for m6Am catalysis is characterized by an NPPF motif, common for mammalian methyltransferases and connected to the aforementioned WW domain via the helical domain [32]. The WW and helical domain form a positively charged binding pocket that shows high affinity for single stranded 5'-capped RNA, hereby distinguishing PCIF1 in its substrate specificity from all other methyltransferases [32]. Sendinc et al. showed that Am is readily converted to m6Am on capped, but not decapped mRNA, as well as less efficiently on mRNA less than 20nt long [24]. Boulias et al. also showed that PCIF1 binding affinity was approximately 7x higher on 2'-O-methylated mRNA [33]. Thus, the ideal substrate for PCIF1 is capped and 2'-O-methylated adenosine in mRNA of a specific minimum length located in the nucleus. Due to WW-domain mediated binding to Serine 5-phosphorylated RNAPII C-terminal domain (CTD), it was concluded that m6Am methylation occurred co-transcriptionally and may influence transcription efficiency of numerous transcript targets and important cellular pathways.

However, all four groups reported slight differences in molecular impact upon loss of the m6Am mark. These discrepancies are likely attributable to the different cell lines used for each study, conflicting methods for transcription start site and 5' transcript isoform detection, as well as sequencing methods developed to enable m6Am mapping. Akichika et al. showed no significant change in transcriptional abundance in HEK293T cells, contradicting the hypothesis that had been circulated until then by Mauer et al. that methylation next to the cap stabilizes transcripts start-

ing in A by rendering them resistant to DCP2 decapping [32, 35]. Instead, they showed that the increase in m6Am gene expression could be traced to upregulated translational efficiency. On the other hand, Sendinc et al. showed a decrease in translation of m6Am marked genes in melanoma cell lines (MEL264) [24]. Boulias et al. also showed little transcriptional change on global mRNA in HEK293T and a mild, but generally repressive, effect of the methyl mark on translation [33]. However, low-abundance transcripts were inspected more closely and determined to be stabilized by m6Am, as opposed to eliciting changes on the global transcriptional level.

These studies, as well as research generated on PCIF1 in the following years, make it challenging to reach a consensus regarding PCIF1's specific molecular function and underline how the use of different cell lines and sequencing techniques can lead to significantly different conclusions. Boulias et al. reasonably suggested that an m6Am dependent effect may be highly specific to the subsequent transcript sequence, as well as dependent on different methods of decapping employed for different mRNA types [33, 35]. Overall, the four studies show that PCIF1 methylates cap-adjacent 2'-O-methylated ribose (Am) with higher affinity than cap-adjacent unmethylated adenosine (A), is dependent on m7G cap binding, and is not required for HEK293T or MEL264 cell proliferation. Interestingly, Akichika et al. propose that a physiological effect of PCIF1 reveals itself in cell-stress conditions during treatment of HEK293T PCIF1 knockout (KO) cells with H_2O_2 to induce oxidative stress, which reduced proliferation of the treated KO cells, perhaps connecting a functional role for m6Am in overcoming oxidative stress and reactive oxygen species (ROS) to PCIF1 mechanisms [32].

FTO (Fat Mass and Obesity-Associated gene), is the only known m6Am eraser and has multi-

faceted roles depending on subcellular localization, cellular-, substrate- and sequence-specific contexts [35, 36, 37]. While a cap-m6Am substrate preference has been suggested in the cytoplasm, internal m6A is also bound by FTO in the nucleus to regulate alternative splicing [35, 38, 39]. The disproportionate abundance of internal m6A compared to cap-adjacent m6Am as well as the recent development of better sequencing technologies enabling accurate differentiation between m6A and m6Am complicate the interpretation of FTO demethylation mechanisms. In a cancer phenotype context, FTO is upregulated in AML and correlates with proliferation and drug resistance by negatively regulating mRNA transcript stability of tumor suppressors in an m6A-dependent manner [40].

According to results from proximity labeling experiments by Covelo-Molares and colleagues, PCIF1 likely has a rich interactome composed of CTD-binding proteins as well as other mediators of transcriptional regulation [41]. As expected, PCIF1 co-precipitates with RNAPII through Ser5-CTD interaction. Furthermore, PCIF1 was also reported to interact with several other mRNA processing enzymes (CMTR1, integrator complex subunits INT4, INT6, INT12, PCF11, SCAF8, SPT5, NELFA), DNA helicases and methyltransferases (SETD2, RECQ5, KMT2D and SETD1A/B), as well as RNAPII-interacting proteins (WAC, CRML (CRAMP1), GPN1) whose detailed function is still unknown [41].

Recently, PCF11 was followed up on mechanistically and identified to be sequestered to the cap by the deposited m6Am mark, hereby unable to perform its transcription elongation termination function and thus being the first validated m6Am reader protein [42]. It would therefore follow that the m6Am mark has a stabilizing effect on mRNA through sequestration away from the mRNA 3'

end undergoing productive elongation. PCF11 is likely one of many putative readers for m6Am, as quantitative proteomics of factors that preferentially bound cap-m6Am as opposed to cap-Am yielded additional hits besides PCF11 [42], and PCF11 was also identified as a putative cofactor in PCIF1 pull-down assays in the study by Covelo-Molares and colleagues [41].

SCAF8, one of the other proteins identified in the earlier screen to interact with PCIF1 (via RNAPII) [41] prevents early alternative polyadenylation of mRNA transcripts (in complex with SCAF4) and promotes RNAPII elongation [43]. SCAF8 could therefore be another m6Am reader or PCIF1 modulating enzyme, although no studies investigating whether SCAF8 can bind m6Am directly, or whether SCAF8 forms a complex with PCIF1 and RNAPII, exist to date.

Other interaction hits from the screen included mRNA processing enzymes, such as SPT5, which stabilizes RNAPII and promotes pausing and transcript elongation, and NELF, which is phosphorylated and disassociates from RNAPII to enable transcript elongation [44, 44]. It is yet to be determined whether a catalytic m6Am-based crosstalk or non-catalytic PCIF1 direct interaction exists between PCIF and components of transcriptional stalling and elongation.

PCIF1 has a preference for m7G capped mRNA and methylates uncapped mRNA with an approximately 5-fold lower efficiency than capped [45, 46], whereas other studies reported no cap-independent methylation at all [33, 24, 34]. The potential to methylate uncapped RNA becomes important in the field of viral infections and host interactions, a many RNA viruses are uncapped in the host cytoplasm [47]. PCIF1 has been found to methylate VSV (Vesicular stomatitis virus) RNA and diminish the antiviral response seen upon treatment with IFN-β [48]. In HIV, the viral machinery targets host PCIF1 for ubiquitination to enable HIV replication, which would other-

wise be restricted by m6Am [49]. As for SARS-CoV-2, the m6Am mark has been found to have a stabilizing effect on transcripts encoding receptors that facilitate viral infection of lung epithelial cells [50]. This viral RNA methylation is not only an interesting focus for treatment of infectious diseases, but also raises the question of PCIF1 location, which, due to its RNAPII binding domain has been described to be nuclear, but immunofluorescence images show some cytoplasmic location ([24], as well as results of this thesis). VSV, HIV and SARS-CoV are single-stranded RNA viruses, of which VSV and SARS-CoV2 replicate entirely in the cytoplasm after viral entry, while HIV counts as an RNA retrovirus, which is reverse transcribed in the cytoplasm and subsequently integrated into host DNA [51, 52, 53]. Uncapped viruses are known to generate a cap structure and 2'-O-methylate the cap-adjacent ribose to gain stability and be less distinguishable from host mRNA to hijack the host translation machinery [54, 55]. The question arises about the timing of host PCIF1 methylation of viral RNA, whether it occurs before or after the virus has generated the cap. If PCIF1 were indeed able to methylate the uncapped viral RNA, it would suggest that PCIF1 has nuclear export and cytoplasmic MTase function.

1.1.3 PCIF1: oncogene or tumor suppressor?

A study investigating TCGA cancer and GTex normal tissue data [56] showed that PCIF1 protein expression was different in clear cell RCC, LUAD, and UCEC, correlated with overall survival (OS) or disease free survival (DFS) in ACC, KIRC, KIRP, MESO and THCA, and showed a positive correlation with tumor infiltration in CD8+ T-cells, neutrophils, macrophages and B-cells of different cancers.

PCIF1 was reported as a hit in an in vivo RNAi screen identifying bladder cancer tumor sup-

pressors [57, 58]. PCIF1 shRNA-mediated knockdown in non-tumorigenic bladder cancer cells and subsequent implantation into immunocompromised mice enabled malignant transformation of bladder cancer cell lines. However, due to the then undiscovered MTase capabilities of PCIF1, no mechanistic follow up was performed. It remains to be seen whether PCIF1 indeed acts as a tumor suppressor in bladder cancer.

The first study implicating PCIF1 as a tumor oncogene with mechanistic insight was performed in gastric cancer (GC). Knocking down PCIF1, thus decreasing m6Am at the +1 position from the 5' end of mRNA, increased polysome occupation on TM9SF1 mRNA, a membrane autophagocytic marker with context specific tumor suppressor and oncogenic abilities [59]. The depletion of PCIF1 in GC led to decreased proliferation and metastatic capability in vitro as well as in vivo. Importantly, this increase in translation was specifically seen for TM9SF1 mRNA, but not across global transcripts [59]. Thus, the first cancer study concluded an oncogenic effect for PCIF1.

Following quickly after, however, Gao and colleagues published findings that indicated PCIF1 to have a tumor suppressive role in glioblastoma multiforme (GBM) [26]. However, m6Am sequencing was not performed for this study, so there is no specified target transcript or translational regulation reported. Overexpression of both WT and catalytically dead PCIF1 produced a suppressive effect, albeit to a lesser extent in the mutant, indicating and enzymatic and non-enzymatic role for PCIF1 in tumor suppression [26].

In colorectal carcinoma (CRC), Wang et al showed that *PCIF1* gene expression is highly upregulated and associated with poor prognosis in TCGA patient data sets [60]. In vivo, they showed that N6-methyladenosine on the TSS stabilizes FOS mRNA which promotes tumor growth and

$TGF-\beta$ expression to suppress anti-tumor immunity. Knockout of PCIF1 also seemed to up-regulate *Stat1* and *Ifitm3* mRNA, which increased the IFN-γ response and was beneficial for anti-PD-1 therapy. The authors show that while m6Am occupancy is decreased on all three transcripts of interest, the relative mRNA abundance as well as stability upon actinomycin-D treatment is only decreased for *Fos* mRNA, while *Stat1* and *Ifitm3* mRNA is upregulated according to qPCR experiments of control vs PD-1 treated tumors (actinomycin-D assay was either not reported, or not performed, for *Stat1* and *Ifitm3*). Whether the depletion of PCIF1 directly leads to an increase in Stat1 and Ifitm3 via m6Am, or whether it occurs indirectly, can therefore not be concluded. Validating this result could imply that PCIF1 and m6Am not only have tumor context specific, but also transcript specific effects within the same model context, as hypothesized in previous studies [35].

In head and neck squamous cell carcinoma (HNSCC), PCIF1 was found to colocalize with the cotranscriptional activator CTBP2 (C-terminal binding protein 2), which facilitates deposition of the m6Am mark and suppresses the translation of TET2 tumor suppressor, and would therefore suggest PCIF1 to be a tumor oncogene [61]. CTBP2 acts as a transcriptional corepressor by recruiting HDACS and HMTS. Interestingly, CTBP2 has been identified to also have NADH/NAD+ as well as fatty acyl-CoA binding capabilities, which would make PCIF1 an interesting target for metabolite sensing and redox homeostasis [62, 63], perhaps similar to the phenotype suggested by Akichika and colleagues showing PCIF1 KD generates sensitivity to oxidative stress [32]. Indeed, numerous studies disclosing a comprehensive list of differentially expressed genes (DEGs) following perturbation of PCIF1 expression find that a significant proportion of these are involved in metabolic regulation of lipids [64].

In addition to the study in HNSCC, the same group investigated PCIF1 specifically in esophageal squamous cell carcinoma (OSCC), the main subtype of HNSCC, but indicated oncogenic functions instead through m6Am methylation and downregulation of tumor suppressor MTF2 translation [61, 65]. MTF2 signaling is indispensable for maintenance of the PRC2-H3K27me3 signature, which could implicate a wider chromatin compaction effect of PCIF1 [65]. Both studies from cancers of head and neck epithelium therefore show that PCIF1 conveys a repressive translational effect on tumor suppressors that have functions in reprogramming the global epigenetic landscape.

Sugita et al. found that PCIF1 mediated m6Am has transcript specific effects on stability, as they show that depletion of m6Am via PCIF1 knockdown from *RAB23* and *CNOT6* transcripts has the opposite effect on stability in HeLa cells [66]. They attribute this to different decapping mechanisms, as hypothesized earlier [35], as *CNOT6*, which is destabilized by lack of m6Am, relies on DCP-mediated decapping and *RAB23* does not [66]. *CNOT6* has 3'-5' RNase activity, which leads to the downregulation of specific transcripts, further underlining that differentially expressed genes could be direct targets of PCIF1, or indirectly via regulation of transcript regulators [66].

In order to understand the impact of PCIF1 in cancer, the influence on the immune system should not be disregarded, as the tumor immune microenvironment (TME) plays an important role in anti-tumor immunity and PD-L1 therapy. Xiang et al. report that conditional KO (cKO) of PCIF1 in murine CD8+ T-cells shows no transcriptional or mRNA stability changes, but elevated translation of m6Am methylated ferroptosis suppressor and T-cell activation genes, which increases tumor infiltrating cytotoxic T-cells [67]. In another immune system related context, Song et al. show that PCIF1 m6Am regulates macrophage migratory and cytotoxic capabilities in a murine PCIF1

macrophage cKO model of periodontal inflammation [68]. The decrease of transcript stability upon loss of m6Am on an alternative TSS of CSF1R (colony stimulating factor-1 receptor) results in downregulation of macrophage phagocytosis and migration and alleviated peridontal bone loss [68].

The divergent effects of PCIF1 effect on mRNA transcription, stability, and translation is likely a consequence of context-specific mechanisms (cell line, cancer-context, sequence motifs), however, a major limitation in the field of m6Am epitranscriptomics is the difficulty in obtaining reliable sequencing results that unambiguously map m6Am on mRNA and consider the transcript isoform diversity arising from alternative transcription start sites [58, 56, 69]. The available techniques approach mapping m6Am on transcripts differently: MeRIP-seq (m6A-seq) [70], miCLIP [71], and m6Am-exo-seq [24] are based on immunoprecipitation of transcripts using an m6A specific antibody and then calling transcription start sites in sequenced fragments, but the antibody specificity yields cross-talk between methylation marks as well as 5'UTR TSS isoforms make ensuring uniformity even within these methods challenging [72, 73]. Jianheng and colleagues recently published CROWN-seq, an m6Am sequencing method that enables single transcription start nucleotide (TSN) level detection of m6Am [69]. Uniquely, this method uses a deamination step, which converts non-N6-methylated ribose (Am) to 2'-O-methylinosine, which is sequenced as G, while m6Am is not converted and sequenced as A [69, 74]. Importantly, the results generated by CROWN-seq in seven different human cell lines show that m6Am is stochiometrically dense, found on most transcripts that encode TSN-A, and seems to have a role in transcriptional regulation of transcripts with specific TSS motifs that in turn depend on specific transcription initiation complexes for RNAPII gene transcription, thus linking the enhanced expression of mRNA

to upregulated transcription initiation [69]. Their sequencing approach also revealed more precise m6Am maps, especially on previously unannotated TSSs, shedding light on the need to improve methods for detecting and calling 5' transcript isoforms.

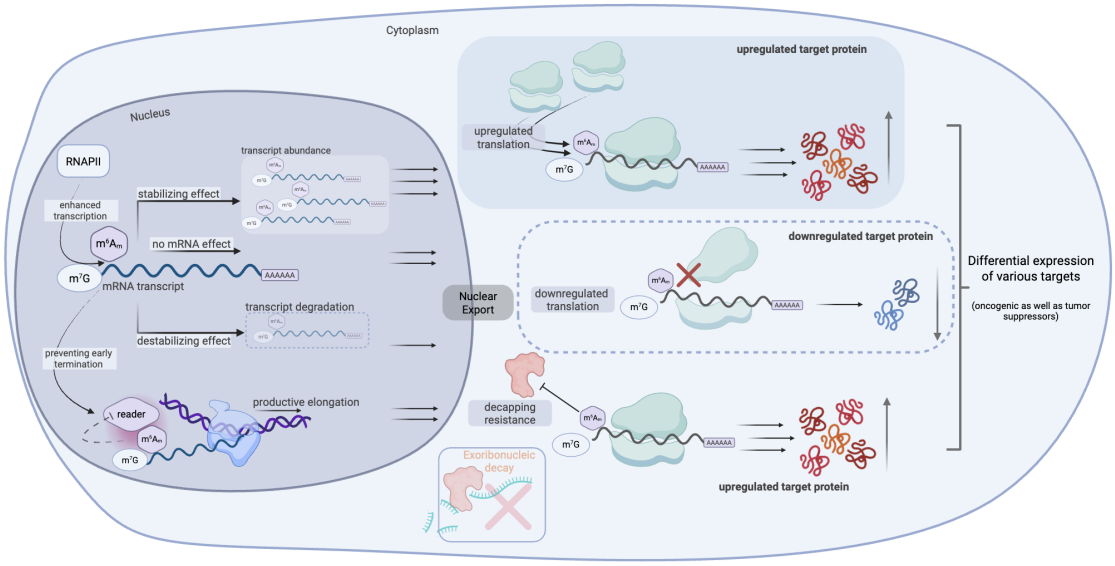

Figure 1.2. Multifaceted roles of m6Am. m6Am is deposited on the +1 position after the TSS on mRNA. While some studies show that m6Am is a stabilizing feature of mRNA, other studies show a decreased abundance on transcripts, while yet others see no effect on the global transcriptome. Translation efficiency showed similarly contradicting outcomes. Some studies hypothesize that m6Am may increase resistance to certain types of decapping. Other studies show transcriptional enhancement, As the mRNA cap structure and cap-adjacent nucleotide is important for translation initiation, ribosome profiling was also assessed by most studies, identifying a reader that is sequestered away from the elongating transcript and inhibits early termination.

Mapping N6,2'-O-dimethyladenosine of the cap-adjacent nucleotide has proven to be complex and, while many studies report that thousands of transcripts are m6Am methylated, they also note that only a small subset appear to be differentially expressed upon PCIF1 perturbation. It should therefore not be overlooked that the prevalent method of TSS mapping does not optimally represent all TSN isoforms, which may generate some false negatives in previous sequencing studies, as well as potential non-catalytic or co-factor interactions of PCIF1 to influence transcription and

translation.

In summary, numerous studies investigating the role of PCIF1 in cancer, the immune system, virus-host interactions, and other disease contexts have been published in the five years since the characterization of PCIF1 cap-dependent m6Am function, and there are likely many more studies currently underway or already in review. Some studies show m6Am enhances target transcript stability [33, 60, 66, 75], while others show a decrease in transcript availability [23, 35, 66]. Controversially, some groups found no change in global transcript abundance and instead report either an increase in polysome occupation and translational efficiency of transcripts targeted by PCIF1 [32, 76] or a decrease in translation machinery recruitment and efficiency of specific targets [24, 33, 59, 61, 65]. Much more is to be gained from optimizing m6Am sequencing strategies as well as expanding knowledge on the contexts in which PCIF1 elicits a phenotype.

1.2 Introduction to Acute Myeloid Leukemia (AML)

Acute Myeloid Leukemia (AML) is defined by the uncontrolled clonal expansion of myeloid precursors in the bone marrow or peripheral blood, resulting in the accumulation of immature blasts and a decline of hematological functions [77, 78]. Leukemic cells have an increased capacity for self-renewal, differentiation blockade as well as an ability to evade cell death and immunogenic detection [78]. Initiation events of clonal hematopoesis and leukemic transformation remain incompletely resolved, but the identification of genomic drivers has allowed for the stratification of AML into subgroups depending on somatic abnormalities that define the blast population [77, 78, 79].

1.2.1 AML Subtypes

Before characterization into genetic subtypes, the classification of AML relied on cytochemical and morphological attributes of blast cells, also known as the FAB (French-American-British) nomenclature [80]. The FAB system defined six groups (M1-M6) based on the direction of differentiation (granulocytic, monocytic, erythroblastic) as well as the degree of maturation of the blasts assessed from Romanowsky stained bone marrow and peripheral blood smears [80]. While this nomenclature allowed for a more uniform disease definition of patient cases between hospitals and institutions, the FAB system does not take cytogenetic and molecular abnormalities into account. Systematic study of cytogenetic rearrangements and gene fusion events by The Cancer Genome Atlas (TCGA) represented the first catalog of leukemia driver genes, however, approximately 50% of AML patients have a normal karyotype and require further genetic profiling [77, 79]. To date

the 5th edition of WHO (World Health Organization) Classification and the International Consensus Classification (ICC) provide a thorough directory of myeloid neoplasms and leukemias used for diagnosis and risk stratification [81, 82].

Patients diagnosed with AML can present with one or more mutations in these recurrent genetic abnormalities, which can be classified into functional groups: AML with mutations in signaling and kinase pathways (*FLT3*, *KRAS*, *NRAS*, *KIT*, *PTPN11*, and *NF1*), epigenetic modifiers (*DNMT3A*, *IDH1*, *IDH2*, *TET2*, *ASXL1*, *EZH2*, and *MLL*/*KMT2A*), nucelophosmin (*NPM1*), transcription factors (*CEBPA*, *RUNX1*, and *GATA2*), tumor suppressors (*TP53*), spliceosome complex (*SRSF2*, *U2AF1*, *SF3B1*, and *ZRSR2*), and cohesin complex (*RAD21*, *STAG1*, *STAG2*, *SMC1A*, and *SMC3*) [78, 84]. Mutations in signaling pathway mediators are among the most common in adult AML and detection of these mutations are commonly associated with a poor outcome [82, 84]. Internal-tandem duplication in *FLT3* (FMS-like tyrosine kinase 3) result in constitutively active signaling of RAS/RAF/MEK/mTOR and the PI3K/Akt pathway, enabling cellular proliferation and a differentiation blockade [84, 85]. The adverse treatment prognosis for *FLT3* mutated AML has improved since the approval of targeted FLT3 inhibitors such as quizartinib, however, acquired resistance and clonal selection advantage of resistant clones remains a challenge in the clinic [85]. Conversely, the disruption of hematopoietic differentiation driven by transcription factor RUNX1 caused by gene fusion with *RUNX1T1* (t(8;21)(q22;q22.1)) is associated with a favorable outcome [86]. Presenting with a particularly aggressive phenotype are patients carrying KMT2A rearranged leukemias (KMT2A-r), which can occur with different fusion partners and result in dysregulation of histone 3 lysine 4 methylation (H3K4me3) and an overexpression of oncogenic pathways via *HOXA*/*MEIS1* [87].

Table 1.1. Major ICC categories of myeloid neoplasms and acute leukemias. Amended from [82]

Acute myeloid leukemia
Acute promyelocytic leukemia (APL) with t(15;17)(q24.1;q21.2)/*PML::RARA* $\geq$ 10%
APL with other *RARA* rearrangements $\geq$ 10%
AML with t(8;21)(q22;q22.1)/*RUNX1::RUNX1T1* $\geq$ 10%
AML with inv(16)(p13.1q22) or t(16;16)(p13.1;q22)/*CBFB::MYH11* $\geq$ 10%
AML with t(9;11)(p21.3;q23.3)/*MLLT3::KMT2A* $\geq$ 10%
AML with other *KMT2A* rearrangements $\geq$ 10%
AML with t(6;9)(p22.3;q34.1)/*DEK::NUP214* $\geq$ 10%
AML with inv(3)(q21.3q26.2) or t(3;3)(q21.3;q26.2)/*GATA2*; *MECOM*(*EVI1*) $\geq$ 10%
AML with other *MECOM* rearrangements $\geq$ 10%
AML with other rare recurring translocations $\geq$ 10%
AML with t(9;22)(q34.1;q11.2)/*BCR::ABL1* $\geq$ 20%
AML with mutated *NPM1* $\geq$ 10%
AML with in-frame bZIP *CEBPA* mutations $\geq$ 10%
AML and MDS/AML with mutated *TP53* 10–19% (MDS/AML) and $\geq$ 20% (AML)
AML and MDS/AML with myelodysplasia-related gene mutations 10–19% (MDS/AML) and $\geq$ 20% (AML): Defined by mutations in *ASXL1*, *BCOR*, *EZH2*, *RUNX1*, *SF3B1*, *SRSF2*, *STAG2*, *U2AF1*, or *ZRSR2*
AML with myelodysplasia-related cytogenetic abnormalities 10–19% (MDS/AML) and $\geq$ 20% (AML): Defined by detecting a complex karyotype ($\geq$ 3 unrelated clonal chromosomal abnormalities in the absence of other class-defining recurring genetic abnormalities), del(5q)/t(5q)/add(5q), –7/del(7q), +8, del(12p)/t(12p)/add(12p), i(17q), –17/add(17p) or del(17p), del(20q), and/or idic(X)(q13) clonal abnormalities
AML not otherwise specified (NOS) 10–19% (MDS/AML) and $\geq$ 20% (AML)
Myeloid sarcoma
Acute leukemia of ambiguous lineage
Acute undifferentiated leukemia
Mixed phenotype acute leukemia (MPAL) with t(9;22)(q34.1;q11.2); *BCR::ABL1*
MPAL, with t(v;11q23.3); *KMT2A* rearranged
MPAL, B/myeloid, NOS
MPAL, T/myeloid, NOS
Myeloproliferative Neoplasms
Myeloid/lymphoid neoplasms with eosinophilia and tyrosine kinase gene fusions
Myelodysplastic/myeloproliferative neoplasms
Premalignant clonal cytopenias and myelodysplastic syndromes
Pediatric and/or germline mutation-associated disorders
Myeloid proliferations associated with Down syndrome

Abbreviations: AML = acute myeloid leukemia; APL = acute promyelocytic leukemia; MDS = myelodysplastic syndrome; MPN = myeloproliferative neoplasms; MPAL = mixed phenotype acute leukemia; NOS = not otherwise specified; TK = tyrosine kinase; inv() = inversion; t() = translocation; p/q() = short/long chromosome arm. Percentages indicate minimum diagnostic blast percentage.

Table 1.2. 2022 ELN genetic risk classification at initial diagnosis

Risk category	Genetic abnormalities
Favorable	t(8;21)(q22;q22.1)/*RUNX1::RUNX1T1* inv(16)(p13.1q22) or t(16;16)(p13.1;q22)/*CBFB::MYH11* Mutated *NPM1* without *FLT3*-ITD bZIP in-frame mutated *CEBPA*
Intermediate	Mutated *NPM1* with *FLT3*-ITD Wild-type *NPM1* with *FLT3*-ITD (without adverse-risk genetic lesions) t(9;11)(p21.3;q23.3)/*MLLT3::KMT2A* Cytogenetic and/or molecular abnormalities not classified as favorable or adverse
Adverse	t(6;9)(p23.3;q34.1)/*DEK::NUP214* t(v;11q23.3)/*KMT2A*-rearranged t(9;22)(q34.1;q11.2)/*BCR::ABL1* t(8;16)(p11.2;p13.3)/*KAT6A::CREBBP* inv(3)(q21.3q26.2) or t(3;3)(q21.3;q26.2)/*GATA2*, *MECOM*(*EVI1*) t(3q26.2;v)/*MECOM*(*EVI1*)-rearranged -5 or del(5q); -7; -17/abn(17p) Complex karyotype or monosomal karyotype Mutated *ASXL1*, *BCOR*, *EZH2*, *RUNX1*, *SF3B1*, *SRSF2*, *STAG2*, *U2AF1*, and/or *ZRSR2* Mutated *TP53*

Source: European Leukemia Network (2022) [83]

Pathogenesis of AML follows the concept of a two-hit model, in which clonal hematopoiesis results from the mutation of a class I hit (eg. FLT3, RAS) which provides proliferative advantage over other clones in the hematopoietic pool. The second mutational hit (class II) enables a blockade of differentiation, arresting the clone in an immature blast state (eg. epigenetic modifiers) [84, 88]. Mutation in either class can therefore lead to myeloproliferative neoplasms or disorders, but a single mutation event is likely not sufficient to cause leukemia [88]. Clonal expansion without induction of AML is an observation made particularly in patients aged >45 years and requires close observation [84].

At initial diagnosis, patients who are eligible for intensive induction chemotherapy receive high-dose cytarabine (AraC) via continuous intravenous infusion for seven days as well as an anthra-

cycline (usually daunorubicin) during the first 3 days of induction chemotherapy (7+3 regimen) [83]. Cytarabine, a pyrimidine analog, hinders DNA synthesis by inhibiting DNA polymerase and stalling at replication forks and the anthracycline daunorubicin elicits DNA damage by intercalating into the helix and inhibiting topoisomerase II [83, 89, 90]. Upon complete remission, less intensive consolidation therapy and/or an allogeneic hematopoietic stem cell transplant (allo-HSCT) is performed if the patient is eligible [83]. In the presence of specific (cyto)genetic features, additional treatment with inhibitors targeting pro-proliferative signaling pathways are included (Midostaurin for FLT3-ITD) [83, 91]. Patients deemed not eligible for intensive induction chemotherapy (usually due to advanced age or existing comorbidities) can be administered low-dose cytarabine in combination with venetoclax, an inhibitor targeting the B-cell lymphoma 2 proto-oncogene (BCL-2), which is overexpressed in many cancers to circumvent apoptosis [83, 92]. Use of azacitidine (Aza) or decitabine alone or in combination with venetoclax have been adopted into standard care for older patients [83]. Azacitidine and decitabine are cytosine analogs and induce cytotoxicity through DNMT3A (DNA methyltransferase) inhibition and DNA hypomethylation [10]. The development of novel small molecule therapeutics for different subtypes of AML has significantly improved prognosis, but issues surrounding resistance or the significant side-effects that come with intensive induction chemotherapy warrant further investigation into novel targets [84, 93].

1.2.2 Epigenetics and Leukemia

Compared to solid cancers, AML has a low genetic mutational burden, with only a few chromosomal translocations and point mutations contributing to pathogenesis, and nearly 50% of AML cases harbor mutations in chromatin modifiers (*KMT2A*r, *EHZH2*, *ASXL1*) and/or DNA methyl-

transferases (*DNMT3A*, *TET2*, *IDH1/2*) [79, 9]. Due to the frequently altered, highly plastic and reversible nature of epigenetic marks that lead to widespread changes and leukemogenesis, targeting of writers, readers and erasers for therapy in AML has become a meaningful clinical intervention in recent years [9]. More recently, RNA epigenetics and the N6-methyladenosine mark deposited by METTL3/METTL14 complex has shifted into focus due to emerging evidence of m6A as a contributor to leukemogenesis [9]. METTL3 targets, such as *BCL2* and c-*MYC*, are stabilized to contribute to the expansion of the clone, while detection of m6A in differentiation genes is detected by cytoplasmic reader YTHDF2 and mediates RNA decay, thus downregulating important factors for hematopoietic differentiation [9, 94, 95]. Research on m6A, as well as clinical trials involving a METTL3 inhibitor in AML, is currently ongoing [96]. Fat mass and obesity-associated protein (FTO) as well as ALKBH5 are erasers of m6A and have been implicated in contributing to leukemia phenotypes [40, 97]. FTO is highly expressed in certain AML subtypes (*FLT3*, *NPM1* mutated) and has an oncogenic role through demethylation and negative regulation of target genes that affect differentiation processes in an m6A-dependent manner [40]. Importantly, FTO has also been identified as the demethylase of 5' cap-adjacent m6Am, which is catalyzed by PCIF1 and has yet to be investigated in the context of AML [35, 38].

2 | Rationale, aims and objectives

Acute myeloid leukemia (AML) heterogeneity, drug resistance and therapeutic limitations, especially in patients aged >60 years, remain a major clinical challenge. Despite advances in chemotherapy, targeted agents and immunotherapy, many patients are still faced with a poor prognosis and unsatisfactory curative treatment chances, underscoring the need to explore novel leukemia vulnerabilities for therapy. Due to low somatic mutational burden compared to other solid cancers, AML is described to be an epigenetically driven cancer and pre-clinical studies targeting m6A modulators have shown promising results for leukemia sensitivity to epitranscriptomic targeting. Phosphorylated CTD interacting factor 1 is the only human cap-adjacent mRNA methyltransferase and has been the subject of in-depth analysis since its characterization six years ago. However, its exact molecular mechanism remains controversial and multi-faceted. *PCIF1* gene expression is dysregulated in several malignancies and previous studies have reported and impact on transcriptional/translational regulation of proliferation, metabolism and oncogenic signaling, warranting detailed molecular mechanistic investigation in the so far unstudied AML context.

This work aims to contribute to existing knowledge on the disease mechanisms of epitranscriptomic writer PCIF1, specifically in the context of AML, by addressing three basic questions:

1. Is PCIF1 differentially expressed across human tissues and cancer cell lines in public data?
2. Are AML cell lines sensitive to the loss of PCIF1 in vitro?
3. What are the targets of PCIF1 in AML?

3 | Materials and Methods

3.1 Methods

3.1.1 Cell culture and maintenance

MOLM-13, THP-1 and U937 were cultured in RPMI (GIBCO) supplemented with 10% fetal bovine serum and 1x pen/strep solution. Kasumi-1 cells were cultured in RPMI (GIBCO) supplemented with 20% fetal bovine serum and 1x pen/strep solution. SKNO-1 cells were cultured in RPMI (GIBCO) supplemented with 10% fetal bovine serum and 10ng/mL human GM-CSF (Biotechne, Cat: NBP2-34893). Cells were expanded until 90% confluent and divided in a ratio of 1:8 (MOLM-13, THP-1 and U937), 1:5 (SKNO-1) or 1:3 (Kasumi-1), depending on the growth rate of each cell line. HEK293T cells were cultured in DMEM supplemented with 10% fetal bovine serum and split when confluent at a 1:10 ratio. Culture supernatants were routinely submitted for mycoplasma testing (Lonza MycoAlert, Cat: LT07-318) or by PCR according to published protocol [98].

3.1.2 Lentivirus production and transduction of AML cell lines

Knockdown and knockout mediated loss of gene expression was achieved using a lentiviral transduction protocol for suspension cells. Lentivirus was produced by calcium-phosphate mediated transfection of HEK293T cells using 10µg pLKO.1 puro vector (Addgene #8453) (for shRNA constructs) or LentiCRISPRv2 (Addgene #52961) (for CRISPR sgRNA constructs), 5µg of pCMV-VSV-G (Addgene #8454) and 8µg of pCMV-dR8.2 (Addgene #8455). A transfection mixture

containing the guide vector, packaging, and envelope vectors was prepared, as well as 62.5µL of $CaCl_2$ and H_2O up to 500µL per 10 cm plate. An equal amount of 2x Hanks buffered saline solution (HBSS) was added to a separate Eppendorf tube and the transfection mixture was added dropwise to the HBSS solution under gentle agitation by vortexing at low speed. The solution was incubated at room temperature for 10-20 minutes before gently dispensing 1mL of the mixture onto 70% confluent HEK293T cells on a 10cm plate and gently swirling. HEK cells were seeded 24h before transfection in DMEM + 10% FBS medium. Transfection was performed in the afternoon and the mixture was incubated on the cells overnight in a 37°C 5% CO_2 incubator. Media was replaced 12-18 hours after transfection with fresh FBS containing media and left inside the incubator for 24 hours before first viral supernatant was harvested. 24-hour, 48-hour, and 72-hour supernatant was collected carefully without disturbing the cells using a 10mL syringe, filtered through a 0.45µm filter, pooled into a 50mL Falcon tube and stored at 4°Cuntil all timepoints were harvested. Pooled viral supernatants were aliquoted and stored at -80°C.

For stable transduction of AML cell lines with lentiviral particles, 200µl or lentiviral particles were added to 25,000-35,000 AML cells in 800µl culture medium containing 6µg/mL per 12-well and swirled to ensure even distribution in the well. 12-well plates containing cells and viral particles were centrifuged at $1000 \times g$, 25°C for one hour. Cells were transferred to the incubator for at least 4 hours before 1mL of fresh culture medium was added to each well and left overnight. Spinfection was repeated on the following day. Culture plates were briefly spun down to collect cells close to the bottom of the well and 500-700µL of media was gently removed before adding fresh lentiviral particles with 6µg/mL polybrene to each well. Cells were allowed to recover from infection for 12-24 hours before adding selective pressure for 2 - 4 days. Selection media was refreshed

after 48h if selecting for 4 days. Cells were allowed to recover for 24 - 48 hours before levels of knockdown were assessed and experiments were performed within four weeks after infection. The appropriate puromycin concentration was assessed using a kill curve assay. Briefly, wildtype cells from every cell line was seeded at 50% confluency in a 12-well plate and puromycin added to an end concentrations between 0 - 20µg/mL. Cell death was assessed visually with a light microscope as well as using trypan blue and the concentration that induced >90% cell death within 48h was used for selection. Wildtype cells were left in selection media for 72 hours and then reseeded and passaged in non-selective media for two weeks to assess whether cells were capable of recovering or acquired resistance after re-challenge. Concentrations of puromycin were additionally optimized in the knockdown cells and adjusted for all future experiments according to greatest difference in protein level seen after selection. The following concentrations of puromycin were used for selection: Kasumi-1: 1µg/mL, MOLM-13: 6µg/mL, THP-1: 8µg/mL, SKNO-1: 12µg/mL, U937: 15µg/mL.

3.1.3 Proliferation assays

Proliferation and viability of AML cell lines after knockdown or knockout were assessed by automatic cell count with trypan blue (BioRad, TC20 Automated Cell Counter) and CellTiter-Glo (CTG) Assay (Promega, G7570). For automatic counting experiments, cells were seeded in duplicate in 12-well plates in 2mL appropriate growth medium for 7 days. Equal numbers of cells were seeded at concentrations that would allow for confluency to be reached around day 7. On indicated days, cells were briefly mixed by pipetting and each well was counted twice.

CellTiter-Glo (CTG) ATP quantification assay using firefly luciferase to assess viability were per-

formed in parallel with automatic cell counting. 100ul of cells from suspensions used for 12-well automatic counting proliferation assays were seeded in triplicates in separate 96-well plates for day 0, day 5 and day 7 timepoints and topped up to 150ul appropriate growth medium at numbers that allow for confluency to be reached around day 7. On indicated days, plates were taken out of the incubator and room temperature (RT) CellTiter-Glo reagent was added at a 1:1 ratio to the wells, mixed by pipetting three times and transferred into a white flat-bottom luminescence 96-well plate (Corning, CLS3922). The mixture was incubated at RT for 10 minutes away from light before taking measurements on a BMG Fluostar Omega microplate reader (luminescence, emission 560nm, no filter, gain 3000). Relative viability was calculated using the formula:

$$\boxed{\text{Relative Cell Proliferation} = \frac{\textbf{T}\text{est} - \textbf{B}\text{lank}}{\textbf{C}\text{ontrol} - \textbf{B}\text{lank}}}$$

where $T =$ Test well at specified time point

$B =$ Average of blank values (containing only medium)

$C =$ Average of scramble control at time point or day 0 of the same condition

3.1.4 EC50/IC50 treatment protocol with chemotherapeutic compounds

For in vitro drug treatments, cells in log-phase growth were seeded in duplicates or triplicates at varying drug concentrations and relative cell viability was measured using CellTiter-Glo. Drugs were resuspended in DMSO to 10mM and experiments were either performed as an EC50/IC50 treatment curve, or dose escalation treatment (low, medium, high concentrations), and a negative

DMSO-vehicle treatment was included for every experiment. Cells were tested for DMSO toxicity (comparing DMSO treated vs untreated) with each new drug concentration optimized. Cells were cultured with drug treatment for 48-72 hours before cell proliferation assays. Relative viability (normalized to DMSO-treated control) was plotted in a dose-response curve on a log-transformed x-axis (concentrations) and the concentration at which 50% viability compared to DMSO vehicle was observed calculated by fitting a sigmoidal curve to the datapoints, or normalized to the scrambled control (in the case of low, medium, high concentrations used). A comprehensive list of all treatments can be found in table 3.4.

3.1.5 May-Grünwald Giemsa staining

Cells for differentiation staining were taken 5 to 10 days after selection ended. Clean reusable cytofunnels (Fisher Scientific, Cat No: SLE5207) were assembled onto glass poly-L-lysine microscopy slides with disposable filter cards (Fisher Scientific, Cat No: SLE5210) between in a metal cytospin clamp. $200\mathrm{ul}$ cell suspensions (between 0.2-0.5 million cells/mL) were loaded one double cytofunnel and centrifuged at $900 \times g$ for 4 minutes using a Shandon CytoSpin 4 (Shandon, Thermo Scientific). Slides were fixed in cold methanol in coplin jars for 10 minutes and then incubated with May-Grünwald solution (Sigma, Cat No:63590) for 8 minutes. Slides were washed three times with H_2O for 3-5 minutes each and then placed into 1:20 diluted Wright-Giemsa (SLS, Cat No: WG128-4L) staining solution for 40-60 minutes. Stained slides were washed in H_2O three times for five minutes each and then placed into a 35°C hybridization oven until dry (approximately 30 minutes). Slides were mounted using Eukitt Quick-hardening mounting medium (Sigma-Aldrich, Cat No: 03989-100ML) and left on a flat surface to harden overnight under a

fume hood. Slides were stored in the dark at room temperature until visualized using a digital slide scanner (Hammamatsu NanoZoomer). Samples were assessed for morphological signs of differentiation and cell types in one region of interest (ROI) counted in a blinded fashion (sample names were hidden while manually counting). Differentiation was qualitatively assessed according to the presence of multiple parameters of morphological differentiation in the PCIF1 shRNA transduced cells compared to the scramble shRNA transduced cells: irregular nucleus/cell shape, decreased nuclear to cytoplasmic ratio (ie. cytoplasmic area visually perceived to be increased in the knockdown samples compared to the scramble samples), cytoplasmic vesicles/granules. Cells that showed signs of apoptosis/death were not included into the group classified as "differentiation". "Differentiated" cells in one region of interest (ROI) were counted and the total number of cells in the ROI divided by the number of differentiated cells to yield a percentage of differentiation per ROI. Three ROIs (25x25uM) were evaluated for each cytospun sample. QuPath (version 0.6.0) was used for visualization and counting.

3.1.6 Immunofluorescence staining and confocal microscopy

Cells for immunofluorescence staining were prepared and spun onto microscope slides as described for Grünwald Giemsa staining. After cytocentrifugation, a hydrophobic barrier was drawn around the sample areas (Thermo Fisher, Cat No: R3777). Samples were fixed with 4% paraformaldehyde diluted in PBS for 10 minutes, washed twice in 1xPBS for 5 minutes and then permeabilized for with 0.25% Triton-X/PBS for 10 minutes at room temperature. Slides were washed three times for 5 minutes after permeabilization to ensure complete removal of detergent before blocking for 30 minutes with 5% BSA/PBS at RT. Primary antibody solutions were prepared in

1% BSA/PBS at the following dilutions: (full-length) Anti-PCIF1 antibody produced in mouse (Sigma, SAB1407847-50UG), (N-terminus) anti-PCIF1 (Atlas antibodies, HPA049517): 1:200 dilution, (internal region) PCIF1 Antibody (A-9) (Santa Cruz Biotechnology, sc-374406): 1:100 dilution. Full-length PCIF1 antibody was determined to be the most specific. Samples were incubated in primary antibody for 3 hours at room temperature or overnight at 4°C. Samples were washed thoroughly with PBS 3 times for 5 minutes each before incubation with staining mixture containing with secondary antibody , DAPI (1:1000) and phalloidin (F-actin, 1:5000) for 1 hour at room temperature in the dark. Secondary antibody solutions were prepared at 1:2000 dilutions. Samples were washed three times with PBS for 5 minutes before mounting with Prolong Gold Antifade (ThermoFisher, Cat. P36934) and left to harden overnight. Slides were stored at 4°C until visualized under a Zeiss confocal laser scanning microscope. The imaging parameters were selected by adjusting the settings to the brightest sample and using the same settings throughout one experiment. Unstained and secondary antibody solution only samples were included to assess autofluorescence or unspecific binding of secondary antibodies. A comprehensive list of antibodies and dilutions used in this work can be found in table 3.3.

3.1.7 Flow cytometry

Staining of cells for analysis of hematological differentiation markers was performed 5-12 days after selection ended. Cells in log-phase growth were harvested, spun down at $400\times g$ for 5 minutes, resuspended in PBS and transferred to a V-bottom 96-well plate. Samples were blocked using 100µL Human TruStain FcX (Fc Receptor Blocking Solution) (BioLegend, Cat No: 422302) or Human FcR block (Miltenyi, Cat No: 130-059-901) for 20 minutes at 4°C for 10 minutes and then

spun down and washed with 1xPBS. Primary antibodies were prepared in 1xPBS with Live-Dead Near-IR (Thermo Fisher, Cat No.: L34992) (1:1000 dilution). Antibodies were used at concentrations recommended by the manufacturer or titrated and prepared using the concentration with the greatest separation index of peaks [99]. A comprehensive list of antibodies and their dilutions used in this work can be found in 3.3. Cells were stained with primary antibody and LIVE/DEAD Fixable Near-IR Dead Cell Stain (Thermo Fisher, L34975) for 30 minutes at 4°C and then washed with 1xPBS. Samples that run on the Fortessa X-20 on the same day were resuspended in FACS Buffer (1xPBS Calcium and Magnesium free, 2% FBS/0.5mM-EDTA) and kept at 4°C in the dark until assayed. Samples that were not run on the same day were fixed in fixing solution (formaldehyde containing) for 30 minutes at room temperature before being resuspended in FACS Buffer and kept at 4°C in the dark until assayed.

Apoptosis and cell cycle staining was performed 7-14 days after selection ended to give cells enough time to recover from selective pressure and resume normal cycling for at least two passages. Cells assessed for apoptosis and cell cycle were taken from cultures in log-phase growth. For cell cycle analysis, 50µL Hoechst 33342 Ready Flow Reagent was added to cells in 500µL normal growth medium with for one hour in the dark at 37°C according to the manufacturer's protocol. Samples were run on a BD Fortessa X-20 on the same day.

Annexin-V FITC + 7-AAD (7-amino-actinomycin-D, Biolegend, Cat No: 420403) or PI (Propidium Iodide, Biologend, Cat No: 640914) was used to assess levels of apoptosis. 500 000 cells/mL were harvested in log-phase growth, washed with PBS and resuspended in Annexin-V Binding Buffer (BioLegend, Cat No: 422201). Cells were incubated with Annexin-V FITC (Biolegend,

Cat No: 640905) and PI or 7-AAD (1:100 or 1:200) in Annexin-V binding buffer for 20 minutes at room temperature in the dark. 200µL of Annexin-V binding buffer was added after incubation and samples were assayed within one hour. Samples were gated so that single-stained controls had <1.5% positive signal and was applied to all samples.

Flow cytometric measurements were performed on a BD LSRFortessa X-20 Cell Analyzer using the BD FACSDiva and analyzed using FlowJo. A comprehensive list of antibodies and dilutions used in this work can be found in table 3.3.

3.1.8 Methylcellulose colony forming unit (CFU) assay

Cells were prepared for methylcellulose colony forming unit (CFU) assay 15 days after selection ended according to the manufacturers protocol. Briefly, 2000 - 10000 cells (depending on the cell line) of each condition (scramble shRNA, *PCIF1* shRNA-2, and *PCIF1* shRNA-5) in complete growth medium were prepared in 200µL of complete media without antibiotics per replicate. 1.1mL MethoCult Media (type: H4535 Enriched without EPO, StemCell Technologies, Cat no.: 04535) was added to each replicate using a 2mL stripette set on low, carefully resuspended, and seeded into sterile 35mm cell culture dishes (Cat No: CLS430165). Cultures were placed in a humidified 100mm dish and incubated in a 37°C 5% CO_2 incubator for 7-14 days, until colonies became distinct enough to count. Colony morphology was assessed according to the manufacturer's guide (Technical manual, Human Colony-Forming Unit (CFU) Assays Using MethoCult, Document number 28404, v4.6.0, march 2019).

3.1.9 RNA isolation

Depending on the downstream application, cells were lysed in TRIzol Reagent (Invitrogen, 15596018) and isolated either by column extraction (for qPCR and RNA-sequencing, Zymo Direct-Zol RNA Miniprep Kit, Cat No: R2052) or by phenol-chloroform phase separation (for m6Am quantification by HPLC-(QQQ)MS, according to manufacturer's protocol for reagent 15596018) and RNA concentrations measured with Nanodrop.

RNA used for m6Am detection was isolated by phenol-chloroform phase separation as previously described [24]. 30-60 million suspension cells were harvested per replicate to achieve the yields necessary for downstream applications (minimum 100µL of $\geq$ 2µg/µL total RNA). Cells were washed in PBS and the cell pellet resuspended in Trizol reagent (Invitrogen, 15596026) and processed further or frozen at -80°C until proceeding. Chloroform (Fisher chemical, 11408123) was added to 30% of total lysate volume and spun down in a tabletop centrifuge at maximum speed at 4°C for 20 minutes. The aqueous phase was transferred into a new tube, 100% isopropanol was added in a 1:1 ratio and incubated overnight at -20°C. On the next day, the mixture was centrifuged in a table-top centrifuge at maximum speed for 15 minutes at 4°C to precipitate the RNA. The supernatant was aspirated and the RNA pellet washed twice with 70% ethanol. The RNA pellet was left to air dry for 3 minutes before being resuspended in 100µL Ultrapure DNase/RNase Free Distilled Water (Invitrogen, 10977035). RNA purity and concentration was measured by Nanodrop.

3.1.10 HPLC-QQQ sample preparation and m6Am quantification

RNA samples were prepared for high-performance liquid chromatography (HPLC) coupled with mass spectrometry (MS) according to Sendinc et al. [24]. Briefly, 250µg of total RNA were subjected to polyA+ isolation using NEB Magnetic mRNA Isolation Kit (S1550S), with 100µL of oligo d(T) magnetic beads per sample and eluted in 50µL of DNase/RNase-free water. 1µg of mRNA was de-capped with 0.5U of Cap-Clip enzyme (C-CC15011H) in 20µL reaction volume for 1-2 hours at 37°C and digested with 0.5U of nuclease P1 (NEB, M0660S) in P1 buffer in 50µL reaction at 37°C for two hours. Single nucleotides were dephorphorylated using 1U of rSAP Shrimp-alkaline phosphatase (NEB, M0371S) added to a final reaction volume of 100µL in rCutSmart buffer (NEB, B6004S) for 1 hour at 37°C.

HPLC-QQQ (High-Performance Liquid Chromatography-Triple Quadrupole Mass Spectrometry) measurement of m6Am, m6A, C, G, A and U nucleosides was performed using a 1290 Infinity UHPLC fitted with a Zorbax Eclipse plus C18 column, (1.8µm, 2.1mm 15mm; Agilent) and coupled to a 6495a Triple Quadrupole mass spectrometer (Agilent Technologies) equipped with a Jetstream ESI-AJS source. The gradient used to elute the nucleosides started by a 5-min isocratic gradient composed with 100% buffer A (10mM ammonium acetate, pH 6) and 0% buffer B (100% methanol, Merck-106035) with a flow rate of 0.400ml/min and was followed by step-wise decrease of buffer A ratio to B at the following timepoints during elution: at 8-9 min 94.4% buffer A; at 16 min 86.3% buffer A; 17-21 min 0% buffer A; 24.3-25 min 100% buffer A. The gradient was followed by a 3-min post time to re-equilibrate the column. The raw mass spectrometry data was analyzed by standard curve method of a nucleoside standards dilution series (8uM-2pM, 1:4

dilutions) using the MassHunter Quantitative Analysis Software package (Agilent Technologies, version 10.0).

3.1.11 Quantitative real-time PCR (qPCR)

500µg of total RNA was reverse transcribed using Superscript IV VILO Mastermix (Thermo Fisher, 11756050) or Maxima H Minus Reverse Transcription cDNA synthesis kit (Thermo Fisher, K1651). SYBR Select Mastermix (Applied Biosystems, Cat No: 4472908) was used according to manufacturer's recommendations for quantitative real-time PCR. 5ng cDNA template input was used for one duplicate reaction. $\Delta\Delta$CT qPCR protocols were performed on a QuantStudio 3 Real-Time PCR System (Applied Biosystems, A28567). A full list of primers used can be found in table 3.2.

3.1.12 Western Blotting

Approximately 0.5-2 million cells were harvested for protein detection by western blot and lysed with RIPA Buffer (SLS, R0278-50ML) for 20 minutes on ice. The cell lysate was then centrifuged at 13 000$\times$g for 10 minutes in a 4°C table-top centrifuge and the supernatant transferred to a new tube. Proportional loading was ensured by measuring protein concentration using the Pierce BCA Protein Assay (Thermo Scientific, 23227) or by manual counting prior to lysis. Samples were prepared for loading by adding sample buffer (Lamelli buffer + 10% β-mercaptoethanol) and incubating at 95°Cfor 10 minutes. Samples were loaded into Bio-Rad 4-20% TGX SDS-PAGE gels. The Bio-Rad Transfer Blot Turbo system was used for transferring protein onto nitrocellulose membrane. Membranes were incubated with Ponceau stain for 5 minutes to assess transfer

efficiency and protein loading distribution before being washed with 1xPBST (1xPBS/1%Triton-X) and blocked in 5% milk/PBST for 30 minutes. Membranes were transferred from blocking solution into primary antibody solution (primary antibody in blocking buffer) and incubated for at least 1 hour at room temperature or at 4°Covernight with rocking. Membranes were washed with 1xPBST 3x 5 minutes each before adding secondary antibody solution (secondary antibody in 5% milk) for one hour. Membranes were washed 1xPBST 3x 5 minutes each before being visualized using BioRad-HRP. A full list of primary and secondary antibodies and their dilutions can be found in 3.3.

3.1.13 Cloning of plasmids and gene constructs

A full list of plasmid names and guide sequences can be found 3.2. For shRNA mediated knockdown of *PCIF1*, guide sequences were taken from Broad MIT and cloned into lentiviral pLKO.1 puro vector according to protocol (a gift from Bob Weinberg [100], Addgene #8453). For generating genetic knockout cell lines, guide sequences were taken from querying ChopChop and IDT tools and cloning into LentiCRISPRv2 backbone according to protocol (a gift from Feng Zhang, Addgene #52961). Plasmids encoding full-length and catalytic mutant (APPA) PCIF1 were made previously as described [24]. All plasmids were sequenced using Azenta Genewiz sanger sequencing services or Plasmidsaurus Nanopore while plasmid sequencing services to verify accurate insert and backbone sequences.

3.1.14 mRNA sequencing and analysis

RNA was harvested for bulk-RNA sequencing as described above and samples were enriched for polyA+ RNA using NEBNext Poly(A) mRNA Magnetic Isolation Module (NEB, E7490). Library preparation was performed according to manufacturer's protocol (NEB Ultra II Directional Kit, E7760S) with NEBNext Single Index Primers. Quality and quantity of RNA as well as cDNA libraries were checked using the TapeStation 4150 system (Agilent) and sequenced using an Illumina NextSeq 2000 (P2 flow cell). Reads were processed using the nf-core pipeline and data was analysed in R studio using DESeq2. The DESeq object was constructed from raw counts with filtering (rowSums >= 10) and effect size shrinkage (lFCshrink = apeglm [101]) applied. Differential gene expression was defined at absolute log2-fold change > 0.75 and adjusted p-value < 0.05.

For differential transcript detection, raw transcript count files were analyzed analogously to create DESeq2 objects using Transcript IDs instead of Gene IDs. For TSS annotation, (protein coding) transcript sequences of differentially regulated genes were downloaded from the ensembl biomart and matched to the transcript identifier from the DESeq2 results object. Transcription start nucleotides were extracted from the TSS sequence start site annotation from BioMart downloads.

For gene ontology analysis, significant up-/downregulated DEGs were queried using GO:Profiler in R using gprofiler2 (version 0.2.3) [102]. Gene set enrichment analysis was performed in R using the msigdbr package (version 25.1.1) and human Hallmark gene sets.

3.1.15 Quantification of PCIF1 expression and patient survival in public datasets

Cell line PCIF1 expression data was downloaded from HPA (Human Protein Atlas) or the DepMap (The Cancer Dependecy Map) Portal. Beat-AML (2.0) trial data was downloaded from vizome.org. TCGA (The Cancer Genome Atlas) + GTEx (Genotype-Tissue Expression) data was visualized and plots dowloaded using the GEPIA2 web tool. TCGA-LAML and TARGET-AML (Therapeutically Applicable Research to Generate Effective Treatments) data was visualized using UCSC (University of Santa Cruz) Xena platform (which allowed for visualization of multiple Pan-Cancer studies) and data downloaded from the same platform for further analysis. Further analysis included Kaplan-Meier survival plotting and prognosis interpretations in R using survminer. Normal (non-cancerous) samples used for comparison were different in each study: HPA - non-malignant lymphoma origin, GEPIA2 TCGA - matched patient normal tissue for certain cancer types and GTEx tissue samples (not matched to TCGA). The GTEx normal tissue origin used to match to TCGA AML patient data was whole blood. Cutoff of gene expression into high/low was determined by optimal cutoff using survcutpoint in R [103].

3.1.16 Statistical analysis and replicates

Statistical analysis was performed in Graphpad Prism (version 10.6.1) or R using the rstatix package (version 0.7.2). Statistical tests and correction for multiple testing used are detailed in the figure captions and appendix. The experimental work comprised in this thesis was generated exclusively using human immortalized cancer cell lines, aliquots of which were generously gifted by labs in the Old Road Campus Research Building. In attempt to control for issues connected

to long-term culture of cell lines (genetic drift, genome instability, changes in signaling), multiple aliquots from early cultures were made and subsequently thawed each time a new round of infection was set up. The term biological replicate in this thesis is thus used to describe samples of cells that were thawed from different aliquots and infected with different preparations of lentivirus and at different time points.

Table 3.1. R packages used

Package	**Version**	**Package**	**Version**
R	4.3.2	apeglm	1.22.1
BiocManager	1.30.26	biomaRt	2.56.1
clusterProfiler	4.8.3	ComplexHeatmap	2.16.0
DESeq2	1.40.2	dbplyr	2.3.3
EnhancedVolcano	1.18.0	enrichplot	1.20.3
fgsea	1.26.0	forcats	1.0.0
ggplot2	3.5.2	ggpubr	0.6.0
ggrepel	0.9.3	gprofiler2	0.2.3
msigdbr	25.1.1	org.Hs.eg.db	3.17.0
survminer	0.4.9	patchwork	1.3.1
pheatmap	1.0.13	readxl	1.4.5
rstatix	0.7.2	tidyverse	2.0.0
tidyr	1.3.0	UpSetR	1.4.0
VennDiagram	1.7.3	writexl	1.5.4

3.2 Materials

Table 3.2. List of primers, guide oligos, and siRNAs used in this work

Target	Sequence	Source
Guides		
NT scramble shRNA	CCTAAGGTTAAGTCGCCCTCGC	[104]
PCIF1 shRNA 1	GCAAGGTGGTAGACAAAGGAT	TRCN0000156865
PCIF1 shRNA 2	CGATGTGATTTCGGACCCTTT	TRCN0000157332
PCIF1 shRNA 3	CATCCAGACCAATGCTGTCAT	TRCN0000158063
PCIF1 shRNA 4	CGTGGTCTGCATCCGGTATAA	TRCN0000276215
PCIF1 shRNA 5	ACGACATTCCTATCAGGTTAT	TRCN0000276251
PCIF1 shRNA 6	ATATGAAGATTATGGTTCTGC	TRCN0000276216
sg non-targeting	ATCGTTTCCGCTTAACGGCG	Sendinc et al. [24]
sg *PCIF1* AA	CCACGGGAGTCTTTCAACCG	IDT
sg *PCIF1* AB	GTGCTAGTCTGGACTGCTGG	IDT
sg *PCIF1* N25	GAGATGGCCAATGAGAATCA	ChopChop [105]
sg *PCIF1* N33	TCCCTGCTGAGTCACTCCCC	ChopChop [105]
sg *PCIF1* F3	ATTCACCAACCAGTCCCTGT	Sendinc et al. [24]
Primers		
beta-actin	fwd: CACCATTGGCAATGAGCGGTTC rev: AGGTCTTTGCGGATGTCCACGT	Origene/IDT
qPCR *PCIF1*	fwd:CTCCGGGCAGCTGCTGAT rev:AAGGAAAGGCCTGCAGGAAG	Sendinc et al. [24]
qPCR CD11b	fwd:GGAACGCCATTGTCTGCTTTCG rev:ATGCTGAGGTCATCCTGGCAGA	Origene/IDT
qPCR HLA-DRA	fwd:AGCTGTGGACAAAGCCAACCTG rev:CTCTCAGTTCCACAGGGCTGTT	Origene/IDT
qPCR CD14	fwd:CTGGAACAGGTGCCTAAAGGAC rev: GTCCAGTGTCAGGTTATCCACC	Origene/IDT
qPCR CD86	fwd:CCATCAGCTTGTCTGTTTCATTCC rev:GCTGTAATCCAAGGAATGTGGTC	Origene/IDT
qPCR CD80	fwd:CTCTTGGTGCTGGCTGGTCTTT rev:GCCAGTAGATGCGAGTTTGTGC	Origene/IDT
qPCR CD163	fwd:CCAGAAGGAACTTGTAGCCACAG rev:CAGGCACCAAGCGTTTTGAGCT	Origene/IDT
qPCR TGF-b	fwd:TACCTGAACCCGTGTTGCTCTC rev:GTTGCTGAGGTATCGCCAGGAA	Origene/IDT
qPCR FADS1	fwd:CTGTCGGTCTTCAGCACCTCAA rev:CTGGGTCTTTGCGGAAGCAGTT	Origene/IDT
qPCR FADS2	fwd:TGCAACGTGGAGCAGTCCTTCT rev:GGCACATAGAGACTTCACCAGC	Origene/IDT
qPCR ELOVL6	fwd:CCAGAGCACTAATGGCTTCCTC rev:CCAGAGCACTAATGGCTTCCTC	Origene/IDT
Plasmids		
pKLO.1		Addgene #8453
pLentiCRISPRv2		Addgene #52961

abbrv. TRC = The RNAi Consortium

Table 3.3. List of antibodies used in this work

Antibody	Source	Identifier
Flow cytometry		
7-AAD Viability Staining Solution	Biolegend	420404
FITC Annexin-V	Biolgened	640906
BV421 Mouse Anti-Human CD54	BD Biosciences	566262
BV421 Mouse Anti-Human CD33	BD Biosciences	560956
BUV395 Mouse Anti-Human CD274	BD Biosciences	740320
APC Mouse Anti-Human CD86	BD Biosciences	560956
PE anti-mouse/human CD11b	Biolegend (clone M1/70)	101208
Western Blotting		
CAPAM/PCIF1 (E8B1B) Rb mAb	Cell Signaling Technology	59921
Cas9 (7A9-3A3) Ms mAb	Cell Signaling Technology	14697S
Confocal Microscopy		
Anti-PCIF1 antibody produced in mouse	Sigma-Aldrich Technology	SAB1407847-50UG
Anti-PCIF1, Rabbit 100ul	SLS	HPA049517
PCIF1 (A-9), Monoclonal Antibody, 200ug/ml	Santa Cruz Biotechnology	sc-374406
ANTI-PCIF1	SLS	HPA049517-100UL

Rb = Rabbit, Ms = Mouse, mAb = monoclonal antibody, pAb = polyclonal antibody

Table 3.4. List of small molecules and chemotherapeutics

Reagent	Source	Identifier
Small Molecules and Chemotherapeutics		
Quizartinib	MedchemExpress	HY-13001
Midostaurin	MedchemExpress	HY-10230
Azacitidine	MedchemExpress	HY-10586
Venetoclax	MedchemExpress	HY-15531
Sorafenib	MedchemExpress	HY-10201
FADS1/2 inhibitor CP-24879	MedchemExpress	HY-115319
FADS2 inhibitor SC-26196	MedchemExpress	HY-107410

4 | Results

PCIF1 is an mRNA cap-adjacent methyltransferase with uncertain molecular mechanisms on transcription, mRNA stability and translation and has been reported to have oncogenic as well as tumor-suppressive roles in different cancer types. While the number of studies on PCIF1 remain limited since the characterization of its catalytic activity (53 results from 2019-2025, PubMed), research output investigating this protein is increasing. In a pan-cancer analysis of PCIF1, Jin and colleagues noted that *PCIF1* gene is upregulated in most tumor types compared to normal tissue, but had low tissue and lineage specificity and significant expression variance within one cancer, indicating that PCIF1 may be differentially expressed in across prognoses and subtypes within one cancer type or non-metastatic/metastatic samples, as suggested to be the case in colorectal carcinoma (CRC) by Relier and colleagues [56, 106]. Given the complex and context-dependent relationship between PCIF1 expression and patient survival in cancer, comprehensive analysis of public data from different sources across different patient subgroups of a specific disease is vital. Chapter 4.1 focuses on insights gained from analyzing *PCIF1* expression in cell lines and tissue as well as overall survival from pan-cancer as well as AML-specific studies. Chapter 4.2 investigates the phenotype triggered by PCIF1 protein depletion in AML cell lines and Chapter 4.3 follows up on the transcriptomic landscape and possible mechanisms by which the phenotype may be elicited.

4.1 Exploring *PCIF1* gene expression in human tissue, cell lines and cancer

PCIF1 gene expression in public data sets was queried to get a better impression of transcript and protein levels across different tissue types, cell line lineages and disease (HPA - Human Protein Atlas, GTEx - The Genotype Tissue Expression Portal, DepMap Portal - Cancer Dependency Map). Various pan-cancer projects (TCGA - The Cancer Genome Atlas, TARGET - Therapeutically Applicable Research to Generate Effective Treatments) as well as AML-specific trials (Beat-AML) were used to analyze *PCIF1* expression and survival in patients across AML subtypes, prognoses and history of dysplasia.

4.1.1 *PCIF1* expression in human tissues and gene/cancer essentiality scores

Analysis of *PCIF1* gene expression in human tissue showed that *PCIF1* is expressed in across all 50 tissue types queried in transcriptomic studies by HPA and GTEx (Figure 4.1A). Cerebellum, ovary and skeletal muscle tissue scored the highest, while other female reproductive tissues, as well as skin and bone marrow, scored among the top 10 highest expressing tissue types. Transcriptomic analysis of 1192 different cell lines recorded in the HPA revealed that median *PCIF1* mRNA levels were higher in all cancer cell lines compared to non-cancerous cell lines (n=63), especially in leukemia (n=93) and lymphoma (n=76) cell lines (Figure 4.1B).

PCIF1 expression data was also queried in datasets from the DepMap initiative (release: DepMap Public 25Q3), which contains RNA sequencing from 1699 different cell lines. The DepMap project provides data on transcript abundance, copy number, and mutation status of a certain gene

for cell lines across 32 different primary sites (Oncotree Lineage). Additionally, the data also includes gene essentiality scores, which are based on genome-wide CRISPR/Cas9 fitness (proliferation) screens to identify and catalog cancer vulnerabilities [107]. PCIF1 transcript and protein expression was plotted for each lineage or cancer subtype which contained n>3 cell line data points (Figure 4.1C-E, appendix A.1). *PCIF1* mRNA expression was the highest in T- and B-cell acute lymphoblastic leukemia (T-/B-ALL), as well as lung neuroendocrine tumor cell lines, and lowest in cutaneous squamous cell carcinoma and cell lines from non-cancerous origins. AML cell lines ranked 14th highest in a list of 57 cancer types (Figure 4.1C). Analogously to HPA datasets, DepMap *PCIF1* transcript expression was higher in cancer cell lines of cancerous compared to non-cancerous origin.

Transcript levels used to infer gene expression should ideally be supplemented with protein quantification, given that mRNA abundance may not always be exactly proportional to protein expression. The DepMap Portal also provided proteomics data for some of the cell lines in the RNA-seq datasets, which revealed the highest median PCIF1 expression in AML cancer cell lines (Harmonized Public Proteomics 24Q4) (Figure 4.1D). To summarize, transcript and protein expression data from HPA and DepMap show that PCIF1 is highly expressed in cancer cell lines, especially in cells from the myeloid lineage (appendix A.1 and AML cell lines compared to other lineages and cancer types.

The DepMap Consortium also provides data from CRISPR knockout screens to assess the (cancer) essentiality of a gene in specific cell line. A negative Chronos score is interpreted as negative selection of a specific sgRNA (in this case PCIF1), indicating a dropout of the sgRNA from the

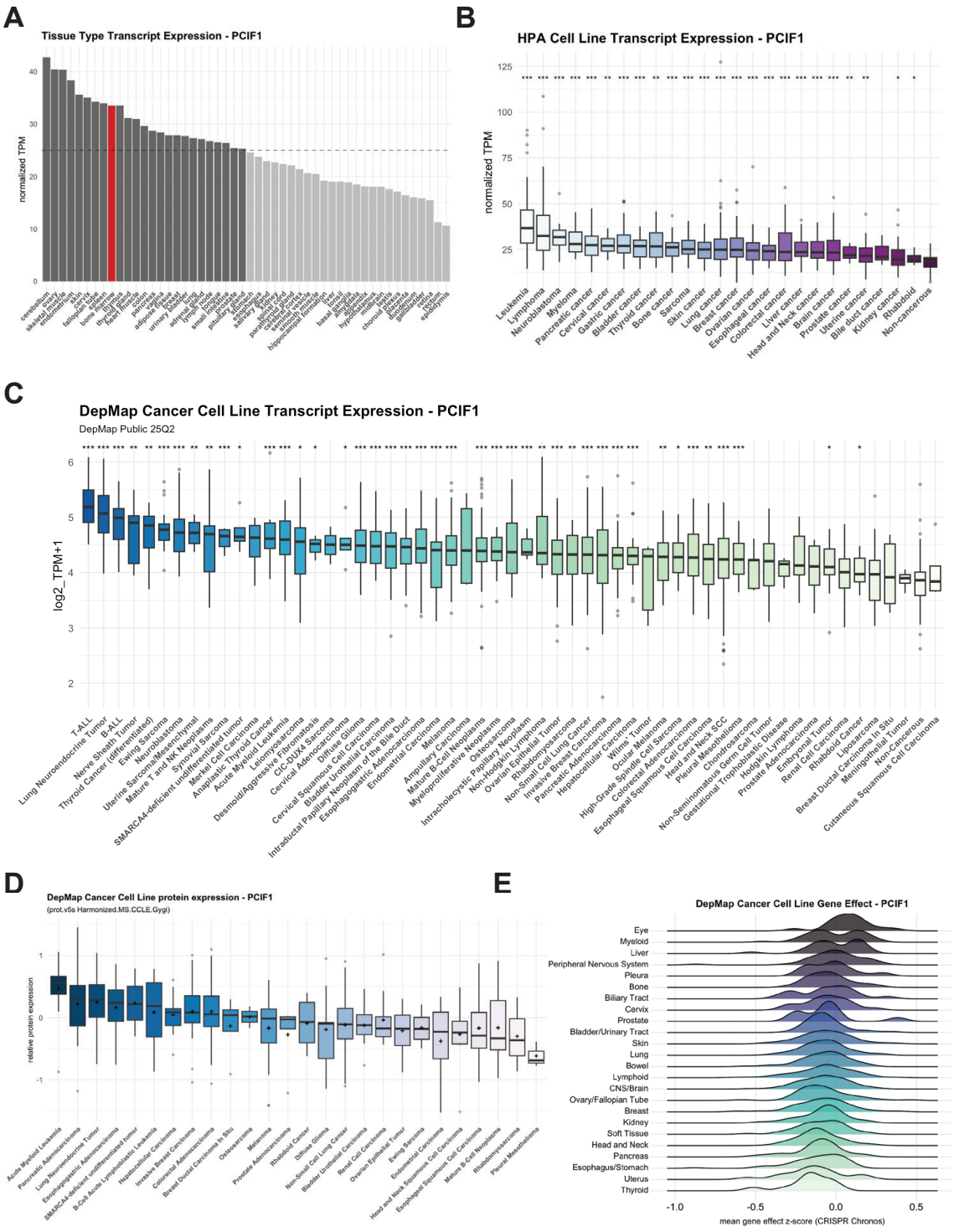

Figure 4.1. PCIF1 expression and sensitivity across tissues and cell lines. **A.** *PCIF1* transcripts per million (TPM) in human tissue types from HPA. Data downloaded from HPA-RNA expression (consensus).

Figure 4.1. (continued) **B.** *PCIF1* transcript expression in 1192/1206 human cell lines downloaded from The Human Protein Atlas (version 24.0). Boxplots represent IQR and median expression in cell lines from a specific cancer type or non-cancerous cell lines, outliers depicted in grey. **C.** *PCIF1* median (IQR) transcript and **D.** protein expression across cancer cell lines. **E.** *PCIF1* gene effect (essentiality for fitness) in cancer cell line lineages. Z-score of -1.0 is considered common essential. All statistical tests: two-tailed t-test comparing means of PCIF1 expression in cancer vs non-cancerous (*P < 0.05; **P < 0.01; ***P < 0.001). Values and multiple testing correction (FDR) see appendix A.1.

infected pool [108, 109, 107]. A pan-essential gene would therefore map at -1.0, while a non-essential gene at 0.0. To predict possible gene effects of PCIF1, CRISPR gene effect scores were mapped as a density distribution between -1.0 and +0.5 and showed that *PCIF1* is generally non-essential across cell line lineages. Gene effect and protein expression was compared in myeloid and lymphoid lineage subgroups, revealing no association between *PCIF1* expression and gene dependency in different blood lineages (appendix A.1).

In summary, PCIF1 is significantly upregulated in many cancer cell lines on the transcript level compared to cell lines of non-cancerous origin, but did not show specific cancer essentiality for any cell line according to DepMap. Unfortunately, not all cell lines queried by the DepMap Consortium with RNA-seq were included for proteomic analysis. AML cell line *PCIF1* mRNA expression ranked in the top 25% of primary diseases, and it was the highest expressing primary disease on the protein level. While categorizing leukemia cell lines into their tissue of origin showed that cell lines of the lymphoid lineage scored lower for *PCIF1* expression than leukemia cell lines of the myeloid lineages A.1, categorizing cell lines more specifically into their primary diseases revealed that T- and B-cell Lymphoblastic Leukemia *PCIF1* expression was the highest whereas Hodgkin lymphoma was in the bottom 10 based on transcript expression, revealing a more pronounced difference in *PCIF1* expression between cancer subtypes of lymphoid origins compared to myeloid origins.

4.1.2 *PCIF1* TCGA pan-cancer expression

Considering that in vitro models posses limited physiological relevance compared to clinical data, *PCIF1* expression was additionally assessed in patient samples from TCGA, Beat-AML and TARGET-AML trials. TCGA data was queried using the GEPIA2 webtool, Beat-AML data was accessed through the vizome portal and queried in RStudio, and TARGET-AML data was downloaded from the UCSC Xena browser and queried in RStudio. Kaplan-Meier survival plots were generated using the survminer [110, 111, 112, 103].

The Cancer Genome Atlas (TCGA) Research Network is a collective initiative to analyze different cancer and normal tissues across 33 different tumor types [79, 113]. TCGA efforts also included matching primary tumor biopsies with healthy tissue samples, although not all cancer types had patient matched tissue (eg. AML). In the case of AML, leukemic expression was compared to non-matched whole blood samples from healthy donors as part of the GTEx study in the GEPIA2 workflow. Figure 4.2A shows *PCIF1* expression in tumor (red) and normal (green) matched tissue across all TCGA matched cancer types. Comparing *PCIF1* expression in between TCGA tumor and TCGA normal matched + GTEx revealed that *PCIF1* was significantly upregulated in Cholangio carcinoma (CHOL), Pancreatic adenocarcinoma (PAAD), and Thymoma (THYM) (Figure 4.2B). Interestingly, while a study shows that *PCIF1* is upregulated in tumors of HNSC patients and is oncogenic in mechanistic studies, TCGA data from GEPIA2 does not replicate this effect [61]. The upregulation in AML patient samples was also not significant compared to GTEx normal whole blood samples. Conversely, Uterine Corpus Endothelial Carcinoma (UCEC) samples downregulated PCIF1, underscoring that *PCIF1* oncogenic and tumor-suppressive effects are

likely context dependent.

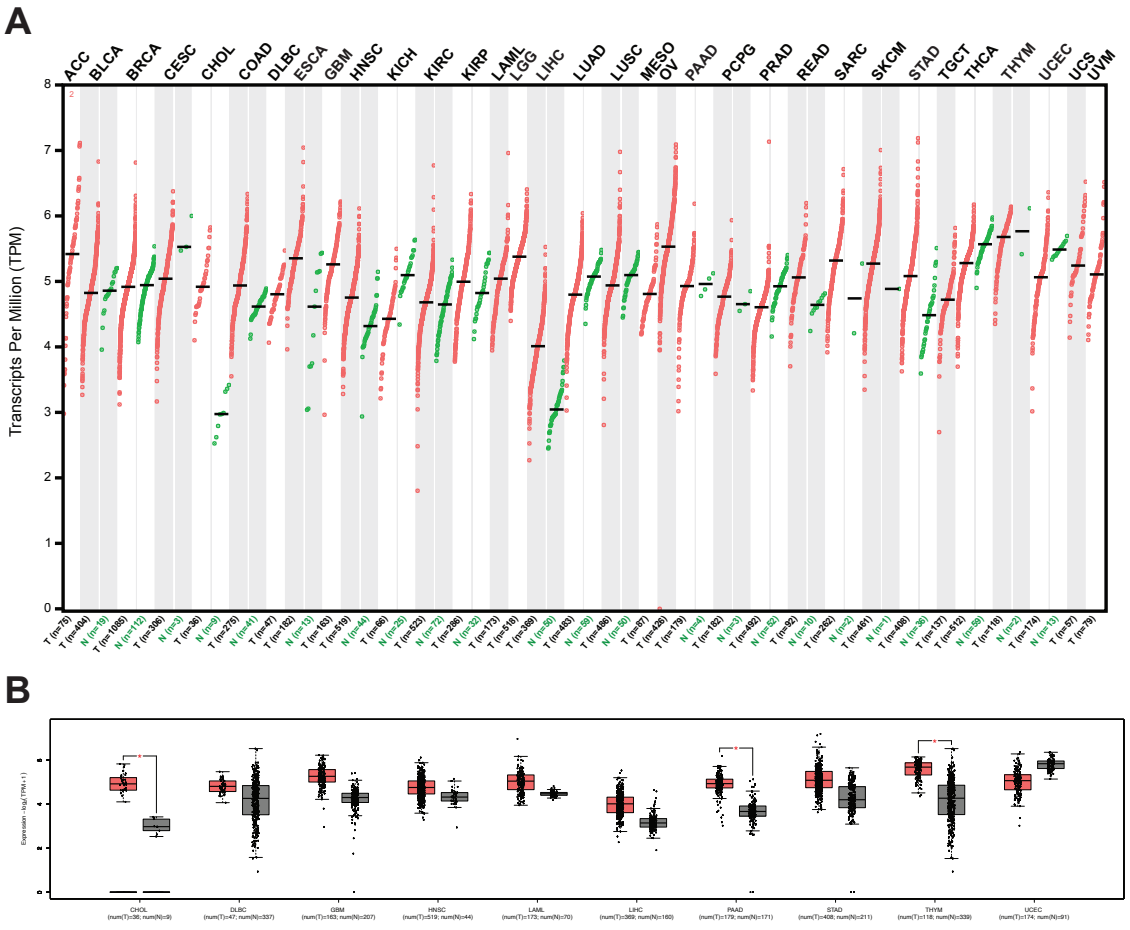

Figure 4.2. Pan-cancer expression of *PCIF1* queried in GEPIA2. **A.** PCIF1 transcripts per million in TCGA patients tumor (red) and normal tissue (green). Not all cancers have matched normal TCGA tissue, see appendix A.4 for TCGA+GTEx normal. **B.** *PCIF1* transcripts per million in TCGA patients comparing tumor tissue (red) with GTEx and normal tissue (grey). Cancers that did not have matched normal tissue in **A.** were matched with normal tissues from the GTEx study. Boxplots show IQR of *PCIF1* log(TPM+1) mRNA expression for cancer types that are significant and/or in which *PCIF1* has a reported oncogenic or tumor suppressive effect. significance: |Log2FC| > 1, pvalue < 0.05

4.1.3 *PCIF1* expression and patient survival in the Beat-AML trial

As described in 1.2, leukemia is a highly heterogeneous disease that can be characterized by various gene rearrangements and blast percentage, allowing for a more refined investigation of specific leukemic subtypes based on driver mutation, prognosis and prior myelodysplastic / myeloprolif-

erative disease states. The Oregon Health and Science University (OHSU) Beat-AML cohort contains detailed clinical annotation, DNA and RNA sequencing, as well as *ex vivo* drug sensitivity testing of 805 patients and is provided as a comprehensive platform accessible for download via vizome.org [111, 114]. For survival analysis of patients within the Beat-AML trial, *PCIF1* (mRNA) expression was stratified into high and low using survminer::survcutpoint, which created an optimal cutpoint using the density distribution of gene expression across samples [103]. Visualizing survival of all patients in the Beat-AML trial regardless of subtype and categorizing them into *PCIF1* high and *PCIF1* low showed no significant difference between expression and survival (appendix A.5C-D), so further sub-grouping into disease specific attributes was performed to determine whether PCIF1 may have a subtype specific effect.

PCIF1 expression was plotted across AML subtypes to analyze whether *PCIF1* transcript levels were associated with a specific driver mutation. Average *PCIF1* transcript expression was significantly upregulated in *CEBPA* (C/EBPα) mutated AML patients compared to bone marrow mononuclear cells (BM MNC) from healthy donors (Figure 4.3A). The higher cancer transcript expression was also accompanied by a lower survival probability in *PCIF1*-high + *CEBPA*-mut compared to *PCIF1*-low + *CEBPA*mut AML patients (n=25, high: n=11, low: n=14, logrank p = 0.026 (**)) (Figure 4.3B). While *PCIF1* was not significantly differentially expressed in *NPM1* mutant AML compared to healthy BM MNC, *PCIF1*-high + *NPM1*-mut leukemia patients had a worse prognosis than *PCIF1*-low + *NPM1*-mut patients (n=94, high:n=28, low:n=66, logrank p=0.04). *FLT3*-ITD (internal tandem duplication) status was recorded in the dataset for every patient and *FLT3*-ITD+/*PCIF1* high showed negative survival trend, however was not significant (Figure 4.3B (bottom)). *KMT2A* rearranged (*KMT2A*-r), *RUNX1-RUNX1T1*, and *PML-RARA*

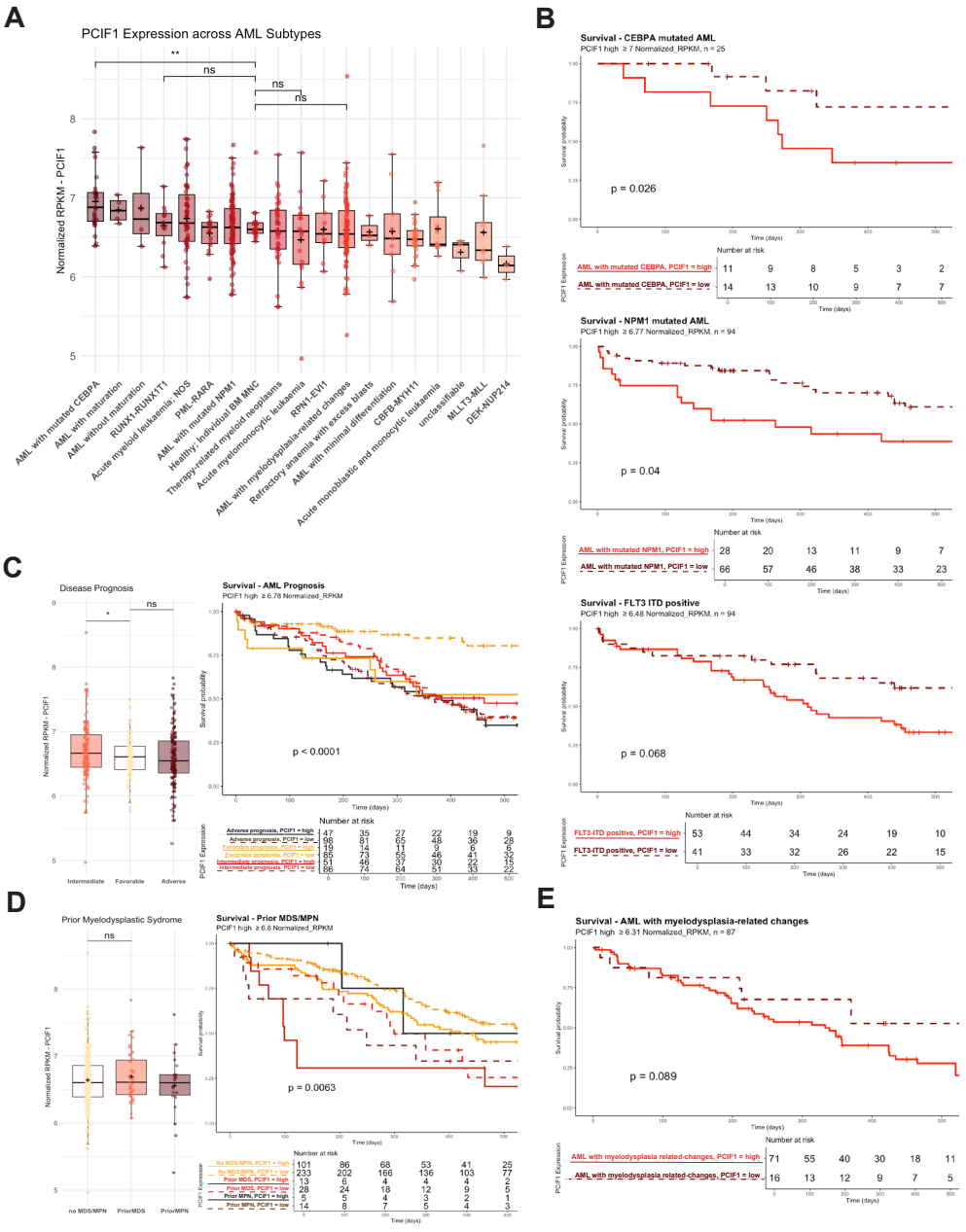

Figure 4.3. *PCIF1* expression and patient survival in the Beat-AML trial. **A.** *PCIF1* transcript expression across AML subtypes. Boxplots depict IQR with median, mean as "+". Subtypes filtered for n>2 (see appendix A.5 for all subtypes). **B.** Survival of high vs low *PCIF1* expression in patients with CEBPA mutated AML (top), NPM1 mutated AML (middle), FLT3 ITD positive mutant AML (bottom). **C.** *PCIF1* expression (left) and survival (right) of *PCIF1* high/low in patients across disease prognosis. **D.** *PCIF1* expression (left) and survival (right) in patients with/without a history of MDS or MPN prior to AML diagnosis. **E.** Survival of AML patients of *PCIF1* high/low in MDS subtype. *PCIF1* low = dashed, *PCIF1* high = full. Statistics expression: two-tailed unpaired t-test. Statistics survival: Log-Rank Statistic. *P < 0.05; **P < 0.01; ***P < 0.001. p-values in plots represent p-statistic for all groups, corrected for multiple testing in the appendix (see A). Optimal expression cutoff determined using (R)survminer::survcutpoint().

leukemic subtypes were also analyzed, but showed no significant correlation and low patient subgroups. Thus, *CEBPA*- and *NPM1*-mutant subtypes with high *PCIF1* expression have worse prognosis, which signify a subtype that would be worth targeting for future therapeutic approaches with *PCIF1*.

PCIF1 expression and patient survival was also assessed in prognostic risk groups (favorable, intermediate, adverse), which are determined by factors such as aforementioned cytogenetic abnormalities, but also by age, blast percentage, and prior dysplasia-related disease [81, 82, 77]. Low or favorable prognostic risk is associated with AMLs carrying chromosomal translocation t8;21 (RUNX1:RUNX1T1), inv16, and t15;17 (APL), while genetic mutations in FLT3, TP53, EZH2 and others, as well as patients aged >60 years are usually associated with higher risk and intermediate to adverse prognosis [115]. Median *PCIF1* expression was higher in patients with intermediate prognosis, and elevated *PCIF1* correlated with lower patient survival in the favorable prognosis group, but intermediate and adverse prognosis patient groups did not show a significant difference in patient survival between high and low expression groups. Average *PCIF1* expression did not differ between patients with and without prior myelodysplastic syndrome (MDS) or myeloproliferative neoplasms (MPN), although the survival trend indicated that *PCIF1* high cohorts with prior MDS exhibited lower survival probability (Figure 4.3D and E). Overall, investigating possible gene effects at subtype level may yield better context dependent insights into PCIF1 significance for AML, although larger patient group sizes would be necessary to draw significant conclusions.

4.1.4 *PCIF1* in TARGET vs TCGA pan-cancer patient cohorts

Another pan-cancer visualization of *PCIF1* using the University of California Santa Cruz' Xenabrowser [116] revealed the overexpression of *PCIF1* in the induction-failure substudy of the TARGET-AML patient trials 4.4A. TARGET-AML-Induction Failure (IF) delineates a group of patients that were refractory to treatment and unable to enter a state of remission after standard two rounds of induction chemotherapy, measured by the presence of >15% myeloblasts [117]. Patients exhibiting primary induction failure are generally confronted with poor prognosis and very few treatment options, the only curative option being allogenic hematopoetic stem cell transplantation (allo-HSCT) [84]. Survival of the AML-IF patient cohort was plotted against the survival of patients that achieved remission after standard therapy (Figure 4.4B). Optimal cutoff of *PCIF1* expression stratified all AML-IF patients into the high group (Figure 4.4C), which resulted in only three patient subgroups (AML with *PCIF1* high, AML with *PCIF1* low, and AML-IF with *PCIF1* high (all AML-IF)). Patients of the AML-IF cohort had worse survival than the AML patients, however whether the upregulated expression of *PCIF1* is the determining factor contributing to this effect could not be able to be determined from just this data (appendix A.6).

PCIF1 expression across pan-cancer TCGA and TARGET groups showed that TCGA-AML was generally not enriched for *PCIF1* expression, while the leukemias of the TARGET studies all showed higher *PCIF1* expression (Figure 4.4A). The TARGET trials focus on untreated, primary childhood tumors [117, 118]. This distribution suggests that *PCIF1* is upregulated in pediatric leukemia patients and may exhibit *PCIF1* dependent sensitivities not otherwise observed in adult AML.

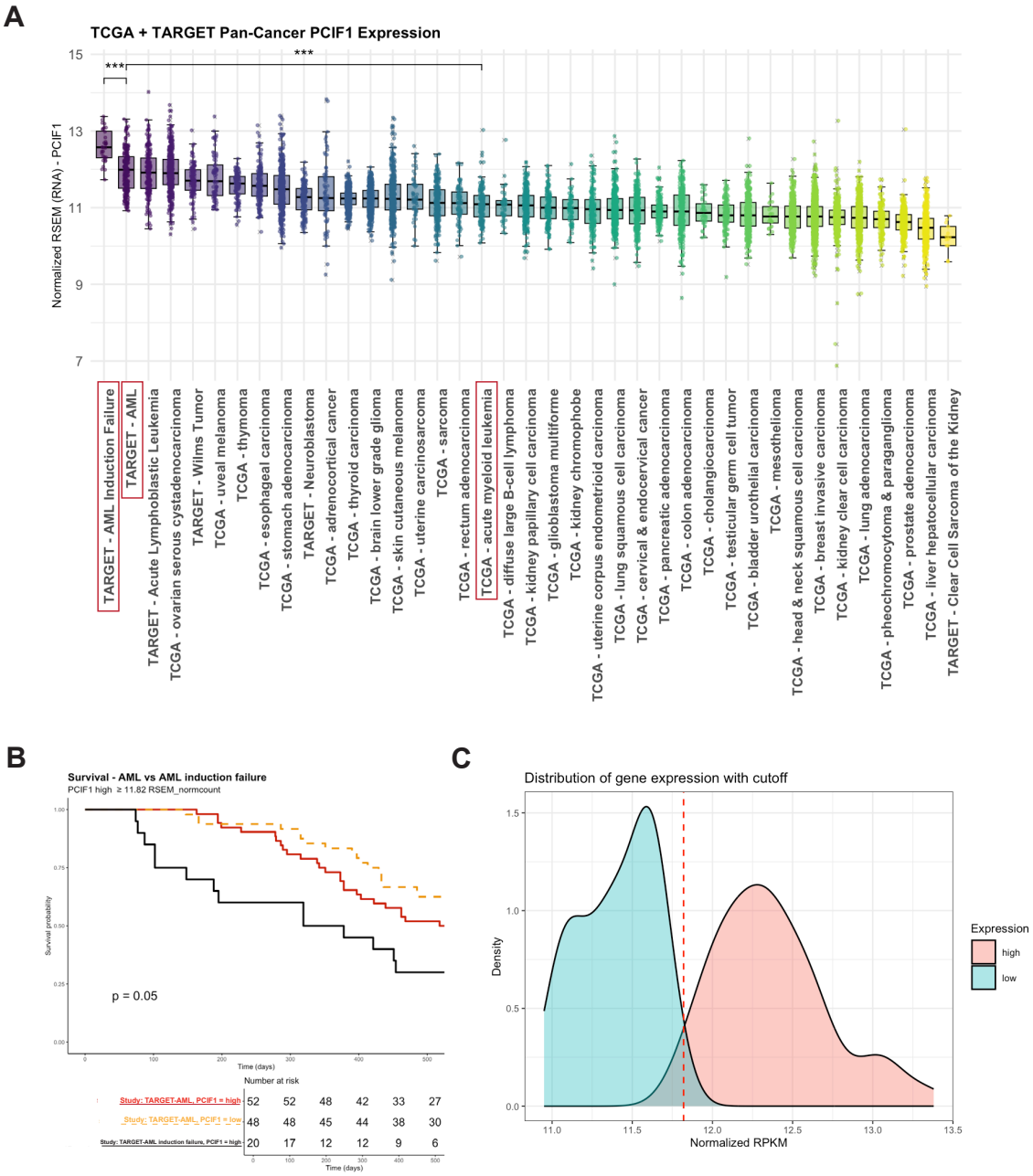

Figure 4.4. *PCIF1* expression and patient survival across TARGET and TCGA cancer tissues. **A.** *PCIF1* transcript expression across all TCGA and TARGET cancer tissues. Boxplots depict IQR with median, filtered for n>2. **B.** Comparing the survival of patients with *PCIF1* high/low in TARGET AML vs TARGET AML Induction Failure (IF) subproject. p-value denotes significance value of all curves. **C.** Distribution of *PCIF1* expression in patients from the TARGET AML vs TARGET AML Induction Failure (IF) subproject. *PCIF1* low = dashed, *PCIF1* high = full. Statistics expression: two-tailed unpaired t-test. Statistics survival: Log-Rank Statistic. *P < 0.05; **P < 0.01; ***P < 0.001. Optimal expression cutoff determined using (R)survminer::survcutpoint().

The aspect of gene up- or downregulation in tumor vs normal tissue commonly forms the foundation and rationale behind further investigation into disease implications in many cancer studies. This data can vary greatly depending on cohorts used, possible statistical transformations and normalizations applied, as well as tissues of origin of the matched normal tissue, as mirrored by data from various studies in this chapter. Overall, this data shows that TCGA AML compared to GTEx whole blood samples shows an upregulation in *PCIF1* expression. Further, *PCIF1* overexpression correlates with worse patient survival in *CEBPA*- and *NPM1*-mutant leukemia and may be more influential in pediatric leukemia (TARGET dataset) compared to non-pediatric leukemia (TCGA-AML).

An impact of PCIF1 protein has been described in various cancers, including studies in gastric cancer (GC) [59], head and neck squamous cell carcinoma (HNSCC) [61], colorectal cancer (CRC) [60], CD8+ T-cells [67], and glioblastoma (GBM) [26], and there is little doubt that more studies in other cancers are currently in progress or already under review. A number of the publications describing PCIF1 in cancer build their rationale for investigating PCIF1 in differential expression seen in public data from cancer studies, certain articles specifically citing pan-cancer studies used in this chapter (see GEPIA2) [59, 65, 76]. HNSCC and KIRC do not show clear significance of upregulated *PCIF1* expression in GEPIA2 TCGA data, similar to AML, although further experiments in published research robustly show that there is an effect.

Therefore, public patient expression data can be helpful for guiding initial investigation, however further targeted experiments should always be performed to decide on a gene's cancer relevance. As PCIF1 has thus far not been investigated in the context of AML and further experimental

follow-up is warranted to elucidate this protein's potential contribution to leukemogenesis.

4.2 The effect of PCIF1 depletion on AML cell lines

This chapter describes and characterizes the phenotypic effect observed in acute myeloid leukemia cell lines upon depletion of PCIF1. Before establishing the phenotype, the first subchapters give a brief overview of cell lines used for this project, as well as describe different protein depletion strategies that were trialed and optimized. The remainder of the chapter is structured into subchapters describing the effects of PCIF1 depletion on proliferation, differentiation, and altered sensitivity to chemotherapeutic agents.

4.2.1 Background and aims

Targeted genetic silencing has become an integral approach to studying the function of a protein in fundamental biology. The use of RNA interference as a method for ablating gene function came about in the late twentieth century when Napoli, Lemieux and Jorgensen first documented their observation observation that genetic introduction of a transgene into petunia flowers resulted in a decrease of the endogenous gene and loss of petal pigmentation [119, 120]. Previously, targeted loss of function studies were performed by incorporation of a DNA fragment carrying the desired mutation into the host genome via homologous recombination and gene substitution events [121]. Later discoveries and a more thorough understanding of genetics enabled the spread of RNA interference methods, such as small-interfering RNAs (siRNAs) and short-hairpin RNAs (shRNAs). The first truly targeted genome editors were introduced at the end of the 20th century and were based on zinc-finger nucleases (ZFN) and non-homologous repair of double-strand breaks (DSB) [122, 123].

Methods trialed for targeted protein depletion in this project include siRNA, dTAG, shRNA and CRISPR/ Cas9. Ultimately, shRNA and CRISPR/Cas9 were used in experiments that generated results for this thesis. A brief part of subchapter 4.2.3 will outline the different methodologies tested and show why protein knockdown using shRNA proved to be the superior choice above complete knockout for a PCIF1 depletion model. Subsequent subchapters aim to answer whether the depletion of PCIF1 impacts acute myeloid leukemia biology in vitro by investigating AML cell proliferation, differentiation and sensitivity to different cytotoxic agents.

4.2.2 Selection of AML cell lines used for protein depletion studies

A panel of AML cell lines that represented different AML subtypes and had been reported in literature were selected as models to assess the impact of PCIF1 depletion. Table 4.1 gives an overview of AML cell lines used in this work, according to World Health Organization (WHO) and International Consensus Classification (ICC) classification.

Table 4.1. Overview of AML cell lines used for experiments

Cell line	**Driver mutation**	**Add. mutations / p53 status**	**Status**
MOLM-13	KMT2A::MLLT3, *FLT3*-ITD	*CDKN2A* LoF, *MTAP* LoF, p53 WT	Relapse
SKNO-1	t(8;21)(q22;q22.1)/ *RUNX1::RUNX1T1*	c-KIT GoF, p53 LoF	2nd relapse
THP-1	*KMT2A::MLLT3*	*CDKN2A* LoF, *MTAP* LoF, *NRAS* GoF, p53 LoF	ns
U937	*CALM::AF10*	*PTEN* LoF, p53 LoF	N/A
Kasumi-1	t(8;21)(q22;q22.1)/ *RUNX1::RUNX1T1*	c-KIT GoF, p53 LoF	Relapse
NOMO-1	*KMT2A::MLLT3*	*CDKN2A* LoF, *MTAP* LoF, *KRAS* GoF, p53 LoF	Relapse

Abbreviations: WT = wild type; GoF = gain of function (mutation); LoF = loss of function (mutation); ITD = internal tandem duplication; ns = not specified, N/A = not applicable. Gene fusions shown using "::"

The MOLM-13 cell line belongs to the *KMT2A* rearranged (specifically *MLLT3::KMT2A*, also known as MLL-AF9, or t(9;11)) category of leukemia cell lines and was established from the peripheral blood of a 20-year old male patient, who relapsed with AML after an initial myelodysplastic syndrome (MDS) with trisomy 8 diagnosis and treatment with granulocyte colony-stimulating factor (G-CSF) [124, 91]. The cell line also carries an internal tandem duplication (ITD) mutation in the fms-like tyrosine kinase (FLT3) receptor, which is reported to promote aberrant proliferation in AML [91].

SKNO-1 cells have a *RUNX1::RUNX1T1* fusion (also known as AML1-ETO, translocation t(8;21)) and were harvested from the bone marrow of a 22-year old male patient in second relapse after remission following combination chemotherapy with cytarabine (Ara-C), mitoxantrone, 6-mercaptopurine (6-MP) and prednisolone (PSL) with high-dose Ara-C consolidation therapy, which was preceded by treatment with enocitabine (BH-AC), daunorubicin hydrochloride, 6-MP and PSL [125]. The cell line is dependent on recombinant human granulocyte-macrophage colony-stimulating factor (GM-CSF) media supplementation during culture [125]. As outlined in the introduction 1.2, *RUNX1::RUNX1T1* prevents the expression of hematopoietic differentiation genes, but the prognosis for patients of this subtype is usually associated with a favorable outcome.

THP-1 cells, like MOLM-13, also belong to the KMT2A::MLLT3 subtype but do not have a mutation in FLT3. The cells were harvested from the peripheral blood of a 1-year old male patient diagnosed with acute monocytic leukemia [126]. The case report does not specify whether the patient had received prior treatment and whether this was a relapse case [127].

U937 cells were harvested from the pleural effusion of a 37-year old male patient with histiocytic

lymphoma, but were reported to express specific monoytic markers and properties [128, 129, 130, 131]. At the point of harvest, the patient presented with rapid tumor growth, which spread to other lymph nodes within 2 months of the initial supraclavical lymph node biopsy [128]. Cells are reported to excrete lysozyme and have phagocytic capacity [128].

Kasumi-1, like SKNO-1, cells also belong to the *RUNX1::RUNX1T1* translocation leukemic cell lines and were harvested from peripheral blood samples of a 7-year old male patient with an initial acute myeloid leukemia diagnosis, who had relapsed after a successful bone-marrow transplantation (BMT) [132]. Second remission after mitxantrone and AraC treatment preceded BMT [132]. Despite showing azurophilic granules representative of a granulocytic delineation, they differentiated into macrophage lineages after treatment with differentiation agents and expressed monocyte/macrophage markers [132].

NOMO-1 cells were derived from the bone marrow of a 31-year old female patient with acute myeloid leukemia at second relapse and also carry the KMT2A::MLLT3 cytogenetic anomaly [133].

All cells, with one exception of SKNO-1 and Kasumi-1, were grown in RPMI supplemented with 10% FBS and antibiotics. For SKNO-1 cell culture, GM-CSF was supplemented additionally and Kasumi-1 cells were cultured in 20% FBS supplemented RPMI that was additionally filtered. Use of the NOMO-1 cell line was discontinued after two unsuccessful culturing and transduction attempts, and thus only results for this thesis are based on MOLM-13, SKNO-1, THP-1, U937 and Kasumi-1 cell lines.

4.2.3 Establishing and optimizing a protein depletion strategy

Different methods to achieve targeted protein depletion of PCIF1 were trialed and optimized in this project. The efforts that went into testing the feasibility of small-interfering RNA (siRNA), CRISPR-Cas9 knockout, degradation tag system (dTAG) and short-hairpin RNA interference (shRNA) based protein depletion systems are described in the subsequent subchapters. Ultimately, this chapter demonstrates why shRNA mediated knockdown was best-suited and implemented in the experimental design for all following results chapters. Limitations of this model are discussed as part of the discussions 4.2.7.

4.2.3.1 siRNA-mediated knockdown of PCIF1

small-interfering RNA (siRNA) mediated knockdown is based on interference of short antisense RNA with the host target mRNA and degradation via the RISC (RNA-induced silencing) complex [134]. siRNA is usually transfected into cells either by cationic lipids, which encapsulate the RNA duplex and facilitate the uptake of the complex across the negatively charged cell membrane, or by electroporation, which applies electric pulses to enable the cell temporarily permeable for siRNA duplexes. This downregulation of specific mRNA leads to the transient depletion of the target protein and can last for up to 96 hours depending on the doubling rate of the host cell [134].

Ready-made siRNA duplexes were purchased from Quiagen and transfected using lipofectamine RNAiMax. Knockdown was assessed using qPCR and western blotting (data not shown) two days after transfection. siRNA construct 4 achieved approximately 50% knockdown of endogenous *PCIF1* mRNA, while other guides showed less than 40% knockdown of the endogenous transcript

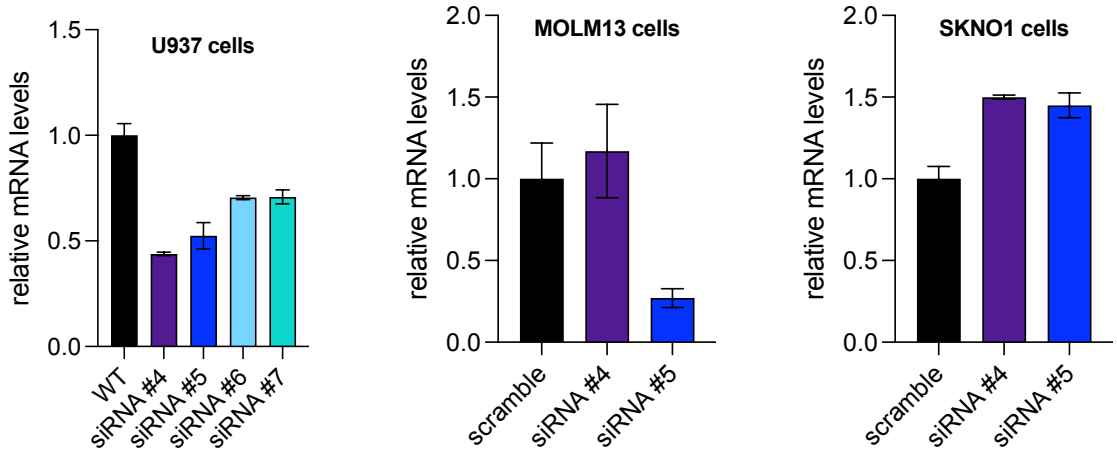

Figure 4.5. AML cell lines transfected with predesigned siRNA against *PCIF1* using Lipofectamine RNAiMAX. Different siRNA constructs were trialed in U937 cells (**A.**) and the best candidates selected for testing in MOLM13 (**B.**) and SKNO1 (**C.**) cells. Residual *PCIF1* mRNA was assessed using qPCR 48h after transfection for all experiments. Data represented as means ± SEM of n=2 replicates.

as detected by qPCR (Figure 4.5A). The level of knockdown varied substantially between experimental replicates as well as different cell lines, and was detectable for no longer than three days after transfection in U937 cells. MOLM-13 and SKNO-1 cells assayed at the same timepoint after transfection did not show the same knockdown effect as U937 cells. siRNA mediated protein depletion was therefore concluded to be an insufficient method to produce a robust significant knockdown of PCIF1 in different cell line models that was useful for downstream testing.

4.2.3.2 CRISPR/Cas9 mediated knockout of PCIF1

To assess the function of PCIF1 in a more durable model, CRISPR/Cas9 mediated knockout was trialed. Single-guide RNA (sgRNA) sequences for *PCIF1* were taken from literature as well as queried using IDT (Integrated DNA Technologies) predesigned Alt-R CRISPR-Cas9 guide RNAs and online tools such as ChopChop [24, 33, 32, 105]. Two methods were optimized (Figure 4.6A). The first method included guide RNA delivery as a two-part system (crRNA+tracrRNA from IDT)

complexed with Cas9 and delivered as a ribonucleoprotein (RNP). The second method comprised lentiviral transduction of sgRNAs using the lentiCRISPRv2, which contains the S. pyogenes Cas9 and the guide RNA scaffold on two different expression cassettes, as well as a puromycin resistance sequence for stable selection [135]. Custom 20 basepair guide oligonucleotide sequences were cloned into the scaffold and transfected into HEK293T cells with packaging and envelope vectors for lentiviral particle production and subsequent spinfection of AML cells.

Multiple guides were assessed for their efficacy of achieving a PCIF1 knockout. Nucleofection (crRNA+tracrRNA RNP), as well as lentiviral transduction (lentiCRISPRv2) of guides AA and AB allowed for puromycin selection and showed stable Cas9 expression in whole cell lysates by western blotting (Figure 4.6B). However, there was no reduction in the level of PCIF1 protein compared to WT or Cas9 only (in RNP protocol) nucleofected populations. This experiment was also performed in HEK293T cells to ensure that the failed knockout was not because of cell line specific incompatibilities. The two guides that were recommended for this experiment failed to produce a stable knockout even in HEK293T cell lines despite showing puromycin resistance, indicating that the Cas9 RNP/lentiCRISPRv2 vector was transfected effectively but the sgRNA used did not lead to proper cleavage at the target site (Figure 4.6B).

Therefore, additional guide sequences reported in previous publications [24, 32, 33, 34] and guides mined using the ChopChop tool [105]. Single guides N25 and N33 were originally designed for the purpose of creating a dTAG (degradation Tag) fused the N-terminus of PCIF1 were found to be able to produce PCIF1 depletion in polyclonal populations in those trial experiments, while sgF3 was taken from literature [24, 60]. Guides N25 and F3 showed a 60%-80% reduction of PCIF1

protein levels in U937 polyclonal bulk population, while guide N33 showed a 50% reduction of PCIF1 protein compared to the non-targeting (NT) infected cell population (Figure 4.6C). Single-cell clones were isolated by serial dilution strategy to obtain a pure clonal population of PCIF1 knockout. Ultimately, this produced viable single-cell PCIF1 knockout clones in U937 cells with a 20% and 80% incidence rate of a good knockout for guides N25 and F3 respectively (Figure 4.6C-E). SKNO-1 cells were also seeded by serial dilution strategy to obtain single-cell PCIF1 knockout clones, however, this yielded in only a very limited number of SKNO-1 clones due to poor proliferation. PCIF1 loss was detected in only in one of the clones (Figure 4.6F), which also did not survive further culture.

It is also worth noting that the levels of residual PCIF1 protein and Cas9 expression varied between the polyclonal populations of U937 and SKNO-1 cell lines (Figure 4.6C). Furthermore, decreased levels of PCIF1 KO and increased Cas9 expression remained stable in the polyclonal U937 population over a prolonged culture period with minimal selection (<1ug/ml). Conversely, polyclonal KO SKNO-1 cells express similar levels of PCIF1 protein compared to the sgNT after 4 weeks in culture (Figure 4.6D). It is conceivable that SKNO-1 PCIF1 knockout cells failed to proliferate at the same rate as PCIF1 intact cells, and perhaps even dropped out of the cell cycle entirely during the prolonged culture period, hinting at a possible PCIF1 gene sensitivity in SKNO-1. MOLM-13 AML cells were also trialed for PCIF1 knockout, however failed to produce a viable polyclonal knockout population after selection and recovery (data not shown).

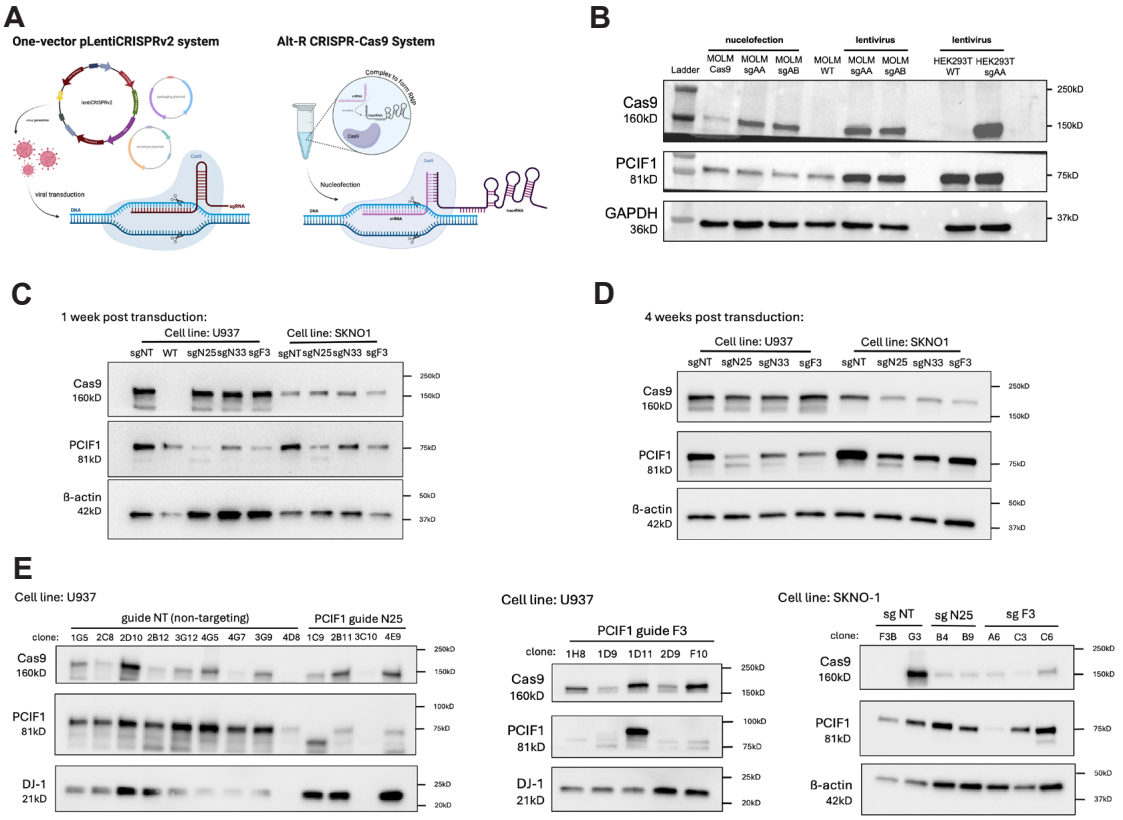

Figure 4.6. Optimizing polyclonal and single clone PCIF1 knockouts in AML cells. **A.** Schematic of two different methods employed. Left: pLentiCRISPRv2 mediated knockout is based on lentiviral infection with a single plasmid containing Cas9, scaffold and guide. Right: Alt-R CRISPR-Cas9 System is based on in vitro complexing of Cas9 protein,scaffold and guide to for the ribonucleoparticle for subsequent electroportation into cells. Figure created with Biorender **B.** Western blot of comparing both methods with two different guides in MOLM13 and HEK293T cells. **C.** Western Blots of polyclonal lentiviral PCIF1 KO using three different guides for PCIF1 in two different cell lines. **D.** Protein levels of polyclonal PCIF1 KO populations assessed 3 weeks later. SKNO PCIF1 KO populations lose Cas9 expression and regain PCIF1, or KO cells dropped out of the population. **E.** Left: Western blot of single clone PCIF1 KO (U937 cells, non-targeting and PCIF1 N25 guide) seeded 1 week after transduction and expanded for a month. Middle: Western blot of U937 single clone PCIF1 guide F3. All clones expanded, sgNT-2D10, sgN25-1C9, sgF3-1H8 and 2F10 used in subsequent experiments. Right: Western blot of single clone PCIF1 KO (SKNO-1 cells, all three guides) seeded 1 week after transduction and expanded for close to two months. clone A6 shows no PCIF1 signal and was expanded, but failed to proliferate shortly after.

4.2.3.3 pLKO.1 shRNA-mediated stable knockdown of PCIF1

Lentiviral infection with short-hairpin RNA (shRNA) constructs allows for a stable and selectable RNAi mediated protein knockdown. Briefly, shRNA sequences used in this project were reported as part of the RNAi consortium shRNA library project and cloned into a the pLKO.1 lentiviral vector to generate lentiviral particles in HEK293T cells for double spinfection of AML cell lines [136]. Infected cells were selected with puromycin for 2-4 days and left to recover before being used for downstream assays within approximately 5 weeks of knockdown generation. Remaining *PCIF1* mRNA and protein was measured 24-48 hours post selection to ensure recovery from selection and good quality protein and RNA for the assays. Puromycin is an antibiotic that mimics the 3' end of aminoacetylated tRNA and inhibits ribosomal protein synthesis by preventing further extension of elongating polypeptide chains [137]. On a physiological level, puromycin treatment is associated with significant cellular stress, which could have various effects on the model. Cells successfully transduced with the pLKO.1 plasmid carry the puromycin resistance transgene encoding for N-acetyltransferase and should be able to counteract puromycin-induced cell stress responses [137]. Stably transduced cells are therefore able to be enriched while genotypically wildtype cells will succumb to puromycin-related inhibition of protein synthesis. Since cell lines differ in their sensitivity to antibiotics, a kill curve assays determining the lowest antibiotic concentration were performed on wildtype cells. This assay showed that AML cell lines used in this project were susceptible to concentrations as low as 1-3$\mu g/ml$ after 48 hours. However, it was observed that cells treated with low concentrations of puromycin showed some remaining viability and slow recovery after ten days in culture without puromycin (data not shown). Since

the phenotypic effect that this project investigated is proliferative in nature, a short-term but intense antibiotic selection procedure was adopted to ensure that transduced cells were enriched effectively without missing the time window where the effects of PCIF1 depletion become visible.

Multiple shRNAs were cloned and tested to determine clones with highest efficiency of knockdown. The RNAi Consortium (TRC) reports five validated shRNA sequences for human PCIF1. Western blot analysis of cell lysates from transduced AML cells showed that shRNA#2 (TRCN0000158063) and shRNA#5 (TRCN0000276251) produced the most effective PCIF1 knockdown in multiple cell lines (Figure 4.7A). This knockdown was verified on the mRNA level using SYBRgreen qPCR as well as on the protein level with western blotting and immunofluorescence (Figure 4.7B-C). The level of residual *PCIF1* mRNA and protein was monitored regularly throughout the culture period, showing that the knockdown remained stable for 4-7 weeks under minimal puromycin selection (Figure 4.7D and A).

N6,2'-O-dimethyladenosine levels in PCIF1 depleted cell lines:

PCIF1 is the sole m6Am methyltransferase (see chapter 1.1.2). Therefore an effective depletion of functional protein via shRNA/sgRNA should be measurable by the reduction of m6Am on mature mRNA. For this, total RNA was harvested from cells by phenol-chloroform extraction, polyA enriched and processed for HPLC-MS (QQQ) (High-Performance Liquid Chromatography-Triple Quadrupole Mass Spectrometry) according. Total RNA was purified and digested according to a published protocol by a previous member of the lab and was employed with minor adaptations for AML cells in this project [24]. Firstly, the number of suspension cells required for sufficient mRNA after all processing steps proved to be more than four times greater than for adherent

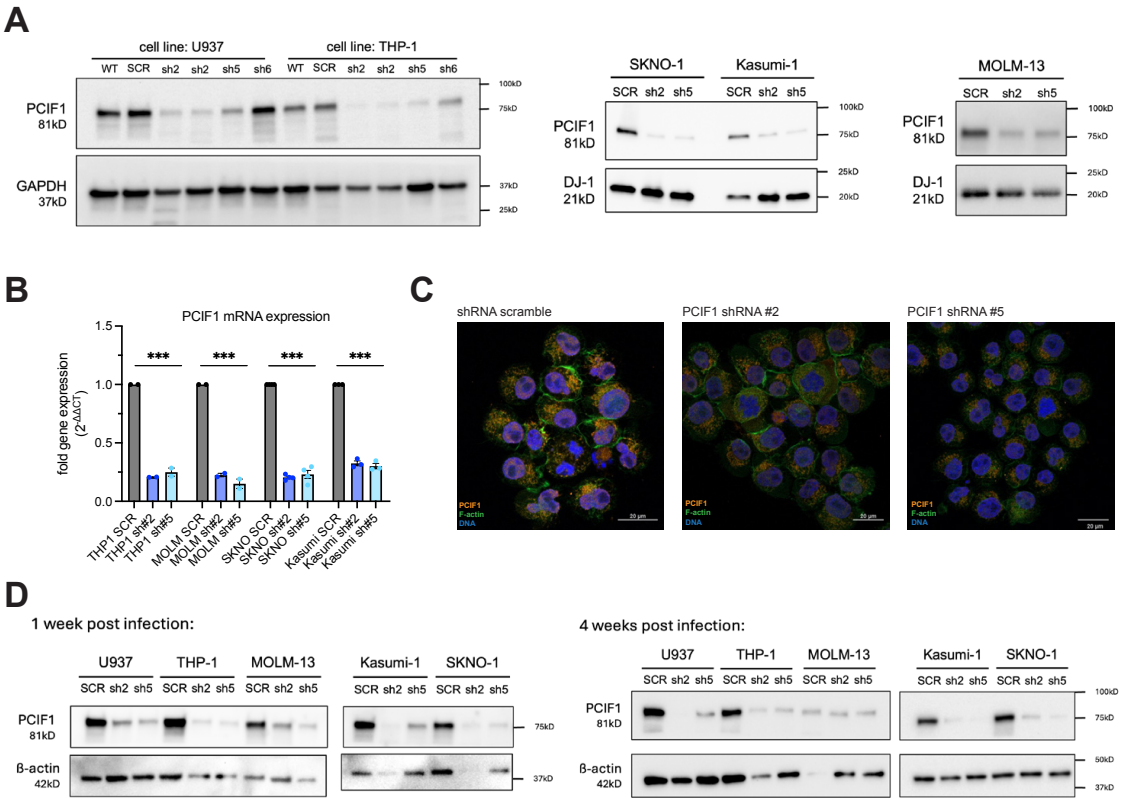

Figure 4.7. AML cell lines infected with lentiviral particles containing pLKO.1 against *PCIF1* mRNA or a scrambled control. **A.** Western blot showing cell lysates of AML cell lines lentivirally transduced with pLKO.1 vector encoding different PCIF1 shRNAs, as well as a scrambled sequence (non-targeting). shRNA2 and shRNA5 showed a >75% knockdown of PCIF1 protein and were selected as guides for all further experiments. Western blot images are representative of 4-8 independent experiments. **B.** (C) $2^{-\Delta\Delta CT}$ *PCIF1* mRNA expression normalized to the scrambled control in different AML cell lines. Knockdown with shRNA shows 75%-85% depletion of *PCIF1* mRNA. Data presented as means ± SEM of n=2-4 independent replicates. Unpaired two-tailed t-test (ΔCT) *P < 0.05; **P < 0.01; ***P < 0.001. **C.** Laser-scanning confocal images of immunofluorescently stained U937 cells transduced with scramble (left), PCIF1 shRNA #2 (middle), PCIF1 shRNA #5 (right). 63x oil, scale bar = 20 µm. PCIF1 = A546, F-actin = FITC(488), DNA = DAPI(405). **D.** Left: PCIF1 knockdown AML cell populations 1 week post infection and at least 48h of recovery after puromycin selection. Right: PCIF1 knockdown AML cell populations 4 weeks post infection with 3 weeks of recovery in normal medium.

cells, as was tested during the protocol optimization stage by comparing yields of MOLM-13 and U937 cells with HEK293T. It was hypothesized that the reason for this may be the difference in cell size and cytoplasmic content, leading to higher RNA content in adherent cells. Ultimately, approximately 60mL of confluent suspension cell culture (approximately 60-76 million cells) was harvested per technical replicate to ensure sufficient RNA for polyA mRNA isolation. The second adaptation to the protocol decreased the number of rounds for magnetic bead mRNA isolation to 1x instead of 2x, due to preventing further loss of yield. Purity assessed by nanodrop did not differ significantly between one and two rounds of isolation.

The enrichment of intact poly(A)+ mRNA via Oligo d(T)25 magnetic beads resulted in a 10% yield compared to the original input. This not surprising, as mRNA is not the most abundant RNA species in the mammalian cell and tRNA, which is more abundant, is (usually) not polyadenylated [138]. The drop in yield compared to the input after bead purification is therefore predominantly a consequence of the ratio of polyadenylated RNA within the total RNA population. The kit protocol was optimized to minimize loss of RNA during bead washes and maximize elution, however, the most effective method to increase poly(A)+ mRNA yield was to increase the first RNA-bead incubation period, as well as increase the amount and purity of total RNA for the input.

High-performance liquid chromatography (HPLC) coupled with mass spectrometry (MS) enables detection and quantification of nucleosides starting from abundances as low as the femtomolar range [139]. Oligonucleotides are digested completely before separation by polarity on the HPLC column, undergoing ionization and separation by mass-to-charge ratio in a triple quadrupole-based mass spectrometer. Isolated mRNA was digested into single nucleotides using Cap-Clip phos-

phatase, rSAP (shrimp alkaline phosphatase) and P1 nuclease and alkaline phosphatase. The Cap-Clip enzyme hydrolizes phosphate bonds, yielding mRNA with 5'monophosphate groups, which rSAP dephosphorylates. Ultimately, the P1 endonuclease cleaves the mRNA molecule into mononucleotides that are loaded for mass-spec analysis.

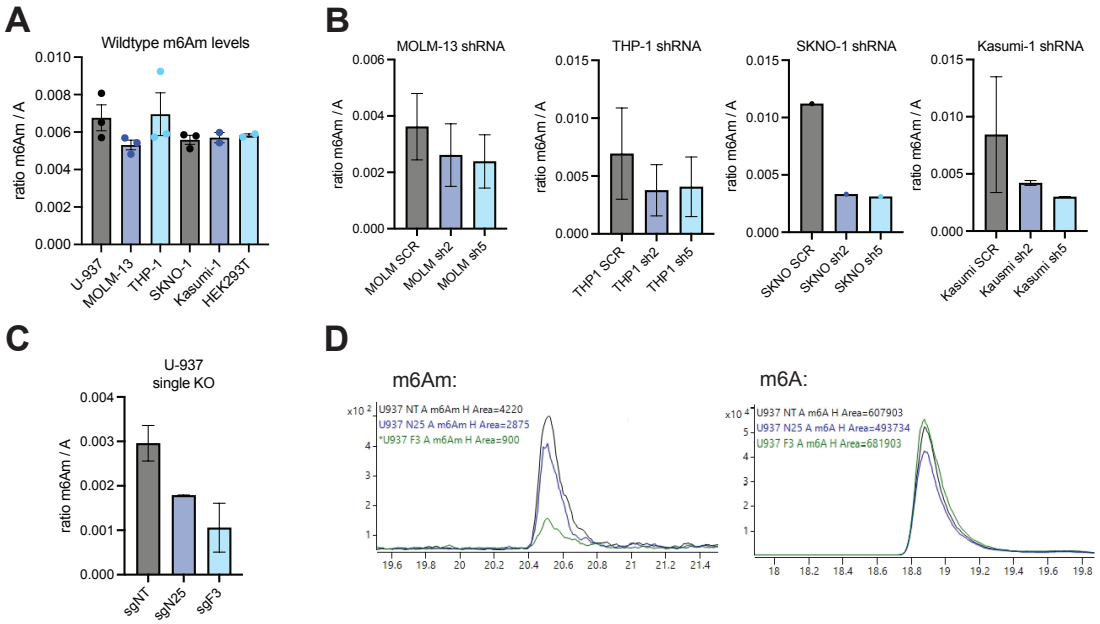

Figure 4.8. Ratio of m6Am / A measured with LCMS. **A.** m6Am levels (normalized to adenosine) in wildtype AML cell lines, as well as HEK293T cells. Data presented as means ± SEM of n=2-3 biological replicates. **B.** m6Am levels of MOLM-13, THP-1, SKNO-1 and Kasumi-1 PCIF1 KD samples. **C.** m6Am levels of U937 PCIF1 knockout. **D.** On the right: Overlay of U937 NT and KO peaks (m6Am and m6A). Chromatography peak graph generated with MassHunter Quantitative Analysis Software (Agilent).

1µg of purified and digested mRNA was loaded onto the LC-MS for detection of m6Am and m6A, while a 1:10 dilution of each sample was loaded for the detection of all other nucleosides. The reason for this lies in the abundance of each mark and the detection limit of the mass spectrometer (see appendix A.8A-B). Integrated response (IR) values for nucleotides A, C, G, and U fell outside the calibration range and detection limit in the undiluted samples, whereas nucleosides m6A and m6Am fall just above the lower bound of the external calibration range in undiluted samples.

Therefore, m6Am and m6A were quantified for each condition by dividing the IR values of m6Am in the undiluted samples by the IR values of A in the 1:10 diluted samples (10x).

In wildtype conditions, the ratio of m6Am/A remains similar across cell lines (Figure 4.8A). Measurements of PCIF1 knockdown cell lines show that mRNA and protein depletion results in a depletion of m6Am (Figure 4.8B). Curiously, the reduction of m6Am in the knockdown cell lines was not as substantial as expected from mRNA and protein reduction. Levels of m6A did not reduce proportionally with m6Am reduction, although there was variation between cell lines and replicates (see appendix A.8). The ratio of m6Am/A was also assessed in U937 PCIF1 KO cell line, however, the abundance of m6Am was higher than expected for a single clone selected knockout cell line (Figure 4.8C). There are multiple possibilities that might explain this outcome:

1. The knockout was not complete or the single clone selection was contaminated with PCIF1 intact cells
2. mRNA purification was suboptimal in this replicate and other RNA species were carried over into the sample, leading to detection of m6Am on the cap of ncRNA
3. CRISPR/Cas9 double-strand breaks at the N-terminus of the *PCIF1* gene created a truncated version of the PCIF1 protein that retained its methyltransferase activity.

The clone that was used for m6Am detection in N25 was in fact the clone 1C9 that seemed to show an approximately 20kD shift in PCIF1 protein size on the western blot (Figure 4.6E). As detailed in 1.1.2, the RNA polymerase 2 (RNAPII) interaction is encoded by the WW-domain at the N-terminal protein end. sgN25 targets *PCIF1* approximately 100bp upstream of this domain, and part of the WW-domain was seen to be mutated in Sanger sequencing from genomic DNA

(data not shown). According to Akichika et al., PCIF1 is able to bind the mRNA cap position +1 without its WW domain [32]. It would be interesting to investigate this subclone further to elucidate potential impact of impaired WW domain integrity on methyltransferase activity.

In summary, different methodologies to achieve loss of PCIF1 mRNA and protein and were trialed. While siRNA lead to an incomplete and difficult to replicate knockdown, CRISPR-Cas9 knockout attempts gave rise to viable single clone populations only for some cell lines, while others never recovered from selection, did not expand in the single clone state, or dropped out of the polyclonal population, as became evident through tracking the population over time. U937 cells retained Cas9 expression and steady levels of KO in the polyclonal population, while SKNO-1 cells lost Cas9 and regained PCIF1 expression over time, perhaps hinting at a dropout of PCIF1 KO cells from the cell cycle, which would corroborate with the low viability and recovery seen with these cells (not shown). Lentiviral CRISPR Cas9 KO was therefore not a useful technique as the main model for this thesis, as it would not have been able to be applied to all cell lines. shRNA KD lead to decreased mRNA and protein in all tested cell lines, which remained stable over a period of more than 2 weeks, which allowed for enough time to observe, characterize and collect cells for downstream assays.

4.2.4 Effect of PCIF1 depletion on proliferation, apoptosis and cell cycle

One of the goals of cancer target discovery is to uncover novel genetic vulnerabilities that will decrease the rate of proliferation, induce differentiation and/or immunogenic death of a cancer cell. The purpose of this subchapter is to observe the function of PCIF1 in the context of acute myeloid leukemia and evaluate whether loss PCIF1 impacts AML cell biology.

4.2.4.1 MOLM-13 and SKNO-1 AML cell lines show decreased proliferation and viability upon loss of PCIF1

To answer whether PCIF1 protein impacts the growth and viability of AML cell lines in vitro, the two shRNA sequences against *PCIF1* that produced the best knockdown were transduced via lentiviral spinfection into different AML cell lines and assessed for their proliferative capacities. Cell lines were infected with puromycin resistant pLKO.1 constructs, selected for 2-4 days and left to recover for at least two days before mRNA and protein samples were collected for quantification of knockdown. A difference in proliferation and viability between knockdown and scramble populations became apparent within 48 hours post selection. The depletion of PCIF1 was found to negatively impact the proliferation of two AML cell lines (SKNO-1 and MOLM-13), as assessed by manual counting as well as CellTiter-Glo (Figure 4.9). PCIF1 depleted SKNO-1 cells showed 2.5x - 2.8x less live cells (shRNA#2: p=0.0012 and shRNA#5: p=0.0016) and a 64%-50% reduction in viability (Figure 4.9A). MOLM-13 PCIF1 KD cells grew 2.4x-1.6x (shRNA#2: p=0,0006 and shRNA#5: p=0.0148) more slowly and had a 68%-57% reduction in cell viability (Figure 4.9B). Kasumi-1 PCIF1 KD cells were not found to be negatively impacted and indeed seemed to have a proliferative advantage over Kasumi-1 shRNA scramble infected cell populations (Figure 4.9 C, F). THP-1 and U937 AML cells were also not found to be significantly impacted upon loss of PCIF1 (Figure 4.9 D-E). Based on proliferation responses, MOLM-13 and SKNO-1 cell lines were therefore categorized as "sensitive" cell lines, while THP-1 U937, Kasumi-1 cell lines were classified as "resistant" to loss of PCIF1.

Despite the downregulation of cell proliferation, PCIF1 knockdown was stable in all cell lines and

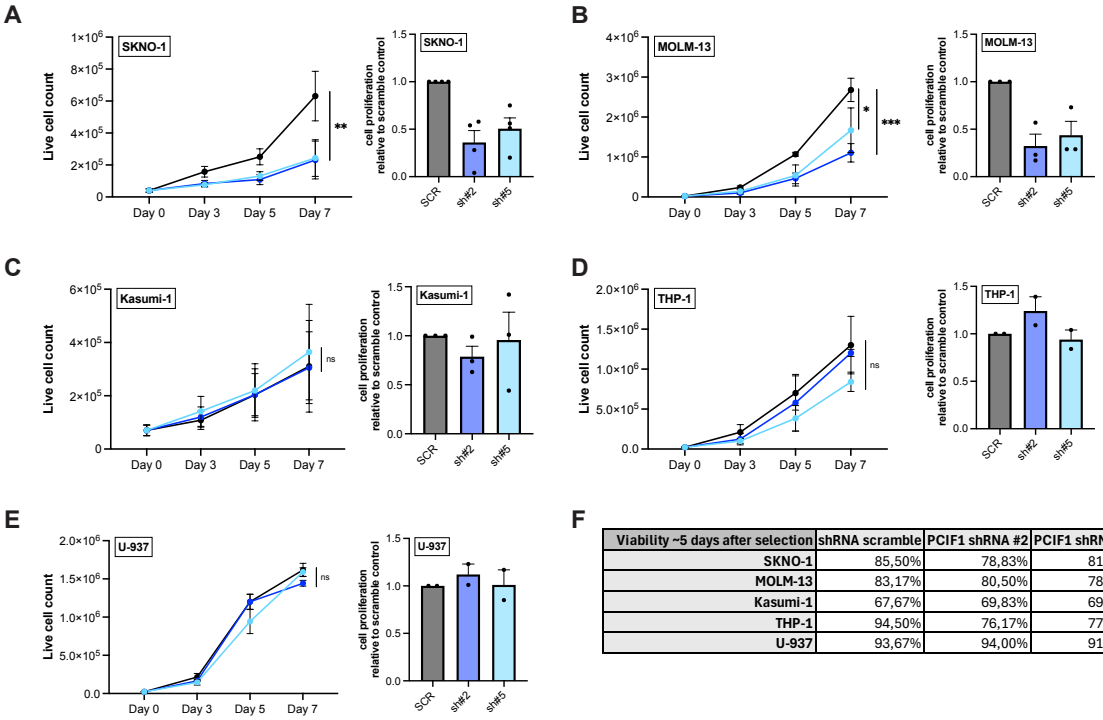

F

Viability ~5 days after selection	shRNA scramble	PCIF1 shRNA #2	PCIF1 shRNA #5
SKNO-1	85,50%	78,83%	81,33%
MOLM-13	83,17%	80,50%	78,00%
Kasumi-1	67,67%	69,83%	69,33%
THP-1	94,50%	76,17%	77,33%
U-937	93,67%	94,00%	91,00%

Figure 4.9. Proliferation and viability of all AML cell lines infected with scramble shRNA or *PCIF1* shRNA. **A-E.** Live cell count (left) and relative viability measured by CellTiter-Glo (right) for each cell line. Error bars show the SEM of the mean of 2-4 independent experiments. **F.** Viability of cell lines approximately five days after selection, after recovery of transfected cells from puromycin pressure. Datapoints represent mean cell counts / CTG luminescence relative to SCR. Significance analyzed by ANOVA with Tukey multiple comparisons test and shown as means ± SEM of n=2-4 independent replicates: *P < 0.05; **P < 0.01; ***P < 0.001.

detectable in culture for over 4 weeks (Figure 4.7 and appendix A.7). Even sensitive cell lines were able to maintain the stable knockdown, indicating that the decrease in cell number did not originate from an immediate cell cycle block and drop out from the active culture. The level of knockdown was still assessed at regular intervals for each independent knockdown experiment performed. Furthermore, each independent experiment describes a fresh infection, in order for the timeline from knockdown to manifestation of phenotype to be maintained for all replicates (. PCIF1 KD cell lines also showed suboptimal recovery from freezing/thawing (data not shown), underscoring the need for an experimental setup from scratch for each replicate.

4.2.4.2 PCIF1 sensitive knockdown cells show increased levels of apoptosis

Inhibiting malignant uncontrolled proliferation is a central focus of cancer research and therapy efforts. Cancer cells respond to intra- and extra-cellular changes in their signaling pathways or environment through modulating cell cycle control, DNA repair pathways, and activation of various cell death cascades [140]. After establishing that MOLM-13 and SKNO-1 cells are sensitive to PCIF1 depletion in preliminary cell growth assays, it was investigated whether this effect was accompanied by an apoptotic phenotype and changes in the cell cycle.

Annexin-V staining:

Annexin-V / Propidium Iodide or 7-Aminoactinomycin D viability dye (AV/PI or AV/7AAD) staining is based on flow cytometric detection of a fluorescent conjugated antibody (annexin-V) that recognizes phosphatidylserine (PS), a phospholipid predominantly located in the inner cell membrane bilayer, which becomes exposed to the extracellular space during early apoptosis [141].

Annexin-V antibody staining is combined with DNA and RNA intercalating viability dyes, such as propidium iodide (PI) or 7-Aminoactinomycin D (7-AAD), which cells only stain positive for during late stages of apoptosis, when the cell membrane is broken down and becomes permeable.

To assess levels of apoptosis in PCIF1 intact and depleted states, infected and selected AML cells were stained with annexin-V-FITC in calcium ion containing staining buffer with either PI or 7-AAD (viability dye) on the day of flow cytometric acquisition (approximately 4-7 days post recovery). Populations that stained positive for either annexin-V only or annexin-V plus viability dye are summarized into a "total apoptosis" population. Positive signal was distinguished from background signal by bounding gates according to single stained annexin-V and viability dye samples, as well as an unstained control (see appendix A.9B). SKNO-1 PCIF1 KD cells showed a significant increase in apoptotic cells (shRNA#2: 2.3x increase p=0.005, shRNA#5: 2x increase p=0.01) across five independent experiments (Figure 4.10A). MOLM-13 PCIF1 KD cells showed a 3.2x (p=0.06) and 2.9x (p=0.23) increase in apoptosis for shRNA#2 and shRNA#5 respectively, but this trend was not significant, as the portion of apoptotic cells in the bulk cell population varied substantially between biological replicates. THP-1 cells were established to be insensitive in cell proliferation experiments, but showed a mild increase in annexin-V upon loss of PCIF1 (shRNA#2: 1.4x and shRNA#5: 1.2x), which was not significant. Kasumi-1 and U937 cells were found to maintain a similar staining profile regardless of PCIF1 status; certain biological replicates performed for Kasumi-1 surprisingly had less apoptosis in the PCIF1 KD population, emulating the observation that Kasumi-1 KD cells were more amenable to culturing.

Caspase activation:

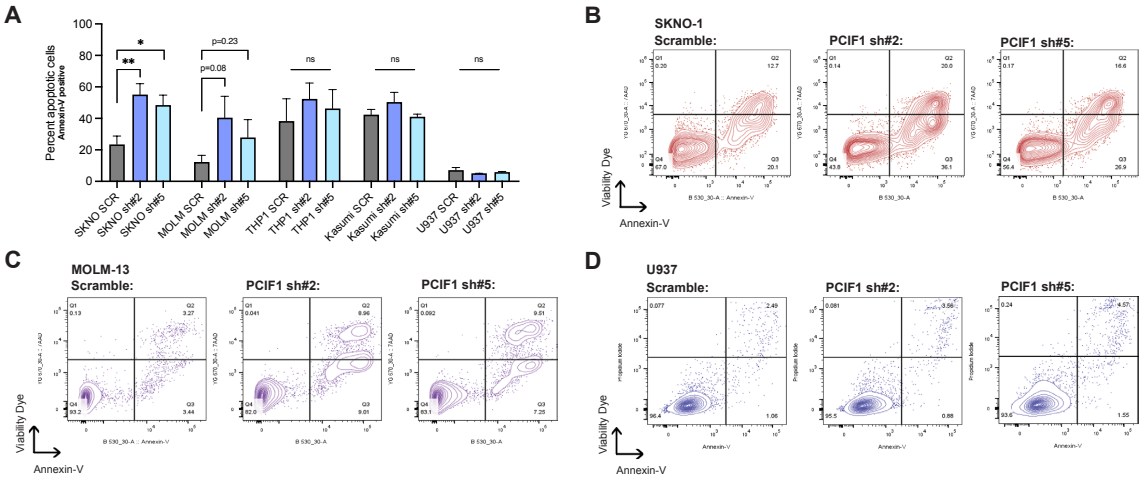

Figure 4.10. Annexin-V + Propidium Iodide or Annexin-V + 7AAD viability dye staining of AML cells in culture 1 week post selection.(A) Summary of percent apoptotic populations in SCR and PCIF1 KD conditions. bars represent averages ± SEM of n=2-5 independent replicates, two-tailed unpaired t-test: *P < 0.05; **P < 0.01. **B.** Gating of SKNO-1 **C.** MOLM-13, and **C.** U937 shRNA SCR, *PCIF1* shRNA2, *PCIF1* shRNA5 knockdown cells stained with annexin-V and 7AAD. Q2 and 3 of each plot shows single cells undergoing apoptosis.

Increased levels of annexin-V can indicate the activation of programmed cell death pathways by caspase activity. During programmed cell death, also known as apoptosis, initiator caspases can be activated by intrinsic or extrinsic factors to in turn trigger the activity of effector caspases, with the aim of breaking down internal cell structures to effectuate cell death [142]. There are two types of apoptosis, depending on the procaspases (initiator caspases) involved and the upstream pathway that activates them. Extrinsic apoptosis is triggered by the binding of cytokines, DAMPs (damage-associated molecular patterns) or PAMPs (pathogen-associated molecular patterns) to an external death receptor, triggering the dimerization of caspase-8 and the subsequent activation of caspases -3, -6, and -7 [142]. Intrinsic apoptosis is triggered by various cellular stresses, such as changes in nutrient and oxygen levels (hypoxia), DNA and cytoskeletal damage, as well as through the unfolded protein response, and lead to the the activation of the cell death signaling cascade and cytochrome C influx from the mitochondrial intermembrane space (IMS) into the

cytosol [142, 143]. Some extrinsic apoptosis pathways require the activation of players from the intrinsic pathway, leading to the release of cytochrome C from the IMS. Apoptosis is tightly regulated by a balance of pro-apoptotic (Bim, Bax, Bid, Puma, Noxa etc) and anti-apoptotic (Bcl-2, Mcl-2) Bcl-2 family proteins that enable efflux of cytochrome C or inhibit anti-apoptotic proteins to enhance the signal and promote cytochrome C binding to APAF-1 (apoptotic protease-activating factor-1) to form the apoptosome [143]. Importantly, mitochondrial membrane permeability can be triggered by other stressors such as mitochondrial membrane damage, cytoskeletal instability and dysregulation of the electron transport chain (ETC). This process can therefore release cytochrome C and trigger cell death pathways independently of caspases [143]. Besides apoptosis, other cell death pathways, which do not require activation of caspases for proteolytic cleavage of intracellular components, such as autophagy, necrosis and necroptosis, as well as pyroptosis, and ferroptosis, exist and are commonly exploited for cancer cell treatment [142, 144, 145].

Caspase activity involvement in PCIF1-related cell death was assessed briefly using two different methods. Primary antibodies raised against human full-length as well as cleaved caspase 3 were used for western blot detection in whole cell lysates of AML cells within one week post selection (Figure 4.11A). A normalization factor was calculated for each sample lane using β-actin band volumes to correct for sample loading variability. The volume of the 17kD band was then measured and normalized to the scrambled control of each cell line while taking the sample-specific normalization factor into account. The results showed that there is a 1.28-fold and 2.54-fold increase in cleaved 17kD caspase-3 signal in MOLM-13 *PCIF1* shRNA#2 and shRNA#5 respectively, as well as a 1.19-fold and 1.60-fold increase in SKNO-1 *PCIF1* shRNA#2 and shRNA#5 respectively. This effect was accompanied by a decrease in full-length caspase-3 levels in SKNO-1

PCIF1 KD populations compared to the scrambled control. However, full-length caspase-3 levels seemed to increase in the MOLM-13 and U937 PCIF1 KD populations. This is surprising, as it would follow that an increase in cleaved / active caspase-3 product would result in a concomitant decrease of the full-length form of caspase-3 due to proteolytic cleavage. Apoptosis detection by flow cytometry was performed in parallel to the WB and showed the same pattern of upregulated annexin-V+ in sensitive cell lines. A Caspase 3/7 luminescent detection assay (Caspase-Glo, Promega) was employed to quantify caspase activity more reliably. Sensitive PCIF1 KD cell lines had a higher activity of caspase 3/7 activity, while THP-1 and U937 cells maintained the same levels regardless of PCIF1 status (Figure 4.11C).

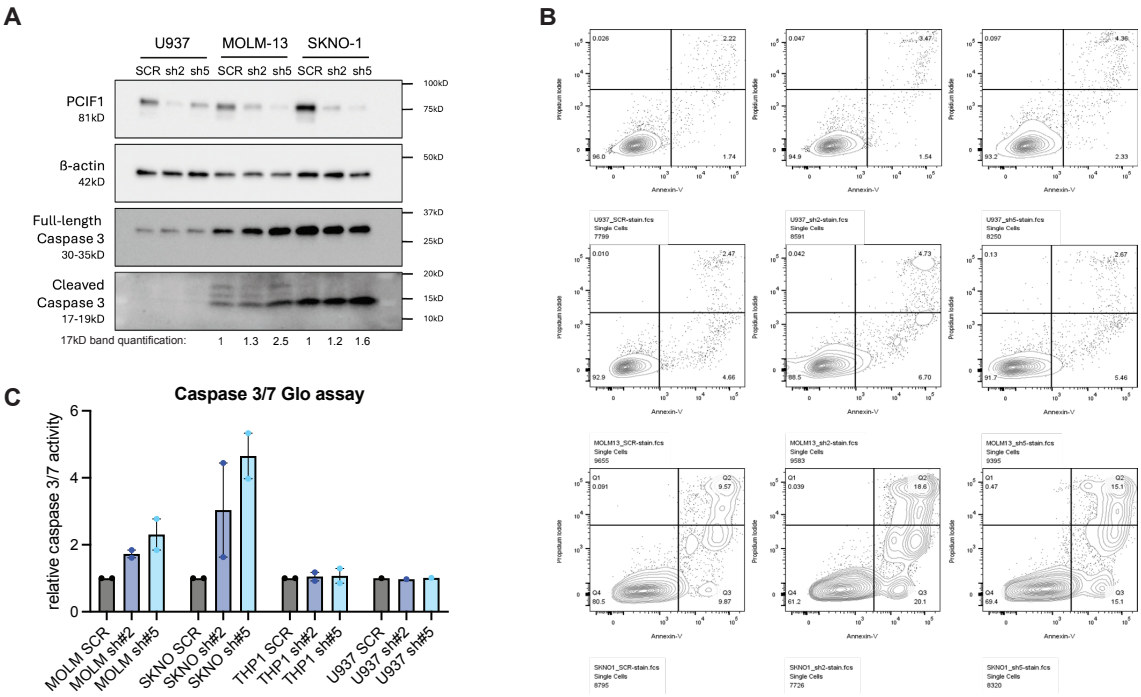

Figure 4.11. Caspase analysis in resistant and sensitive AML cell lines. **A.** Western blot of whole cell lysates from resistant U937, and sensitive MOLM-13 and SKNO-1 cells transduced with scramble and *PCIF1* shRNA. Detection with full-length and cleaved caspase 3 antibody shows an increase in the 17kD band, quantified using the denominator method with background subtraction and loading normalization in Image Lab. **B.** Annexin-V + PI staining in replicates sued for Caspase WB. **C.** Caspase 3/7 Glo Luciferase assay (Promega) levels of caspase cleavage in AML cell populations taken from cells in active culture 10 days post selection. Results depicted as means ± SEM of two technical replicates.

Cell cycle analysis:

Sustained proliferation and replicative immortality count as two defining hallmarks of cancer [6]. Non-proliferating cells exit the cell cycle to become quiescent and/or commit apoptosis. Having established that apoptotic cell signals are increased in PCIF1 knockdown AML cell populations that show a proliferation defect, it was next investigated whether cells were arrested at a specific cell cycle checkpoint.

Cell cycle analysis was performed by staining live cells in healthy culture conditions with Hoechst 33342, which binds to double stranded DNA preferentially at the A-T base rich regions and emits fluorescence that can be measured using flow cytometry [146]. Cell cycle phases can be distinguished by partitioning the detected population according to distinct peaks seen along the linear scale of Hoechst 33342 range, which correspond to stoichiometric DNA content within the cell [147, 148, 149]. The longest part of the cycle is spent in the G1-phase, which is represented by the first and in normal cycling cells the largest peak, where DNA exists in the 2n diploid state [147, 150]. Actively proliferating cells will then enter S-phase and duplicate their DNA content in preparation for mitosis. Cells will present with 4n chromosome content just before undergoing mitosis and therefore peak at double the value of the G1-peak. This phase is called G2/M. Cell cycle analysis was performed using the Watson Pragmatic algorithm and peaks were constrained to equal coefficients of variation (CV), with G2+M gate set to reach its peak at double that of G1 [150]. Cell cycle analysis of all five cell lines showed that while there is an increase of cells in the sub-G0/G1 phase with a tradeoff in the proportion of cells residing in G1 and S-phase for the sensitive cell lines upon PCIF1 knockdown, no other cell cycle arrest was observed (Figure 4.12A). The cell cycle changes were therefore considered to be minor compared to the proliferation defect

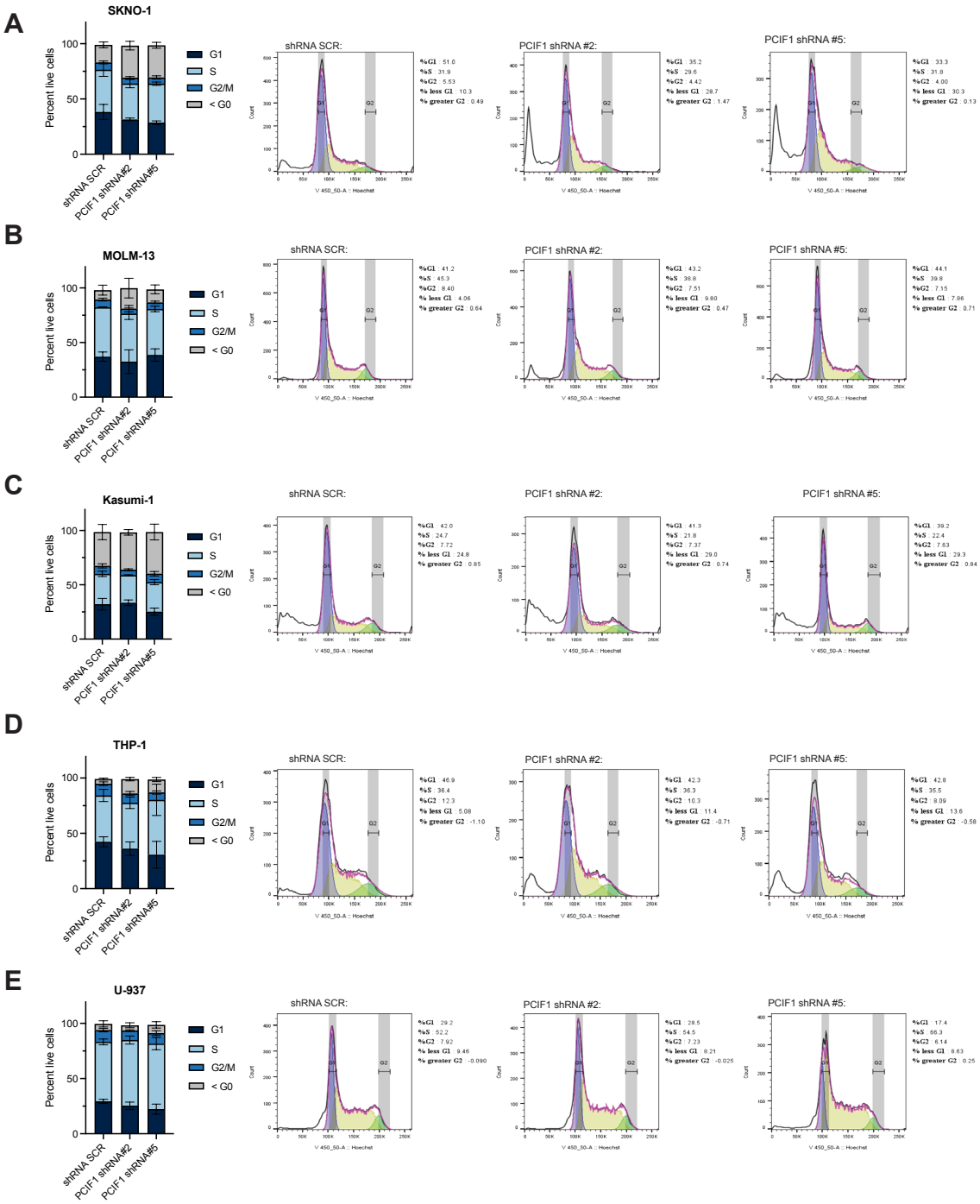

Figure 4.12. Cell cycle analysis of AML cell lines infected with shRNA for scramble control or PCIF1. Data shown as means ± SEM of n=2-5 independent replicates. Bar graphs representative of biological replicates in individual cell lines accompanied by Hoechst cell cycle watson-pragmatic gates of one representative replicate. Results horizontally for **A.** SKNO-1, **B.** MOLM-13, **C.** Kasumi-1, **D.** THP-1, **E.** U937.

and apoptosis increase observed in other experiments. Nonetheless, PCIF1 knockdown remained stable for several weeks in sensitive cell lines, leading to the conclusion that some PCIF1 depleted cells likely still contribute to the actively cycling cell population in order to maintain representation in the culture. It would be interesting to assess the timing and duration of one cell cycle progression on a single cell level using live cell microscopy, which could give an insight into the timing of cell cycle checkpoints in each cell population and answer whether sensitive PCIF1 KD cells cycle more slowly in addition to other cell death and proliferation phenotypes.

The signal detected to the left of the G0/G1 peak represents cells that may stain for less DNA for any of the following reason: first, they may be undergoing internucleosomal DNA fragmentation through endonuclease activity as part of the apoptotic process [149]; second, they could have micronuclei as a result of cell cycle dysregulation [148]; or third, possible fragmented nuclei due to cell lysis during the experimental setup [147]. The third possibility is less likely, as all cells were processed simultaneously and all population would have shown a sub-G0/G1 peak, regardless whether they are sensitive or insensitive to loss of PCIF1, if rough handling were the cause. The presence of micronuclei was also excluded as part of immunofluorescent detection of PCIF1 experiments (shown in 4.2.3) as well as in images of Giemsa stained cytospins (see 4.2.5). Since signs of apoptosis were already established with annexin-V staining, it was therefore concluded that the sub-G0/G1 peak is likely an indicator of apoptotic cells. As the molecular basis for the existence of this peak lies in DNA fragmentation and therefore cannot be taken as stoichiometric measurement, the sub-G0/G1 percentage arising from the watson pragmatic algorithm is not a direct measurement of individual apoptotic cells. Additionally, it is also important to note that it is possible for cells to undergo apoptosis from the S- or G2-phase, which would lead to DNA frag-

ments not overlapping with the traditional sub-G0/G1 peak and possibly overlapping with the G1 peak [149]. An indication of this would be wide peaks left of the G1 peak, indicating the presence of S and G2/M cells with more DNA content due to duplication but undergoing DNA fragmentation. However, should apoptotic G2/M cells peak in early S-phase or G1-phase, then these would be erroneously misclassified as cycling cells, which cannot be excluded in this analysis. It would be useful therefore to measure DNA breaks using the TUNEL assay, which allows for fluorescent labeling of free 3'-hydroxyl ends of DNA [151]. Thus, it was concluded that AML cells sensitive to loss of PCIF1 show an increase in apoptosis that could be accompanied by internucleosomal DNA fragmentation.

4.2.5 Effect on differentiation

As outlined in chapter 1.2, leukemia is defined by an expansion of immature blasts in the bone marrow niche, resulting in the accumulation of dysfunctional progenitor-like cells that fail to differentiate into hematopoietic cell types [152, 153, 154]. Acute myeloid leukemia diagnosis requires the presence of >10% or >20% blast cells, depending on the genotype, and is also an indicator of patient prognosis [81, 82, 152]. Differentiation therapy is one of the gold standards for certain types of leukemia, as is the case for acute promyelocytic leukemia (APL), where All-trans retinoic acid (ATRA) is implemented in the clinic and associated with curative potential [154, 155, 156, 157, 158]. However, various symptoms that accompany treatment with ATRA, such as fever, infection and renal failure (broadly differentiation syndrome) must also be considered before and during treatment [159]. To assess whether loss of PCIF1 impacts AML differentiation, shRNA transduced leukemic cell lines were assessed using hematological staining

techniques, here, May-Grünwald Giemsa stain, clonogenic capacity in semi-solid methylcellulose medium and the expression of markers associated with hematological differentiation.

4.2.5.1 AML cells sensitive to PCIF1 loss show morphological signs of monocyte/macrophage differentiation

The May-Grünwald Giemsa (MGG) staining belongs to the Romanowsky group of dyes and is commonly used in hematological studies on peripheral blood smears and bone marrow aspirations to detect parasites such as malaria plasmodium and assess blood cell morphology and lineages present in the sample [160]. MGG is a two-step staining procedure, in which the May-Grünwald stain is distinct from the Giemsa stain. The May-Grünwald stain mainly consists of eosin and methylene blue, while Giemsa contains additional azure dye [161]. Incubating samples in these stains nuclei dark purple, while the cytoplasm colors more lightly, and granules will retain the stain differently depending on their acidity profile [160]. Cells can then be categorized into hematopoietic lineages based on morphology and staining characteristics. The hematopoietic lineage can be broadly separated into the monocytic and lymphoid lineage, which give rise to progenitor cells and mature blood cells with distinct function (Figure 4.13).

Acute myeloid leukemia cell lines for May-Grünwald Giemsa staining (MGG) were harvested during the exponential growth phase at least a week after the end of puromycin selection and cytospun onto glass slides before fixation in 100% methanol and staining with MG stain and Giemsa dye. Cells were assessed for signs of morphological differentiation and the number of cells showing a small nuclear to cytoplasmic ratio (N/C), irregular nuclear and cell shape and/or cytoplasmic granules were counted in three distinct regions of interest (ROI) and quantified as a percentage of

differentiated cells compared to the total cell number in the ROI ($200\,\mu m^2$) (Figure 4.14). Cells that stained faintly in the cytoplasm and nucleus, that did not have an intact cell membrane and were visibly undergoing cell death, were not counted into the differentiation category, as the apoptotic phenotype was already assessed using more appropriate methods in chapter 4.2.4.2. Cells that were obviously undergoing chromosome condensation in preparation for mitosis were also not included into the counted population, as the nuclear to cytoplasmic ratio is easy to misinterpret and may lead to false positive results.Features of differentiation taken from images in the image bank of the American Society of Hematology (ASH) [162] and [155, 163] were used as a reference.

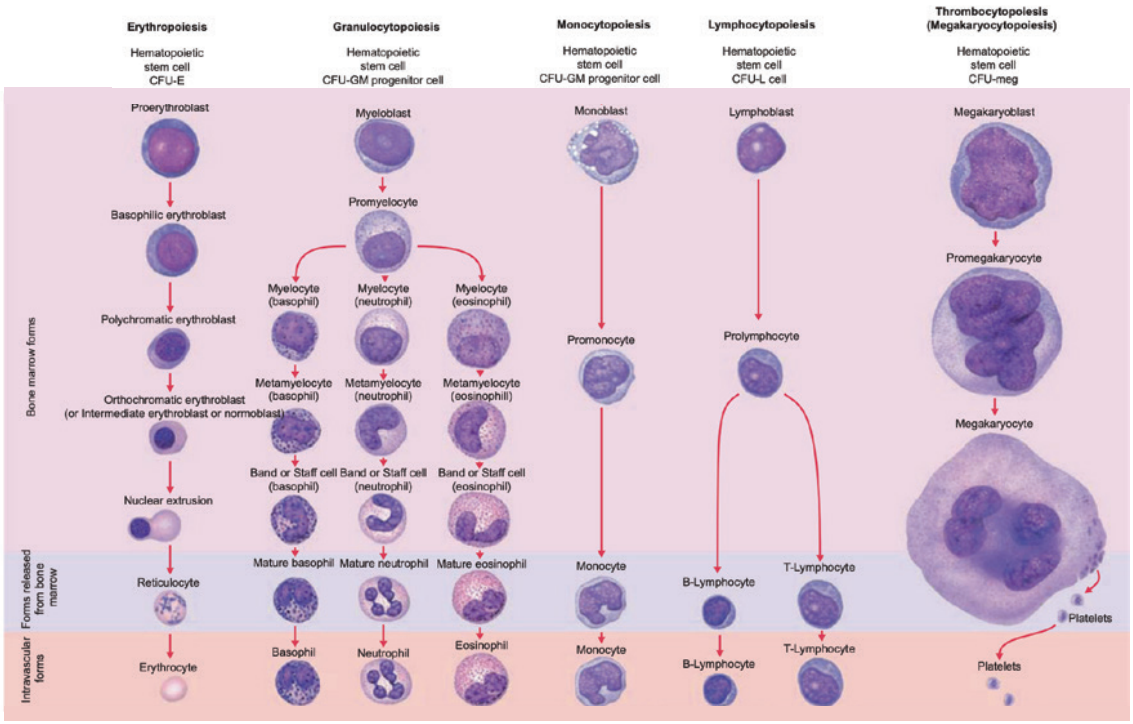

Figure 4.13. Stages of hematological differentiation (myeloid lineage) with histological samples. Image adapted from Ward et al. (2018). Comparative Anatomy and Histology (Second Edition) [164]

Hematological staining of AML cell populations revealed that sensitive lines show distinct morphological changes compared to the scramble control (Figure 4.14C-F). PCIF1 depleted SKNO-1

cells showed a decreased N/C ratio in the KD compared to the control population, irregular nuclear and cell shape, as well as an increased number of cytoplasmic vesicles towards the cell membrane. This could indicate upregulated cytolytic pathways or increased phagocytosis (Figure 4.14C). MOLM-13 PCIF1 KD cells showed a decreased N/C ratio, as well as an irregularly shaped cell membrane. Both sensitive cell line knockdown populations also showed suboptimal cell health and apoptotic phenotypes, evident by the presence of faded dying cells and debris on the slide (Figure 4.14D).

Kasumi-1 insensitive cells did not show the same differentiation phenotype as SKNO-1 and MOLM-13 cells upon PCIF1 knockdown. In fact, Kasumi-1 PCIF1 KD cells had a healthier looking cell morphology, despite obvious signs of debris from cell death scattered across the slide, which was present in both the scrambled and knockdown conditions and are a testimony to the low viability observed throughout their culture (Figure 4.14E). This beneficial effect of PCIF1 was also seen in cell cycle analysis (4.12) and general viability (4.9). THP-1 cells did not show increased morphological differentiation specific to the knockdown conditions, showing irregular cell membrane and nuclear shapes in the control as well as the knockdown conditions (Figure 4.14F). U937 cells also did not show increased signs of differentiation in the knockdown conditions, recapitulating the insensitive effect established with the proliferation and apoptosis assays (data not shown). Cell line cultures in wildtype conditions were also briefly assessed using MGG to verify that the lentivirus infection itself did not elicit phenotypic changes and that the shRNA-SCR transduced samples replicated the morphology of the wildtype (see appendix A.10).

An attempt was made to measure nuclear/cytoplasmic ratio using advanced imaging analysis by

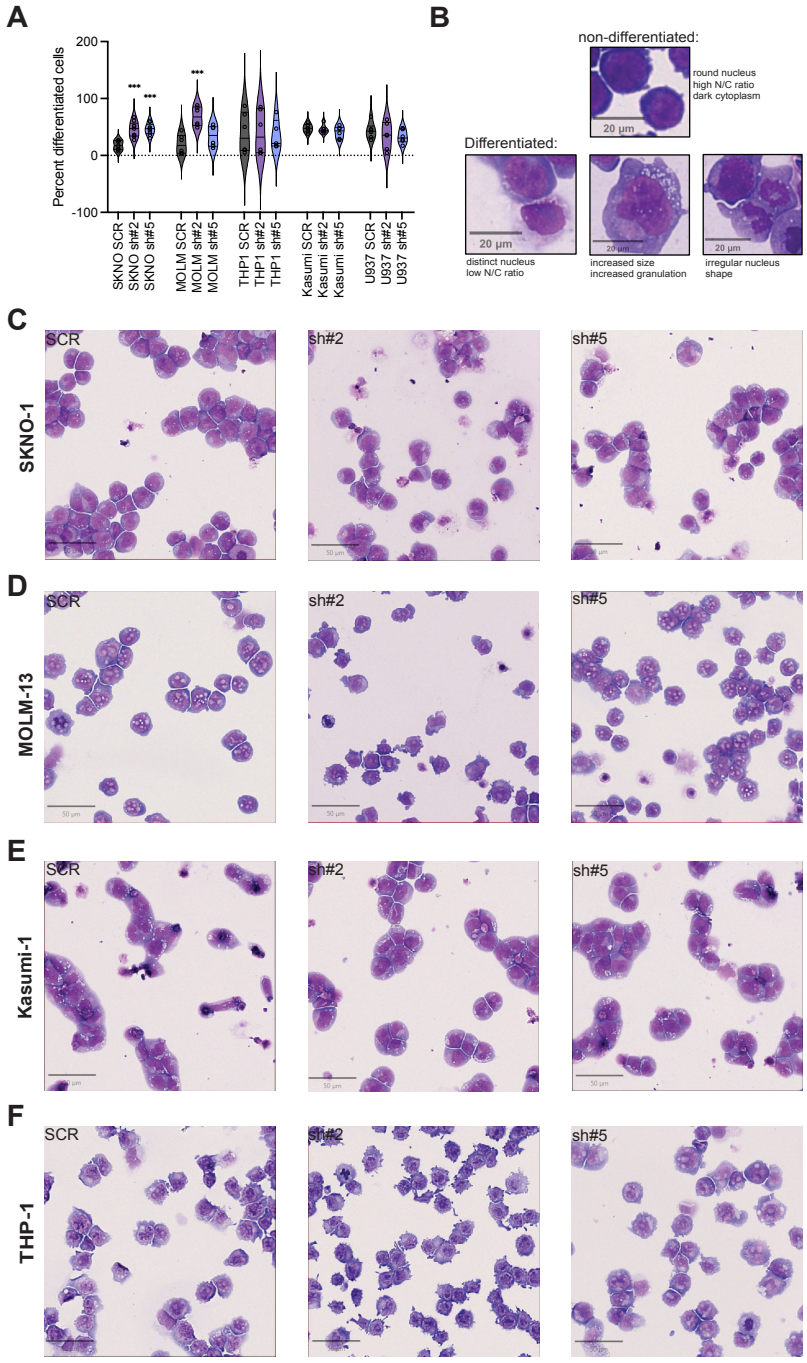

Figure 4.14. May Grünwald Giemsa staining for hematological differentiation.

Figure 4.14. (continued) **A.** Violin plots showing the percentage of differentiated cells out of total cells in a $200\,\mu m^2$ ROI. Three ROIs per biological replicate (n=2-4) were counted manually and analyzed using a two-tailed unpaired t-test *P < 0.05; **P < 0.01; ***P < 0.001. **B.** Example morphology of differentiated cells. Snapshots taken from MOLM-13 and SKNO-1 populations stained for this experiment. **C-F** Representative snapshots of SKNO-1, MOLM-13, Kasumi-1, and THP-1 cell lines infected with lentiviral shRNA scramble (left), shRNA *PCIF1* #2 (middle) and shRNA *PCIF1* #5 (right). Scale bar $50\,\mu m$. Images taken with a digital slide scanner (Hammamatsu NanoZoomer) and evaluated using manual annotation in Quantstudio.

quantifying the gray scale overlays of the darker nuclear component with the wider total cell and also by quantifying the intensity (higher intensity equals darker nucleus). Unfortunately, the image quality did not allow for easy reliable quantification. Thus, the differentiation percentages rely on counting of qualitatively assessed cells exhibiting hallmarks of morphological differentiation.

Results from MGG staining assays indicate that cells sensitive to PCIF1 depletion in proliferation and apoptosis show subtle signs of morphological monocyte/ macrophage lineage differentiation. The spread out, irregular cell shape acquired by MOLM-13 PCIF1 knockdown cells could be indicative of a macrophage or myeloid dendritic morphology. However, although these cells acquire key features (as referenced using the image bank of the American Society of Hematology (ASH) [162] and [155, 163]), the phenotypes observed in this project are subtle and not exemplary of terminal differentiation. Furthermore, AML cell lines are immortalized and cultured in serum culture conditions unfavorable of differentiation. Nonetheless, morphological changes upon loss of PCIF1 is a promising sign that PCIF1 pathways play a role in maintaining the differentiation block typical for leukemia.

4.2.5.2 Sensitive cell lines produce fewer and smaller colonies in methylcellulose medium conditions upon loss of PCIF1

Besides morphological staining, assessing clonogenic abilities of leukemic cell lines in semi-solid media via colony forming unit (CFU) assay serves to demonstrate long-term reproductive growth, engraftment and stemness [165]. One colony is considered to be at least 50 cells and hematopoietic stem cells seeded in suitable Methocult media can give rise to specific lineage colonies [165, 166].

Leukemic cell lines were seeded in methocult with 10% culture media and assessed for their colony forming abilities. SKNO-1 sensitive cell lines showed decreased colony number as well as number of cells per colony and diameter (Figure 4.15A). MOLM-13 cells, while sensitive in all other proliferation, apoptosis, and differentiation tests, did not show a significant difference in colony number. However, a difference was uncovered when classifying colony types (here: "dense" = compact core and "diffuse" = spread out core, no clear center) (Figure 4.15B). While the scrambled condition showed an equal number of dense and diffuse colonies, knockdown conditions decreased the number of dense colonies, indicating that MOLM-13 PCIF1 knockdown cells also had a decreased ability to form colonies with a compact center. Kasumi-1 PCIF1 KD cells, similarly to the more viable morphology seen in MGG staining and easier handling observed in active culture, showed a few more colonies than the control condition. Fewer colonies were counted in THP-1 sh#2 condition, but this effect was not replicated by sh#5. Overall, the CFU assay showed that AML cells sensitive to the loss of PCIF1 in proliferation and differentiation also formed fewer or, in the case of MOLM-13 cells, less compact, colonies in semi-solid medium.

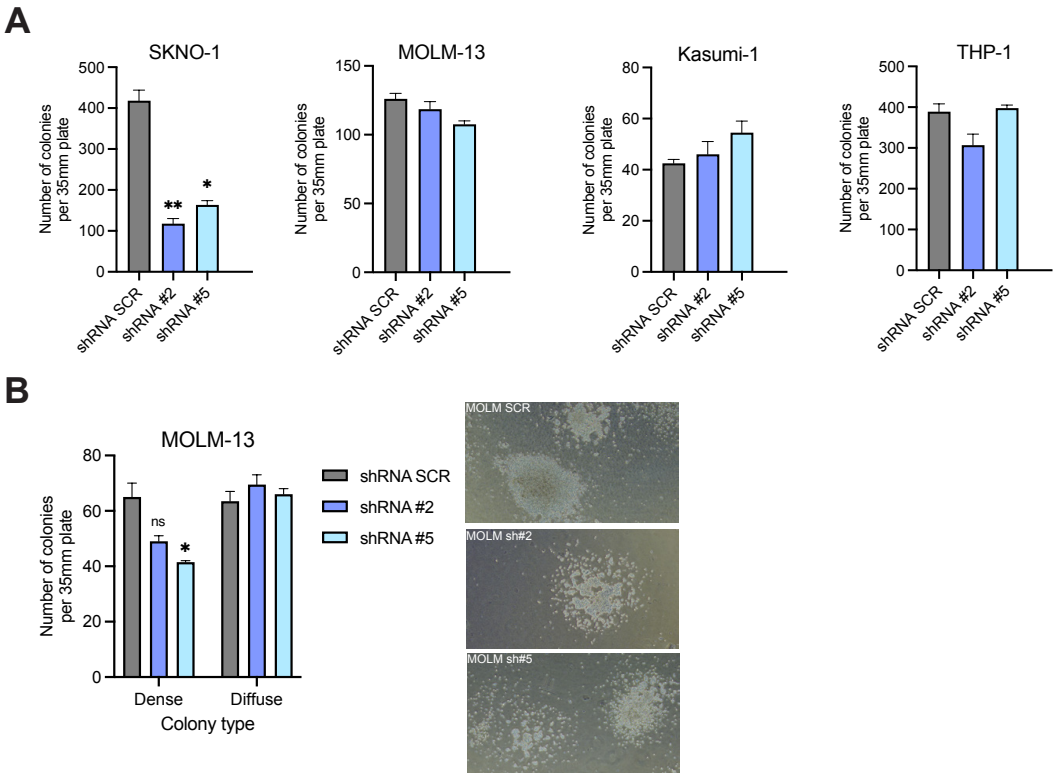

Figure 4.15. Analysis of colony forming capabilities of AML cells upon PCIF1 knockdown. **A.** Number of colonies formed by AML cells with different PCIF1 status seeded in $35\,\mathrm{mm}^2$ plates in Methocult. **B.** Comparison of dense and diffuse colony numbers in MOLM-13 cells. Representative images of MOLM-13 colonies taken on a Nikon Eclipse Ts2 microscope (10x). Results representative of n=2 biological replicates, depicted means ± SEM of technical replicates of one experiment two-tailed unpaired t-test *P < 0.05; **P < 0.01

4.2.5.3 Loss of PCIF1 induces the expression of monocytic surface markers CD11b, CD14 and CD86

Flow cytometry-based measurement of specific cluster of differentiation molecules (CD) generates a more holistic as well as quantitative understanding of lineages of differentiation. CD molecules are cell surface markers differentially expressed by stem cells and differentiated cells. The CD markers most commonly associated with myelomonoytic differentiation are CD11b and CD14 [167, 168]. CD11b is an integrin primarily found on the surface of monocytes, macrophages, neutrophils and other immune cells that, together with CD18, forms macrophage-1 antigen (Mac-1)

[169]. It belongs to the class of pathogen recognition receptors (PRR) and plays a role in activation, cytotoxicity, chemotaxis and adhesion in differentiated leukocytes [169, 170]. Its expression gradually increases upon differentiation from the negative/low myeloblast stage to the positive/high neutrophils and monocytes [168, 171]. CD11b is also expressed on some AML blasts and has been associated with a poor prognosis [172].

CD14 is associated with monocytic differentiation/activation and acts as a coreceptor to TLR4, binding pathogen associated molecular patterns such as LPS (lipopolysaccharide) and inducing NfkB signaling downstream of the surface receptor. CD11b and CD14 have been previously shown to be upregulated upon All-trans retinoic acid (ATRA) treatment in Acute Promyelocytic Leukemia (APL) and their expression is therefore seen as a factor indicative of positive differentiation treatment [157, 167].

CD86 and HLA-DR are pro-inflammatory markers expressed on antigen presenting cells and are therapeutic markers for immune cell infiltration in AML [173]. CD86 and HLA-DR have also been reported to be stimulated and upregulated in response to granulocyte-macrophage-colony stimulating factor (GM-CSF) treatment, shifting cells into a pro-inflammatory M1 macrophage phenotype [174].

PCIF1 knockdown AML cells were assessed for the mRNA as well as protein expression of different surface markers using qPCR and flow cytometry. The SKNO-1 cell line was compared to the Kasumi-1 cell line, as they represent two cell lines of the same subtype (*RUNX1::RUNX1T1*) with opposite phenotypes upon loss of PCIF1 (Figure 4.16). Flow cytometric and qPCR analysis showed that differentiation markers were inversely up-/downregulated in SKNO-1 vs Kasumi-

1 PCIF1 knockdown cells. Specifically, CD11b and CD86 are upregulated in SKNO-1 PCIF1 knockdown cells compared to the scrambled control condition on both the mRNA and protein level, while these markers were expressed at similar or even decreased levels in Kasumi-1 PCIF1 knockdown cells compared to the scramble condition (Figure 4.16A and C). CD14 mRNA and protein was upregulated in SKNO-1 PCIF1 knockdown cells and downregulated in Kasumi-1 PCIF1 depleted cells on the mRNA level (Figure 4.16B). However, there was generally significant variability between Kasumi-1 biological replicates, making it challenging to reach a consensus. *HLA-DRA* was downregulated on the mRNA level in SKNO-1 cells and also in one Kasumi-1 shRNA condition. On the protein level, HLA-DR expression remained the same in Kasumi-1 cells and decreased in SKNO-1 PCIF1 KD cells (Figure 4.16D).

Other cell surface markers such as CD47 (immune regulation known as a "don't eat me" marker [175]), CD115 (also known as CSF-1R, associated with macrophage activation, recently shown to be correlated with PCIF1 expression in peridontal inflammation [68]), CD33 (hematopoietic differentiation marker, also targeted in leukemia therapy with gemtuzumab ozogamicin) and more were also quantified with flow cytometry (see appendix A.13B-I). Wildtype levels of differentiation markers were referenced from annotations in the DSMZ cell line repository and data pages of each cell line. Notably, the Kasumi-1 cell line is CD34+ and HLA-DR- in wildtype conditions, while the wildtype SKNO-1 cell line is CD34- and HLA-DR+, reflecting a diverse range of maturity between these two cell lines (see Table 4.2 [133, 176]. CD34 is a human hematopoietic stem cell surface marker, while cells differentiating into effector cells will gradually lose CD34 expression [177]. Overall, PCIF1 knockdown may induce the expression of cell surface markers indicative of differentiation and activation along the monocytic lineage, although the differences

between PCIF1 intact and knockdown populations were moderate with some variance between replicates, showing that better follow up with a more precise panel to assess monocytic differentiation is warranted.

Table 4.2. Immunophenotypic marker expression of wildtype AML cell lines from cell line repository

Cell line	Markers
SKNO-1	CD3−, CD4+, CD13+, CD14−, CD15−, CD19−, CD33+, CD34−, HLA-DR(+)
Kasumi-1	CD3−, CD4+, CD13+, CD14−, CD15(+), CD16(+), CD19−, CD33+, CD34+, CD38+, CD71+, HLA-DR(+)

Source: Reference flow cytometry data provided by cell line repository Leibnitz Institute DSMZ [133, 176].

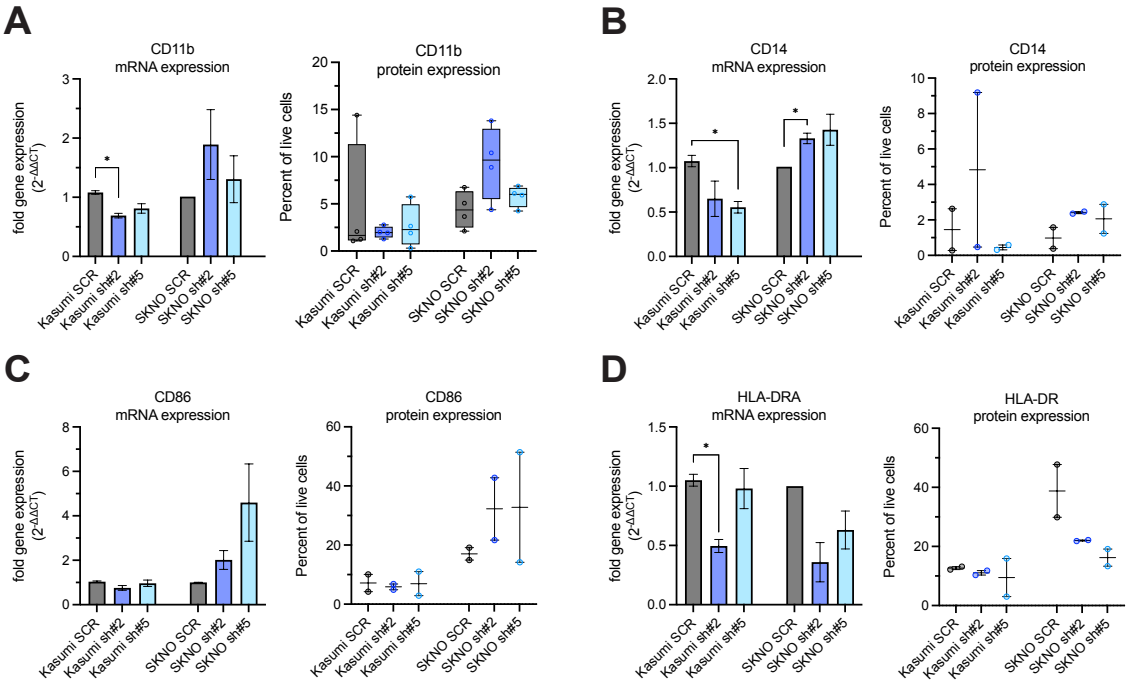

Figure 4.16. Expression of monocytic surface markers in PCIF1 depleted AML cell lines. Each panel: left = mRNA expression measured using $2^{-\Delta\Delta C_T}$ qPCR relative to the scrambled condition, right = protein expression measured with fluorescent antibody flow cytometry. Data presented as means ± SEM of n=2-4 independent replicates. Unpaired two-tailed t-test (ΔC_T) *P < 0.05; **P < 0.01; ***P < 0.001. Gating strategy see appendix A.11 and A.12.

4.2.6 PCIF1 depleted AML cells respond differently to chemotherapeutics

One aspect of investigating the role of PCIF1 in acute myeloid leukemia was to explore whether it would be an interesting synergistic target for existing AML therapy. Relapse and therapy resistance is a common obstacle in AML patient care and candidates that may overcome acquired therapy resistance or synergize with existing therapies is an important aspect of fundamental cancer science. Using the proliferation readout by quantification with CellTiter-Glo, AML cell viability in scramble and PCIF1 knockdown conditions, as well as PCIF1 knockout conditions in U937 cells was assessed. Primarily, these experiments were conducted to investigate whether resistant cell lines would be rendered more sensitive to treatment with AML chemotherapeutics and other death inducing treatments. A second question that came up in the course of these experiments was whether PCIF1 sensitive cells would require lower drug concentrations, which would be beneficial in a clinical setting.

4.2.6.1 Choice of therapeutic drugs

As discussed in chapter 1.2.1, the treatment strategy employed depends greatly on the driver mutation and therapy toleration factors, such as age and fitness, myeloproliferative history and prior treatment. Generally for AML, patients will receive 7+3 induction therapy, which consists of chemotherapeutics cytarabine for 7 days and anthracycline on the first 3 days. A FLT3 inhibitor may be given additionally to patients with FLT3 mutated AML. The aim is to reduce the number of leukemic blasts entirely (remission), or into a state of minimal residual disease (MRD), both of which are accompanied by post-remission or post-consolidation therapy. Less intensive

induction therapy may be used in older patients or young patients who may not tolerate high-dose chemotherapy. Low-dose cytarabine, venetoclax, azacitidine, decitabine and targeted drugs such as gemtuzumab ozogamicin (for CD33+ AML) and IDH inhibitors (for IDH mutated AML) are often used in these cases.

4.2.6.2 PCIF1 depletion does not confer sensitivity to venetoclax treatment

IC50 dose-response experiments were set up in 96-well plates using concentrations ranging from 10uM to 19,5nM for venetoclax (Ven), azacitidine (Aza), as well as Ven+Aza as a combination treatment, in which both compounds were used at equimolar concentrations (ie 10µM each, 20µM total). Dose-response curves showed no improvement in treatment outcome in PCIF1 depleted conditions (Figure 4.17A-B). Interestingly, U937 knockout cells seemed less sensitive to Aza treatment conditions, showing higher IC50 values for the KD treated than the scramble treated group. Venetoclax belongs to the class of Bcl-2 inhibitors, which target the oncogenic protein Bcl-2 and enable leukemic cells to overcome the differentiation blockade and trigger apoptosis [178]. U937 cell lines have been reported not to be dependent on Bcl-2 for leukemia maintenance, according to the DepMap Consortium [107, 129]. Loss of PCIF1 also did not render them more sensitive to the treatment (Figure 4.17A). A chemoresistant effect was also seen in the MOLM-13 cell line treated with Ven only (4.17D) as well as Sorafenib. The inhibitor Sorafenib targets Raf/MEK/ERK to induce apoptosis and downregulates another anti-apoptotic protein (Mcl-1) [179]. Sorafenib is also a reported ferroptosis activator and has also been shown to induce apoptosis especially in *FLT3* mutant leukemia [180, 181]. While MOLM-13 WT cells were highly sensitive to sorafenib treatment, PCIF1 KD rendered them less sensitive compared to their scrambled counterpart, enhancing

the chemoresistant effect even more than with Ven (Figure 4.17D-E). Notably, MOLM-13 cells are characterized by a *KMT2A::MLLT3* (MLL-AF9) rearrangement as well as a *FLT3* mutation and are sensitive to FLT3 inhibitors. The sensitivity of MOLM-13 WT vs PCIF1 KD cells was also tested by treatment with Quizartinib and Midostaurin, two FDA-approved FLT3 inhibitors, and showed the same chemo-insensitive trend in the KD condition (data not shown). Unfortunately, these chemotherapeutic/inhibitor experiments were only repeated within one biological replicate and it would be vital to confirm this effect in an additional replicate.

It would additionally be of worth to establish whether sorafenib is better tolerated by both sensitive PCIF1 sensitive cell lines (ie MOLM-13 as well as SKNO-1 PCIF1 KD) in additional replicate experiments. Should this be the case, it would be important to understand the mechanism underlying this effect of sorafenib, and potentially other ferroptosis and kinase inhibitor treatments, to potentially shed light on the mechanism that governs PCIF1 sensitivity. It would be highly interesting if PCIF1 can indeed elicit such contrary (pro-apoptotic but also chemoresistant) effects in different AML cell lines. This further highlights how the m6Am mark deposited on 5' mRNA contributes to a finely tuned, cell and cancer-type specific landscape.

4.2.7 Chapter summary, discussion and limitations

Summarizing observations from experiments to assess phenotypic changes brought about by PCIF1 knockdown, the results show that only certain AML cell lines (MOLM-13 and SKNO-1) are sensitive to the loss of PCIF1 and respond with decreased proliferation and viability, increased apoptosis, subtle changes in cell morphology and expression of monocytic differentiation markers (CD11b, CD14 and CD86). Resistant cell lines seem to be unperturbed by the loss of PCIF1 and

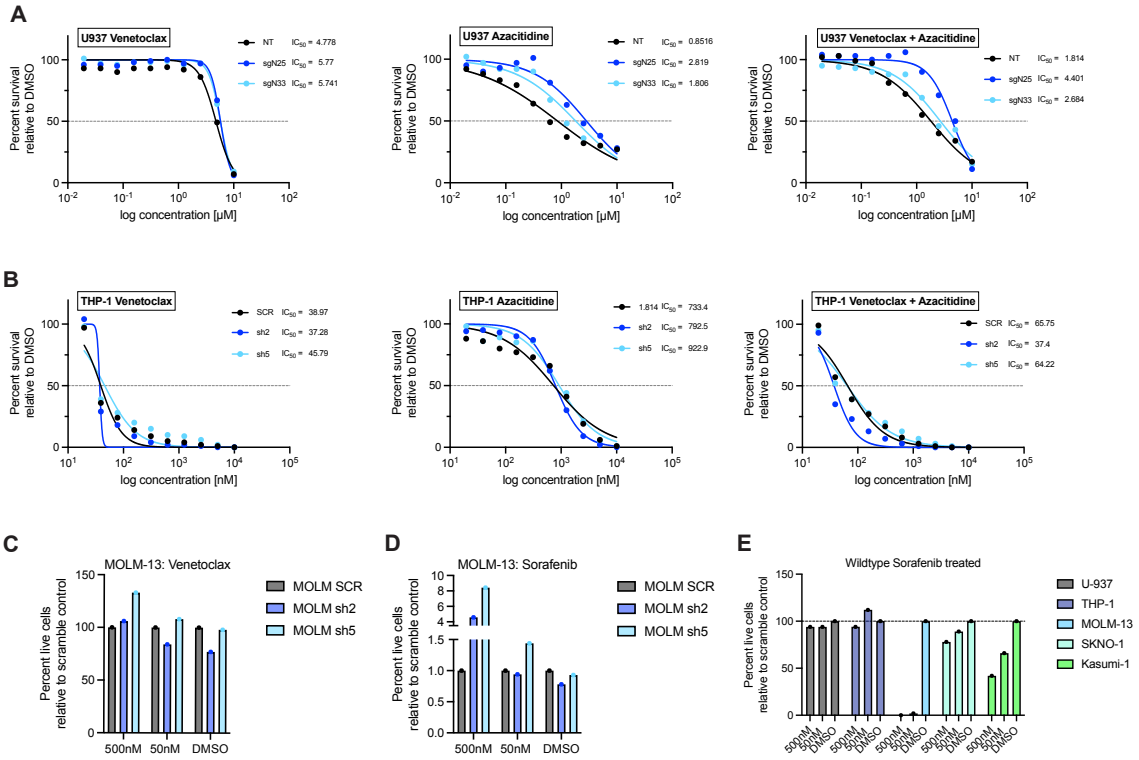

Figure 4.17. Viability of AML cell lines treated with Venetoclax (BCL2i) and Sorafenib (Ras-pathway inhibitor). **A.** IC50 dose-response curves in U937 PCIF1 knockout cells treated with venetoclax, azacitidine, and the combination at equimolar concentrations indicated on the x-axis in log. **B.** IC50 dose-response curves in THP-1 PCIF1 knockdown cells teated with venetoclax, azacitidine, and the combination at equimolar concentrations indicated on the x-axis in log. Data representative of 2 independent replicates. **C.** MOLM-13 scramble and PCIF1 knockdown cells treated with venetoclax only at different concentrations. Data represented as mean or luminescence (viability) normalized to SCR (n=1). **D.** MOLM-13 scramble and PCIF1 knockdown cells treated with sorafenib only at different concentrations. Data represented as mean or luminescence (viability) normalized to SCR (n=1). **E.** Wildtype AML cells treated with sorafenib to assess basal sensitivity. Data represented as mean or luminescence (viability) normalized to SCR (n=1).

continue to proliferate normally without upregulation of monocytic maturation markers.

The hypothesis that PCIF1 sensitivity relies on AML subtype specific biology was thoroughly considered, but set aside over the course of these experiments. The first PCIF1 knockdown experiments were performed in only SKNO-1, MOLM-13, THP-1 and U937 cell lines, and thus generated a hypothesis that perhaps the *RUNX1::RUNX1T1* subtype may generally sensitive to loss of PCIF1. However, follow-up experiments in the Kasumi-1 cell line showed the inverse phenotype, seemingly proliferating more readily after PCIF1 knockdown. Moreover, MOLM-13 and THP-1 cell lines are both derived from *KMT2A* rearranged leukemia, but only MOLM-13 cells were consistently sensitive in knockdown experiments. Therefore, *RUNX1::RUNX1T1* and MLLT3::KMT2A leukemic subtypes were not counted as a determining factors in PCIF1 sensitivity. An additional difference between MOLM-13 and THP-1 cell lines is a gain of function mutation in *FLT3* (ITD) in MOLM-13 cells. It would be interesting to investigate whether a *FLT3*-ITD, as well as its allelic status, might impact PCIF1 sensitivity. MOLM-13 cells retain one WT copy of *FLT3*, while MV4-11 carries two mutant alleles [91]. Follow-up experiments in other *KMT2A* rearranged AML subtypes are currently ongoing and include Monomac-1, Shi-1 and MV4-11 cell lines.

AML subtype driver mutations are not the only characteristics that should be considered when assessing possible patterns for selective sensitivity. p53 mutational status, relapse status, and treatment with chemotherapeutics prior to cell line establishment from patient blood or bone marrow were also considered. The cancer dependency tool for cell lines developed by the DepMap Consortium was used to assemble a more holistic overview of AML cell lines [109, 129]. AML

cell lines were plotted according to expression and sensitivity to PCIF1 knockout (reported by DepMap) and then categorized according to various characteristics (p53 status, relapse, secondary mutations, etc) but no clear pattern was discernible (see DepMap.org, Data Explorer Tool). It is worth mentioning that the DepMap z-score (delineating the level dependency of a cancer cell line on a given gene, in this case PCIF1) for the MOLM-13 cell line was above the threshold for sensitivity, meaning that these cells were resistant to PCIF1 knockout in their experiments. This could be due to different methodologies and culture conditions used, but also signifies that the biological effect of PCIF1 may not be absolute and information from public datasets should assessed with caution.

There are significant limitations to the model and method with which PCIF1 significance was assessed. Firstly, while cell lines are valuable model systems for cancer research, genetic drift and failure to mimic inherent physiological characteristics are significant shortcomings. Assessing PCIF1 in patient primary cell lines as well as measuring leukemic manifestation in in vivo mouse models would be of significant scientific value in future experiments. Secondly, the pLKO.1 shRNA model for protein depletion requires selection and recovery after lentiviral infection, during which the effects of PCIF1 loss manifest. Thus, the data presented in this work does not provide insight into the immediate effects after PCIF1 knockdown, which may provide insight into disease mechanisms. Generation of an inducible model (dTAG) was attempted, yet knock-in of the modified N- or C-terminal PCIF1 domain proved to be challenging and time-consuming and was put on hold. Inducible knockdown using the pLKO.1-Tet-ON plasmid are currently ongoing. A significant worry was also the loss of PCIF1 knockdown cells in sensitive cell lines due to dropout from the cell cycle and actively proliferating population. This was observed in the creation

of single clone knockouts for both resistant and sensitive cells, but only U937 cells were able to expand productively enough for isolation of single-cell derived clones. PCIF1 knockdown was assessed over the course of multiple weeks to ascertain whether the stable knockdown persisted long enough for adequate measurement to be performed. Knockdown cultures in sensitive and resistant cell populations proved to be stable under minimal selection for up to 3 weeks. Nonetheless, in order to ensure that measurements across experiments and replicates were comparable, sample harvest and experimental setups were carried out within the three week time window set out in chapter 4.2.3.2, protein levels assessed before every major measurement, and infections repeated anew for sensitive as well as resistant cell lines for every biological replicate. Freezing and thawing aliquots of the same resistant knockdown populations was considered and trialed, however not taken into practice because PCIF1 KD cell lines did not recover well after thawing, even though the shRNA-SCR counterparts recovered comparably to the wildtypes. It could be postulated that PCIF1 may play a role in mediating recovery from low-temperature storage even in cell lines that seem resistant in "unstressed" conditions.

In conclusion, the work from this chapter established that PCIF1 depletion results in apoptosis and differentiation in certain AML cell lines. The effect was not attributable to one specific subtype and further investigation into the transcriptomic landscape of these cells is necessary to uncover the mechanism behind PCIF1-related cell death.

4.3 Changes in the transcriptomic landscape upon loss of PCIF1

Transcriptomic analyses of biological processes shed light on complex regulatory networks of changes in transcriptional rates and splicing that would remain unexplored without the help of high-throughput sequencing technologies. Even though assessing RNA transcript abundance with techniques such as qPCR and hybridization experiments had been possible before the advent of RNA-sequencing (RNA-seq), next-generation sequencing (NGS) allowed for a rapid and robust high-throughput approach to deep-profiling of transcriptional networks. To investigate the PCIF1-dependent effect on AML cells more closely, RNA sequencing on four cell lines (two sensitive and two resistant) was performed and analyzed for general differential gene expression, as well as transcript variant abundance.

4.3.1 Bulk RNA-sequencing reveals differential expression of fatty acid metabolism and oxidative stress genes

Purified total RNA from shRNA scramble and shRNA *PCIF1* infected acute myeloid leukemia cell lines was enriched for polyadenylated (polyA) RNA, fragmented (approximately 200nt fragments), and processed for directional library sequencing on the Illumina Next-Seq 2000 plattform. Data was processed using the nf-core/rna-seq pipeline (v3.18.0) and STAR/RSEM for read alignment (GRCh38) [182, 183]. Gene and transcript counts were analyzed for differential expression using DESeq2 (v1.40.2).

Visualization of differentially expressed genes between the scramble shRNA and two *PCIF1* shRNA conditions (absolute log-2 fold change (l2fc) > 0.75 and FDR adjusted p-value (p.adj)

< 0.05) showed that sensitive *PCIF1* knockdown cells up- and downregulated a much larger number of genes than resistant *PCIF1* knockdown cells (Figure 4.18A-D), further highlighting the phenotypic difference observed in non -omics experiments.

A total of 160 genes were differentially expressed in SKNO-1 *PCIF1* KD cells (up: 115 genes, down: 45 genes) and 87 genes in MOLM-13 *PCIF1* KD cells (up : 42 genes, down: 45 genes). In resistant Kasumi-1 *PCIF1* KD cells, only 8 genes were significantly differentially regulated (up: 6 genes, down: 2 genes) and 24 genes in THP-1 *PCIF1* KD cells showed differential regulation (up: 6 genes, down: 18 genes). Seven transcripts were significantly differentially regulated in both cell lines (*PCIF1*, *FADS2*, *ELOVL6*, *AXL*, *FUCA1*, *CAMK1*, and uncharacterized protein (ENSG00000288841)), none of which overlapped with the resistant DEG list. However, as it is likely that SKNO-1 and MOLM-13 cells may up- and downregulate slightly different gene sets as they undergo cell death, an extended list of 20 (including the 7 previously listed) was defined that included genes that were differentially expressed (absolute l2fc > 0.75) in at least one of the cell lines and had an adjusted p.value < 0.05 in both cell lines (Figure 4.18F). This list of 20 genes was defined as common sensitive DEGs. Clustering analysis of the expression of these 20 genes by euclidean distance showed distinct expression patterns between sensitive and resistant cell lines (Figure 4.18E). Specifically the genes *CTSG*, *FADS2*, *FADS1*, *STK39*, *ELOVL6*, *IGFBP2*, and *IFITM1* were upregulated in the resistant state, and either downregulated or unchanged in the sensitive KD state. MOLM-13 sensitive cells upregulated the expression of *MPO*, *CD82*, *ARPC3*, and *COX7C*. SKNO-1 cells upregulated *BTG2*, *LIMK1*, *CDNK1A*, *AHNAK*, *AXL*, *CAMK1* and *FUCA1*. The only gene that was significantly upregulated (l2fc > 0.75) in both of the sensitive cell lines was an uncharacterized protein coding gene (ENSG00000288841) (Figure 4.18F). These genes have par-

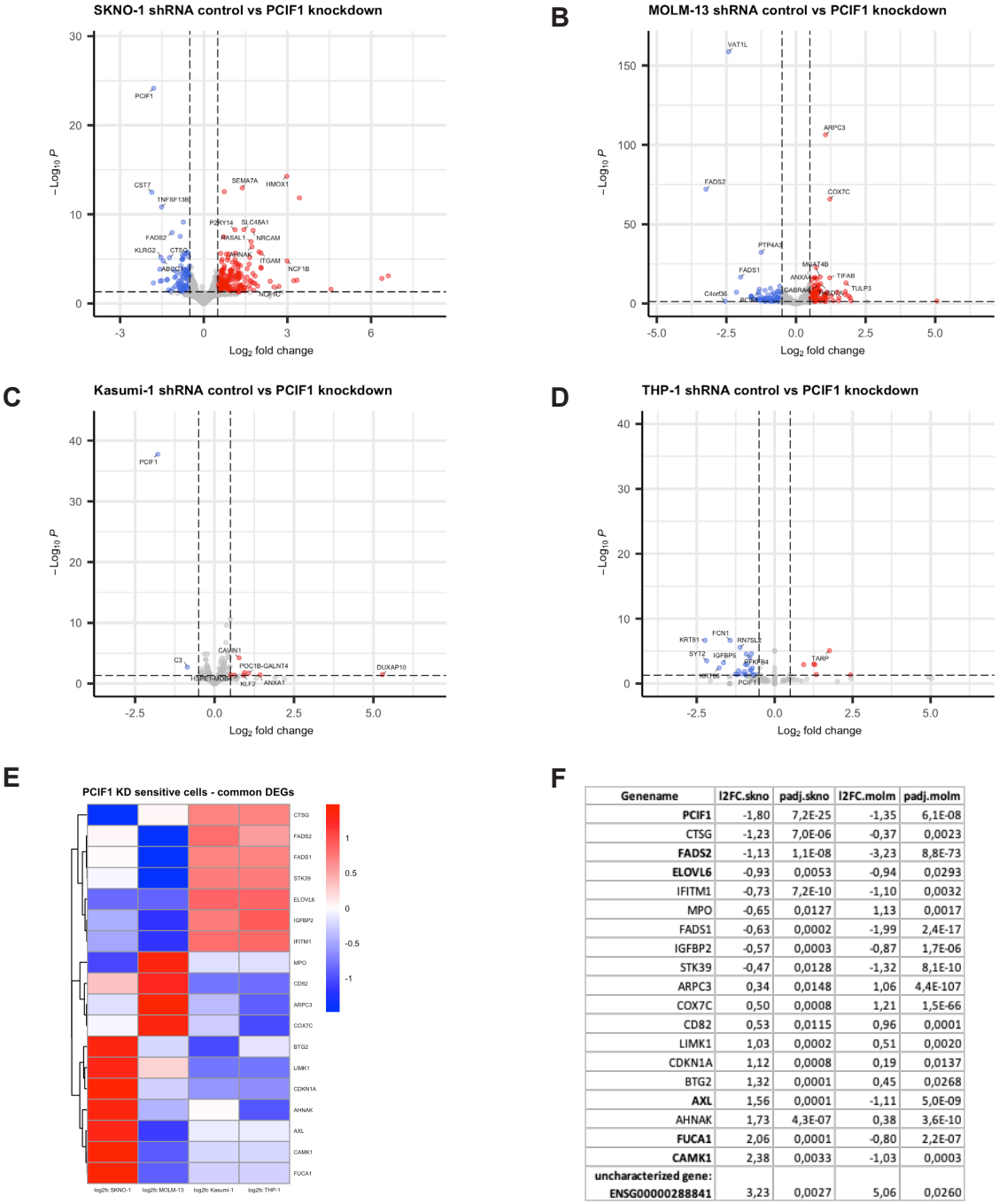

Genename	l2FC.skno	padj.skno	l2FC.molm	padj.molm
PCIF1	-1,80	7,2E-25	-1,35	6,1E-08
CTSG	-1,23	7,0E-06	-0,37	0,0023
FADS2	-1,13	1,1E-08	-3,23	8,8E-73
ELOVL6	-0,93	0,0053	-0,94	0,0293
IFITM1	-0,73	7,2E-10	-1,10	0,0032
MPO	-0,65	0,0127	1,13	0,0017
FADS1	-0,63	0,0002	-1,99	2,4E-17
IGFBP2	-0,57	0,0003	-0,87	1,7E-06
STK39	-0,47	0,0128	-1,32	8,1E-10
ARPC3	0,34	0,0148	1,06	4,4E-107
COX7C	0,50	0,0008	1,21	1,5E-66
CD82	0,53	0,0115	0,96	0,0001
LIMK1	1,03	0,0002	0,51	0,0020
CDKN1A	1,12	0,0008	0,19	0,0137
BTG2	1,32	0,0001	0,45	0,0268
AXL	1,56	0,0001	-1,11	5,0E-09
AHNAK	1,73	4,3E-07	0,38	3,6E-10
FUCA1	2,06	0,0001	-0,80	2,2E-07
CAMK1	2,38	0,0033	-1,03	0,0003
uncharacterized gene: ENSG00000288841	3,23	0,0027	5,06	0,0260

Figure 4.18. Differential Gene Expression analysis of *PCIF1* KD AML cell lines.**A-D.** Volcano plots of differential gene expression analysis. DESeq2 objects were filtered for low counts and shrinkage of effect size (lfcshrink) was applied. Significantly upregulated genes (absolute l2fc > 0.75 and p.adj < 0.05) in red, downregulated in blue. **E.** Heatmap plot of euclidean distance clustering of 19 common differentially regulated genes. **F.** Statistics of 20 common differentially expressed genes in sensitive cell lines.

tially overlapping roles in fatty acid metabolism (*FADS1*, *FADS2*, *ELOVL6*), oxidative stress and ROS (*MPO*, *COX7C*, *AXL*), inflammation and lysosomal maturation (*CTSG*, *IFITM1*, *IGFBP2*, *FUCA1*) membrane-bound ion transporters (*CAMK1*, *STK39*, *AHNAK*), and cell cycle and actin polymerization (*ARPC3*, *LIMK1*, *CDNK1A*, *CD82*). A detailed insight into molecular pathways that these players contribute to and links to existing *PCIF1* literature is outlined in the chapter discussion (see 4.3.1.3).

4.3.1.1 Gene ontology and gene set enrichment analysis of DEGs in *PCIF1* KD AML cells reveal downregulation of mTORC1 signaling, bile acid and cholesterol homeostasis pathway players

After establishing differentially regulated genes, pathway analyses were performed to shed light on the biological significance and molecular networks that these genes are involved in. Gene ontology (GO) analysis relies on cumulative hypergeometric tests followed by multiple testing correction (here Benjamini-Hochberg (BH) false discovery rate) to identify functional enrichment of pathways and lineages [102]. Importantly, the l2FC of each DEG is not taken into account in hypergeometric tests for GO, but is considered when running gene set enrichment analysis (GSEA). First, GO analysis was performed using the gprofiler2 tool package (v 0.2.3) and significantly differentially regulated genes (abs.l2fc > 0.75 and p.adj < 0.05).

Cellular stress response gene ontology terms, specifically responses to reactive oxygen species (ROS) pathways, were among the highest scoring GO terms in both sensitive cell lines (Figure 4.19 A-B). Small molecule metabolic processes (encompassing fatty acid biosynthetic processes), were commonly enriched in both cell lines, but not significantly in SKNO-1 cell lines. Interestingly,

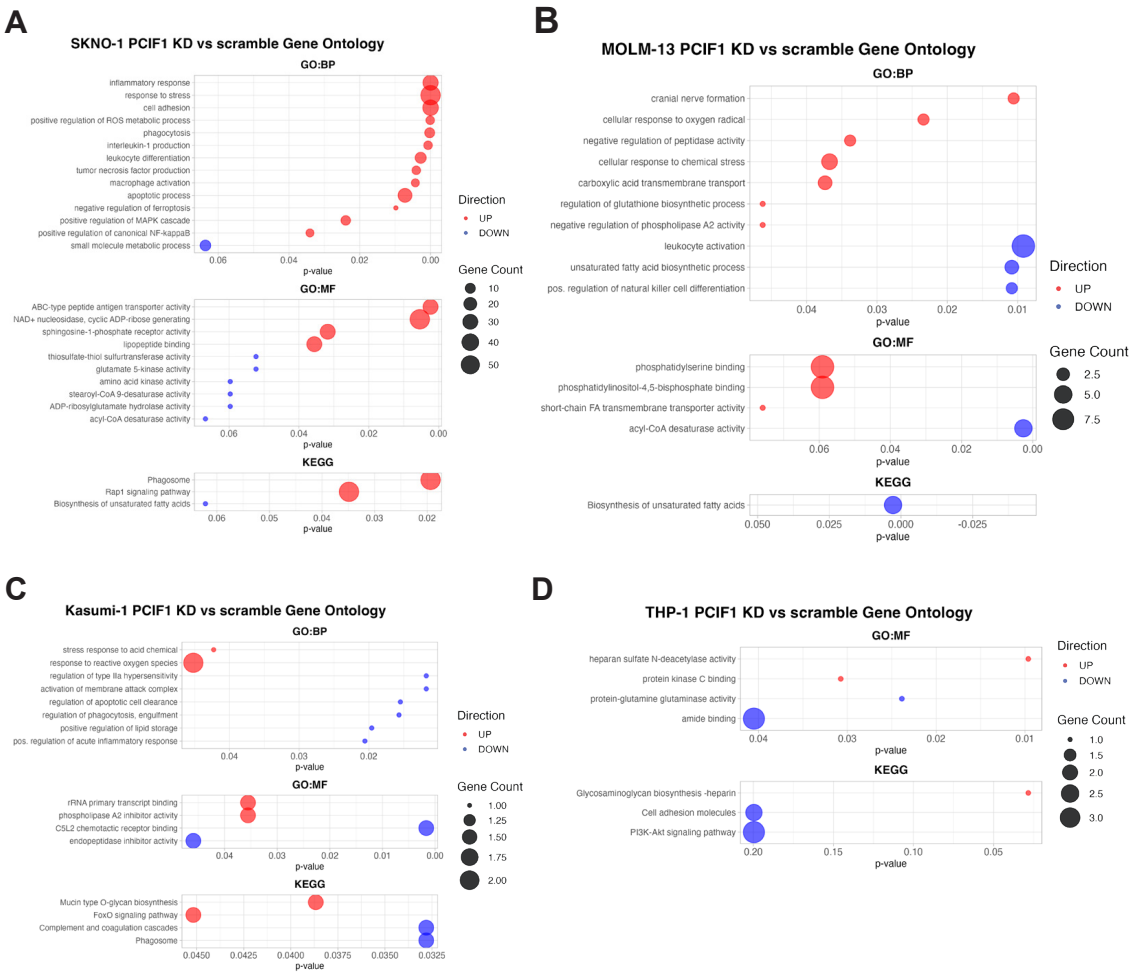

Figure 4.19. Gene Ontology (gProfiler) pathways in *PCIF1* KD cells. Bubble plots represent up-(red) and downregulated (blue) ontology terms upon loss of PCIF1. Number of genes that intersect with GO term represent radius of bubble and GO terms are ranked from top-to-bottom by ascending p-value. Enrichment determined using cumulative hypergeometric probability test (Fischer's one-tailed) and corrected for multiple comparison using FDR (BH) method [102] GO:BP = Biological process, MF = Molecular function, KEGG = Kyoto Encyclopedia of Genes and Genomes.

SKNO-1 scored highly for inflammatory and monocytic activation pathways. However, this was not significantly reflected in MOLM-13 cells. MOLM-13 cells scored highly for upregulation of ROS response terms and downregulation of fatty acid metabolic processes. In line with the low variance seen in DEG analysis for resistant cell lines, there were not many significant GO terms. Remarkably, phagocytosis ontology was downregulated in both resistant cell lines, in line with the upregulation in the respective sensitive AML subtype counterparts.

Enrichment of certain gene ontologies between cell lines warranted further investigation into pathways. The increased inflammatory potential of SKNO-1 cells could be attributed to the upregulation of transcription factor signatures that were downstream of $TGF - \beta$ signaling (Figure 4.20 A). While gene ontology analysis is a well-proven approach for pathway analysis, the input gene list is not ranked and does not take into account the fold-changes that define each gene. Therefore, gene-set enrichment analysis (GSEA) using the Human Molecular Signatures Database (MSigDB) Hallmark gene sets was performed to gain further insight into pathways impacted by *PCIF1* [184]. Genes and their corresponding l2fc values from DESeq2 were ranked against MSig Hallmark gene sets and plotted from most upregulated to most downregulated to return a normalized enrichment score (NES) for each hallmark gene set. The four cell lines were queried for gene-set enrichment and NES scores of significant hallmarks that overlapped in the sensitive cell lines were plotted (Figure 4.20 B). This revealed that mTORC1 signaling, inflammatory response, cholesterol homeostasis and bile acid metabolic gene sets were most enriched across both sensitive cell lines. Notably, these four significant gene sets in sensitive cells did not overlap with the resistant cell lines (non-significant NES scores, therefore not depicted). Resistant cell lines were not enriched for gene sets like the sensitive cell lines were, wherein only Kasumi-1 cell lines showed downregula-

tion of genes enclosed in the oxidative phosphorylation signaling, which was not recapitulated in THP-1 cells (Figure A.15).

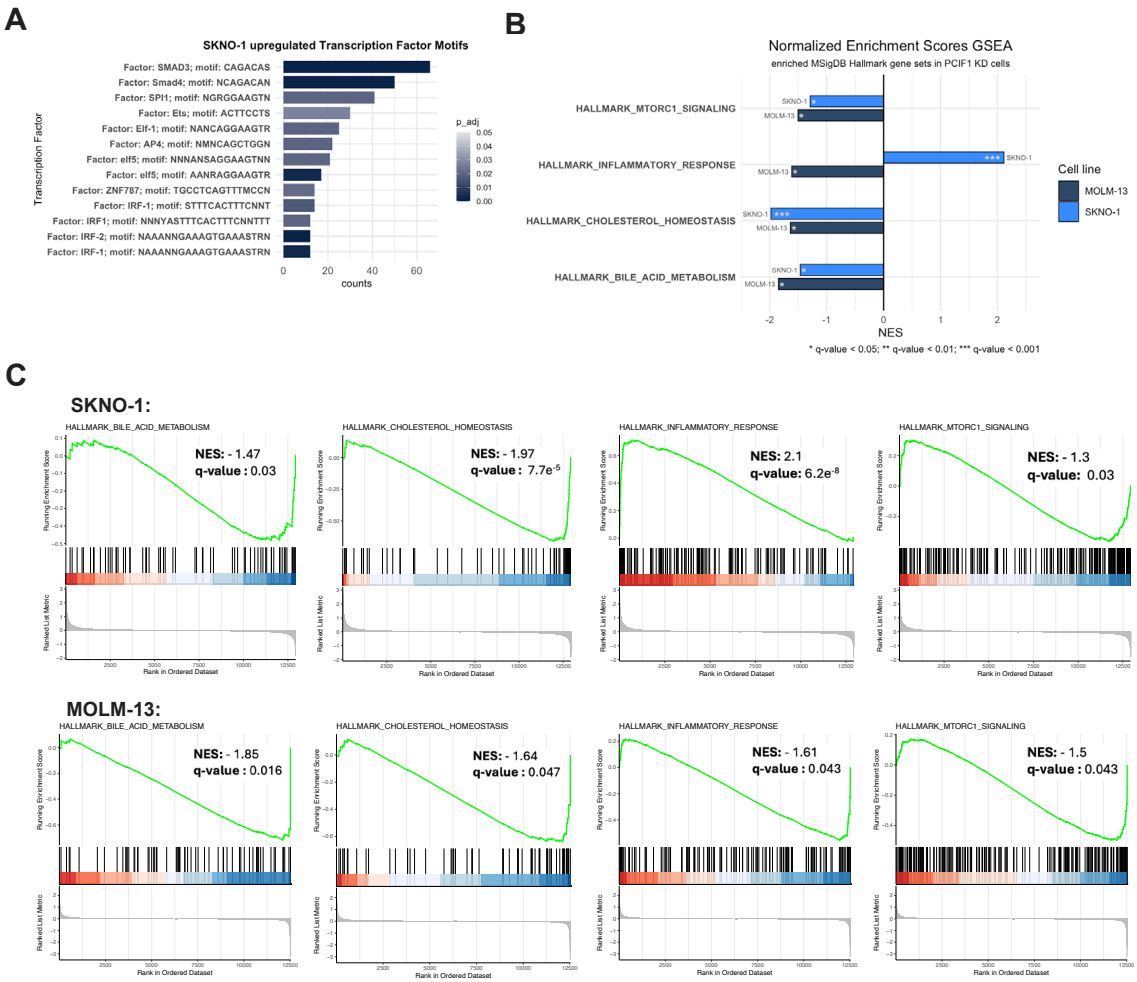

Figure 4.20. Transcription factor motif and Gene Set Enrichment Analysis (GSEA). **A.** Upregulated TF motifs of SKNO-1 differentially expressed genes from RNA-seq. **B.** Summary of significant MSig Hallmark gene sets in gene set enrichment analysis for MOLM-13 and SKNO-1 cell lines. Bars represent normalized enrichment scores common in both sensitive cell lines. Asterisks represent significance of FDR q-values (*FDR-q < 0.05; **FDR-q < 0.01; ***FDR-q < 0.001. Top 10 enriched gene sets in all 4 cell lines see Appendix. A.15 **C.** Visualization of enrichment results. For statistics see Appendix. A.15 **D.** Heatmap plot by euclidean distance of significant hallmark gene sets in all four cell lines.

Interestingly, MOLM-13 and SKNO-1 cells show opposite enrichment in inflammatory response pathway, reflecting the trend observed in GO analysis and perhaps hinting at a convergence of

two different pathways that lead to the same *PCIF1* proliferation phenotype. The most differentially regulated common sensitive genes according to DESeq2 (FADS2) is included in the bile acid metabolism and cholesterol homeostasis hallmark gene sets, which broadly include genes implicated in lipid metabolic processes (*FADS1*, *FADS2*, *FASN*, *SCD*, *ELOVL5*, *HMGCS1*, *AMACR*, *ABCA1*, *HSD17B6*) through desaturation, lipid transporter or peroxidation activity and inhibition of Sterol Regulatory Element-Binding Proteins (SREBPs) [185, 186].

Overall, analyzing the enriched pathways in sensitive and resistant *PCIF1* KD cells reflected the implications derived from literature behind the common differentially regulated genes.

4.3.1.2 Differential transcript isoform expression analysis of common dysregulated sensitive genes

PCIF1 is responsible for catalyzing the addition of a methyl group on the N6 position of cap-adjacent dimethyladenosine on mRNA [32, 33, 34, 24]. The impact of m6Am on transcriptional rate, mRNA stability, nuclear export and/or translational efficiency is being explored by various groups, but remains contentious. Due to the substrate specificity of PCIF1, it is therefore necessary to inspect the transcription start nucleotide (TSN) of the differentially expressed transcripts (DETs) found in transcriptomic analysis, to determine whether a DET has the potential to be a target of PCIF1.

To assess general presence of transcript variants, the transcript counts output file from the nf-core tool RSEM for isoform expression was analyzed for differential transcript analysis. Figure 4.21 (left) shows the TSN of all commonly differentially expressed genes in sensitive cell lines (A. - SKNO-1 B. - MOLM-13). Performing differential expression analysis on transcript isoforms

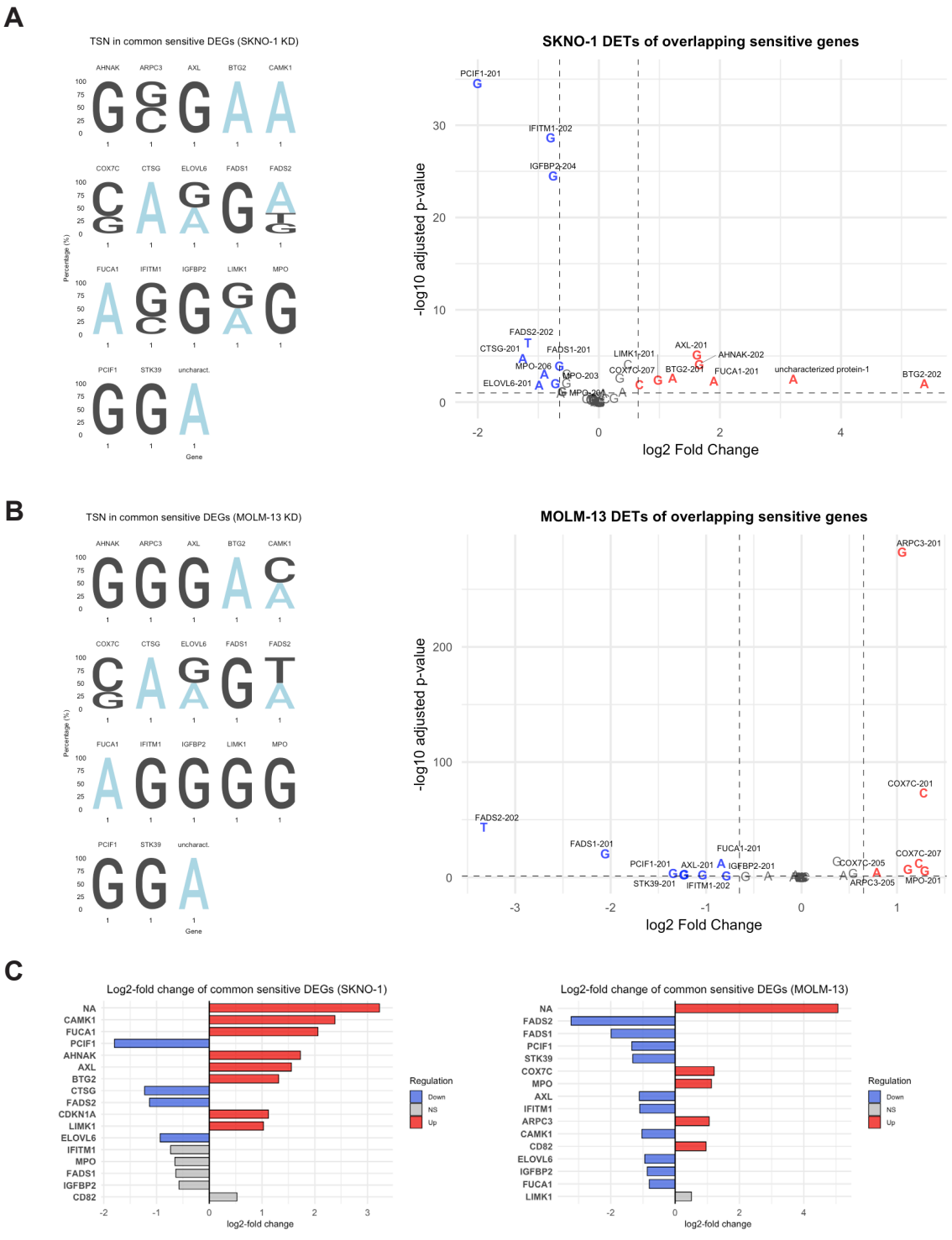

Figure 4.21. Transcription start nucleotide (TSN) analysis of common sensitive differentially expressed genes.

Figure 4.21. (continued) **A.** SKNO-1 and **B.** MOLM-13: left - TSN percent representation of common sensitive DEGs after DESeq2 analysis and right - volcanoplot of l2fc and adjusted p-values of each transcript isoform with TSN notation, showing which isoforms have the highest differential expression. **C.** Ranking of common sensitive DEGs lg2fc for total gene values in SKNO-1 (left) and MOLM-13 (right) cell lines. DEGs with significant adj p-values in only one cell line are shown in grey for the non-significant cell line.

showed that it was not necessarily the transcript isoforms starting with "A" that were driving the total differential gene expression (Figure 4.21 right). Full tables of l2fc and adjusted p-values for each transcript variant are listed in the appendix (A.16). Interestingly, uncharacterized protein coding gene "ENSG00000288841" was upregulated in both sensitive cell lines and ensembl reported the single transcript isoform to start with an "A". SKNO-1 cells also differentially expressed two isoforms of *BTG2* starting in A. *FADS1*, *FADS2*, and *ELOVL6* genes, which were among the most downregulated genes in the sensitive phenotypes, encode transcript isoforms starting in A that showed a decrease in log2FC, making them potential candidates for driving the overall downregulated effect on the gene level (appendix A.15). However, the most differentially regulated transcripts in DET analysis did not show a specific enrichment in A-TSN transcripts, leading to the conclusion that the differential expression of several of the sensitive DEGs is indirectly regulated by *PCIF1* via another mediator, or that the differential effect would be better visualized by analysis of translational efficiency, as suggested by other studies showing that m6Am positively affects translation efficiency [24, 32, 65]. This further underlines that assessing transcriptional changes for *PCIF1* mechanisms is likely not sufficient, since it is just as likely that transcripts in the non-significant, non-differentially regulated gray area of the volcano plots are directly regulated on the translational level by enhancing ribosome occupancy and other translation machinery, and therefore are interesting downstream targets of *PCIF1* without showing it on the transcript level. This rudimentary analysis of TSN in DEGs should therefore be supplemented with polysome profiling

and m6Am sequencing experiments in order to come to a conclusion on the impact of *PCIF1* the expression of these transcripts in AML.

4.3.1.3 Chapter summary and discussion

In chapter 4.3.1, global transcriptomic changes seen upon loss of *PCIF1* were analyzed in sensitive and resistant cell lines, with the aim of identifying pathways that lead to the observed proliferation phenotype.

Bulk-RNA sequencing of *PCIF1* KD AML cell lines revealed a more differentially regulated transcriptome in sensitive MOLM-13 and SKNO-1 cell lines compared to resistant cell lines THP-1 and Kasumi-1. A common set of 20 genes differentially regulated in sensitive cell lines and not in the resistant counterparts was identified and showed that sensitive and resistant cell lines oppositely regulate these. Gene ontology (GO) showed that sensitive cell lines show upregulated terms for stress responses, ROS metabolic processes, phagocytosis, MAPK and NF-kappaB pathways, while downregulating fatty acid and acyl-CoA biosynthetic processes. Importantly, phagocytosis was downregulated in the Kasumi-1 resistant cell line, while THP-1 only showed amide binding as a significant GO term with a count > 0. Interestingly, sensitive cell lines showed opposite regulation of GO terms related to inflammation, which indicates that there may be cell/subtype specific signaling involved. Gene set enrichment analysis not only further validated the difference in inflammatory response, but further focused the results into the downregualtion of three hallmark responses in both sensitive cell lines: mTORC1 signaling, cholesterol homeostasis, and bile acid metabolism. Further analysis into specific subcollections and curated experimental datasets of signatures describing specific chemical or genetic perturbation states would be interesting and

may potentially give rise to a more in depth perspective on specific subsets of these large hallmark sets.

Due to the m6Am catalytic function of PCIF1, the transcription start nucleotides (TSN) of differentially expressed transcripts (and isoforms) observed in bulk-RNA sequencing were cataloged using Ensembl and NCBI RefSeq annotated sequences. Querying aligned transcripts using the Ensembl Biomart provided a fast and straightforward method of TSN calling without the requirement for advanced computational methods or experimentally challenging sequencing methods that would require large amounts of input RNA. However, this is not an optimal approach to assessing TSNs, as it relies on reported sequences across various studies and omits possible TSS-isoforms. Profiling TSNs of DEGs shows that not all differentially expressed genes posses transcript isoforms beginning with A (and therefore are more likely to be m6Am methylated) that are detectable in AML cells, and that different transcript isoforms contribute to the overall gene expression to different degrees. Interestingly, only analysis in the SKNO-1 cell line showed that differential gene expression of *FUCA1*, *BTG2*, and uncharacterized protein ENSG00000288841 were driven by transcription start isoforms encoding adenosine, according to ensembl MANE select annotations. In the downregulated genes of SKNO-1, *ELOVL6* downregulation seemed to be driven by the A-TSN transcript, while the single *CTSG* transcript reported started in A as well.

This part of the analysis constituted an exploration of what was possible to be gleaned from public ensembl data without much cost or extra effort invested into specialized sequencing techniques. However, and in light of evidence presented by the Jaffrey group [69], this analysis is overshadowed by the fact that TSN isoforms are more spurious and plentiful than previously assumed,

are often misannotated and require more sophisticated detection techniques in order to make genuine claims. As outlined previously in the introduction (see chapter 1.1.2), bulk-RNA sequencing does not offer powerful evidence for transcriptional or mRNA stability control of differentially expressed genes. In order to assess transcript stability, experiments involving translation inhibition using actinomycin D followed by qPCR of samples collected over 4-6 hours would help shed light on the rate of degradation of potential *PCIF1* target mRNAs. However, some published studies report no effect on mRNA stability; instead demonstrating an impact on translational efficiency, which would not be quantifiable on an mRNA level. Translational efficiency is better tested by polysome profiling of *PCIF1* KD AML cells, which should be performed in this study to gain knowledge on the translational status of global transcripts. Moreover, these experiments for transcriptional and translational control must be paired with a TSS-m6Am mapping techniques, such as m6Am-exo-seq [24] or CROWN-seq [69], to gain insight on whether identified differentially regulated transcripts indeed are m6Am-methylated.

The transcriptomic analysis therefore illuminates the processes that *PCIF1* KD AML cell lines are undergoing in order to adapt to the genetic perturbation. It is possible that these results reflect indirect rather than directly causal effects of m6Am downregulation. Using MOLM-13 and SKNO-1 overlapping differentially expressed genes generated a focused group that allowed for a detailed literature analysis of these genes in connection to the cancer context, as well as possible links in existing *PCIF1* literature.

Summary of molecular mechanisms associated with the DEGs according to published literature:

Common differentially regulated genes in the sensitive cell lines broadly fell into five (interrelated) categories: genes related to fatty acid metabolism (*FADS1*, *FADS2*, *ELOVL6*), oxidative stress and ROS (*MPO*, *COX7C*, *AXL*), inflammation, chemotaxis and lysosomal maturation (*CTSG*, *IFITM1*, *IGFBP2*, *FUCA1*) membrane-bound ion transporters (*CAMK1*, *STK39*, *AHNAK*), and cell cycle and actin polymerization (*ARPC3*, *LIMK1*, *CDNK1A*, *CD82*).

1. Phagocytosis and inflammation:

MPO and *CTSG* are among the top 12 most enriched genes in the bone marrow (according to The Human Protein Atlas). *CTSG* (Cathepsin G) is a serine protease found in lysosomes and azurophilic granules of neutrophils and plays a role in phagolysosomal host defense mechanism against pathogens [187]. In t(8;21)(q22;q22) (*RUNX1/RUNX1T1*) leukemia, *CTSG* has been found to be specifically repressed by the *RUNX1-RUNX1T1* fusion gene, enabling an escape of the oncogoene from proteolytic cleavage and contribute to leukemogenesis, and its targeted depletion in AML is associated with cell death and differentiation [188]. *MPO* belongs to the class of heme peroxidases and generally resides in granules of neutrophils (commonly) and monocytes (less commonly) [189]. It it responsible for generating hypochlorous acid ($HOCl$) from H_2O_2, hereby creating a highly oxidative environment, leading to stress, lipid oxidation and DNA-damage [189]. *MPO* is often upregulated in cancer, but has shown conflicting results in AML. Kim et al. showed in a retrospective study that *MPO*-low AML was associated a negative prognostic effect, but that *MPO*-high and *MPO*-low allogenic stem cell transplant patient groups showed no significant difference in disease free survival (DFS) [190]. ROS is also associated with chemotherapy resistance in AML and inhibiting *MPO* was seen to render certain AML cell lines sensitive to Cytarabine (AraC) treatment [191]. *IFITM1* belongs to the interferon-inducible transmembrane (IFITM) pro-

tein family and its upregulation has recently been linked as a marker of cytokine release syndrome in CAR-T treated B-cell acute lymphoblastic leukemia patients [192]. However, *IFITM1* expression is also correlated with better survival in high-risk chronic myeloid leukemia (CML) patient groups and improve the phagocytic and anti-metastatic capacity of lung cancer cell lines [193]. The *FUCA1* gene encodes for the α-L-fucosidase enzyme that cleaves the fucose residue from glycoproteins within the lysosome and has been reported as a p53 target with tumor-suppressive functions in ccRCC [194]. α-L-fucosidase deficiency is associated with lysosomal storage defects and neuroinflammation [195]. Induction of the phagolysosome and cathepsin G activity is associated with *MPO* (Myeloperoxidase) and IGFBP2 (Insulin-like growth factor binding protein 2) activity [187, 196, 197].

2. OXPHOS and ROS:

Intracellular ROS is a symptom arising from many different possible pathways, but is generally an indication for cellular stress, lipid peroxidation, and ferroptosis [144]. ROS is also generated as a byproduct of the electron transport chain (ETC) [198, 199]. *COX7C*, a subunit of cytochrome C oxidase complex IV, is responsible the last step of the electron transport chain in which it transfers one electron from cytochrome C to oxygen required for oxidative phosphorylation and the generation of ATP [200, 201]. *COX7C* activity is not directly involved in the generation of ROS. Missense mutations in complex IV are associated with a poor prognosis in AML [202, 203]. p53 has a function in mitochondrial respiration by translocation and activating cytochrome C release during stress-response to trigger the apoptosome [143, 204] and SKNO-1 and MOLM-13 AML cell lines differ in their p53 mutational status (SKNO-1 = mut [125], MOLM-13 = WT, [124]), which may explain some of the differences of in DEGs upon *PCIF1* KD. Major signaling path-

way mediator *AXL*, a receptor tyrosine kinase, was differently regulated between sensitive *PCIF1* knockdown cell lines (up in SKNO-1, down in MOLM-13). *AXL* has been connected to increased *BCL2* expression in adult de-novo leukemia [205], and is more highly expressed in in *KMT2A* rearranged and/or *FLT3*-ITD AML compared to non-*KMT2A* rearranged AML [206, 207]. *AXL* signaling activates pro-proliferative pathways as well as migratory and cell differentiation pathways, and has additionally been linked to be activated by hydrogen peroxide in vascular smooth-muscle cells [207, 208]. Controversial roles of ROS, either as signaling for proliferation and hijacked for cancer cell function, but too much can also trigger macromolecular damage, cell senescence and death [198, 209]. In *PCIF1* sensitive KD cell lines, Gene Ontology terms related to responses to chemical stress and ROS are upregulated while GSEA analysis shows mTORC1 downregulation. The mTOR pathway plays a complex role in oxidative stress, but has been shows to induce ROS by changing mitochondrial metabolism, intracellular GSH synthesis and concentration as well as prevent the activation of ROS inhibitors [210]. Cancer cells are known to upregulate ROS in order to accommodate for their increased need in nutrients and redox imbalance is also defined as a cancer hallmark [6, 210]. More research is required to untangle the complex interplay between mTORC1 and ROS, although recent developments have seen mTORC1 influence on *FADS2* activity in cancer (expanded on in subsequent paragraphs).

3. Ion transport and membrane trafficking:

Ion transport across organelle membranes plays an important role in intrinsic apoptosis. *AHNAK*/desmoykin is a large scaffold protein that was identified to function as an important calcium channel in T-cell function, enabling calcium ion influx and IL-6 secretion in CD4+ T-cells [211, 212, 213]. In triple-negative breast cancer, *AHNAK* has been identified to have tumor sup-

pressor role [214], but is associated with more severe disease outcomes in PDAC and HCC [215], therefore conveying context specific functions in different cancers. Serine/threonine kinase 39 (*STK39* or *SPAK*) has been shown to be upregulated in AML patients and its downregulation leading to decreased proliferation of AML cells [216]. *STK39* is also implicated in pathological hypertension through phosphorylative activation of ion co-transporter *SLC12A1* [217]. *STK39* is activated by hypotonic stress response and phosphorylates Na-K-Cl cotransporters activating ion influx and blocking other cotransporters to block ion efflux [218]. *AHNAK* ability to trigger calcium ion influx, may activate calmodulin and calmodulin dependent kinases, such as *CAMK1*, which is positively regulated in SKNO-1 cells. *CAMK1* is a ser/thr kinase activated by calcium influx and has been linked to support AML stem-cell self renewal [219]. Calcium sensors have been shown to tightly regulate actin nucleators responsible for actin filament formation [220].

4. Actin polymerization and cytoskeleton:

A subset of common differentially regulated genes between the two sensitive cell lines were *ARPC3*, *LIMK1*, and *CDNK1A*, which are implicated in cytoskeleton maintenance [221, 222, 223]. *ARPC3* constitutes a subunit of the ARP2/3 complex that facilitates actin polymerization and macrophage integrin function [224]. ARP2/3 activity is regulated by Rho GTPase G-protein *RAC1* and intermediate signaling proteins to trigger migration, lamellipodia formation, endocytosis, adherence and intracellular trafficking [221]. The complex signaling cascade confers functions in many different cell types and contexts. Stabilized actin translates to the mitochondria to induce apoptosis. *RAC1* (and Cdc42) also activate *LIMK1* via p21-activated kinases (PAK). The serine/threonine kinase *LIMK1* is involved in actin filament processes through its ability to phosphorylate cofilin, hereby abolishing cofilin's actin depolymerization function [225, 222]. In AML,

LIMK1 carries a negative correlation with patient survival and its knockdown was found to induce the expression of tumor suppressor *BTG2* and decrease colony forming capacity of *FLT3*+ ITD mutant AML cell line MOLM-13 [226, 222]. Furthermore, small-molecule inhibition of *LIMK1* synergized with *FLT3* inhibitor treatment, highlighting *LIMK1* as a potential therapeutic target [227]. B-cell translocation gene 2 (*BTG2*) is a known tumor suppressor in B-cell leukemia and solid tumors [228]. Its activation by p53 and p21, as well as oxidative and genotoxic stress response genes triggers mRNA polyA-tail deadenylation and global reduction of protein translation, resulting in an anti-proliferative effect [228, 229]. It is interesting that *ARPC3* and *LIMK1* are regulated differently in each sensitive cell line, perhaps providing two different pathways of actin stabilization. The observation made in a previous study linking *LIMK1* expression with the down-regulation of tumor suppressor *BTG2* was not mirrored in this thesis' RNA-seq results, where both genes seemed to be upregulated in *PCIF1* KD SKNO-1 cells, perhaps hinting that the regulation of both factors is not necessarily correlated. A recent piece of work postulated that *BTG2* is regulated by *RUNX1C*, a TF that is differentially expressed across AML cell lines and which SKNO-1 cells have a *RUNX1*::*RUNX1T1* (loss-of-function) mutation [230]. *CDNK1A* (cyclin-dependent kinase inhibitor 1A) gene encodes for p21 protein, which is controlled by the p53 pathway and inhibits cell cycle progression through G1. *CDKN1A* in disease is associated with upregulated macrophage phagocytosis by transcriptional repression of *SIRP1*α [223] and positively regulated lipid oxidaiton and free fatty acid uptake in metabolic dysfunction-associated steatotic liver disease [231]. *CD82* was originally identified to have metastasis suppressive functions in solid tumors through its canonical integrin biding function to maintain cell shape and enable cell adhesion [232, 233]. In leukemia, *CD82* activation triggers many signaling cascades that are a part of the

tetraspanin microdomain signaling hub, which has been associated with leukemic stem cell functions in pediatric leukemia [234].

5. Lipid metabolism and unsaturated fatty acid biosynthesis:

Fatty acid desaturase 1 and 2 (*FADS1* and *FADS2*), as well as elongase of very long-chain fatty acids 6 (*ELOVL6*) are involved in polyunsaturated fatty acid synthesis and are commonly downregulated in sensitive *PCIF1* KD cells, while upregulated in the resistant cells. *ELOVL6* is the rate-limiting enzyme in the synthesis of very-long chain fatty acids (VLCFA), both saturated and monounsaturated. It is responsible for catalyzing the addition of two carbons to palmitic acid (C16:0) and palmitoleic acid (C16:1, monounsaturated) to elongate them into stearic acid (C18:0) and oleic acid (C18:1), respectively [235]. There are seven different human ELOVL enzymes that are involved in elongating fatty acids and each have their own very specific substrate and tissue expression [235, 236](see Figure 4.22A). *ELOVL6* is ubiquitously expressed across tissues, but especially enriched in lipid-rich tissues (liver, adipose tissue, brain) and its expression is induced by ChREBP and SREBP transcritpion factors, which are sensitive to changes in cellular glucose and insulin levels [235, 236, 237]. In the context of disease, *ELOVL6* has been found to be overexpressed in type-2 diabetes and mediate insulin resistance, [238], have a negative clinical factor in operable breast cancer patients [239], promote demyelination and an inflammatory phenotype in multiple sclerosis (MS) [240], promote fatal ROS lipid peroxidation / ferroptotic cell death partly via *ACSL4* signaling in apatinib treated colorectal cancer (CRC) [241], and show upregulation in acute myeloid leukemia, with a case report detailing a rearrangement t(4;16)(q25;q23.1) [242]. Furthermore, *ELOVL6* knockout decreased the hematopoietic stem cell engraftment and leukemic potential of mouse BM (and *MLL::AF9* transduced BM cells) via impaired *CXCL12*-PI3K-*Rac1*

cytoskeletal remodeling [243]. Fatty acid desaturase 1 and 2 are involved in catalyzing the double bond in long chain fatty acids to generate poly-unsaturated fatty acids (PUFAs), which are long chain fatty acids with two or more double bonds. Their substrates, linoleic acid (LA, C18:2) and α-linoleic acid (ALA, C18:3) are derived from essential dietary omega-6 and omega-3 fatty acids that cannot be synthesized de novo, although plants have Δ-12 desaturase and Δ-15 desaturase and can convert oleic acid (OA,C18:1) into LA and ALA [244]. *FADS2* has an equal affinity for LA and ALA to catalyze the synthesis of a double bond at position 6 to generate γ-linoleic acid (GLA) and stearidonic acid (SDA, which are both further elongated by *ELOVL5* before *FADS1* catalyzes the addition of a double bond at position C5 to create arachidonic acid (ARA or AA) and eicosapentanoic acid (EPA), and finally conversion into docosapentaenoic (DPA) and docosahexaenoic acid (DHA). These PUFAs provide glycerophospholipids and sphingolipids for cell membrane, as well as signaling molecules in various cellular responses. In membrane contexts, double bonds in the fatty acid chains generate "kinks" in the FA tails that bestow increased fluidity upon the membrane [245]. The increased presence of saturated fatty acids in the cell membrane is associated with chemoresistance, based on the premise that saturated fatty acid phospholipids in the membrane bilayer being less susceptible to ROS and oxidative stress by inducing membrane rigidity and mobilize machinery for molecule efflux [185, 246]. Conversely, multidrug resistance in cancer has also been associated with MUFA and PUFA increase [247]. However, a recent study in pancreatic cancer show that specific PUFAs as well as the cellular context impact the cell response, meaning that chemoresistive potential does not increase proportionally with double bond number [248]. PUFA intermediates also provide the precursors for leukotrines and prostaglandin inflammatory signaling molecules.

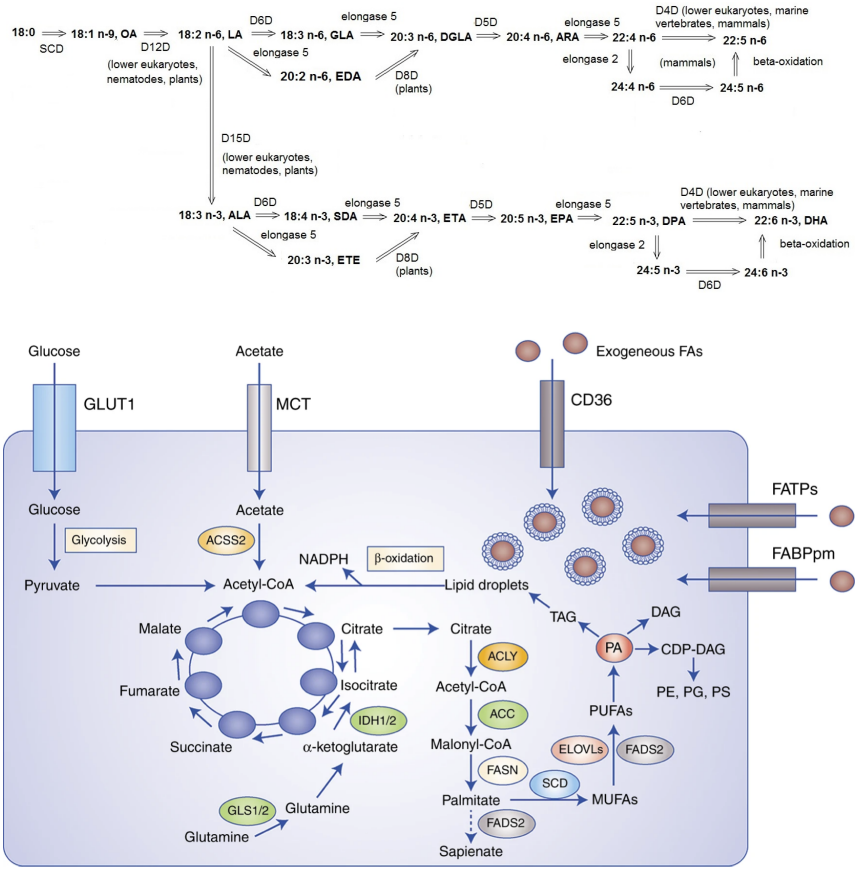

Figure 4.22. Overview of fatty acid desaturation process. **A.** Omega-6 and Omega-3 fatty acid desaturation process (poly-unsaturated fatty acid (PUFA) biosynthesis. Figure source: [249]. **B.** De novo lipogenesis pathways are enhanced in cancer cells to serve proliferative purposes. Figure source: [250]

Maintaining the optimal balance of saturated. mono- and poly-unsaturated fatty acids is important for maintaining cellular homeostasis and cancer cells often hijack these pathways to provide the basis for chemoresistance, inflammation or a metabolically more favorable environment see Figure 4.22B). *FADS2* has recently been discovered to posses de-novo mono-unsaturated fatty acid biosynthesis capabilities, which had previously been ascribed only to Steroyl-CoA desaturase (Δ9D), and can co-opt oleic acid from SCD to produce sapienate, a C16 fatty acid and usually only observed in sebocytes [251]. The fatty acid pool is therefore a lot more dynamic than initially supposed and minor changes to the balance within the cell, or yet to be discovered alternative metabolic pathways in cancer, contributing to the malignancy of the disease [252]. It has been proven that fatty acid desaturation processes may play important roles in various cancers, including leukemia, where leukemic stem cells harvested from relapsed AML patients were shown to rely on fatty acid metabolism [253, 254] and that pharmacological inhibition of *FADS1* and *FADS2* in therapy resistant AML cells decreases the citric-acid cycle metabolism and resensitized them to Ven/Aza treatment [255]. Furthermore, it has been shown that *FADS2* sapienate biosynthesis activity is regulated by *SREBP*-1 and *SREBP*-2 and mTOR signaling in mouse embryonic fibroblasts as well as glioblastoma cells, and that *FADS2* activity and substrate affinity is highly tumor context as well as FA profile dependent [186, 256].

This shows that cancer cells adopt a plethora of different tools to gain metabolic plasticity, enabling superior growth and chemoresistance, and that the uniform downregulation of fatty acid metabolism genes seen in both sensitive cell lines indeed has a physiological connection to inflammation, oxidative stress and apoptosis seen in the panel of differentially expressed genes, albeit SKNO-1 and MOLM-13 cell lines seem to oppositely regulate some genes (see Figure 4.18

F: *AXL*, *FUCA1*, CAMK1).

4.3.2 Preliminary investigations of reactive oxygen species and poly-unsaturated fatty acid biosynthesis pathways in *PCIF1* KD AML cell lines

Reactive oxygen species:

Results from GSEA imply that the reactive oxygen species metabolic process is dysregulated upon *PCIF1* KD. As discussed, mTORC1 is implicated to influence the accumulation of levels of reactive oxygen species (ROS) through regulation of mitochondrial metabolism. The DCFDA (2',7'-dichlorodihydrofluorescein) assay, which is based on oxidation of DCFDA by ROS inside the cell to emits fluorescence that can be detected in microplate readers and flow cytometry, was used to detect the levels of intracellular ROS [257]. In addition, TBHP (tert-butyl hydroperoxide) ROS inducing agent treatment for one hour was performed in parallel and served as a positive control for the experiment (see Appendix A.18A).

DCFDA fluorescent measurement showed that at least one of the *PCIF1* KD conditions upregulated intracellular ROS in SKNO-1, MOLM-13 and U937 cell lines (Figure 4.23A). The positive control induced ROS in all cell conditions and the difference was the greatest in U937 treated vs untreated cells (see Appendix A.18A), and *PCIF1* knockdown cells also showed higher levels of compared to the shSCR under treatment (Figure 4.23B). Interestingly, ROS levels were shown to be increased no matter the sensitivity phenotype of the cell line. Further replicates and experiments investigating intracellular levels of different ROS will be necessary in order to validate the ROS effect.

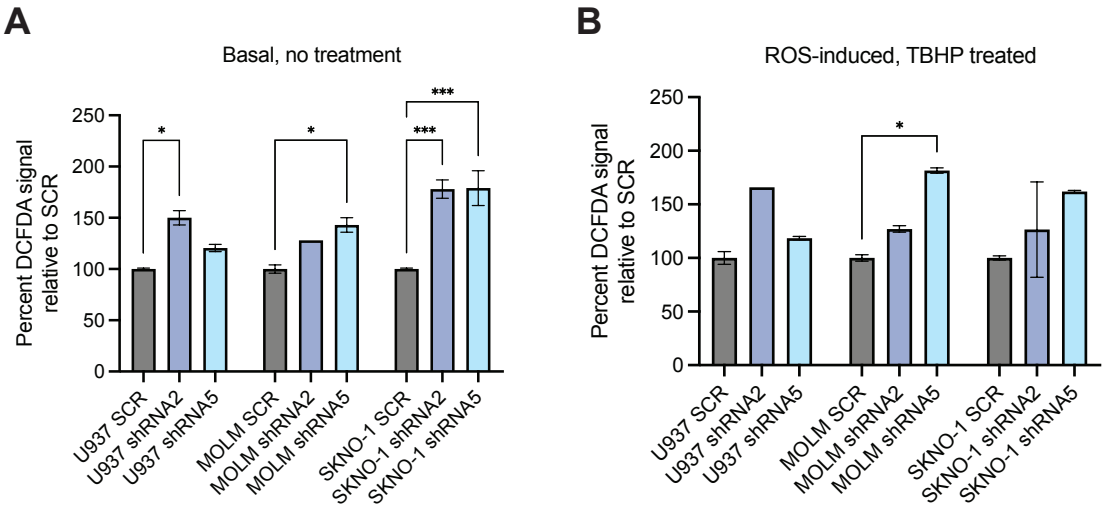

Figure 4.23. Reactive oxygen species are elevated in SKNO-1 *PCIF1* KD cells. The cellular redox state of *PCIF1* KD cell lines was measured using DCFDA assay kit. **A.** Cells were stained with DCFDA for 30 minutes, seeded in 96-well plates and positive control wells **B.** treated with 20 µM TBHP (tert-butyl hydroperoxide) for 1 hour to induce oxidative stress in each condition. Bars represent means ± SEM of n=2 (technical) replicates, statistical significance tested with ANOVA and Holm-Sidak post-test: *P < 0.05; **P < 0.01; ***P < 0.001.

It is worth noting the limitations of the DCFDA assay: while it is one of the more common approaches for measuring ROS and the methodology is straightforward using commercially provided kits, the probe is not selective for a specific species of reactive oxygen and may omit signal from other ROS forms and the assay can be influenced by local O_2 levels and pH [258]. Therefore, follow up with more rigorous tests for specific ROS species in additional replicates would be necessary to consolidate this ROS phenotype.

Fatty Acid Metabolism:

As previously highlighted, fatty acid metabolism is known to play a role in PI3K/Akt/mTOR signaling, ROS pathways, as well as inflammatory potential of cancer cells. Additionally, the primary fatty acid desaturase and elongase enzymes were most obviously differentially regulated across both cell lines, generating a hypothesis that they could be crucial in regulating the sensitive pheno-

type seen upon *PCIF1* knockdown. Multiple lines of investigation into fatty acid metabolism were launched. Firstly, as *FADS1*, *FADS2* and *ELOVL6* were not commonly significantly downregulated in THP-1 and Kasumi-1 cell lines, it was investigated whether deliberate pharmacological inhibition of these enzymes in the *PCIF1* KD background would generate a sensitive phenotype in the primarily resistant cell lines. Secondly, supplementation of the fatty acid intermediates of *FADS1*, *FADS2* and ELOV6 in cell culture media was performed to answer whether the proliferative defect in *PCIF1* KD cells would be ameliorated or rescued.

FADS1 and *FADS2* mRNA expression was assessed in additional biological replicates to confirm that this differential regulation was not an artifact in the populations for which RNA-sequencing libraries were prepared (Figure 4.24A-B). Indeed, in the sensitive phenotypes, *FADS1* and 2 were consistently downregulated across replicates, however the expected upregulation of these transcripts in the resistant knockdowns was not as consistent and prominent across shRNAs as RNA-seq euclidian clustering of differentially expressed genes (see 4.18E) made it seem. Transcript level expression was probed with polyclonal antibodies against regions of *FADS1* and *FADS2* in western blots (Figure 4.24C). Detection of *FADS2* and *FADS1* signal was challenging due to suboptimal signal and antibody optimization is therefore ongoing, however, preliminary results indicate no obvious change in FADS1/2 protein levels. Basal WT transcript expression of PCIF1, *FADS1*, and *FADS2* was assessed using data from the LL-100 project in the visualization tool offered by the cell line repository (The Leibniz Institute DSMZ [176]) and showed that *PCIF1* expression seemed to be positively associated with FADS1/2 expression in the five cell lines used in this work (Figure 4.24D). A similar analysis was performed on the protein level in wildtype AML cell lines queried as part of the DepMap portal and showed a non-significant association

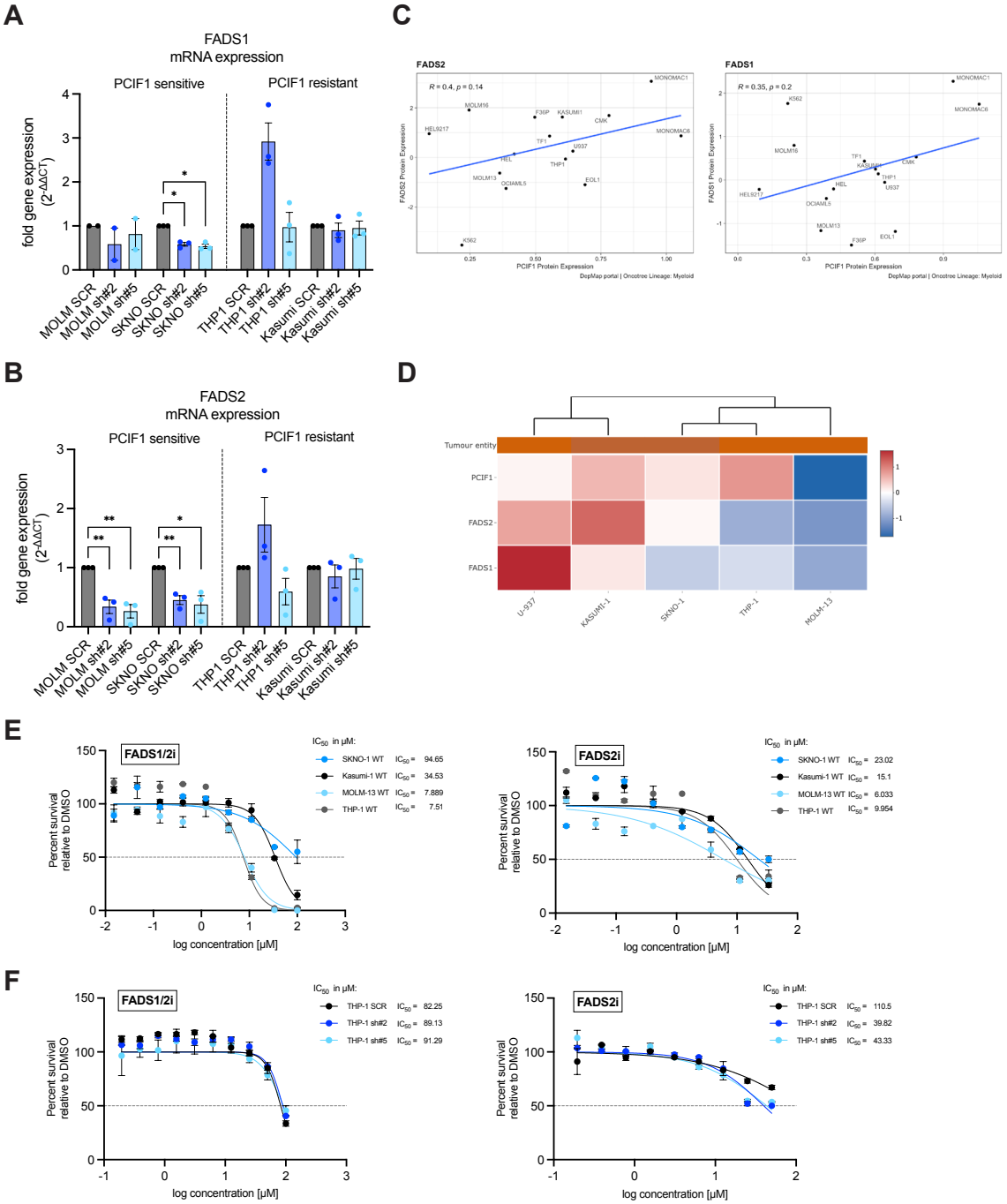

Figure 4.24. Fatty Acid Desaturase 1 and 2 (*FADS1* and *FADS2*) expression in AML cell lines and viability upon inhibition.

Figure 4.24. (continued) qPCR analysis of MOLM-13, SKNO-1, THP-1, and Kasumi-1 scramble and knockdown cell lines for the expression of **A.** *FADS1* and **B.** *FADS2* mRNA expression. Bars representing means ± SEM of n=2-3 biological replicates, asterisks two-tailed unpaired t-test *P < 0.05; **P < 0.01; ***P < 0.001. **C.** Association trend plots of *PCIF1* expression vs protein expression of different DEGs observed from RNA-seq (continued in appendix A.17). **D** Euclidean clustering of RNA-seq expression of *PCIF1* and sensitive DEGS *FADS2* and *FADS1* in WT AML cells. Data generated using DSMZCellDive [176] from the LL-100 sequencing project. **E.** IC50 dose-response curves in WT AML cells for *FADS1/2*i (left) and FADS2i (right). Dots represent average viability (assessed by CTG after 48h) of ± SEM of n=2 technical replicates **F.** IC50 dose-response curves in THP1 *PCIF1* KD AML cells. Dots represent average viability of ± SEM of n=2 technical replicates.

between *PCIF1* and DEG expression (Figure 4.24E). *ELOVL6* did not follow a similar pattern in WT AML cell RNA and proteomics data from the DSMZ and DepMap Portals, respectively (see Appendix A.17).

This data shows that *FADS1* and 2 are more consistently downregulated in *PCIF1* sensitive knockdown cells and may be the driving factor behind cell line specific sensitivity to loss of PCIF1. Inhibitors for fatty acid desaturase 2, as well as an inhibitor that targets both 1 and 2, are commercially available and were tested in IC50 dose-response curves in four of the WT AML cell lines used for this thesis to shed light on any subtype or cell line specific effect upon inhibition of these players that mirrored that seen for *PCIF1* (Figure 4.24F). Unfortunately, these inhibitors showed a poor dosage profile, requiring concentrations in the micromolar range to show a decrease in cell viability. In light of this, it can only be cautiously surmised that WT cell lines of the *KMT2A*::*MLLT3* subtype (ie MOLM-13 and THP-1 WT) seem to have a 5x lower IC50 compared to the *RUNX1::RUNX1T1* subtype. The question whether inhibition of fatty acid desaturase activity would have a greater effect on *PCIF1* KD resistant cell lines, tipping them into a sensitive phenotype, was tested by performing the dose-response assay in THP1 *PCIF1* KD cell lines (Figure 4.24G). Keeping in mind the suboptimal in vitro concentration profiles of these inhibitors, it seems that *PCIF1* KD cells may indeed show higher sensitivity to inhibition of *FADS2*. These

experiments are currently being repeated for validation, in addition to genetic knockdown and proliferation assays of the fatty acid desaturases, which will circumvent the dosage issues encountered with the inhibitors.

Due to the suboptimal dosage and potential risk of unspecific interaction of the small molecule inhibitors against FADS1/2 and FADS2, a genetic knockdown using shRNA sequences taken from TRC specific for *FADS1*, *FADS2*, and *ELOVL6* were cloned into the lentiviral pLKO.1 vector [136]. Cell lines that showed sensitivity (MOLM-13) or resistance (U937 and THP-1) to PCIF1 depletion were infected with lentivirus targeting the fatty acid metabolism genes under the same protocol as for shRNAs targeting *PCIF1*, selected with puromycin and assessed for potential proliferation defects that mirror the phenotype seen with PCIF1. qPCR analysis of FADS1 shRNAs showed shRNA#2 resulted in an approximately 70% depletion of *FADS1* transcript in both U937 and MOLM-13 cell lines, shRNA#3 only achieved a good knockdown in the MOLM-13 but not U937 cell line (Figure 4.25A). Cell-TiterGlo experiments performed after cells had recovered from puromycin selection showed that cell lines resistant to PCIF1 depletion were overall also resistant to FADS1 depletion and MOLM-13 cells, which were sensitive to PCIF1 depletion, depleted of FADS1 were less viable (shRNA#3) or not viable at all (shRNA#2) (Figure 4.25B). However, MOLM-13 FADS1 shRNA#2 populations were not viable enough to yield suitable amounts of RNA for qPCR analysis and it can therefore only be speculated that the cell death stemmed from depletion of FADS1. MOLM-13 FADS1 shRNA#3 cells showed a 50% reduction in proliferation over 7 days. For FADS2 knockdown AML cell lines, MOLM-13 cells of either shRNA did not recover, wheras PCIF1 resistant cell lines again also proliferated well under FADS2 knockdown (4.25C). Similarly, MOLM-13 cells did not yield good amount of RNA for qPCR and thus only

the knockdown levels assessed for U937 can be used as reference to assess knockdown in sensitive cell lines. In MOLM-13 cells infected with shRNA for ELOVL6, cells recovered and showed adequate levels of knockdown and a slight decrease in proliferation over three days after the end of selection (Figure 4.25E), but recovered more two weeks after selection ended and proliferated similarly to the scrambled control (data not shown). Thus, judging by these preliminary results from depletion of few of the topmost hits from the RNA sequencing, MOLM-13 cell lines also seem dependent on intact FADS1, FADS2, and ELOVL6. These genes could be driving the proliferation defect seen upon PCIF1 depletion in sensitive cell lines and are interesting targets for further investigation, even though further repeats as well as follow up in the sensitive SKNO-1 cell line is still warranted to consolidate this finding.

The question of fatty acid metabolism involvement in *PCIF1* KD effects was then approached from the an angle of rescue, instead of inhibition, of possible downstream *PCIF1* targets. Therefore, downstream metabolites of the omega-3 and omega-6 desaturase pathways, which *FADS1*, *FADS2*, and *ELOVL6* belong to, were supplemented in complete medium and cell viability assessed with CellTiter-Glo over 8 days. Omega-6 (linoleic acid - LA) and omega-3 (α-linoleic acid - ALA) fatty acids (FA) belong to the family of essential FAs that cannot be de novo synthesized in homo sapiens and must be consumed in a balanced diet [236, 245]. The first step after entry into the cell involves *FADS2* (otherwise known as Delta-6 Desaturase, *D6D*) catalyzing a double-bond in the long fatty acid chains and subsequent elongation to produce the substrates for *FADS1* (also *D5D*), which produces arachidonic acid (ARA) and eicosapentaenoic acid. *FADS2* reenters the reaction cascade in the last step prior to beta-oxidation to catalyze an additional double-bond to generate poly-unsaturated fatty acids (PUFAs) that can be stored in lipid droplets or readily used

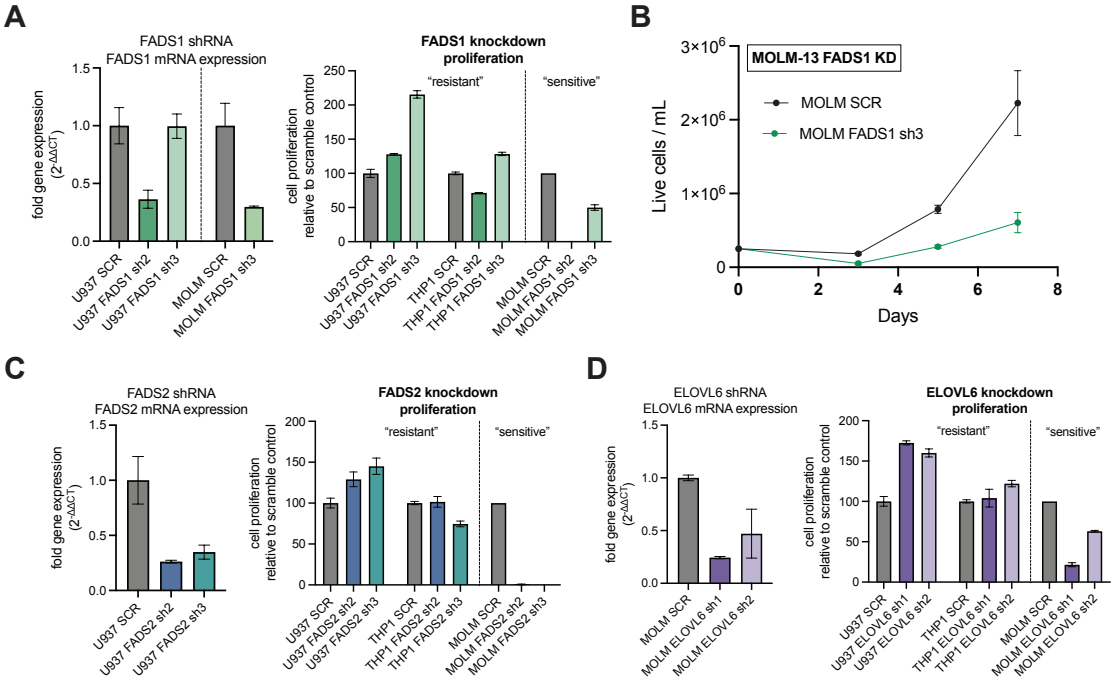

Figure 4.25. shRNA mediated knockdown of FADS1, FADS2, and ELOVL6. **A.** qPCR analysis of FADS1 knockdown efficiency in U937 and MOLM-13 cells and cell proliferation relative to the shRNA scramble control of the same cell line over three days, directly post recovery from selection. **B.** 7-day live cell counting assays using trypan blue of the only viable shRNA population of FADS1 knockdown in MOLM-13 cells. **C.** qPCR analysis of FADS2 knockdown efficiency in U937 cells (MOLM-13 population did not recover to levels fit for RNA extraction) and cell proliferation relative to the shRNA scramble control of the same cell line over three days. **D.** qPCR analysis of ELOVL6 shRNA knockdown efficiency in MOLM-13 cells and cell proliferation relative to the shRNA scramble control of the same cell line over three days. Error bars represent ± SEM of n=3 technical replicates. Preliminary data, one independent experiment.

for catabolic breakdown for acyl-CoA generation, which can enter the TCA-cycle to produce ATP required for cancer growth. Besides this classic fatty acid pathway, *FADS2* has recently been identified to be able to desaturate palmitate to generate sapienate, a fatty acid that had been associated with presence in sebaceous cells, and is co-opted as an alternative metabolic pathway in some cancers [251]. Furthermore, positive regulation of the mTORC1 pathway has been shown to drive *FADS2* sapienate biosynthesis processes [256].

Thus, it was hypothesized that, with the downregulation of these fatty acid desaturases and elongases, AML cells are deprived of essential metabolites from the omega-6 and omega-3 fatty acid pathways and are unable to proliferate as a result of metabolite deprivation. Experimental conditions to test this required optimization of concentrations and BSA conjugation ratios. Not only are fatty acids challenging to maintain in cell culture media due to their inclination to oxidize, but the method of uptake into cell lines requires optimization of the BSA (bovine serum albumin) to FA ratio [259, 260]. Excessive concentrations of fatty acids or BSA can trigger inflammatory responses and cell death. This experiment was therefore performed at four different concentration in two different molar ratios of FA:BSA (3:1 and 6:1) each, with addition of fresh FA:BSA media every 2 days, and assessed for viability over the course of 8 days after cells recovered from infection and puromycin selection, which is when their peak proliferative defect was observable. Shown in Figure 4.26A are the results of AA, EPA, PA, GLA, SDA supplementation, as well as the BSA vehicle control, in MOLM-13 *PCIF1* knockdown cell lines normalized to the scramble control, while Figure 4.26B shows the same experiment normalized to the BSA vehicle control.

Tracking the *PCIF1* proliferative defect over 8 days with an without FA revealed that cell viability

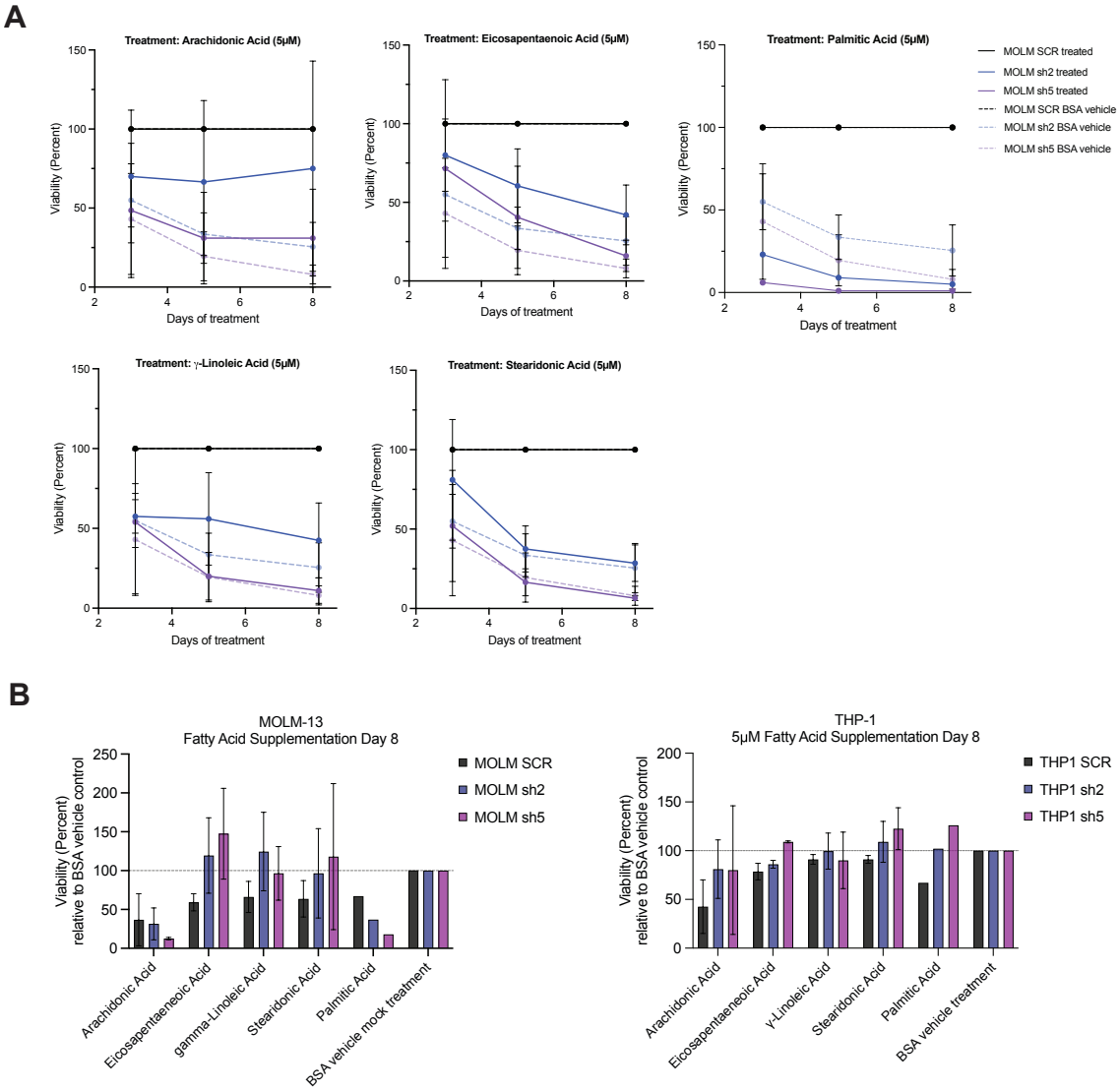

Figure 4.26. Proliferation analysis of fatty acid desaturase pathway intermediate metabolites supplementation in media (CellTiterGlo). **A.** Viability of MOLM-13 *PCIF1* knockdown cell lines with AA, EPA, GLA, SDA supplementation, as well as the BSA vehicle control (dashed line in each graph), normalized to the scramble control over 8 days assessed with CTG. Data representing mean ± SEM of n=2 biological replicates. **B.** Viability of MOLM-13 and THP-1 *PCIF1* knockdown cell lines supplemented with AA, EPA, PA, GLA, SDA, on Day 8, normalized to BSA vehicle control. Data representing mean ± SEM of n=2 biological replicates.

still decreases over time in the KD population in all treatments, but potentially at a slower rate in the EPA treated populations compared to the BSA vehicle control. While the effects seen in both independent replicates, was the same, there were significant fluctuations in cell viability at identical time points, which is likely due to unconscious differences in infection, selection and culture procedures leading up to and during the FA supplementation experiment itself. Although treatments with AA seem to pause the proliferative defect from day 5-8, it is important to contextualize the shRNA-SCR normalized results in 4.26A with the vehicle normalized results in 4.26B, which will reveal that on day 8, AA-treated scramble cells showed less than 50% viability compared to their BSA-mock treated counterparts, meaning that proliferation was comparable to the knockdowns and would lead to a false positive when comparing the different *PCIF1* states only. Interestingly, the *PCIF1* KD THP-1 cells also proliferated better in FA containing medium compared to their BSA vehicle counterpart, but their viability slowly decreased over time (with the exception of AA) compared to the scramble, possibly because of chronic FA overload and FA-related inflammation and lipid peroxidation (Figure 4.26 and appendix A.18).

Overall, the FA supplementation experiments replicate the complex metabolic niches that each intermediate has the potential to fill. Free arachidonic acid has been shown to be toxic in many culture conditions due to its contribution to prostaglandin and leukotrine synthesis [261]. Whether eicosapentaenoic acid is truly able to counteract the effects *PCIF1* can only be tentatively proposed, as fatty acid experiments are challenging and the effects observed were not as akin to a rescue as it would be expected. However, this could still be biologically relevant, even though the experimental process requires optimization to fully appreciate this. Furthermore, the role of *FADS2* in the biosynthesis of sapienate and mTOR dependent *FADS2* regulation is published and

being investigated to have a role in cancer metabolism switching. Preliminary results using sapienate in the cell culture medium however do not convincingly show a rescue effect that would support this hypothesis in the context of PCIF1. Validation of hits from the RNA-seq data by shRNA knockdown show that MOLM-13 cells, which are sensitive to PCIF1 depletion, also have decreased proliferative capacity, while U937 and THP-1 cells, which are resistant to PCIF1 depletion, do not seem impacted by knockdown of fatty acid desaturase enzymes.

4.3.2.1 Chapter summary and discussion

It is important to acknowledge that, at this point in the project, the lipid profile of *PCIF1* knockdown cells has not yet been assessed. Therefore, the hypothesis regarding the influence of polyunsaturated fatty acids in driving the sensitivity phenotype cannot be verified until lipidomics have been performed. Aspects that prevented this to be performed for the completion of this thesis were related to time and cost constraints considering extensive optimization of lipid extraction protocols that would be necessary for high quality readouts.

In this last chapter, we identify multiple fatty acid and ROS metabolism genes, to be affected by *PCIF1* KD in sensitive cells. This could be explained by downregulation of mTORC1 signaling, as research has shown that mTORC1 signaling activates SREBP binding of *FADS2* genes and promotes sapienate biosynthesis [256, 262]. mTORC1 is an important regulator of cell growth and lipid metabolism is regulated by many different factors, most prominently the PI3K/Akt/mTOR pathway, but also nutrient levels, where low levels of AMPK inhibit mTORC1, as well as ROS, although this regulation is still less well understood [256, 263]. To confirm this pathway, the downregulation of mTORC1 will need to be validated by examining the activation / phospho-

rylation of S6, S6K1, and eukaryotic translation initiation factor 4E-binding protein 1 (4EBP1) phosphorylation in *PCIF1* KD cell lines [256]. Important in the context of PCIF1, the TSS nucleotides for differentially expressed transcripts were cataloged and transcript isoforms starting in A were not seen to be significantly lost or gained in differential expression analysis upon loss of PCIF1. m6Am-exo-seq or CROWN-seq will be performed to generate a transcriptome-wide map of m6Am levels on transcription start nucleotides. We validated the increase in cellular stress and ROS levels by measuring DCFDA dye fluorescent signal in *PCIF1* knockdown cells, which showed mild levels of upregulation even in resistant cell lines. It could therefore follow that ROS upregulation is either better tolerated by the resistant cells, or they show lower ROS compared to other sensitive cell lines. The precise regulation of ROS in cancer is complex and the terms "Goldilocks zone" or the metaphor of a double-edged sword have been used to describe its implications in cancer; too little may not be beneficial to cell metabolism, while too much may trigger mitochondrial stress and apoptosis. Supplementation of certain fatty acid metabolites in culture media of *PCIF1* knockdown cell lines did not seem to significantly rescue the proliferation phenotype, however, the role of *FADS2* in sapienic acid biosynthesis was not considered in the "feeding" experiments, which is currently being rectified.

Overall, the transcriptomic analysis of differential pathways in sensitive versus resistant *PCIF1* knockdown cell lines sheds light on interesting potential follow-up experiments to uncover the reason behind the phenotypic effect of *PCIF1* on some AML cell lines. Future work could involve investigating a regulatory effect of *PCIF1* on the mTOR/SREBP/*FADS2* axis, as well as investigate the effect of ROS in this context in more detail.

5 | Discussion, limitations and future directions

5.1 Summary of key findings and discussion

In this work, we investigated the role of the writer of methylated adenosine, *PCIF1*, in the context of Acute Myeloid Leukemia. We started by examining *PCIF1* expression in public datasets of cancer cell lines and AML patients, and found that *PCIF1* protein expression is upregulated in cell lines of the myeloid lineage and in TCGA AML vs GTEx healthy whole blood samples. In comparison to other cancers, patients of the TARGET AML cohort, especially the induction failure subproject, show higher *PCIF1* mRNA expression. In the Beat-AML study, patients of the *CEBPA* and *NPM1* mutant subtypes with upregulated *PCIF1* had a worse prognosis than patients belonging to the same subtypes with low *PCIF1* expression. This chapter concluded that, although AML does not show significant differential expression or patient survival in the context of *PCIF1*, investigating disease subtypes as well as different cancer studies may yield specific associations between *PCIF1* and prognosis. In work included in the next chapter, we found that in vitro depletion of *PCIF1* resulted in a proliferation defect, but only in MOLM-13 (*KMT2A::MLLT3*) and SKNO-1 (*RUNX1::RUNX1T1*) AML cell lines. We further show that sensitive cell lines have increased annexin-V and caspase 3/7 activation, as well as upregulated morphological signs as well as cell surface markers of monocytic differentiation. It was concluded that this effect is unlikely to be driven by the cytogenetic subtype, since the resistant THP-1 and Kasumi-1 cell lines have a similar mutational landscape to the sensitive cell lines. Importantly, there are additional differences, such as *FLT3*-ITD and p53 status between resistant cell lines and sensitive counterparts, which may contribute significantly to the phenotype. Thus, while we revealed that *PCIF1* must

play an important role in leukemic maintenance, we were not able to define a pattern that may rationalize why certain subtypes are sensitive, although more experiments are currently underway to gain more insight into *FLT3*-ITD mutations contributing to the phenotype.

In the final chapter, the transcriptomic landscape of *PCIF1* knockdown cell lines was assessed using bulk-RNA sequencing, which revealed that sensitive cell lines downregulate gene sets involved in the mTORC1 signaling pathway, bile acid metabolism, and cholesterol homeostasis and upregulated genes involved in reactive oxygen species (ROS) response gene ontologies. Importantly, differentially regulated genes were assessed in the context of their transcription start nucleotides (TSN) and we found that the differential gene expression was not necessarily driven by transcripts encoding adenosine as their TSN. However, we know from existing studies RNA-seq and categorizing transcripts by ensembl reported TSSs does not adequately quantify the variance in transcript isoforms or m6Am stochiometry on the first adenosine [69]. The genes that stood out from the list of DEGs that were downregulated in both sensitive cell lines were *FADS2*, *FADS1* and *ELOVL6*, which are all directly involved in desaturation and elongation of polyunsaturated fatty acids (PUFAs). The involvement of fatty acids in cancer metabolism and chemoresistance is intensely studied, however, *FADS1*/2 contribution to OXPHOS and the TCA is by comparison still understudied. Recent work on depleting *FADS2* and *FADS1* in AML in vitro also show a proliferative defect and differentiation effect [254, 264]. Interestingly, unsaturated fatty acid biosynthesis and upregulation of fatty acid oxidation has been shown to underlie leukemic stem cell (LSC) potential and therapy resistance to Ven+Aza via *FADS1*/2 [253, 254, 255] and that *FADS2* in cancer can synthesize sapienate via an alternative pathway, which has been shown to be upregulated in cancer by mTORC1 and *SREBP-1*/2 activation in mouse embryonic fibroblasts (MEFs) and U87 glioblas-

toma cells and decreased cancer growth upon depletion [251, 256]. These findings are relevant to the results of this thesis, as they may provide mechanistic background for the phenotype observed in AML. Interestingly, supplementation of fatty acid intermediates of the canonical *FADS2* pathway only show a minor improvement to AML cell proliferation, while supplementation with palmitate significantly reduced cell viability. Experiments on impact of sapienate supplementation on knockdown cell proliferation, as well as phosphorylation levels of mTORC1 pathway mediators are in progress. These experiments will deliver a new perspective on the potential of the non-canonical *FADS2* pathway being involved in the *PCIF1* phenotype.

An additional term referenced in GO analysis showed that many of the commonly differentially regulated genes of the sensitive phenotype involve response to reactive oxygen species. It is established that unsaturated fatty acids have a higher redox potential, and thus downregulation of fatty acids reduces ROS generation and increases resistance to ROS inducing agents. Levels of ROS were briefly assessed in sensitive and resistant *PCIF1* knockdown cell lines and showed an upregulation of DCFDA signals, indicative of ROS presence in the cell, in *PCIF1* knockdown cell lines. However, U937 resistant cell lines were only slightly less affected than the sensitive cell lines, concluding that ROS may not be the driving force behind cell death. Interestingly, chemoresistance has been attributed to a cell's ability to metabolize ROS and downregulate pathways that contribute to ROS generation, which we observed briefly in treatments of resistant U937 and THP-1 cell lines with venetoclax and azacitidine.

Tying it all back to the cell line dependent effect of *PCIF1* loss, which was initially attributed to AML subtypes, we now hypothesize this to be dependent on cell line specific reliance on fatty

acid metabolic pathways, in which some AML cell line types rely on fatty acid oxidation (FAO) and undergo apoptosis with the downreguation of long chain acyl-CoA substrate generation by *FADS1*/2, while other AML cell line types are able to compensate this gap in their energy supply with other metabolic pathways and evade cell death. Further research into these mechanisms will be necessary to develop a better understanding of PCIF1's contribution to this pathway.

5.1.1 Implications for cancer therapy

If PCIF1 is a viable target for cancer therapy, how might it be best applied in the clinic in combination with other AML treatments? Inhibitors for PCIF1, which are yet to be identified and developed, may specifically synergize with AML therapies that unmask apoptotic vulnerabilities that rely on epitranscriptomic regulation. Possible pathways include induction or transcriptional stress or transcriptional/translational control of signaling pathways. If PCIF1 and m6Am indeed have a destabilizing role on mRNA transcripts or inhibitive function on translation, then targeting contexts in which there is an upregulation of pro-survival mediators would be the most beneficial. However, as the exact molecular mechanisms and targets of PCIF1 remain contested, further studies will be necessary to clarify downstream pathways responsible for leukemic dependencies and inform treatment strategy.

Potential AML patient groups interesting for investigation with PCIF1 therapy may include patients with primary chemoresistance (induction failure), as data from the Target-AML trial indicates that AML cells of these patients express PCIF1 at a particularly high level, hinting at a possible regulatory role of PCIF1 in this response (Figure 4.4). It is worth noting that, while there are to date no published inhibitors on PCIF1, clinical trials investigating inhibition of METTL3

(in non-AML advanced malignancies) are currently underway and could inform on cancer subgroups that respond to epitranscriptomic regulation (Clinical Trial ID NCT06975293). More importantly, potential future clinical investigations involving FTO, an m6Am/m6A eraser protein, should be closely monitored, since recent studies suggest that m6Am is the preferred substrate for demethylase activity, which could signify opposite patient groups to respond. More importantly, prospective investigations targeting FTO, an m6Am/m6A eraser protein, should be closely monitored, as accumulating evidence suggests that a preference for m6Am demethylation, raising the possibility of therapeutic responses more suitable for investigation of a PCIF1 context as opposed to therapeutic potential emerging from m6A-centric models.

If PCIF1 plays a regulatory role in metabolic pathways integral to cancer cell survival and stemness, as results of this thesis and other published studies suggest, employing PCIF1 therapies in cancers that show dependency on alternative metabolism may be beneficial [75, 76, 265]. In leukemia, targeted inhibitors Ivosidenib and Enasidenib against isocitrate dehyrogenase 1 and 2 respectively (IDH1/2) are administered in combination with induction chemotherapy or as a single-agent in patients ineligible for intensive chemotherapy with IDH-mutant leukemia [83]. The normal enzymatic function of IDH enzymes involves conversion of isocitrate to alpha-ketoglutarate (aKG), a key step in the citric acid cycle (TCA) [266, 267]. Loss-of-function mutations in the IDH1/2 enzymes affect the catalytic binding pocket of isocitrate and NADPH, triggering the reduction of isocitrate to 2-hydroxyglutarate (2HG) instead of aKG and the inhibition of demethylases, DNA repair pathways and components of the electron transport chain (ETC) [266, 268]. The use of NADPH by IDH mutants to produce 2HG also directly impacts de novo lipogenesis and fatty acid metabolism, as NADPH is also a vital reducing molecule in these processes, and IDH

mutant cancers have been shown to be especially reliant on exogenous lipid import [269, 270]. Thus, pathways affected by the oncometabolite 2HG that lead to aberrant proliferation, a block in differentiation, and metabolic reprogramming overlap with gene sets enriched in PCIF1-deficient AML cell lines, which may represent a potential synergistic effect for future application of PCIF1 therapies.

Metabolic reprogramming is one of the cancer hallmarks used by tumor cells to satisfy their energy demand. One such example was described by Otto Warburg, in which cancers resort to glycolysis, even in the presence of oxygen, instead of mitochondrial oxidation. Besides the Warburg effect, some cancers reprogram their energy demand to rely on fatty acid and lipid oxidation (β-oxidation) instead of amino acid metabolism [271]. Fatty acid oxidation (FAO) supplies the cancer cell with acetyl-CoA for the TCA, as well as $NADH$ and $FADH_2$ for the electron transport chain (ETC), thus sustaining cell proliferation. The substrate of FAO are long chain fatty acids, such as PUFAs generated by *FADS1*/2. Targeting the metabolic pathway required by these cancer cells may therefore provide treatment alternatives with reduced toxicity and rates of relapse. FAO has been shown to be upregulated in AML, particularly in in resistant/relapsed (R/R) AML patients, and sustains quiescence of leukemic stem cells (LSCs) in the bone marrow niche. Culp-Hill et al. showed that targeting of *FADS1*/2 resensitized refractory/relapsed (R/R) AML cells to Ven+Aza treatment [255]. Interestingly, we see increased IC50 values in resistant U937 *PCIF1* KD cells treated with Ven+Aza, implicating that *PCIF1* loss enhanced chemoresistance. However, qPCR of sensitive and resistant cell lines shows that resistant cell lines have higher levels of *FADS1*/2, which could lead to increased levels of FAO and chemoresistance. The interplay between *PCIF1*, fatty acid desaturation and chemoresistance in AML therefore requires deeper investigation to be

fully understood, but PCIF1 max signify a promising new AML modulator.

5.1.2 Limitations

Limitations to this thesis work include the type of model system employed and the lack of m6Am and lipid profiling techniques to evaluate mechanistic targets and impact of *PCIF1*. AML cell lines are valuable model systems to investigate the disease, but the lack of a tumor microenvironment in the bone marrow niche make clinical translation challenging. While results from assessing morphological signs as well as cell-surface markers indicate AML cell differentiation induced by the loss of *PCIF1*, other functional experiments, such as phagocytic capacity of AML cells were not measured. Further studies in a broader panel of AML cell lines, as well as patient-derived primary AML cells, may give rise to subtype specific insight not observable in the panel chosen for this thesis. The use of patient-derived xenografts and mouse models would be of additional significant scientific value for future experiments. Further, the pLKO.1 shRNA model for protein depletion requires selection and recovery after lentiviral infection, during which the effects of *PCIF1* loss manifest. Thus, the data presented in this work does not provide insight into the immediate effects after *PCIF1* knockdown, which may provide insight into disease mechanisms. Generation of inducible knockdown and degradation systems would be applicable to elucidate the immediate effects of *PCIF1*.

While we establish that many of the common differentially expressed transcripts between sensitive cell lines may not be m6Am-methylated, the AML phenotype requires further follow up with m6Am sequencing methods such as m6Am-exo-seq, CROWN-seq or m6Am-seq. Furthermore, this prevented us from delineating the function of m6Am in transcriptional and translational

control, for which a consensus in the scientific community is yet to be reached. Thus, polysome profiling would be useful to assess the translational efficiency of transcripts which carry an m6Am-methylated transcription start nucleotide.

An important limitation to address is the type of mRNA enriched for when using the poly(A) mRNA isolation kit for RNA sequencing library preparation and HPLC-MS m6Am detection. By enriching specifically for poly-adenylated RNA, the RNA yield should consist mostly of intact, full-length messenger RNA. As a result, any mRNA transcripts that were terminated prematurely and not poly-adenylated, perhaps due to yet to be characterized functions of the PCIF1-RNAPII interaction, would be excluded from preparation and downstream analysis. Premature transcriptional termination is an important mechanism for quality control as well as gene expression [272]. Prematurely terminated transcripts can also be polyadenylated, leading to the generation of stable mRNAs encoding for small regulating RNAs or mRNA isoforms with protein function. Genes can have numerous intronic alternative 3' polyadenylation sites [273]. Indeed, a study has reported a correlation between alternative transcription start sites, which may influence whether or not the first transcribed nucleotide is an A, correlate with the "choice" of alternative 3' cleavage and polyadenylation site [274]. Thus the selection for polyadenylated mRNA may have biased results from m6Am mass spec and mRNA sequencing.

Ultimately, while the biological implication of *PCIF1* in fatty acid metabolism and reactive oxygen species response is curious, follow-up experiments with catalytic active and inactive genetic rescues of *PCIF1*, as well as genetic depletion of *FADS1*/2 instead of the inhibitors, which may lack target specificity, are necessary to confirm this phenotype. Additionally, this work would

benefit from the addition of further biological replicates as well as supplementation experiments with other fatty acid metabolites that were overlooked in the main results.

5.1.3 Remaining questions and future directions

The work in this thesis provides interesting future avenues for further investigation of *PCIF1* in the context of AML. Relevant questions that remain to be answered relate to identifying the pattern that governs *PCIF1* sensitivity of AML cell lines as well as the molecular impact behind fatty acid metabolism and ROS regulation directly or indirectly via m6Am deposition on transcription start nucleotides. Why does *PCIF1* trigger a proliferative defect only in certain cell lines? Does *PCIF1* directly or indirectly impact the differentially expressed genes seen in sensitive versus resistant cell lines? Importantly, does *PCIF1* have an overarching role in lipid metabolism, given that several published studies link *PCIF1* perturbation with a change in metabolism? Further studies exploring the potential role of sapienic acid alternative pathway will be necessary to unveil how fatty acid metabolism contributes to the *PCIF1* phenotype. In future work, we would also like to clearly address these mechanisms more closely, and conduct preclinical assessments to make our finding more applicable to the clinical setting.

Metabolism and epigenetic rewiring are closely interlinked cancer hallmarks and show significant potential for future therapies [6]. It is known that metabolic switching of cancer cells impacts epigenetic processes, and vice-versa, but further investigation is necessary to understand these mechanisms. Fatty acids and ROS metabolites have important functions as cell messengers and regulate cellular states. Whether *PCIF1* could be another link between epigenetics/epitranscriptomics and cancer metabolism will be an exciting question to cover in future investigations.

Bibliography

[1] Crick F. Central Dogma of Molecular Biology [Journal Article]. Nature. 1970;227(5258):561-3. Available from: https://doi.org/10.1038/227561a0.

[2] Henikoff S. Beyond the central dogma [Journal Article]. Bioinformatics. 2002;18(2):223-5. Available from: https://doi.org/10.1093/bioinformatics/18.2.223.

[3] Cobb M. 60 years ago, Francis Crick changed the logic of biology [Journal Article]. PLoS Biol. 2017;15(9):e2003243. Available from: https://www.ncbi.nlm.nih.gov/pubmed/28922352.

[4] Hanahan D, Weinberg RA. The hallmarks of cancer [Journal Article]. Cell. 2000;100(1):57-70.

[5] Hanahan D, Weinberg RA. Hallmarks of cancer: the next generation [Journal Article]. Cell. 2011;144(5):646-74. Available from: https://www.ncbi.nlm.nih.gov/pubmed/21376230.

[6] Hanahan D. Hallmarks of Cancer: New Dimensions [Journal Article]. Cancer Discov. 2022;12(1):31-46. Available from: https://www.ncbi.nlm.nih.gov/pubmed/35022204.

[7] Cui L, Ma R, Cai J, Guo C, Chen Z, Yao L, et al. RNA modifications: importance in immune cell biology and related diseases [Journal Article]. Signal Transduct Target Ther. 2022;7(1):334. Available from: https://www.ncbi.nlm.nih.gov/pubmed/36138023.

[8] Esteve-Puig R, Bueno-Costa A, Esteller M. Writers, readers and erasers of RNA modifications in cancer [Journal Article]. Cancer Lett. 2020;474:127-37. Available from: https://www.ncbi.nlm.nih.gov/pubmed/31991154.

[9] Schrezenmeier J, Huntly BJP. Epigenetic dysregulation in acute myeloid leukemia [Journal Article]. Semin Hematol. 2025.

[10] Simonicova K, Janotka L, Kavcova H, Sulova Z, Breier A, Messingerova L. Different mechanisms of drug resistance to hypomethylating agents in the treatment of myelodysplastic syndromes and acute myeloid leukemia [Journal Article]. Drug Resist Updat. 2022;61:100805. Available from: https://www.ncbi.nlm.nih.gov/pubmed/35227933.

[11] Stelmach P, Trumpp A. Leukemic stem cells and therapy resistance in acute myeloid leukemia [Journal Article]. Haematologica. 2023;108(2):353-66. Available from: https://www.ncbi.nlm.nih.gov/pubmed/36722405.

[12] Galloway A, Cowling VH. mRNA cap regulation in mammalian cell function and fate [Journal Article]. Biochim Biophys Acta Gene Regul Mech. 2019;1862(3):270-9. Available from: https://www.ncbi.nlm.nih.gov/pubmed/30312682.

[13] Cowling VH. CAPAM: The mRNA Cap Adenosine N6-Methyltransferase [Journal Article]. Trends Biochem Sci. 2019;44(3):183-5. Available from: https://www.ncbi.nlm.nih.gov/pubmed/30679132.

[14] Belanger F, Stepinski J, Darzynkiewicz E, Pelletier J. Characterization of hMTr1, a human Cap1 2'-O-ribose methyltransferase [Journal Article]. J Biol Chem. 2010;285(43):33037-44. Available from: https://www.ncbi.nlm.nih.gov/pubmed/20713356.

[15] Blears D, Lou J, Fong N, Mitter R, Sheridan RM, He D, et al. Redundant pathways for removal of defective RNA polymerase II complexes at a promoter-proximal pause checkpoint [Journal Article]. Molecular Cell. 2024;84(24):4790-807.e11.

[16] Naganuma M, Kujirai T, Ehara H, Uejima T, Ito T, Goto M, et al. Structural insights into promoter-proximal pausing of RNA polymerase II at +1 nucleosome [Journal Article]. Science Advances. 2025;11(10).

[17] Ramanathan A, Robb GB, Chan SH. mRNA capping: biological functions and applications [Journal Article]. Nucleic Acids Res. 2016;44(16):7511-26. Available from: https://www.ncbi.nlm.nih.gov/pubmed/27317694.

[18] Vidya E, Duchaine TF. Eukaryotic mRNA Decapping Activation [Journal Article]. Front Genet. 2022;13:832547.

[19] Picard-Jean F, Brand C, Tremblay-Letourneau M, Allaire A, Beaudoin MC, Boudreault S, et al. 2'-O-methylation of the mRNA cap protects RNAs from decapping and degradation by DXO [Journal Article]. PLoS One. 2018;13(3):e0193804. Available from: https://www.ncbi.nlm.nih.gov/pubmed/29601584.

[20] Galloway A, Kaskar A, Ditsova D, Atrih A, Yoshikawa H, Gomez-Moreira C, et al. Upregulation of RNA cap methyltransferase RNMT drives ribosome biogenesis during T cell activation [Journal Article]. Nucleic Acids Res. 2021;49(12):6722-38. Available from: https://www.ncbi.nlm.nih.gov/pubmed/34125914.

[21] Liang S, Silva JC, Suska O, Lukoszek R, Almohammed R, Cowling VH. CMTR1 is recruited to transcription start sites and promotes ribosomal protein and histone gene expression in embryonic stem cells [Journal Article]. Nucleic Acids Res. 2022;50(5):2905-22. Available from: https://www.ncbi.nlm.nih.gov/pubmed/35212377.

[22] Culjkovic-Kraljacic B, Skrabanek L, Revuelta MV, Gasiorek J, Cowling VH, Cerchietti L, et al. The eukaryotic translation initiation factor eIF4E elevates steady-state m(7)G capping of coding and noncoding transcripts [Journal Article]. Proc Natl Acad Sci U S A. 2020;117(43):26773-83. Available from: https://www.ncbi.nlm.nih.gov/

pubmed/33055213.

[23] Hirose Y, Iwamoto Y, Sakuraba K, Yunokuchi I, Harada F, Ohkuma Y. Human phosphorylated CTD-interacting protein, PCIF1, negatively modulates gene expression by RNA polymerase II [Journal Article]. Biochemical and Biophysical Research Communications. 2008;369(2):449-55. Available from: https://www.sciencedirect.com/science/article/pii/S0006291X08002969.

[24] Sendinc E, Valle-Garcia D, Dhall A, Chen H, Henriques T, Navarrete-Perea J, et al. PCIF1 Catalyzes m6Am mRNA Methylation to Regulate Gene Expression [Journal Article]. Mol Cell. 2019;75(3):620-30 e9. Available from: https://www.ncbi.nlm.nih.gov/pubmed/31279659.

[25] Franco G, Taillebourg E, Delfino E, Homolka D, Gueguen N, Brasset E, et al. The catalytic-dead Pcif1 regulates gene expression and fertility in Drosophila [Journal Article]. Rna. 2023;29(5):609-19.

[26] Gao S, Zhou J, Hu Z, Zhang S, Wu Y, Musunuru PP, et al. Effects of the m6Am methyltransferase PCIF1 on cell proliferation and survival in gliomas [Journal Article]. Biochim Biophys Acta Mol Basis Dis. 2022;1868(11):166498.

[27] Yin J, Liu G, Zhou Y, Zhou J, Guo M, Hu Z, et al. The WW domain presents a promising target for the development of PCIF1 agonists in the treatment of glioma [Journal Article]. NPJ Precis Oncol. 2025;9(1):329. Available from: https://www.ncbi.nlm.nih.gov/pubmed/41131141.

[28] Wei CM, Gershowitz A, Moss B. N6 O2-dimethyladenosine a novel methylated ribonucleoside next to the 5 terminal of animal cell and virus mRNAs [Journal Article]. Nature. 1975;257(5523):251-3. Available from: https://doi.org/10.1038/257251a0.

[29] Fan H, Sakuraba K, Komuro A, Kato S, Harada F, Hirose Y. PCIF1, a novel human WW domain-containing protein, interacts with the phosphorylated RNA polymerase II [Journal Article]. Biochemical and Biophysical Research Communications. 2003;301(2):378-85. Available from: https://www.sciencedirect.com/science/article/pii/S0006291X02030152.

[30] Lee YM, Liou YC. Gears-In-Motion: The Interplay of WW and PPIase Domains in Pin1 [Journal Article]. Front Oncol. 2018;8:469. Available from: https://www.ncbi.nlm.nih.gov/pubmed/30460195.

[31] Iyer LM, Zhang D, Aravind L. Adenine methylation in eukaryotes: Apprehending the complex evolutionary history and functional potential of an epigenetic modification [Journal Article]. Bioessays. 2016;38(1):27-40. Available from: https://www.ncbi.nlm.nih.gov/pubmed/26660621.

[32] Akichika S, Hirano S, Shichino Y, Suzuki T, Nishimasu H, Ishitani R, et al. Cap-specific

terminal N (6)-methylation of RNA by an RNA polymerase II-associated methyltransferase [Journal Article]. Science. 2019;363(6423). Available from: https://www.ncbi.nlm.nih.gov/pubmed/30467178.

[33] Boulias K, Toczydlowska-Socha D, Hawley BR, Liberman N, Takashima K, Zaccara S, et al. Identification of the m(6)Am Methyltransferase PCIF1 Reveals the Location and Functions of m(6)Am in the Transcriptome [Journal Article]. Mol Cell. 2019;75(3):631-43 e8. Available from: https://www.ncbi.nlm.nih.gov/pubmed/31279658.

[34] Sun H, Zhang M, Li K, Bai D, Yi C. Cap-specific, terminal N(6)-methylation by a mammalian m(6)Am methyltransferase [Journal Article]. Cell Res. 2019;29(1):80-2. Available from: https://www.ncbi.nlm.nih.gov/pubmed/30487554.

[35] Mauer J, Luo X, Blanjoie A, Jiao X, Grozhik AV, Patil DP, et al. Reversible methylation of m(6)A(m) in the 5 cap controls mRNA stability [Journal Article]. Nature. 2017;541(7637):371-5. Available from: https://www.ncbi.nlm.nih.gov/pubmed/28002401.

[36] Mauer J, Sindelar M, Despic V, Guez T, Hawley BR, Vasseur JJ, et al. FTO controls reversible m(6)Am RNA methylation during snRNA biogenesis [Journal Article]. Nat Chem Biol. 2019;15(4):340-7.

[37] Li Y, Su R, Deng X, Chen Y, Chen J. FTO in cancer: functions, molecular mechanisms, and therapeutic implications [Journal Article]. Trends Cancer. 2022;8(7):598-614.

[38] Wei J, Liu F, Lu Z, Fei Q, Ai Y, He PC, et al. Differential m(6)A, m(6)A(m), and m(1)A Demethylation Mediated by FTO in the Cell Nucleus and Cytoplasm [Journal Article]. Mol Cell. 2018;71(6):973-85 e5. Available from: https://www.ncbi.nlm.nih.gov/pubmed/30197295.

[39] Bartosovic M, Molares HC, Gregorova P, Hrossova D, Kudla G, Vanacova S. N6-methyladenosine demethylase FTO targets pre-mRNAs and regulates alternative splicing and 3-end processing [Journal Article]. Nucleic Acids Research. 2017;45(19):11356-70.

[40] Li Z, Weng H, Su R, Weng X, Zuo Z, Li C, et al. FTO Plays an Oncogenic Role in Acute Myeloid Leukemia as a N(6)-Methyladenosine RNA Demethylase [Journal Article]. Cancer Cell. 2017;31(1):127-41.

[41] Covelo-Molares H, Obrdlik A, Postulkova I, Dohnalkova M, Gregorova P, Ganji R, et al. The comprehensive interactomes of human adenosine RNA methyltransferases and demethylases reveal distinct functional and regulatory features [Journal Article]. Nucleic Acids Res. 2021;49(19):10895-910. Available from: https://www.ncbi.nlm.nih.gov/pubmed/34634806.

[42] An H, Hong Y, Goh YT, Koh CWQ, Kanwal S, Zhang Y, et al. m(6)Am sequesters PCF11 to suppress premature termination and drive neuroblastoma differentiation [Journal Article].

Mol Cell. 2024;84(21):4142-57 e14. Available from: https://www.ncbi.nlm.nih.gov/pubmed/39481383.

[43] Gregersen LH, Mitter R, Ugalde AP, Nojima T, Proudfoot NJ, Agami R, et al. SCAF4 and SCAF8, mRNA Anti-Terminator Proteins [Journal Article]. Cell. 2019;177(7):1797-813 e18. Available from: https://www.ncbi.nlm.nih.gov/pubmed/31104839.

[44] Yamaguchi Y, Inukai N, Narita T, Wada T, Handa H. Evidence that negative elongation factor represses transcription elongation through binding to a DRB sensitivity-inducing factor/RNA polymerase II complex and RNA [Journal Article]. Mol Cell Biol. 2002;22(9):2918-27. Available from: https://www.ncbi.nlm.nih.gov/pubmed/11940650.

[45] Sugita A, Kuruma S, Yanagisawa N, Ishiguro H, Kano R, Ohkuma Y, et al. The cap-specific m6A methyltransferase, PCIF1/CAPAM, is dynamically recruited to the gene promoter in a transcription-dependent manner [Journal Article]. J Biochem. 2021;170(2):203-13. Available from: https://www.ncbi.nlm.nih.gov/pubmed/33982754.

[46] Yu D, Dai N, Wolf EJ, CorrÃªa J I R, Zhou J, Wu T, et al. Enzymatic characterization of mRNA cap adenosine-N6 methyltransferase PCIF1 activity on uncapped RNAs [Journal Article]. J Biol Chem. 2022;298(4):101751.

[47] Whittaker GR. Virus nuclear import [Journal Article]. Adv Drug Deliv Rev. 2003;55(6):733-47. Available from: https://www.ncbi.nlm.nih.gov/pubmed/12788537.

[48] Tartell MA, Boulias K, Hoffmann GB, Bloyet LM, Greer EL, Whelan SPJ. Methylation of viral mRNA cap structures by PCIF1 attenuates the antiviral activity of interferon-beta [Journal Article]. Proc Natl Acad Sci U S A. 2021;118(29). Available from: https://www.ncbi.nlm.nih.gov/pubmed/34266951.

[49] Zhang Q, Kang Y, Wang S, Gonzalez GM, Li W, Hui H, et al. HIV reprograms host m(6)Am RNA methylome by viral Vpr protein-mediated degradation of PCIF1 [Journal Article]. Nat Commun. 2021;12(1):5543. Available from: https://www.ncbi.nlm.nih.gov/pubmed/34545078.

[50] Wang L, Wang S, Wu L, Li W, Bray W, Clark AE, et al. PCIF1-mediated deposition of 5'-cap N(6),2'-O-dimethyladenosine in ACE2 and TMPRSS2 mRNA regulates susceptibility to SARS-CoV-2 infection [Journal Article]. Proc Natl Acad Sci U S A. 2023;120(5):e2210361120. Available from: https://www.ncbi.nlm.nih.gov/pubmed/36689652.

[51] Green TJ, Luo M. Structure of the vesicular stomatitis virus nucleocapsid in complex with the nucleocapsid-binding domain of the small polymerase cofactor, P [Journal Article]. Proc Natl Acad Sci U S A. 2009;106(28):11713-8.

[52] Wilen CB, Tilton JC, Doms RW. HIV: cell binding and entry [Journal Article]. Cold Spring Harb Perspect Med. 2012;2(8). Available from: https://www.ncbi.nlm.nih.gov/pubmed/22908191.

[53] Jackson CB, Farzan M, Chen B, Choe H. Mechanisms of SARS-CoV-2 entry into cells [Journal Article]. Nat Rev Mol Cell Biol. 2022;23(1):3-20. Available from: https://www.ncbi.nlm.nih.gov/pubmed/34611326.

[54] Hercyk N, Horikami SM, Moyer SA. The vesicular stomatitis virus L protein possesses the mRNA methyltransferase activities [Journal Article]. Virology. 1988;163(1):222-5. Available from: https://www.sciencedirect.com/science/article/pii/004268228890253X.

[55] Park GJ, Osinski A, Hernandez G, Eitson JL, Majumdar A, Tonelli M, et al. The mechanism of RNA capping by SARS-CoV-2 [Journal Article]. Nature. 2022;609(7928):793-800. Available from: https://www.ncbi.nlm.nih.gov/pubmed/35944563.

[56] Jin MZ, Zhang YG, Jin WL, Wang XP. A Pan-Cancer Analysis of the Oncogenic and Immunogenic Role of m6Am Methyltransferase PCIF1 [Journal Article]. Front Oncol. 2021;11:753393. Available from: https://www.ncbi.nlm.nih.gov/pubmed/34888238.

[57] Hensel J, Duex JE, Owens C, Dancik GM, Edwards MG, Frierson HF, et al. Patient Mutation Directed shRNA Screen Uncovers Novel Bladder Tumor Growth Suppressors [Journal Article]. Mol Cancer Res. 2015;13(9):1306-15. Available from: https://www.ncbi.nlm.nih.gov/pubmed/26078295.

[58] Wu Y, Pu X, Wu S, Zhang Y, Fu S, Tang H, et al. PCIF1, the only methyltransferase of N6,2-O-dimethyladenosine [Journal Article]. Cancer Cell Int. 2023;23. Available from: https://cancerci.biomedcentral.com/articles/10.1186/s12935-023-03066-7http://creativecommons.org/publicdomain/zero/1.0/.

[59] Zhuo W, Sun M, Wang K, Zhang L, Li K, Yi D, et al. m(6)Am methyltransferase PCIF1 is essential for aggressiveness of gastric cancer cells by inhibiting TM9SF1 mRNA translation [Journal Article]. Cell Discov. 2022;8(1):48. Available from: https://www.ncbi.nlm.nih.gov/pubmed/35597784.

[60] Wang L, Wu L, Zhu Z, Zhang Q, Li W, Gonzalez GM, et al. Role of PCIF1-mediated 5'-cap N6-methyladeonsine mRNA methylation in colorectal cancer and anti-PD-1 immunotherapy [Journal Article]. EMBO J. 2023;42(2):e111673. Available from: https://www.ncbi.nlm.nih.gov/pubmed/36514940.

[61] Li K, Chen J, Zhang C, Cheng M, Chen S, Song W, et al. The CTBP2-PCIF1 complex regulates m6Am modification of mRNA in head and neck squamous cell carcinoma [Journal Article]. J Clin Invest. 2023;133(20). Available from: https://www.ncbi.nlm.

nih.gov/pubmed/37643007.

[62] Sekiya M, Kainoh K, Sugasawa T, Yoshino R, Hirokawa T, Tokiwa H, et al. The transcriptional corepressor CtBP2 serves as a metabolite sensor orchestrating hepatic glucose and lipid homeostasis [Journal Article]. Nat Commun. 2021;12(1):6315. Available from: https://www.ncbi.nlm.nih.gov/pubmed/34728642.

[63] Sekiya M, Ma Y, Kainoh K, Saito K, Yamazaki D, Tsuyuzaki T, et al. Loss of CtBP2 may be a mechanistic link between metabolic derangements and progressive impairment of pancreatic beta cell function [Journal Article]. Cell Rep. 2023;42(8):112914. Available from: https://www.ncbi.nlm.nih.gov/pubmed/37557182.

[64] Ben-Haim MS, Pinto Y, Moshitch-Moshkovitz S, Hershkovitz V, Kol N, Diamant-Levi T, et al. Dynamic regulation of N6,2-O-dimethyladenosine (m6Am) in obesity [Journal Article]. Nature Communications. 2021.

[65] Li K, Yi Y, Ling R, Zhang C, Zhang Z, Wang Y, et al. PCIF1 drives oesophageal squamous cell carcinoma progression via m6Am-mediated suppression of MTF2 translation [Journal Article]. Clinical and Translational Medicine. 2025;15(4).

[66] Sugita A, Kano R, Ishiguro H, Yanagisawa N, Kuruma S, Wani S, et al. Cap-Specific m(6)Am Methyltransferase PCIF1/CAPAM Regulates mRNA Stability of RAB23 and CNOT6 through the m(6)A Methyltransferase Activity [Journal Article]. Cells. 2024;13(20). Available from: https://www.ncbi.nlm.nih.gov/pubmed/39451207.

[67] Xiang B, Zhang M, Li K, Zhang Z, Liu Y, Gao M, et al. The epitranscriptional factor PCIF1 orchestrates CD8+ T cell ferroptosis and activation to control antitumor immunity [Journal Article]. Nature Immunology. 2025.

[68] Song W, Liu L, Liang H, Cheng H, He W, Yin Q, et al. m6Am Methyltransferase PCIF1 Regulates Periodontal Inflammation [Journal Article]. Journal of Dental Research. 2024;103(11):1130-40. Available from: https://dx.doi.org/10.1177/00220345241271078.

[69] Liu JF, Hawley BR, Nicholson LS, Jaffrey SR. Decoding m6Am by simultaneous transcription-start mapping and methylation quantification [Journal Article]. eLife. 2025;13:RP104139. Available from: https://doi.org/10.7554/eLife.104139.

[70] Schwartz S, Mumbach MR, Jovanovic M, Wang T, Maciag K, Bushkin GG, et al. Perturbation of m6A writers reveals two distinct classes of mRNA methylation at internal and 5' sites [Journal Article]. Cell Rep. 2014;8(1):284-96.

[71] Linder B, Grozhik AV, Olarerin-George AO, Meydan C, Mason CE, Jaffrey SR. Single-nucleotide-resolution mapping of m6A and m6Am throughout the transcriptome [Journal

Article]. Nat Methods. 2015;12(8):767-72.

[72] Cesaro B, Tarullo M, Fatica A. Regulation of Gene Expression by m6Am RNA Modification [Journal Article]. Int J Mol Sci. 2023;24(3). Available from: https://www.ncbi.nlm.nih.gov/pubmed/36768600.

[73] Jin H, Shi Z, Zhou T, Xie S. Regulation of m6Am RNA modification and its implications in human diseases [Journal Article]. Journal of Molecular Cell Biology. 2024;16(3). Available from: https://doi.org/10.1093/jmcb/mjae012.

[74] Liu JF. CROWN-seq reveals m6Am landscapes and transcription start site diversity [Journal Article]. Nature Reviews Genetics. 2025;26(8):509-9. Available from: https://doi.org/10.1038/s41576-025-00861-y.

[75] Pandey RR, Delfino E, Homolka D, Roithova A, Chen KM, Li L, et al. The Mammalian Cap-Specific m(6)Am RNA Methyltransferase PCIF1 Regulates Transcript Levels in Mouse Tissues [Journal Article]. Cell Rep. 2020;32(7):108038. Available from: https://www.ncbi.nlm.nih.gov/pubmed/32814042.

[76] Luo W, Xu Z, Li F, Ding L, Wang R, Lin Y, et al. m6Am Methyltransferase PCIF1 Promotes LPP3 Mediated Phosphatidic Acid Metabolism and Renal Cell Carcinoma Progression [Journal Article]. Adv Sci (Weinh). 2024;11(46).

[77] Papaemmanuil E, Gerstung M, Bullinger L, Gaidzik VI, Paschka P, Roberts ND, et al. Genomic Classification and Prognosis in Acute Myeloid Leukemia [Journal Article]. N Engl J Med. 2016;374(23):2209-21. Available from: https://www.nejm.org/doi/10.1056/NEJMoa1516192.

[78] Chakraborty S, Park CY. Pathogenic Mechanisms in Acute Myeloid Leukemia [Journal Article]. Curr Treat Options Oncol. 2022;23(11):1522-34.

[79] Cancer Genome Atlas Research N, Weinstein JN, Collisson EA, Mills GB, Shaw KR, Ozenberger BA, et al. The Cancer Genome Atlas Pan-Cancer analysis project [Journal Article]. Nat Genet. 2013;45(10):1113-20. Available from: https://www.ncbi.nlm.nih.gov/pubmed/24071849.

[80] Bennett JM, Catovsky D, Daniel MT, Flandrin G, Galton DAG, Gralnick HR, et al. Proposals for the Classification of the Acute Leukaemias French-American-British (FAB) Cooperative Group [Journal Article]. British Journal of Haematology. 1976;33(4):451-8.

[81] Khoury JD, Solary E, Abla O, Akkari Y, Alaggio R, Apperley JF, et al. The 5th edition of the World Health Organization Classification of Haematolymphoid Tumours: Myeloid and Histiocytic/DendriticÂ Neoplasms [Journal Article]. Leukemia. 2022;36(7):1703-19.

[82] Arber DA, Orazi A, Hasserjian RP, Borowitz MJ, Calvo KR, Kvasnicka HM, et al. International Consensus Classification of Myeloid Neoplasms and Acute Leukemias: integrating

morphologic, clinical, and genomic data [Journal Article]. Blood. 2022;140(11):1200-28.

[83] Doehner H, Wei AH, Appelbaum FR, Craddock C, DiNardo CD, Dombret H, et al. Diagnosis and management of AML in adults: 2022 recommendations from an international expert panel on behalf of the ELN [Journal Article]. Blood. 2022;140(12):1345-77. Available from: https://doi.org/10.1182/blood.2022016867.

[84] DiNardo CD, Cortes JE. Mutations in AML: prognostic and therapeutic implications [Journal Article]. Hematology. 2016;2016(1):348-55.

[85] Rataj J, Gorecki L, Muthna D, Sorf A, Krystof V, Klener P, et al. Targeting FMS-like tyrosine kinase 3 (FLT3) in acute myeloid leukemia: Novel molecular approaches and therapeutic challenges [Journal Article]. Biomed Pharmacother. 2025;182.

[86] Al-Harbi S, Aljurf M, Mohty M, Almohareb F, Ahmed SOA. An update on the molecular pathogenesis and potential therapeutic targeting of AML with t(8;21)(q22;q22.1);RUNX1-RUNX1T1 [Journal Article]. Blood Advances. 2020;4(1):229-38.

[87] Zehtabcheh S, Soleimani Samarkhazan H, Asadi M, Zabihi M, Parkhideh S, Mohammadi MH. Insights into KMT2A rearrangements in acute myeloid leukemia: from molecular characteristics to targeted therapies [Journal Article]. Biomark Res. 2025;13(1):73.

[88] Frohling S, Scholl C, Gilliland DG, Levine RL. Genetics of Myeloid Malignancies: Pathogenetic and Clinical Implications [Journal Article]. Journal of Clinical Oncology. 2005;23(26).

[89] Tomic B, Smoljo T, Lalic H, Dembitz V, Batinic J, Batinic D, et al. Cytarabine-induced differentiation of AML cells depends on Chk1 activation and shares the mechanism with inhibitors of DHODH and pyrimidine synthesis [Journal Article]. Sci Rep. 2022;12(1):11344. Available from: https://www.ncbi.nlm.nih.gov/pubmed/35790845.

[90] Thirumaran R, Prendergast GC, Gilman PB. In: Prendergast GC, Jaffee EM, editors. Chapter 7 - Cytotoxic Chemotherapy in Clinical Treatment of Cancer. Burlington: Academic Press; 2007. p. 101-16. Available from: https://www.sciencedirect.com/science/article/pii/B9780123725516500717.

[91] Quentmeier H, Reinhardt J, Zaborski M, Drexler HG. FLT3 mutations in acute myeloid leukemia cell lines [Journal Article]. Leukemia. 2003;17(1):120-4.

[92] Scheffold A, Jebaraj BMC, Stilgenbauer S. Venetoclax: Targeting BCL2 in Hematological Cancers [Journal Article]. Recent Results Cancer Res. 2018;212:215-42.

[93] Vakiti A, Reynolds SB, Mewawalla P. 1. In: Acute Myeloid Leukemia. Treasure Island (FL): Stat Pearls Publishing Copyright 2025, StatPearls Publishing LLC.; 2025. p. 1.

[94] Barbieri I, Tzelepis K, Pandolfini L, Shi J, MillÃ¡n-Zambrano G, Robson SC, et al.

Promoter-bound METTL3 maintains myeloid leukaemia by m6A-dependent translation control [Journal Article]. Nature. 2017;552(7683):126-31.

[95] Paris J, Morgan M, Campos J, Spencer GJ, Shmakova A, Ivanova I, et al. Targeting the RNA m6A Reader YTHDF2 Selectively Compromises Cancer Stem Cells in Acute Myeloid Leukemia [Journal Article]. Cell Stem Cell. 2019;25(1):137-48.

[96] Moser JC, Papadopoulos KP, Ahnert JR, Ofir-Rosenfeld Y, Holz JB. Phase 1 dose escalation and cohort expansion study evaluating safety, PK, PD and clinical activity of STC-15, a METTL-3 inhibitor, in patients with advanced malignancies [Journal Article]. Journal of Clinical Oncology. 2024;42(16):2586-6.

[97] Zheng G, Dahl J, Niu Y, Fedorcsak P, Huang CM, Li C, et al. ALKBH5 Is a Mammalian RNA Demethylase that Impacts RNA Metabolism and Mouse Fertility [Journal Article]. Molecular Cell. 2013;49(1):18-29. Doi: 10.1016/j.molcel.2012.10.015.

[98] Young L, Sung J, Stacey G, Masters JR. Detection of Mycoplasma in cell cultures [Journal Article]. Nat Protoc. 2010;5(5):929-34.

[99] Bonilla DL, Paul A, Gil-Pulido J, Park LM, Jaimes MC. The Power of Reagent Titration in Flow Cytometry [Journal Article]. Cells. 2024;13(20).

[100] Stewart SA, Dykxhoorn DM, Palliser D, Mizuno H, Yu EY, An DS, et al. Lentivirus-delivered stable gene silencing by RNAi in primary cells [Journal Article]. Rna. 2003;9(4):493-501.

[101] Zhu A, Ibrahim JG, Love MI. Heavy-tailed prior distributions for sequence count data: removing the noise and preserving large differences [Journal Article]. Bioinformatics. 2018;35(12):2084-92.

[102] Kolberg L, Raudvere U, Kuzmin I, Adler P, Vilo J, Peterson H. g:Profiler-interoperable web service for functional enrichment analysis and gene identifier mapping (2023 update) [Journal Article]. Nucleic Acids Research. 2023;51(W1):W207-12. Available from: https://doi.org/10.1093/nar/gkad347.

[103] Kassambara A, Kosinski M, P B. Kassambara A, Kosinski M, P B, editors. survminer: Drawing Survival Curves using 'ggplot2' [Generic]. CRAN/datanovia; 2021. R package version 0.4.9. Available from: https://CRAN.R-project.org/package=survminer.

[104] Wagner FF, Benajiba L, Campbell AJ, WeÃ¯wer M, Sacher JR, Gale JP, et al. Exploiting an Asp-Glu "switch" in glycogen synthase kinase 3 to design paralog-selective inhibitors for use in acute myeloid leukemia [Journal Article]. Science Translational Medicine. 2018;10(431):eaam8460.

[105] Labun K, Montague TG, Krause M, TorresÂ Cleuren YN, Tjeldnes H, Valen E. CHOP-

CHOP v3: expanding the CRISPR web toolbox beyond genome editing [Journal Article]. Nucleic Acids Research. 2019;47(W1):W171-4. Available from: https://doi.org/10.1093/nar/gkz365.

[106] Relier S, Ripoll J, Guillorit H, Amalric A, Achour C, Boissiere F, et al. FTO-mediated cytoplasmic m(6)A(m) demethylation adjusts stem-like properties in colorectal cancer cell [Journal Article]. Nat Commun. 2021;12(1):1716. Available from: https://www.ncbi.nlm.nih.gov/pubmed/33741917.

[107] Arafeh R, Shibue T, Dempster JM, Hahn WC, Vazquez F. The present and future of the Cancer Dependency Map [Journal Article]. Nature Reviews Cancer. 2025;25(1):59-73. Available from: https://doi.org/10.1038/s41568-024-00763-x.

[108] Tsherniak A, Vazquez F, Montgomery PG, Weir BA, Kryukov G, Cowley GS, et al. Defining a Cancer Dependency Map [Journal Article]. Cell. 2017;170(3):564-76 e16. Available from: https://www.ncbi.nlm.nih.gov/pubmed/28753430.

[109] Meyers RM, Bryan JG, McFarland JM, Weir BA, Sizemore AE, Xu H, et al. Computational correction of copy number effect improves specificity of CRISPR-Cas9 essentiality screens in cancer cells [Journal Article]. Nature Genetics. 2017;49(12):1779-84. Available from: https://doi.org/10.1038/ng.3984.

[110] Tang Z, Kang B, Li C, Chen T, Zhang Z. GEPIA2: an enhanced web server for large-scale expression profiling and interactive analysis [Journal Article]. Nucleic Acids Res. 2019;47(W1).

[111] Tyner JW, Tognon CE, Bottomly D, Wilmot B, Kurtz SE, Savage SL, et al. Functional genomic landscape of acute myeloid leukaemia [Journal Article]. Nature. 2018;562(7728):526-31. Available from: https://www.ncbi.nlm.nih.gov/pubmed/30333627.

[112] Goldman MJ, Craft B, Hastie M, Repecka K, McDade F, Kamath A, et al. Visualizing and interpreting cancer genomics data via the Xena platform [Journal Article]. Nature Biotechnology. 2020;38(6):675-8.

[113] Liu J, Lichtenberg T, Hoadley KA, Poisson LM, Lazar AJ, Cherniack AD, et al. An Integrated TCGA Pan-Cancer Clinical Data Resource to Drive High-Quality Survival Outcome Analytics [Journal Article]. Cell. 2018;173(2):400-16 e11. Available from: https://www.ncbi.nlm.nih.gov/pubmed/29625055.

[114] Bottomly D, Long N, Schultz AR, Kurtz SE, Tognon CE, Johnson K, et al. Integrative analysis of drug response and clinical outcome in acute myeloid leukemia [Journal Article]. Cancer Cell. 2022;40(8):850-64 e9. Available from: https://www.ncbi.nlm.nih.gov/pubmed/35868306.

[115] Yang JJ, Park TS, Wan TSK. 1. In: Wan TSK, editor. Recurrent Cytogenetic Abnormalities

in Acute Myeloid Leukemia. New York, NY: Springer New York; 2017. p. 223-45.

[116] Caicedo HH, Hashimoto DA, Caicedo JC, Pentland A, Pisano GP. Overcoming barriers to early disease intervention [Journal Article]. Nat Biotechnol. 2020;38(6):669-73. Available from: https://www.ncbi.nlm.nih.gov/pubmed/32444852.

[117] Farrar JE, Schuback HL, Ries RE, Wai D, Hampton OA, Trevino LR, et al. Genomic Profiling of Pediatric Acute Myeloid Leukemia Reveals a Changing Mutational Landscape from Disease Diagnosis to Relapse [Journal Article]. Cancer Res. 2016;76(8):2197-205. Available from: https://www.ncbi.nlm.nih.gov/pubmed/26941285.

[118] Ma X, Liu Y, Liu Y, Alexandrov LB, Edmonson MN, Gawad C, et al. Pan-cancer genome and transcriptome analyses of 1,699 paediatric leukaemias and solid tumours [Journal Article]. Nature. 2018;555(7696):371-6. Available from: https://www.ncbi.nlm.nih.gov/pubmed/29489755.

[119] Napoli C, Lemieux C, Jorgensen R. Introduction of a Chimeric Chalcone Synthase Gene into Petunia Results in Reversible Co-Suppression of Homologous Genes in trans [Journal Article]. Plant Cell. 1990;2(4):279-89.

[120] Sen GL, Blau HM. A brief history of RNAi: the silence of the genes [Journal Article]. FASEB J. 2006;20(9):1293-9. Available from: https://www.ncbi.nlm.nih.gov/pubmed/16816104.

[121] Alberts B. Molecular Biology of the Cell. 2nd ed. New York; London: Garland; 1989.

[122] Chandrasegaran S, Carroll D. Origins of Programmable Nucleases for Genome Engineering [Journal Article]. J Mol Biol. 2016;428(5 Pt B):963-89. Available from: https://www.ncbi.nlm.nih.gov/pubmed/26506267.

[123] Mocellin S, Provenzano M. RNA interference: learning gene knock-down from cell physiology [Journal Article]. J Transl Med. 2004;2(1):39. Available from: https://www.ncbi.nlm.nih.gov/pubmed/15555080.

[124] Matsuo Y, MacLeod RA, Uphoff CC, Drexler HG, Nishizaki C, Katayama Y, et al. Two acute monocytic leukemia (AML-M5a) cell lines (MOLM-13 and MOLM-14) with interclonal phenotypic heterogeneity showing MLL-AF9 fusion resulting from an occult chromosome insertion, ins(11;9)(q23;p22p23) [Journal Article]. Leukemia. 1997;11(9):1469-77.

[125] Matozaki S, Nakagawa T, Kawaguchi R, Aozaki R, Tsutsumi M, Murayama T, et al. Establishment of a myeloid leukaemic cell line (SKNO-1) from a patient with t(8;21) who acquired monosomy 17 during disease progression [Journal Article]. Br J Haematol. 1995;89(4):805-11. Available from: https://www.ncbi.nlm.nih.gov/pubmed/7772516.

[126] Tsuchiya S, Yamabe M, Yamaguchi Y, Kobayashi Y, Konno T, Tada K. Establishment and characterization of a human acute monocytic leukemia cell line (THP-1) [Journal Article]. Int J Cancer. 1980;26(2):171-6. Available from: https://www.ncbi.nlm.nih.gov/pubmed/6970727.

[127] Drexler HG, Quentmeier H, MacLeod RA. Malignant hematopoietic cell lines: in vitro models for the study of MLL gene alterations [Journal Article]. Leukemia. 2004;18(2):227-32.

[128] Sundstrom C, Nilsson K. Establishment and characterization of a human histiocytic lymphoma cell line (U-937) [Journal Article]. Int J Cancer. 1976;17(5):565-77. Available from: https://www.ncbi.nlm.nih.gov/pubmed/178611.

[129] DepMap B. DepMap B, editor. DepMap Public 25Q2 [Dataset]. depmap.org; 2025.

[130] Nascimento CR, Rodrigues Fernandes NA, Gonzalez Maldonado LA, Rossa Junior C. Comparison of monocytic cell lines U937 and THP-1 as macrophage models for in vitro studies [Journal Article]. Biochem Biophys Rep. 2022;32:101383.

[131] Moscicki RA, Amento EP, Krane SM, Kurnick JT, Colvin RB. Modulation of surface antigens of a human monocyte cell line, U937, during incubation with T lymphocyte-conditioned medium: detection of T4 antigen and its presence on normal blood monocytes [Journal Article]. The Journal of Immunology. 1983;131(2):743-8. Available from: https://doi.org/10.4049/jimmunol.131.2.743.

[132] Asou H, Tashiro S, Hamamoto K, Otsuji A, Kita K, Kamada N. Establishment of a human acute myeloid leukemia cell line (Kasumi-1) with 8;21 chromosome translocation [Journal Article]. Blood. 1991;77(9):2031-6.

[133] Quentmeier H, Pommerenke C, Dirks WG, Eberth S, Koeppel M, MacLeod RAF, et al. The LL-100 panel: 100 cell lines for blood cancer studies [Journal Article]. Sci Rep. 2019;9(1):8218. Available from: https://www.ncbi.nlm.nih.gov/pubmed/31160637.

[134] Alshaer W, Zureigat H, Al Karaki A, Al-Kadash A, Gharaibeh L, Hatmal MM, et al. siRNA: Mechanism of action, challenges, and therapeutic approaches [Journal Article]. Eur J Pharmacol. 2021;905:174178. Available from: https://www.ncbi.nlm.nih.gov/pubmed/34044011.

[135] Sanjana NE, Shalem O, Zhang F. Improved vectors and genome-wide libraries for CRISPR screening [Journal Article]. Nat Methods. 2014;11(8):783-4.

[136] Moffat J, Grueneberg DA, Yang X, Kim SY, Kloepfer AM, Hinkle G, et al. A lentiviral RNAi library for human and mouse genes applied to an arrayed viral high-content screen [Journal Article]. Cell. 2006;124(6):1283-98. Available from: https://www.ncbi.nlm.nih.gov/pubmed/16564017.

[137] Aviner R. The science of puromycin: From studies of ribosome function to applications in biotechnology [Journal Article]. Comput Struct Biotechnol J. 2020;18:1074-83. Available from: https://www.ncbi.nlm.nih.gov/pubmed/32435426.

[138] Palazzo AF, Lee ES. Non-coding RNA: what is functional and what is junk? [Journal Article]. Frontiers in Genetics. 2015;6.

[139] Zhang Y, Lu L, Li X. Detection technologies for RNA modifications [Journal Article]. Exp Mol Med. 2022;54(10):1601-16. Available from: https://www.ncbi.nlm.nih.gov/pubmed/36266445.

[140] Feitelson MA, Arzumanyan A, Kulathinal RJ, Blain SW, Holcombe RF, Mahajna J, et al. Sustained proliferation in cancer: Mechanisms and novel therapeutic targets [Journal Article]. Semin Cancer Biol. 2015;35 Suppl(Suppl):S25-s54.

[141] Koopman G, Reutelingsperger CP, Kuijten GA, Keehnen RM, Pals ST, van Oers MH. Annexin V for flow cytometric detection of phosphatidylserine expression on B cells undergoing apoptosis [Journal Article]. Blood. 1994;84(5):1415-20.

[142] McIlwain DR, Berger T, Mak TW. Caspase functions in cell death and disease [Journal Article]. Cold Spring Harb Perspect Biol. 2013;5(4):a008656.

[143] Mustafa M, Ahmad R, Tantry IQ, Ahmad W, Siddiqui S, Alam M, et al. Apoptosis: A Comprehensive Overview of Signaling Pathways, Morphological Changes, and Physiological Significance and Therapeutic Implications [Journal Article]. Cells. 2024;13(22). Available from: https://www.ncbi.nlm.nih.gov/pubmed/39594587.

[144] Yan HF, Zou T, Tuo QZ, Xu S, Li H, Belaidi AA, et al. Ferroptosis: mechanisms and links with diseases [Journal Article]. Signal Transduction and Targeted Therapy. 2021;6(1):49. Available from: https://www.ncbi.nlm.nih.gov/pubmed/33536413.

[145] Nie Q, Hu Y, Yu X, Li X, Fang X. Induction and application of ferroptosis in cancer therapy [Journal Article]. Cancer Cell Int. 2022;22(1):12. Available from: https://www.ncbi.nlm.nih.gov/pubmed/34996454.

[146] Schmid I, Uittenbogaart C, Jamieson BD. Live-cell assay for detection of apoptosis by dual-laser flow cytometry using Hoechst 33342 and 7-amino-actinomycin D [Journal Article]. Nature Protocols. 2007;2(1):187-90. Available from: https://doi.org/10.1038/nprot.2006.458.

[147] Darzynkiewicz Z, Huang X, Zhao H. Analysis of Cellular DNA Content by Flow Cytometry [Journal Article]. Curr Protoc Cytom. 2017;82:7.5.1-7.5.20.

[148] Darzynkiewicz Z, Halicka HD, Zhao H. Analysis of cellular DNA content by flow and laser scanning cytometry [Journal Article]. Adv Exp Med Biol. 2010;676:137-47.

[149] Kajstura M, Halicka HD, Pryjma J, Darzynkiewicz Z. Discontinuous fragmentation of nuclear DNA during apoptosis revealed by discrete "sub-G1" peaks on DNA content histograms [Journal Article]. Cytometry A. 2007;71(3):125-31.

[150] Watson JV, Chambers SH, Smith PJ. A pragmatic approach to the analysis of DNA histograms with a definable G1 peak [Journal Article]. Cytometry. 1987;8(1):1-8. Available from: https://www.ncbi.nlm.nih.gov/pubmed/3803091.

[151] Li H, Liu B, Lian L, Zhou J, Xiang S, Zhai Y, et al. High dose expression of heme oxigenase-1 induces retinal degeneration through ER stress-related DDIT3 [Journal Article]. Mol Neurodegener. 2021;16(1):16. Available from: https://www.ncbi.nlm.nih.gov/pubmed/33691741.

[152] Rubnitz JE, Gibson B, Smith FO. Acute myeloid leukemia [Journal Article]. Hematol Oncol Clin North Am. 2010;24(1):35-63.

[153] Jager P, Geyh S, Twarock S, Cadeddu RP, Rabes P, Koch A, et al. Acute myeloid leukemia-induced functional inhibition of healthy CD34+ hematopoietic stem and progenitor cells [Journal Article]. Stem Cells. 2021;39(9):1270-84. Available from: https://www.ncbi.nlm.nih.gov/pubmed/34013984.

[154] Stubbins RJ, Karsan A. Differentiation therapy for myeloid malignancies: beyond cytotoxicity [Journal Article]. Blood Cancer J. 2021;11(12):193. Available from: https://www.ncbi.nlm.nih.gov/pubmed/34864823.

[155] Chen Q, Ross AC. Retinoic acid regulates cell cycle progression and cell differentiation in human monocytic THP-1 cells [Journal Article]. Exp Cell Res. 2004;297(1):68-81. Available from: https://www.ncbi.nlm.nih.gov/pubmed/15194426.

[156] Sanchez PV, Glantz ST, Scotland S, Kasner MT, Carroll M. Induced differentiation of acute myeloid leukemia cells by activation of retinoid X and liver X receptors [Journal Article]. Leukemia. 2014;28(4):749-60. Available from: https://www.ncbi.nlm.nih.gov/pubmed/23823656.

[157] Iijima K, Honma Y, Niitsu N. Granulocytic differentiation of leukemic cells with t(9;11)(p22;q23) induced by all-trans-retinoic acid [Journal Article]. Leuk Lymphoma. 2004;45(5):1017-24. Available from: https://www.ncbi.nlm.nih.gov/pubmed/15291362.

[158] Sykes DB, Kfoury YS, Mercier FE, Wawer MJ, Law JM, Haynes MK, et al. Inhibition of Dihydroorotate Dehydrogenase Overcomes Differentiation Blockade in Acute Myeloid Leukemia [Journal Article]. Cell. 2016;167(1):171-86.e15.

[159] Montesinos P, Bergua JM, Vellenga E, Rayon C, Parody R, de la Serna J, et al. Differentiation syndrome in patients with acute promyelocytic leukemia treated with all-trans retinoic acid and anthracycline chemotherapy: characteristics, outcome, and prog-

nostic factors [Journal Article]. Blood. 2009;113(4):775-83. Available from: https://www.ncbi.nlm.nih.gov/pubmed/18945964.

[160] Dunning K, Safo AO. The ultimate Wright-Giemsa stain: 60 years in the making [Journal Article]. Biotechnic and Histochemistry. 2011;86(2):69-75. Available from: https://doi.org/10.3109/10520295.2010.515496.

[161] Barcia JJ. The Giemsa stain: its history and applications [Journal Article]. Int J Surg Pathol. 2007;15(3):292-6.

[162] American Society of Hematology A. of Hematology AS, editor. ASH Image Bank [Online Database]. American Society of Hematology; 2025. Available from: www.imagebank.hematology.org.

[163] Josa-Cullere L, Galan SRG, Cogswell TJ, Jackson TR, Jay-Smith M, Mola L, et al. Phenotypic screening identifies a trisubstituted imidazo[1,2-a]pyridine series that induces differentiation in multiple AML cell lines [Journal Article]. European Journal of Medicinal Chemistry. 2023;258:115509. Available from: https://www.sciencedirect.com/science/article/pii/S0223523423004750.

[164] Ward JM, Cherian S, Linden MA. In: Treuting PM, Dintzis SM, Montine KS, editors. 19 - Hematopoietic and Lymphoid Tissues. San Diego: Academic Press; 2018. p. 365-401. Available from: https://www.sciencedirect.com/science/article/pii/B9780128029008000191.

[165] Kaufman DS, Hanson ET, Lewis RL, Auerbach R, Thomson JA. Hematopoietic colony-forming cells derived from human embryonic stem cells [Journal Article]. Proceedings of the National Academy of Sciences. 2001;98(19):10716-21. Available from: https://doi.org/10.1073/pnas.191362598.

[166] Franken NAP, Rodermond HM, Stap J, Haveman J, van Bree C. Clonogenic assay of cells in vitro [Journal Article]. Nature Protocols. 2006;1(5):2315-9. Available from: https://doi.org/10.1038/nprot.2006.339.

[167] Mazzone A, Ricevuti G. Leukocyte CD11/CD18 integrins: biological and clinical relevance [Journal Article]. Haematologica. 1995;80(2):161-75. Available from: https://haematologica.org/article/view/664.

[168] Gorczyca W. Flow Cytometry in Neoplastic Hematology: Morphologic-Immunophenotypic Correlation. Third edition ed. CRC Press; 2017.

[169] Zhou H, Liao J, Aloor J, Nie H, Wilson BC, Fessler MB, et al. CD11b/CD18 (Mac-1) is a novel surface receptor for extracellular double-stranded RNA to mediate cellular inflammatory responses [Journal Article]. J Immunol. 2013;190(1):115-25.

[170] Solovjov DA, Pluskota E, Plow EF. Distinct roles for the alpha and beta subunits in

the functions of integrin alphaMbeta2 [Journal Article]. Journal of Biological Chemistry. 2005;280(2):1336-45. Available from: https://doi.org/10.1074/jbc.M406968200.

[171] Scott CS, Richards SJ, Master PS, Kendall J, Limbert HJ, Roberts BE. Flow cytometric analysis of membrane CD11b, CD11c and CD14 expression in acute myeloid leukaemia: relationships with monocytic subtypes and the concept of relative antigen expression [Journal Article]. Eur J Haematol. 1990;44(1):24-9. Available from: https://www.ncbi.nlm.nih.gov/pubmed/1689668.

[172] Chen MH, Atenafu E, Craddock KJ, Brandwein J, Chang H. CD11b expression correlates with monosomal karyotype and predicts an extremely poor prognosis in cytogenetically unfavorable acute myeloid leukemia [Journal Article]. Leukemia Research. 2013;37(2):122-8. Available from: https://www.sciencedirect.com/science/article/pii/S014521261200392X.

[173] Zhang Q, Ma R, Chen H, Guo W, Li Z, Xu K, et al. CD86 Is Associated with Immune Infiltration and Immunotherapy Signatures in AML and Promotes Its Progression [Journal Article]. J Oncol. 2023;2023:9988405.

[174] Ushach I, Zlotnik A. Biological role of granulocyte macrophage colony-stimulating factor (GM-CSF) and macrophage colony-stimulating factor (M-CSF) on cells of the myeloid lineage [Journal Article]. J Leukoc Biol. 2016;100(3):481-9.

[175] Takimoto CH, Chao MP, Gibbs C, McCamish MA, Liu J, Chen JY, et al. The Macrophage Do not eat me signal, CD47, is a clinically validated cancer immunotherapy target [Journal Article]. Annals of Oncology. 2019;30(3):486-9. Doi: 10.1093/annonc/mdz006. Available from: https://doi.org/10.1093/annonc/mdz006.

[176] Koblitz J, Dirks WG, Eberth S, Nagel S, Steenpass L, Pommerenke C. DSMZCellDive: Diving into high-throughput cell line data [Journal Article]. F1000Res. 2022;11:420. Available from: https://www.ncbi.nlm.nih.gov/pubmed/35949917.

[177] Hughes MR, Canals Hernaez D, Cait J, Refaeli I, Lo BC, Roskelley CD, et al. A sticky wicket: Defining molecular functions for CD34 in hematopoietic cells [Journal Article]. Exp Hematol. 2020;86:1-14. Available from: https://www.ncbi.nlm.nih.gov/pubmed/32422232.

[178] Montero J, Letai A. Why do BCL-2 inhibitors work and where should we use them in the clinic? [Journal Article]. Cell Death Differ. 2018;25(1):56-64. Available from: https://www.ncbi.nlm.nih.gov/pubmed/29077093.

[179] Dahiya M, Dureja H. Sorafenib for hepatocellular carcinoma: potential molecular targets and resistance mechanisms [Journal Article]. J Chemother. 2022;34(5):286-301. Available from: https://www.ncbi.nlm.nih.gov/pubmed/34291704.

[180] Li Q, Chen K, Zhang T, Jiang D, Chen L, Jiang J, et al. Understanding sorafenib-induced ferroptosis and resistance mechanisms: Implications for cancer therapy [Journal Article]. Eur J Pharmacol. 2023;955:175913. Available from: https://www.ncbi.nlm.nih.gov/pubmed/37460053.

[181] Auclair D, Miller D, Yatsula V, Pickett W, Carter C, Chang Y, et al. Antitumor activity of sorafenib in FLT3-driven leukemic cells [Journal Article]. Leukemia. 2007;21(3):439-45. Available from: https://www.ncbi.nlm.nih.gov/pubmed/17205056.

[182] Ewels PA, Peltzer A, Fillinger S, Patel H, Alneberg J, Wilm A, et al. The nf-core framework for community-curated bioinformatics pipelines [Journal Article]. Nature Biotechnology. 2020;38(3):276-8. Available from: https://doi.org/10.1038/s41587-020-0439-x.

[183] Love MI, Huber W, Anders S. Moderated estimation of fold change and dispersion for RNA-seq data with DESeq2 [Journal Article]. Genome Biology. 2014;15(12):550. Available from: https://doi.org/10.1186/s13059-014-0550-8.

[184] Liberzon A, Birger C, Thorvaldsdottir H, Ghandi M, Mesirov JP, Tamayo P. The Molecular Signatures Database (MSigDB) hallmark gene set collection [Journal Article]. Cell Syst. 2015;1(6):417-25.

[185] Kopecka J, Trouillas P, Gasparovic AC, Gazzano E, Assaraf YG, Riganti C. Phospholipids and cholesterol: Inducers of cancer multidrug resistance and therapeutic targets [Journal Article]. Drug Resist Updat. 2020;49:100670. Available from: https://www.ncbi.nlm.nih.gov/pubmed/31846838.

[186] Snaebjornsson MT, Janaki-Raman S, Schulze A. Greasing the Wheels of the Cancer Machine: The Role of Lipid Metabolism in Cancer [Journal Article]. Cell Metab. 2020;31(1):62-76. Available from: https://www.ncbi.nlm.nih.gov/pubmed/31813823.

[187] Pham CTN. Neutrophil serine proteases: specific regulators of inflammation [Journal Article]. Nature Reviews Immunology. 2006;6(7):541-50. Available from: https://doi.org/10.1038/nri1841.

[188] Jin W, Wu K, Li YZ, Yang WT, Zou B, Zhang F, et al. AML1-ETO targets and suppresses cathepsin G, a serine protease, which is able to degrade AML1-ETO in t(8;21) acute myeloid leukemia [Journal Article]. Oncogene. 2013;32(15):1978-87. Available from: https://www.ncbi.nlm.nih.gov/pubmed/22641217.

[189] Lin W, Chen H, Chen X, Guo C. The Roles of Neutrophil-Derived Myeloperoxidase (MPO) in Diseases: The New Progress [Journal Article]. Antioxidants (Basel). 2024;13(1). Available from: https://www.ncbi.nlm.nih.gov/pubmed/38275657.

[190] Kim Y, Yoon S, Kim SJ, Kim JS, Cheong JW, Min YH. Myeloperoxidase expression in

acute myeloid leukemia helps identifying patients to benefit from transplant [Journal Article]. Yonsei Med J. 2012;53(3):530-6. Available from: https://www.ncbi.nlm.nih.gov/pubmed/22476996.

[191] Hosseini M, Rezvani HR, Aroua N, Bosc C, Farge T, Saland E, et al. Targeting Myeloperoxidase Disrupts Mitochondrial Redox Balance and Overcomes Cytarabine Resistance in Human Acute Myeloid Leukemia [Journal Article]. Cancer Res. 2019;79(20):5191-203.

[192] Du M, Zhang Y, Li C, Zhou F, Luo W, Tang L, et al. Effect of interferon induced transmembrane protein 1 (IFITM1) upregulation to cytokine release syndrome in CAR-T-treated B-cell acute lymphoblastic leukemia [Journal Article]. Chin Med J (Engl). 2025;138(10):1242-4. Available from: https://www.ncbi.nlm.nih.gov/pubmed/40204523.

[193] She X, Shen S, Chen G, Gao Y, Ma J, Gao Y, et al. Immune surveillance of brain metastatic cancer cells is mediated by IFITM1 [Journal Article]. The EMBO Journal. 2023;42(7):e111112. Available from: https://www.embopress.org/doi/abs/10.15252/embj.2022111112.

[194] Zhao S, Sun J, Chang Q, Pang S, Zhang N, Fan Y, et al. CTCF-activated FUCA1 functions as a tumor suppressor by promoting autophagy flux and serum alpha-L-fucosidase serves as a potential biomarker for prognosis in ccRCC [Journal Article]. Cancer Cell Int. 2024;24(1):327. Available from: https://www.ncbi.nlm.nih.gov/pubmed/39342260.

[195] Pekdemir B, Bechelany M, Karav S. Fucosidosis: A Review of a Rare Disease [Journal Article]. Int J Mol Sci. 2025;26(1). Available from: https://www.ncbi.nlm.nih.gov/pubmed/39796208.

[196] Reeves EP, Lu H, Jacobs HL, Messina CGM, Bolsover S, Gabella G, et al. Killing activity of neutrophils is mediated through activation of proteases by K+Â flux [Journal Article]. Nature. 2002;416(6878):291-7. Available from: https://doi.org/10.1038/416291a.

[197] Morimoto-Kamata R, Tsuji D, Yui S. Cathepsin G-Induced Insulin-Like Growth Factor (IGF) Elevation in MCF-7 Medium Is Caused by Proteolysis of IGF Binding Protein (IGFBP)-2 but Not of IGF-1 [Journal Article]. Biological and Pharmaceutical Bulletin. 2020;43(11):1678-86.

[198] Hong Y, Boiti A, Vallone D, Foulkes NS. Reactive Oxygen Species Signaling and Oxidative Stress: Transcriptional Regulation and Evolution [Journal Article]. Antioxidants (Basel). 2024;13(3). Available from: https://www.ncbi.nlm.nih.gov/pubmed/38539845.

[199] Raimondi V, Ciccarese F, Ciminale V. Oncogenic pathways and the electron transport chain: a dangeROS liaison [Journal Article]. Br J Cancer. 2020;122(2):168-81. Available from:

https://www.ncbi.nlm.nih.gov/pubmed/31819197.

[200] Van Kuilenburg AB, Van Beeumen JJ, Van der Meer NM, Muijsers AO. Subunits VIIa,b,c of human cytochrome c oxidase. Identification of both 'heart-type' and 'liver-type' isoforms of subunit VIIa in human heart [Journal Article]. Eur J Biochem. 1992;203(1-2):193-9. Available from: https://www.ncbi.nlm.nih.gov/pubmed/1309697.

[201] Kadenbach B, HÃ¼ttemann M. The subunit composition and function of mammalian cytochrome c oxidase [Journal Article]. Mitochondrion. 2015;24:64-76.

[202] Wu S, Akhtari M, Alachkar H. Characterization of Mutations in the Mitochondrial Encoded Electron Transport Chain Complexes in Acute Myeloid Leukemia [Journal Article]. Sci Rep. 2018;8(1):13301. Available from: https://www.ncbi.nlm.nih.gov/pubmed/30185817.

[203] Silkjaer T, Norgaard JM, Aggerholm A, Ebbesen LH, Kjeldsen E, Hokland P, et al. Characterization and prognostic significance of mitochondrial DNA variations in acute myeloid leukemia [Journal Article]. Eur J Haematol. 2013;90(5):385-96. Available from: https://www.ncbi.nlm.nih.gov/pubmed/23444869.

[204] Mihara M, Erster S, Zaika A, Petrenko O, Chittenden T, Pancoska P, et al. p53 has a direct apoptogenic role at the mitochondria [Journal Article]. Mol Cell. 2003;11(3):577-90. Available from: https://www.ncbi.nlm.nih.gov/pubmed/12667443.

[205] Rochlitz C, Lohri A, Bacchi M, Schmidt M, Nagel S, Fopp M, et al. Axl expression is associated with adverse prognosis and with expression of Bcl-2 and CD34 in de novo acute myeloid leukemia (AML): results from a multicenter trial of the Swiss Group for Clinical Cancer Research (SAKK) [Journal Article]. Leukemia. 1999;13(9):1352-8. Available from: https://doi.org/10.1038/sj.leu.2401484.

[206] Niu X, Rothe K, Chen M, Grasedieck S, Li R, Nam SE, et al. Targeting AXL kinase sensitizes leukemic stem and progenitor cells to venetoclax treatment in acute myeloid leukemia [Journal Article]. Blood. 2021;137(26):3641-55. Available from: https://doi.org/10.1182/blood.2020007651.

[207] Vandewalle N, De Beule N, De Becker A, De Bruyne E, Menu E, Vanderkerken K, et al. AXL as immune regulator and therapeutic target in Acute Myeloid Leukemia: from current progress to novel strategies [Journal Article]. Exp Hematol Oncol. 2024;13(1):99. Available from: https://www.ncbi.nlm.nih.gov/pubmed/39367387.

[208] Konishi A, Aizawa T, Mohan A, Korshunov VA, Berk BC. Hydrogen peroxide activates the Gas6-Axl pathway in vascular smooth muscle cells [Journal Article]. J Biol Chem. 2004;279(27):28766-70. Available from: https://www.ncbi.nlm.nih.gov/pubmed/15123721.

[209] Nakamura H, Takada K. Reactive oxygen species in cancer: Current findings and future

directions [Journal Article]. Cancer Sci. 2021;112(10):3945-52. Available from: https://www.ncbi.nlm.nih.gov/pubmed/34286881.

[210] Glorieux C, Enriquez C, Buc Calderon P. The complex interplay between redox dysregulation and mTOR signaling pathway in cancer: A rationale for cancer treatment [Journal Article]. Biochem Pharmacol. 2025;232:116729. Available from: https://www.ncbi.nlm.nih.gov/pubmed/39709038.

[211] Matza D, Badou A, Kobayashi KS, Goldsmith-Pestana K, Masuda Y, Komuro A, et al. A scaffold protein, AHNAK1, is required for calcium signaling during T cell activation [Journal Article]. Immunity. 2008;28(1):64-74.

[212] Sundararaj S, Ravindran A, Casarotto MG. AHNAK: The quiet giant in calcium homeostasis [Journal Article]. Cell Calcium. 2021;96:102403. Available from: https://www.ncbi.nlm.nih.gov/pubmed/33813182.

[213] Li L, Liu Y, Feng T, Zhou W, Wang Y, Li H. The AHNAK induces increased IL-6 production in CD4+ T cells and serves as a potential diagnostic biomarker for recurrent pregnancy loss [Journal Article]. Clin Exp Immunol. 2022;209(3):291-304. Available from: https://www.ncbi.nlm.nih.gov/pubmed/35766885.

[214] Chen B, Wang J, Dai D, Zhou Q, Guo X, Tian Z, et al. AHNAK suppresses tumour proliferation and invasion by targeting multiple pathways in triple-negative breast cancer [Journal Article]. J Exp Clin Cancer Res. 2017;36(1):65. Available from: https://www.ncbi.nlm.nih.gov/pubmed/28494797.

[215] Li K, Song K, Hou Y, Tian Y, Wang H, Sun L, et al. AHNAK Contributes to Hepatocellular Carcinoma Growth by Interacting with IGF-1R [Journal Article]. Molecules. 2022;27(24). Available from: https://www.ncbi.nlm.nih.gov/pubmed/36557813.

[216] Li C, Xin H, Hao J, Miao Y. Decreasing of serine/threonine kinase 39 has tumour inhibiting effects on acute myeloid leukaemia by impacting the PI3K/AKT and Wnt/beta-catenin signalling cascades [Journal Article]. Toxicol Appl Pharmacol. 2024;489:116982. Available from: https://www.ncbi.nlm.nih.gov/pubmed/38821216.

[217] Richardson C, Sakamoto K, de los Heros P, Deak M, Campbell DG, Prescott AR, et al. Regulation of the NKCC2 ion cotransporter by SPAK-OSR1-dependent and -independent pathways [Journal Article]. J Cell Sci. 2011;124(Pt 5):789-800. Available from: https://www.ncbi.nlm.nih.gov/pubmed/21321328.

[218] Biggs O'May J, Vanes L, de Boer LL, Lewis DA, Hartweger H, Kunzelmann S, et al. WNK1-dependent water influx is required for CD4(+) T cell activation and T cell-dependent antibody responses [Journal Article]. Nat Commun. 2025;16(1):1857. Available from: https://www.ncbi.nlm.nih.gov/pubmed/39984435.

[219] Kang X, Cui C, Wang C, Wu G, Chen H, Lu Z, et al. CAMKs support development of

acute myeloid leukemia [Journal Article]. J Hematol Oncol. 2018;11(1):30. Available from: https://www.ncbi.nlm.nih.gov/pubmed/29482582.

[220] Izadi M, Hou W, Qualmann B, Kessels MM. Direct effects of Ca(2+)/calmodulin on actin filament formation [Journal Article]. Biochem Biophys Res Commun. 2018;506(2):355-60. Available from: https://www.ncbi.nlm.nih.gov/pubmed/30093111.

[221] Campellone KG, Lebek NM, King VL. Branching out in different directions: Emerging cellular functions for the Arp2/3 complex and WASP-family actin nucleation factors [Journal Article]. Eur J Cell Biol. 2023;102(2):151301. Available from: https://www.ncbi.nlm.nih.gov/pubmed/36907023.

[222] Villalonga E, Mosrin C, Normand T, Girardin C, Serrano A, Zunar B, et al. LIM Kinases, LIMK1 and LIMK2, Are Crucial Node Actors of the Cell Fate: Molecular to Pathological Features [Journal Article]. Cells. 2023;12(5). Available from: https://www.ncbi.nlm.nih.gov/pubmed/36899941.

[223] Allouch A, Voisin L, Zhang Y, Raza SQ, Lecluse Y, Calvo J, et al. CDKN1A is a target for phagocytosis-mediated cellular immunotherapy in acute leukemia [Journal Article]. Nat Commun. 2022;13(1):6739. Available from: https://www.ncbi.nlm.nih.gov/pubmed/36347876.

[224] Rotty JD, Brighton HE, Craig SL, Asokan SB, Cheng N, Ting JP, et al. Arp2/3 Complex Is Required for Macrophage Integrin Functions but Is Dispensable for FcR Phagocytosis and In Vivo Motility [Journal Article]. Dev Cell. 2017;42(5):498-513 e6. Available from: https://www.ncbi.nlm.nih.gov/pubmed/28867487.

[225] Yang N, Higuchi O, Ohashi K, Nagata K, Wada A, Kangawa K, et al. Cofilin phosphorylation by LIM-kinase 1 and its role in Rac-mediated actin reorganization [Journal Article]. Nature. 1998;393(6687):809-12. Available from: https://doi.org/10.1038/31735.

[226] Jensen P, Carlet M, Schlenk RF, Weber A, Kress J, Brunner I, et al. Requirement for LIM kinases in acute myeloid leukemia [Journal Article]. Leukemia. 2020;34(12):3173-85. Available from: https://www.ncbi.nlm.nih.gov/pubmed/32591645.

[227] Djamai H, Berrou J, Dupont M, Kaci A, Ehlert JE, Weber H, et al. Synergy of FLT3 inhibitors and the small molecule inhibitor of LIM kinase1/2 CEL_Amide in FLT3-ITD mutated Acute Myeloblastic Leukemia (AML) cells [Journal Article]. Leuk Res. 2021;100:106490. Available from: https://www.ncbi.nlm.nih.gov/pubmed/33373830.

[228] Yuniati L, Scheijen B, van der Meer LT, van Leeuwen FN. Tumor suppressors BTG1 and BTG2: Beyond growth control [Journal Article]. J Cell Physiol. 2019;234(5):5379-89. Available from: https://www.ncbi.nlm.nih.gov/pubmed/30350856.

[229] Zhang Z, Chen C, Wang G, Yang Z, San J, Zheng J, et al. Aberrant expression of the p53-inducible antiproliferative gene BTG2 in hepatocellular carcinoma is associated with overexpression of the cell cycle-related proteins [Journal Article]. Cell Biochem Biophys. 2011;61(1):83-91. Available from: https://www.ncbi.nlm.nih.gov/pubmed/21327578.

[230] Han C, Zhang Z, Crosse EI, Sajedi S, Lu B, Wang X, et al. An isoform-specific RUNX1C-BTG2 axis governs AML quiescence and chemoresistance [Journal Article]. Blood Cancer Discov. 2025. Available from: https://www.ncbi.nlm.nih.gov/pubmed/40632085.

[231] Lamas-Paz A, Hionides-Gutierrez A, Guo F, Jorquera G, Moran-Blanco L, Benede-Ubieto R, et al. Loss of Cdkn1a protects against MASLD alone or with alcohol intake by preserving lipid homeostasis [Journal Article]. JHEP Rep. 2025;7(1):101230. Available from: https://www.ncbi.nlm.nih.gov/pubmed/39659733.

[232] Zheng S, Zhang Y, Cai R, Cai B, Luo S, He S, et al. The untold story of CD82: Exploring its non-canonical roles in cancer [Journal Article]. Pathol Res Pract. 2025;270:155979. Available from: https://www.ncbi.nlm.nih.gov/pubmed/40252385.

[233] Liu WM, Zhang F, Moshiach S, Zhou B, Huang C, Srinivasan K, et al. Tetraspanin CD82 inhibits protrusion and retraction in cell movement by attenuating the plasma membrane-dependent actin organization [Journal Article]. PLoS One. 2012;7(12):e51797. Available from: https://www.ncbi.nlm.nih.gov/pubmed/23251627.

[234] Ji H, Chen L, Xing Y, Li S, Dai J, Zhao P, et al. CD82 supports survival of childhood acute myeloid leukemia cells via activation of Wnt/beta-catenin signaling pathway [Journal Article]. Pediatr Res. 2019;85(7):1024-31. Available from: https://www.ncbi.nlm.nih.gov/pubmed/30862962.

[235] Wang X, Yu H, Gao R, Liu M, Xie W. A comprehensive review of the family of very-long-chain fatty acid elongases: structure, function, and implications in physiology and pathology [Journal Article]. Eur J Med Res. 2023;28(1):532. Available from: https://www.ncbi.nlm.nih.gov/pubmed/37981715.

[236] Ferrero E, Vaz FM, Cheillan D, Brusco A, Marelli C. The ELOVL proteins: Very and ultra long-chain fatty acids at the crossroads between metabolic and neurodegenerative disorders [Journal Article]. Mol Genet Metab. 2025;144(3):109050. Available from: https://www.ncbi.nlm.nih.gov/pubmed/39946831.

[237] Guo J, Xue S, Wang X, Wang L, Wen SY. Emerging insights on the role of Elovl6 in human diseases: Therapeutic challenges and opportunities [Journal Article]. Life Sci. 2025;361:123308. Available from: https://www.ncbi.nlm.nih.gov/pubmed/39675554.

[238] Liu Y, Wang F, Yu XL, Miao ZM, Wang ZC, Chen Y, et al. Genetic analysis of the ELOVL6

gene polymorphism associated with type 2 diabetes mellitus [Journal Article]. Braz J Med Biol Res. 2013;46(7):623-8. Available from: https://www.ncbi.nlm.nih.gov/pubmed/23903678.

[239] Feng YH, Chen WY, Kuo YH, Tung CL, Tsao CJ, Shiau AL, et al. Elovl6 is a poor prognostic predictor in breast cancer [Journal Article]. Oncol Lett. 2016;12(1):207-12. Available from: https://www.ncbi.nlm.nih.gov/pubmed/27347126.

[240] Garcia Corrales AV, Verberk SGS, Haidar M, Grajchen E, Dehairs J, Vanherle S, et al. Fatty acid elongation by ELOVL6 hampers remyelination by promoting inflammatory foam cell formation during demyelination [Journal Article]. Proc Natl Acad Sci U S A. 2023;120(37):e2301030120. Available from: https://www.ncbi.nlm.nih.gov/pubmed/37669365.

[241] Tian X, Li S, Ge G. Apatinib Promotes Ferroptosis in Colorectal Cancer Cells by Targeting ELOVL6/ACSL4 Signaling [Journal Article]. Cancer Manag Res. 2021;13:1333-42. Available from: https://www.ncbi.nlm.nih.gov/pubmed/33603479.

[242] Anelli L, Zagaria A, Coccaro N, Tota G, Impera L, Minervini CF, et al. A novel t(4;16)(q25;q23.1) associated with EGF and ELOVL6 deregulation in acute myeloid leukemia [Journal Article]. Gene. 2013;529(1):144-7. Available from: https://www.ncbi.nlm.nih.gov/pubmed/23933272.

[243] Kiyoki Y, Kato T, Kito S, Matsuzaka T, Morioka S, Sasaki J, et al. The fatty acid elongase Elovl6 is crucial for hematopoietic stem cell engraftment and leukemia propagation [Journal Article]. Leukemia. 2023;37(4):910-3. Available from: https://www.ncbi.nlm.nih.gov/pubmed/36890291.

[244] Shetty VV, Shetty SS. Fatty Acid Desaturase: The Yin or Yang of Disease Pathology [Journal Article]. Mol Diagn Ther. 2025. Available from: https://www.ncbi.nlm.nih.gov/pubmed/40587082.

[245] Harayama T, Shimizu T. Roles of polyunsaturated fatty acids, from mediators to membranes [Journal Article]. J Lipid Res. 2020;61(8):1150-60. Available from: https://www.ncbi.nlm.nih.gov/pubmed/32487545.

[246] Hoy AJ, Nagarajan SR, Butler LM. Tumour fatty acid metabolism in the context of therapy resistance and obesity [Journal Article]. Nat Rev Cancer. 2021;21(12):753-66. Available from: https://www.ncbi.nlm.nih.gov/pubmed/34417571.

[247] Qin J, Ye L, Wen X, Zhang X, Di Y, Chen Z, et al. Fatty acids in cancer chemoresistance [Journal Article]. Cancer Lett. 2023;572:216352. Available from: https://www.ncbi.nlm.nih.gov/pubmed/37597652.

[248] Suda A, Umaru BA, Yamamoto Y, Shima H, Saiki Y, Pan Y, et al. Polyunsaturated fatty acids-induced ferroptosis suppresses pancreatic cancer growth [Journal Article]. Sci Rep.

2024;14(1):4409. Available from: https://www.ncbi.nlm.nih.gov/pubmed/38388563.

[249] Bond LM, Miyazaki M, ONeill LM, Ding F, Ntambi JM. 1. In: Ridgway ND, McLeod RS, editors. Chapter 6 - Fatty Acid Desaturation and Elongation in Mammals. Boston: Elsevier; 2016. p. 185-208. Available from: https://www.sciencedirect.com/science/article/pii/B9780444634382000067.

[250] Koundouros N, Poulogiannis G. Reprogramming of fatty acid metabolism in cancer [Journal Article]. Br J Cancer. 2020;122(1):4-22. Available from: https://www.ncbi.nlm.nih.gov/pubmed/31819192.

[251] Vriens K, Christen S, Parik S, Broekaert D, Yoshinaga K, Talebi A, et al. Evidence for an alternative fatty acid desaturation pathway increasing cancer plasticity [Journal Article]. Nature. 2019;566(7744):403-6. Available from: https://www.ncbi.nlm.nih.gov/pubmed/30728499.

[252] Young RSE, Bowman AP, Williams ED, Tousignant KD, Bidgood CL, Narreddula VR, et al. Apocryphal FADS2 activity promotes fatty acid diversification in cancer [Journal Article]. Cell Rep. 2021;34(6):108738. Available from: https://www.ncbi.nlm.nih.gov/pubmed/33567271.

[253] Jones CL, Stevens BM, D'Alessandro A, Reisz JA, Culp-Hill R, Nemkov T, et al. Inhibition of Amino Acid Metabolism Selectively Targets Human Leukemia Stem Cells [Journal Article]. Cancer Cell. 2018;34(5):724-40 e4. Available from: https://www.ncbi.nlm.nih.gov/pubmed/30423294.

[254] Stevens BM, Jones CL, Pollyea DA, Culp-Hill R, D'Alessandro A, Winters A, et al. Fatty acid metabolism underlies venetoclax resistance in acute myeloid leukemia stem cells [Journal Article]. Nat Cancer. 2020;1(12):1176-87. Available from: https://www.ncbi.nlm.nih.gov/pubmed/33884374.

[255] Culp-Hill R, Stevens BM, Jones CL, Pei S, Dzieciatkowska M, Minhajuddin M, et al. Therapy-Resistant Acute Myeloid Leukemia Stem Cells Are Resensitized to Venetoclax + Azacitidine by Targeting Fatty Acid Desaturases 1 and 2 [Journal Article]. Metabolites. 2023;13(4). Available from: https://www.ncbi.nlm.nih.gov/pubmed/37110126.

[256] Triki M, Rinaldi G, Planque M, Broekaert D, Winkelkotte AM, Maier CR, et al. mTOR Signaling and SREBP Activity Increase FADS2 Expression and Can Activate Sapienate Biosynthesis [Journal Article]. Cell Rep. 2020;31(12):107806. Available from: https://www.ncbi.nlm.nih.gov/pubmed/32579932.

[257] Eruslanov E, Kusmartsev S. 1. In: Armstrong D, editor. Identification of ROS Using Oxidized DCFDA and Flow-Cytometry. Totowa, NJ: Humana Press; 2010. p. 57-72. Available from: https://doi.org/10.1007/978-1-60761-411-1_4.

[258] Murphy MP, Bayir H, Belousov V, Chang CJ, Davies KJA, Davies MJ, et al. Guidelines for measuring reactive oxygen species and oxidative damage in cells and in vivo [Journal Article]. Nat Metab. 2022;4(6):651-62. Available from: https://www.ncbi.nlm.nih.gov/pubmed/35760871.

[259] Mbarik M, Biam RS, Robichaud PP, Surette ME. The impact of PUFA on cell responses: Caution should be exercised when selecting PUFA concentrations in cell culture [Journal Article]. Prostaglandins Leukot Essent Fatty Acids. 2020;155:102083. Available from: https://www.ncbi.nlm.nih.gov/pubmed/32126480.

[260] Alsabeeh N, Chausse B, Kakimoto PA, Kowaltowski AJ, Shirihai O. Cell culture models of fatty acid overload: Problems and solutions [Journal Article]. Biochim Biophys Acta Mol Cell Biol Lipids. 2018;1863(2):143-51. Available from: https://www.ncbi.nlm.nih.gov/pubmed/29155055.

[261] Thun MJ, Henley SJ, Patrono C. Nonsteroidal anti-inflammatory drugs as anticancer agents: mechanistic, pharmacologic, and clinical issues [Journal Article]. J Natl Cancer Inst. 2002;94(4):252-66.

[262] Matsuzaka T, Shimano H, Yahagi N, Amemiya-Kudo M, Yoshikawa T, Hasty AH, et al. Dual regulation of mouse Delta(5)- and Delta(6)-desaturase gene expression by SREBP-1 and PPARalpha [Journal Article]. J Lipid Res. 2002;43(1):107-14.

[263] Saxton RA, Sabatini DM. mTOR Signaling in Growth, Metabolism, and Disease [Journal Article]. Cell. 2017;168(6):960-76. Available from: https://doi.org/10.1016/j.cell.2017.02.004.

[264] Sokei J, Kanefsky J, Sykes SM. Reprogramming of Fatty Acid Metabolism in Acute Leukemia [Journal Article]. J Cell Physiol. 2025;240(1):e70000. Available from: https://www.ncbi.nlm.nih.gov/pubmed/39835485.

[265] Cong S, Li Z, Yu L, Liu Y, Hu Y, Bi Y, et al. Integrative proteomic and lipidomic analysis of Kaili Sour Soup-mediated attenuation of high-fat diet-induced nonalcoholic fatty liver disease in a rat model [Journal Article]. Nutr Metab (Lond). 2021;18(1):26. Available from: https://www.ncbi.nlm.nih.gov/pubmed/33691721.

[266] Issa GC, DiNardo CD. Acute myeloid leukemia with IDH1 and IDH2 mutations: 2021 treatment algorithm [Journal Article]. Blood Cancer J. 2021;11(6):107. Available from: https://www.ncbi.nlm.nih.gov/pubmed/34083508.

[267] Heuser M, Maria Araujo Cruz M, Goparaju R, Chaturvedi A. Enigmas of IDH mutations in hematology/oncology [Journal Article]. Experimental Hematology. 2015;43(8):685-97. Doi: 10.1016/j.exphem.2015.05.005. Available from: https://doi.org/10.1016/j.exphem.2015.05.005.

[268] Fruchtman H, Avigan ZM, Waksal JA, Brennan N, Mascarenhas JO. Manage-

ment of isocitrate dehydrogenase 1/2 mutated acute myeloid leukemia [Journal Article]. Leukemia. 2024;38(5):927-35. Available from: https://doi.org/10.1038/s41375-024-02246-2.

[269] Badur MG, Muthusamy T, Parker SJ, Ma S, McBrayer SK, Cordes T, et al. Oncogenic R132 IDH1 Mutations Limit NADPH for De Novo Lipogenesis through (D)2-Hydroxyglutarate Production in Fibrosarcoma Sells [Journal Article]. Cell Rep. 2018;25(4):1018-26.e4.

[270] Han S, Liu Y, Cai SJ, Qian M, Ding J, Larion M, et al. IDH mutation in glioma: molecular mechanisms and potential therapeutic targets [Journal Article]. British Journal of Cancer. 2020;122(11):1580-9. Available from: https://doi.org/10.1038/s41416-020-0814-x.

[271] Lei Y, Cai S, Zhang JK, Ding SQ, Zhang ZH, Zhang CD, et al. The role and mechanism of fatty acid oxidation in cancer drug resistance [Journal Article]. Cell Death Discovery. 2025;11(1).

[272] Kamieniarz-Gdula K, Proudfoot NJ. Transcriptional Control by Premature Termination: A Forgotten Mechanism [Journal Article]. Trends in Genetics. 2019;35(8):553-64. Available from: https://www.sciencedirect.com/science/article/pii/S0168952519300927.

[273] Vlasenok M, Margasyuk S, Pervouchine DD. Transcriptome sequencing suggests that premRNA splicing counteracts widespread intronic cleavage and polyadenylation [Journal Article]. NAR Genom Bioinform. 2023;5(2):lqad051.

[274] Calvo-Roitberg E, Carroll CL, Kim G, Sanabria V, Venev SV, Mick ST, et al. mRNA initiation and termination are spatially coordinated [Journal Article]. Science. 2025;390(6769):eado8279. Available from: https://www.science.org/doi/abs/10.1126/science.ado8279.

A | Appendix

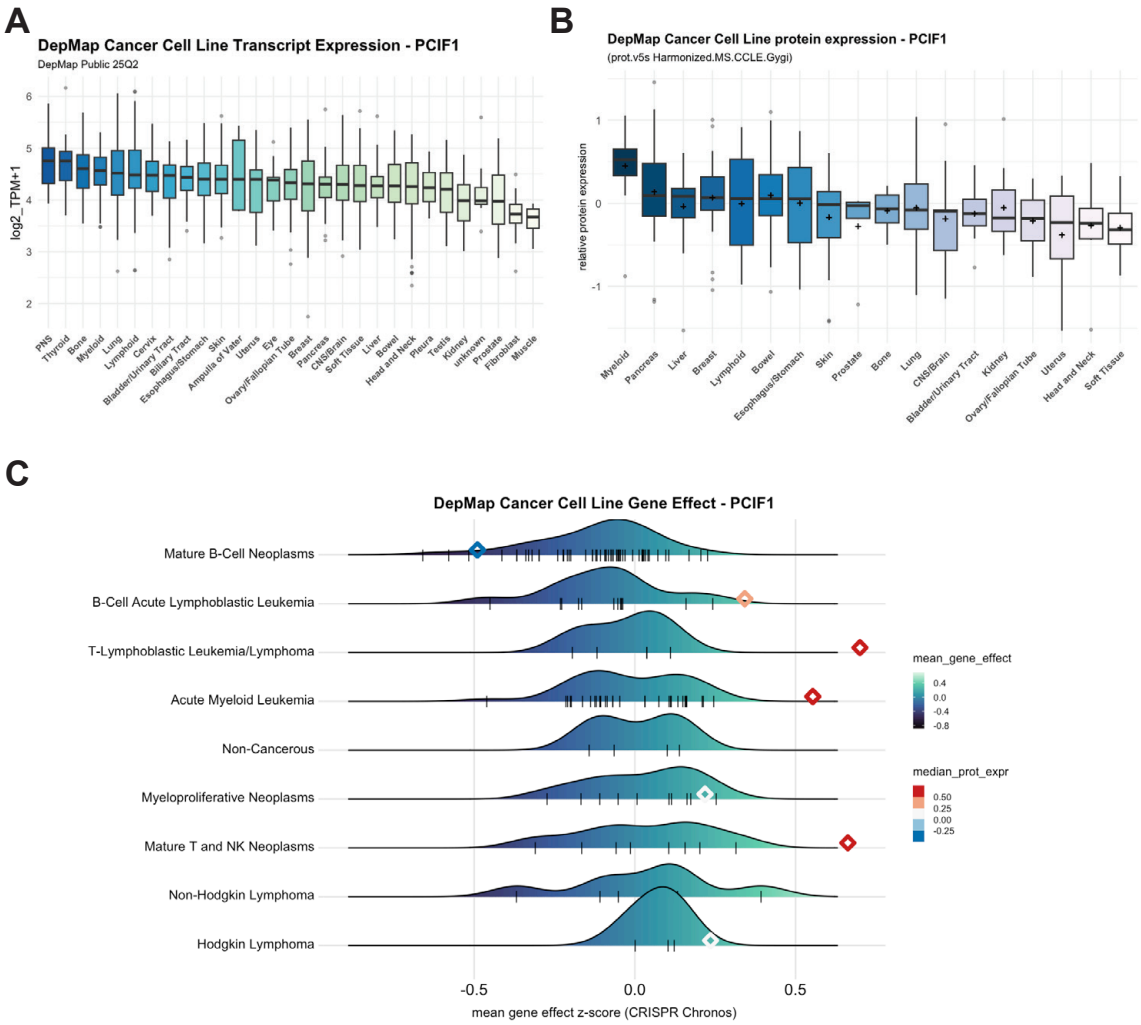

Figure A.1. Appendix: PCIF1 expression in DepMap. **A.** DepMap cell line lineage PCIF1 transcript expression. Data represented as boxplot (median+IQR), outliers depicted in grey, **B.** DepMap cell line lineage PCIF1 protein expression. Data represented as boxplot (median+IQR), outliers depicted in grey, **C.** DepMap gene effect score for PCIF1 in cancer cell lines of the myeloid and lymphoid cell line. Data represented as density plot (gene effect score along x), each event marked by |, diamond represents median PCIF1 protein expression of the cancer type.

Appendix Table A

HPA - Cell lines RNA-seq (ref = non-cancerous)								
.y.	group1	group2	n1	n2	statistic	df	p	p.adj
nTPM	Non-cancerous	Leukemia	63	93	-13,258554	116,290162	5,25E-25	1,31E-23
nTPM	Non-cancerous	Lymphoma	63	76	-9,2210172	87,4781127	1,51E-14	1,26E-13
nTPM	Non-cancerous	Neuroblastoma	63	17	-6,4308019	18,3360989	0,00000432	0,00000771
nTPM	Non-cancerous	Myeloma	63	34	-8,270946	46,8258266	1,04E-10	4,33E-10
nTPM	Non-cancerous	Pancreatic cancer	63	46	-7,8521864	67,4948358	4,25E-11	2,5E-10
nTPM	Non-cancerous	Cervical cancer	63	8	-4,7517609	8,20592205	0,001	0,002
nTPM	Non-cancerous	Gastric cancer	63	42	-6,9342473	53,0195651	5,74E-09	1,79E-08
nTPM	Non-cancerous	Bladder cancer	63	26	-6,0423207	35,1075512	6,71E-07	0,0000014
nTPM	Non-cancerous	Thyroid cancer	63	11	-3,4285778	10,7644389	0,006	0,007
nTPM	Non-cancerous	Bone cancer	63	21	-4,727008	24,9815231	0,0000757	0,000111
nTPM	Non-cancerous	Sarcoma	63	15	-4,6712276	16,8817601	0,000223	0,00031
nTPM	Non-cancerous	Skin cancer	63	62	-7,3075442	107,729465	5E-11	2,5E-10
nTPM	Non-cancerous	Lung cancer	63	232	-9,2178993	246,88071	1,38E-17	1,73E-16
nTPM	Non-cancerous	Breast cancer	63	62	-6,0599542	83,9261365	3,73E-08	9,32E-08
nTPM	Non-cancerous	Ovarian cancer	63	59	-5,5838364	85,0445623	2,76E-07	6,27E-07
nTPM	Non-cancerous	Esophageal cancer	63	27	-4,715643	38,0556613	0,0000321	0,0000502
nTPM	Non-cancerous	Colorectal cancer	63	63	-6,2848071	83,5370324	1,42E-08	3,94E-08
nTPM	Non-cancerous	Liver cancer	63	24	-4,9330053	30,8922215	0,0000262	0,0000437
nTPM	Non-cancerous	Head and Neck cancer	63	38	-5,2202458	55,7657966	0,00000273	0,00000525
nTPM	Non-cancerous	Brain cancer	63	80	-6,772094	125,93483	4,33E-10	1,55E-09
nTPM	Non-cancerous	Prostate cancer	63	8	-3,2737455	9,26466018	0,009	0,011
nTPM	Non-cancerous	Uterine cancer	63	29	-2,8095709	36,0882844	0,008	0,009
nTPM	Non-cancerous	Bile duct cancer	63	7	-2,2670694	6,72791889	0,059	0,059
nTPM	Non-cancerous	Kidney cancer	63	35	-2,416179	47,3013428	0,02	0,021
nTPM	Non-cancerous	Rhabdoid	63	14	-2,3007049	27,4191804	0,029	0,03

Figure A.2. Statistics Table: t-test and FDR p.adj for HPA Cancer cell lines. T-test correction for multiple comparisons (FDR) **Table A.** (belonging to Figure 4.1B) HPA cell lines. Ref group = non-cancerous.

Appendix Table B

DepMap Primary Disease - PCIF1 transcript (ref = non-cancerous)								
.y.	group1	group2	n1	n2	statistic	df	p	p.adj
mean_log2_tpm	Non-Cancerous	Lung Neuroendocrine Tumor	93	60	-15,688227	120,025602	7,53E-31	4,22E-29
mean_log2_tpm	Non-Cancerous	Acute Myeloid Leukemia	93	54	-10,178472	116,200521	8,79E-18	2,46E-16
mean_log2_tpm	Non-Cancerous	Melanoma	93	111	-9,3607745	196,229463	1,88E-17	3,51E-16
mean_log2_tpm	Non-Cancerous	Diffuse Glioma	93	73	-9,0780366	149,386505	6,06E-16	8,1E-15
mean_log2_tpm	Non-Cancerous	Mature B-Cell Neoplasms	93	106	-8,7938769	196,926883	7,23E-16	8,1E-15
mean_log2_tpm	Non-Cancerous	Ewing Sarcoma	93	24	-10,912703	43,0094121	5,69E-14	4,55E-13
mean_log2_tpm	Non-Cancerous	Neuroblastoma	93	36	-9,6958577	61,755433	5,05E-14	4,55E-13
mean_log2_tpm	Non-Cancerous	B-Cell Acute Lymphoblastic Leukemia	93	25	-10,500644	38,5660929	7,22E-13	5,05E-12
mean_log2_tpm	Non-Cancerous	Non-Small Cell Lung Cancer	93	143	-7,4758092	216,524029	1,88E-12	1,17E-11
mean_log2_tpm	Non-Cancerous	T-Lymphoblastic Leukemia/Lymphoma	93	17	-12,781254	23,2811788	5,21E-12	2,92E-11
mean_log2_tpm	Non-Cancerous	Esophagogastric Adenocarcinoma	93	52	-7,4146333	91,0052185	6,13E-11	3,12E-10
mean_log2_tpm	Non-Cancerous	Colorectal Adenocarcinoma	93	84	-6,9122235	169,981121	9,2E-11	4,29E-10
mean_log2_tpm	Non-Cancerous	Intraductal Papillary Neoplasm of the Bile Duct	93	36	-6,774745	71,5304949	2,94E-09	1,27E-08
mean_log2_tpm	Non-Cancerous	Ovarian Epithelial Tumor	93	64	-5,5728442	127,417356	1,43E-07	5,72E-07
mean_log2_tpm	Non-Cancerous	Pancreatic Adenocarcinoma	93	51	-5,3908082	101,864853	4,55E-07	0,0000017
mean_log2_tpm	Non-Cancerous	Bladder Urothelial Carcinoma	93	33	-5,0677792	48,8496908	0,00000617	0,0000216
mean_log2_tpm	Non-Cancerous	Myeloproliferative Neoplasms	93	17	-5,4749534	27,1937859	0,00000833	0,0000274
mean_log2_tpm	Non-Cancerous	Pleural Mesothelioma	93	22	-4,894637	38,4669203	0,000018	0,000056
mean_log2_tpm	Non-Cancerous	Osteosarcoma	93	27	-4,8532401	35,390696	0,0000244	0,0000719
mean_log2_tpm	Non-Cancerous	Synovial Sarcoma	93	6	-7,9716726	8,35307719	0,0000351	0,0000983
mean_log2_tpm	Non-Cancerous	Hepatocellular Carcinoma	93	23	-4,4770761	32,2827325	0,0000888	0,000237
mean_log2_tpm	Non-Cancerous	Invasive Breast Carcinoma	93	63	-4,0584966	94,0995437	0,000102	0,00026
mean_log2_tpm	Non-Cancerous	Endometrial Carcinoma	93	36	-3,8594218	54,3063654	0,000304	0,000709
mean_log2_tpm	Non-Cancerous	Intracholecystic Papillary Neoplasm	93	6	-6,1160687	7,8877379	0,000301	0,000709
mean_log2_tpm	Non-Cancerous	Cervical Squamous Cell Carcinoma	93	13	-4,5845651	14,7505562	0,000373	0,000836
mean_log2_tpm	Non-Cancerous	Anaplastic Thyroid Cancer	93	11	-4,4052954	11,2742093	0,000994	0,002
mean_log2_tpm	Non-Cancerous	Head and Neck Squamous Cell Carcinoma	93	70	-3,486681	112,64204	0,000698	0,002
mean_log2_tpm	Non-Cancerous	Mature T and NK Neoplasms	93	15	-3,8984746	15,9625171	0,001	0,003
mean_log2_tpm	Non-Cancerous	Nerve Sheath Tumor	93	9	-4,5260047	9,02228477	0,001	0,003
mean_log2_tpm	Non-Cancerous	Non-Hodgkin Lymphoma	93	12	-4,0430902	12,404523	0,002	0,003
mean_log2_tpm	Non-Cancerous	Rhabdomyosarcoma	93	20	-3,5798996	25,3044884	0,001	0,003
mean_log2_tpm	Non-Cancerous	Well-Differentiated Thyroid Cancer	93	8	-4,392694	7,84141441	0,002	0,004
mean_log2_tpm	Non-Cancerous	Esophageal Squamous Cell Carcinoma	93	26	-3,0708907	34,5764835	0,004	0,007
mean_log2_tpm	Non-Cancerous	Ocular Melanoma	93	15	-3,1715054	18,0427056	0,005	0,009
mean_log2_tpm	Non-Cancerous	Uterine Sarcoma/Mesenchymal	93	4	-5,5840135	3,59198673	0,007	0,011
mean_log2_tpm	Non-Cancerous	Cervical Adenocarcinoma	93	5	-3,7970758	4,52591685	0,015	0,023
mean_log2_tpm	Non-Cancerous	SMARCA4-deficient undifferentiated tumor	93	4	-4,6314016	3,37235911	0,015	0,023
mean_log2_tpm	Non-Cancerous	Embryonal Tumor	93	19	-2,5499008	26,2524871	0,017	0,025
mean_log2_tpm	Non-Cancerous	Leiomyosarcoma	93	11	-2,661462	10,9723573	0,022	0,032
mean_log2_tpm	Non-Cancerous	Desmoid/Aggressive Fibromatosis	93	3	-4,5060519	2,51575769	0,029	0,041
mean_log2_tpm	Non-Cancerous	Rhabdoid Cancer	93	15	-2,2140231	25,723842	0,036	0,049
mean_log2_tpm	Non-Cancerous	High-Grade Spindle Cell Sarcoma	93	7	-2,4747323	6,8165041	0,043	0,058
mean_log2_tpm	Non-Cancerous	CIC-DUX4 Sarcoma	93	3	-3,2632767	2,22670527	0,071	0,093
mean_log2_tpm	Non-Cancerous	Merkel Cell Carcinoma	93	4	-2,4231998	3,17592795	0,089	0,113
mean_log2_tpm	Non-Cancerous	Hodgkin Lymphoma	93	7	-1,9048663	6,55171733	0,101	0,123
mean_log2_tpm	Non-Cancerous	Renal Cell Carcinoma	93	36	-1,6611164	66,3617154	0,101	0,123
mean_log2_tpm	Non-Cancerous	Ampullary Carcinoma	93	5	-1,980828	4,14867756	0,116	0,138
mean_log2_tpm	Non-Cancerous	Non-Seminomatous Germ Cell Tumor	93	10	-1,5706306	10,0159832	0,147	0,172
mean_log2_tpm	Non-Cancerous	Chondrosarcoma	93	5	-1,4014657	4,56240069	0,225	0,257
mean_log2_tpm	Non-Cancerous	Gestational Trophoblastic Disease	93	3	-1,1828788	2,31251902	0,344	0,385
mean_log2_tpm	Non-Cancerous	Prostate Adenocarcinoma	93	6	-1,0175768	5,48818458	0,352	0,387
mean_log2_tpm	Non-Cancerous	Cutaneous Squamous Cell Carcinoma	93	5	-0,8339527	4,33601705	0,448	0,482
mean_log2_tpm	Non-Cancerous	Liposarcoma	93	12	-0,7631072	12,3603036	0,46	0,486
mean_log2_tpm	Non-Cancerous	Breast Ductal Carcinoma In Situ	93	5	-0,4527868	4,21854705	0,673	0,698
mean_log2_tpm	Non-Cancerous	Meningothelial Tumor	93	4	-0,3253809	4,76040312	0,759	0,773
mean_log2_tpm	Non-Cancerous	Wilms' Tumor	93	5	-0,2315371	4,18767207	0,828	0,828

Figure A.3. Statistics Table: t-test and FDR p.adj for DepMap Cancer cell lines. T-test correction for multiple comparisons (FDR) for **Table B.** (belonging to Figure 4.1C): DepMap Primary disease transcript. Ref group = non-cancerous.

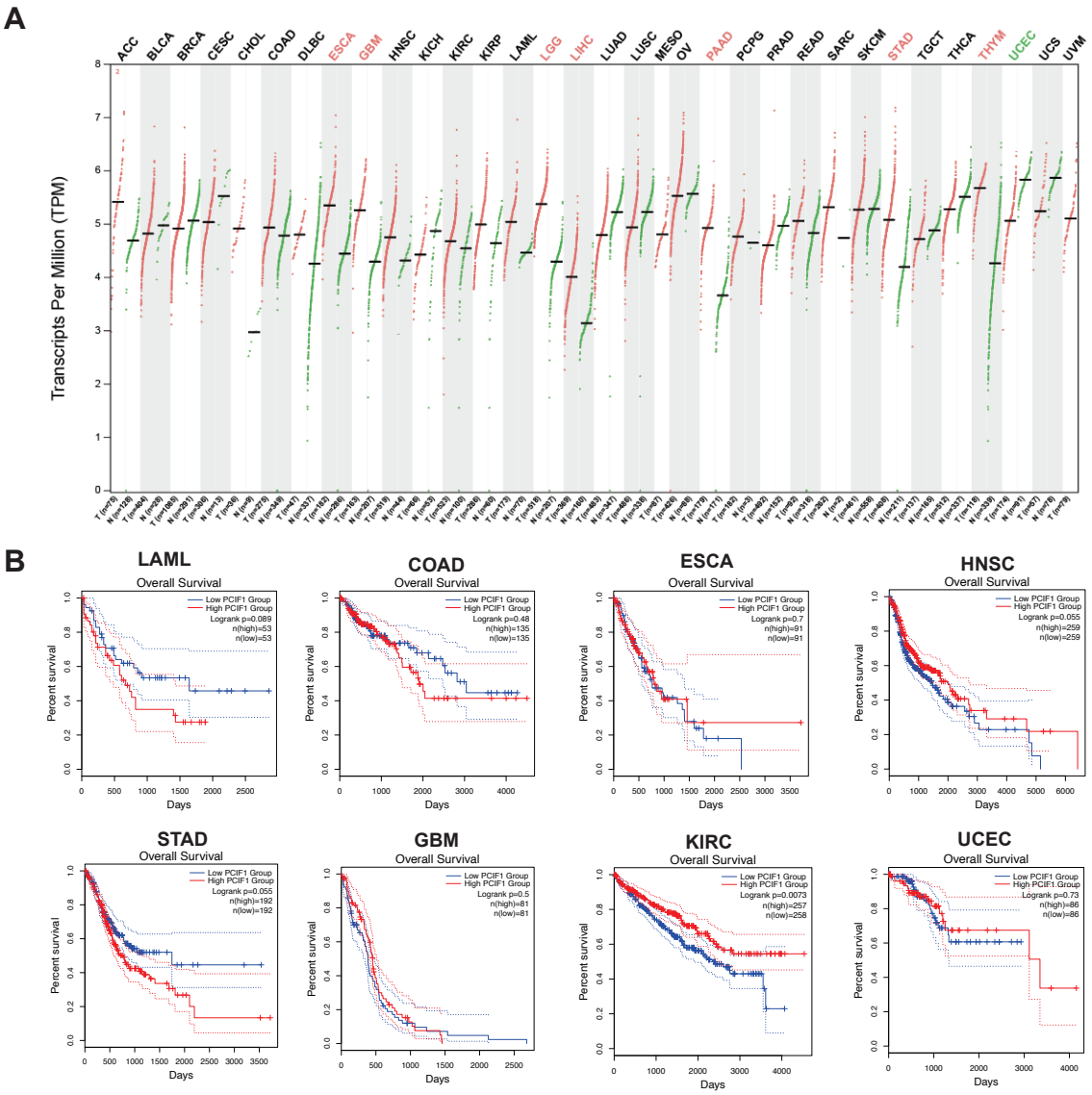

Figure A.4. PCIF1 expression and survival in GEPIA2. **A.** GEPIA2 PCIF1 transcript expression in TCGA tumor and normal matched + GTEx normal tissue. **B.** Survival of patients in TCGA with PCIF1 high/low expression, median cutoff. Abbreviations: LAML = Acute myelid leukemia, COAD = Colorectal Adenocarcinoma, ESCA = Esophageal carcinoma, HNSC = Head and Neck squamous cell carcinoma, STAD = Stomach adenocarcinoma, GBM = Glioblastoma multiforme, KIRC = Kidney renal clear cell carcinoma, UCEC = Uterine Corpus Endometrial Carcinoma.

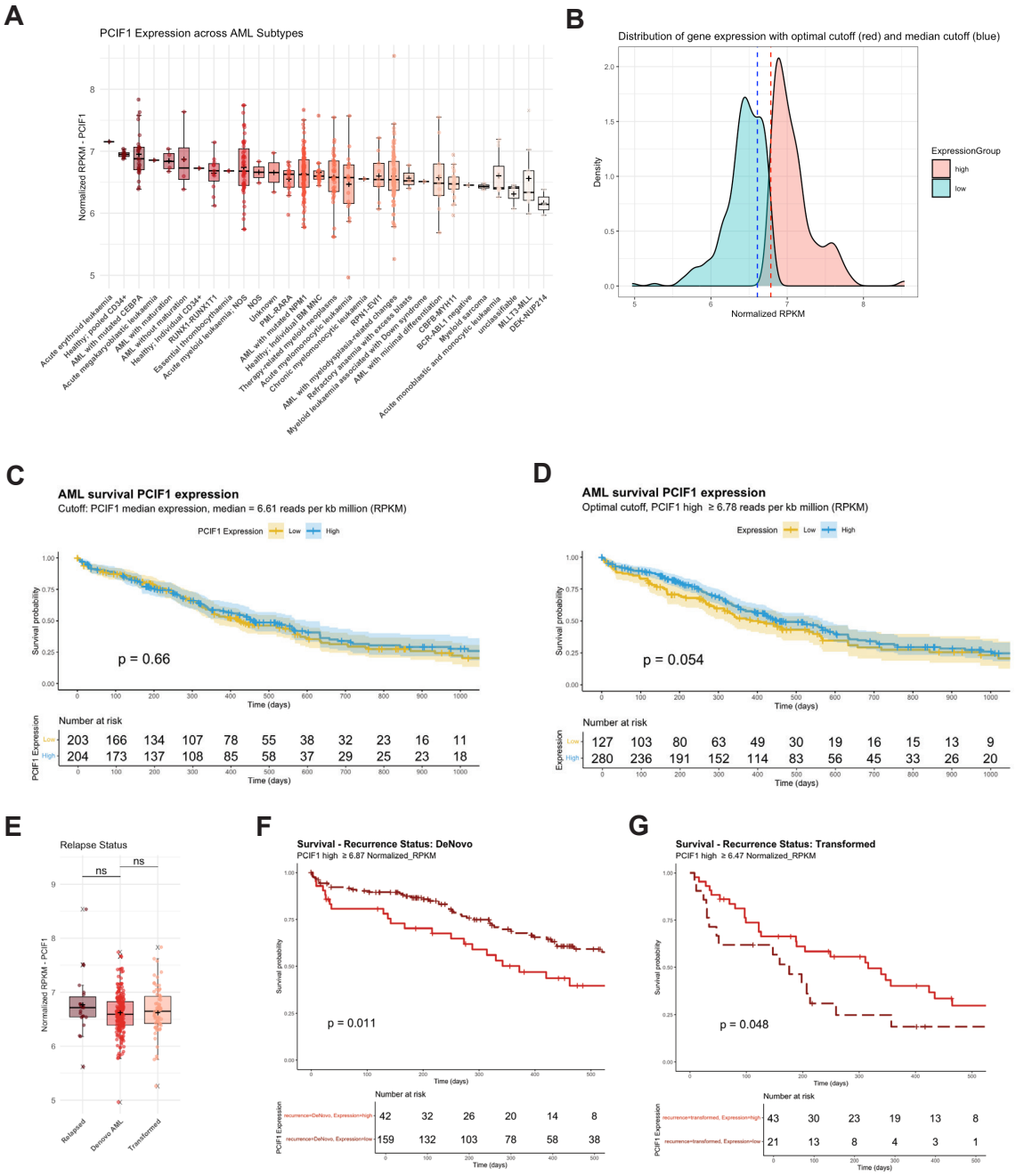

Figure A.5. PCIF1 expression and patient survival in the BEAT-AML trial. **A.** PCIF1 transcript expression across all AML subtypes in Beat-AML trial. **B.** Comparison of expression cutoffs in AML patients from survival plots C and D. Blue dashed line = median cutoff value, red dashed line = optimal cutoff value for biggest difference between two groups, determined by survcutpoint(). **C.** AML patient PCIF1 high/low survival with median cutoff. **D.** AML patient PCIF1 high/low survival with optimal cutoff. p = logRank test. **E.** PCIF1 expression in AML patients grouped by recurrence. Unpaired t-test. **F.** and **G.** Survival of PCIF1 high (light red) and low (dark red dashed) patients with DeNovo (F) or transformed (G) AML.

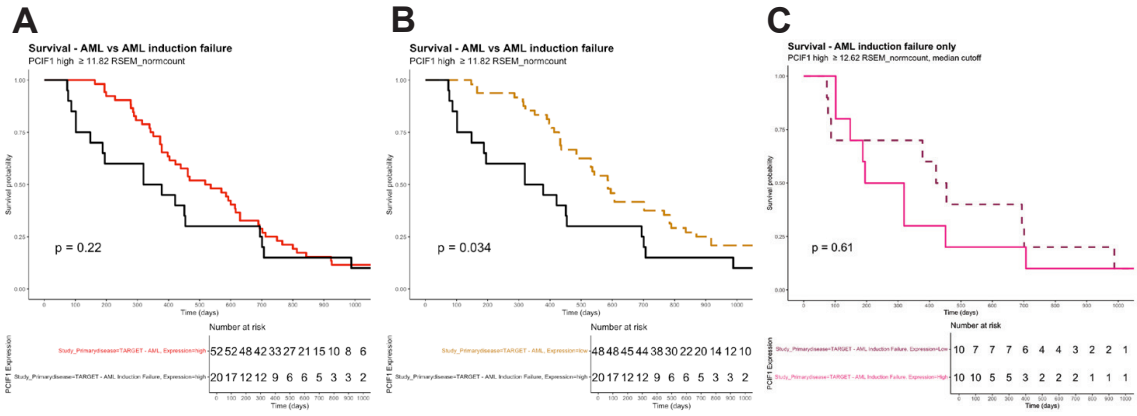

Figure A.6. PCIF1 patient survival in the TARGET AML and TARGET AML-IF subgroup. **A.** Comparison of patient survival TARGET AML PCIF1 high and TARGET AML-IF (all PCIF1 high). **B.** Comparison of patient survival TARGET AML PCIF1 low and TARGET AML-IF (all PCIF1 high). **C.** Comparison of patient survival within the TARGET AML-IF subgroup (PCIF1 expression cutoff = median).

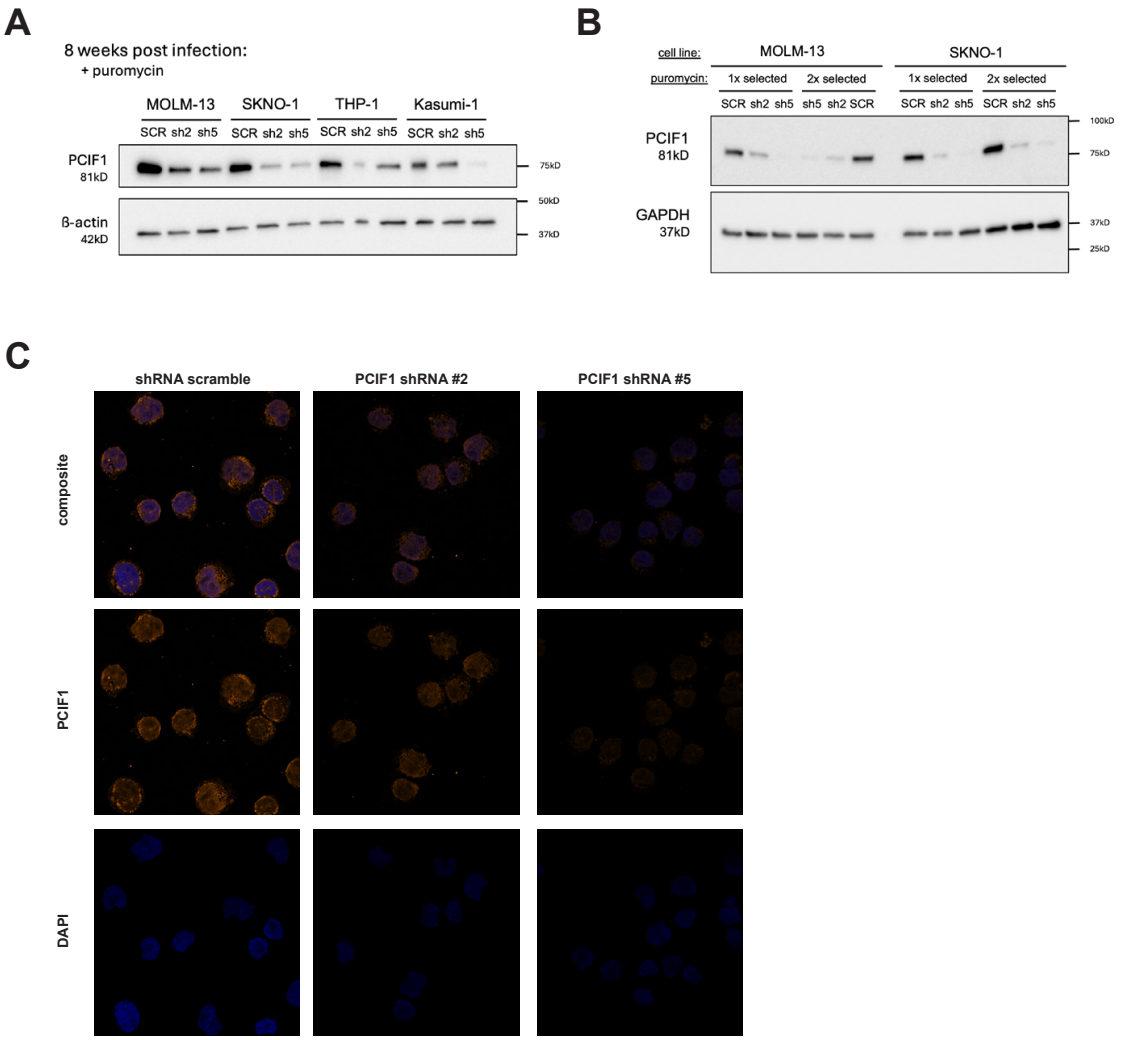

Figure A.7. PCIF1 shRNA mediated knockdown measurements. **A.** Western Blot analysis of PCIF1 over 8 weeks post infection with minimal puromycin selection over the culture period shows a mild re-expression of PCIF1 in MOLM-13 and Kasumi-1 cells. **B.** Western blot analysis of MOLM-13 and SKNO-1 sensitive cell lines within 3 weeks post infection, comparing PCIF1 levels of populations that were treated with a repeated round of puromycin selection before samples were harvested for WB and showed that the level of knockdown was not different between the two conditions. **C.** Confocal immunofluorescence images of MOLM-13 sensitive cell lines stained for PCIF1, phalloidin (not shown) and DAPI. Confocal images of the sensitive cell lines often showed no F-actin staining despite phalloidin addition to the staining mix.

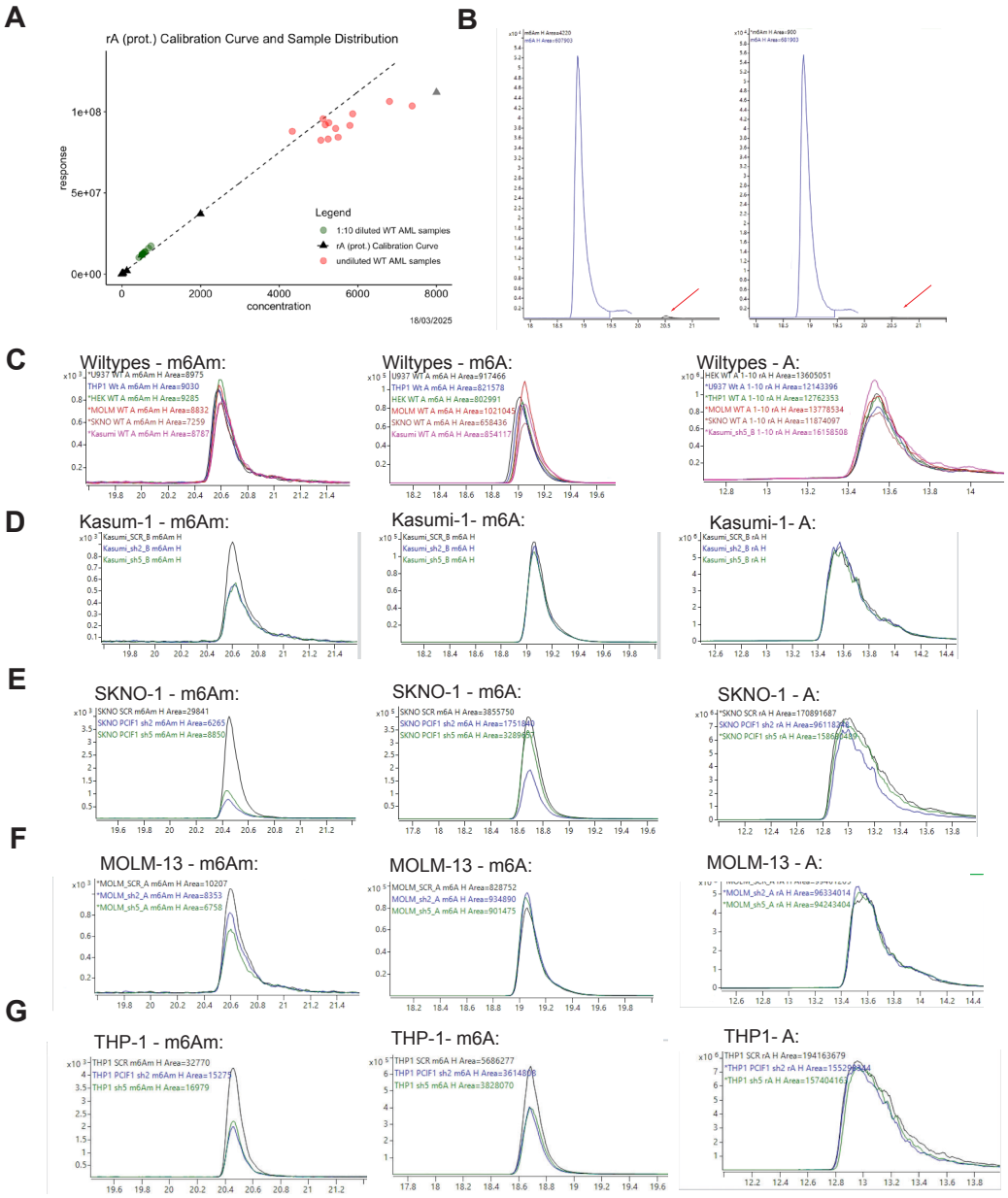

Figure A.8. LCMS acquired measurements of m6Am, m6A and A nucleotides from poly A+ enriched mRNA. **A.** Calibration curve of adenosine standards (black triangles) and measured response (ie integrated peaks) of adenosine nucleotide in AML WT cell lines undiluted (red dots) and 1:10 diluted (green dots), showing that undiluted adenosine peaks were usually detected outside of the standard range of calibration (8pM-2uM) and above the limit of the detector.

Figure A.8. (continued) The detector limit was deemed to have been surpassed if concentrations surpassed the SD of the linear regression for calibration as illustrated by the grey triangle (8uM input of adenosine standard) maxing out. **B.** Comparison of the abundance of m6A (blue peak) and m6Am (black peak indicated with red arrow) in U937 non-targeting guide and PCIF1 sgF3 mRNA. **C-E** Overlay of m6Am, m6A and adeonsine sample peaks for WT (C), Kasumi-1 resistant (D) as well as SKNO-1 sensitive (E) cell lines. m6A levels seem to decrease in this SKNO-1 PCIF1 knockdown replicate.

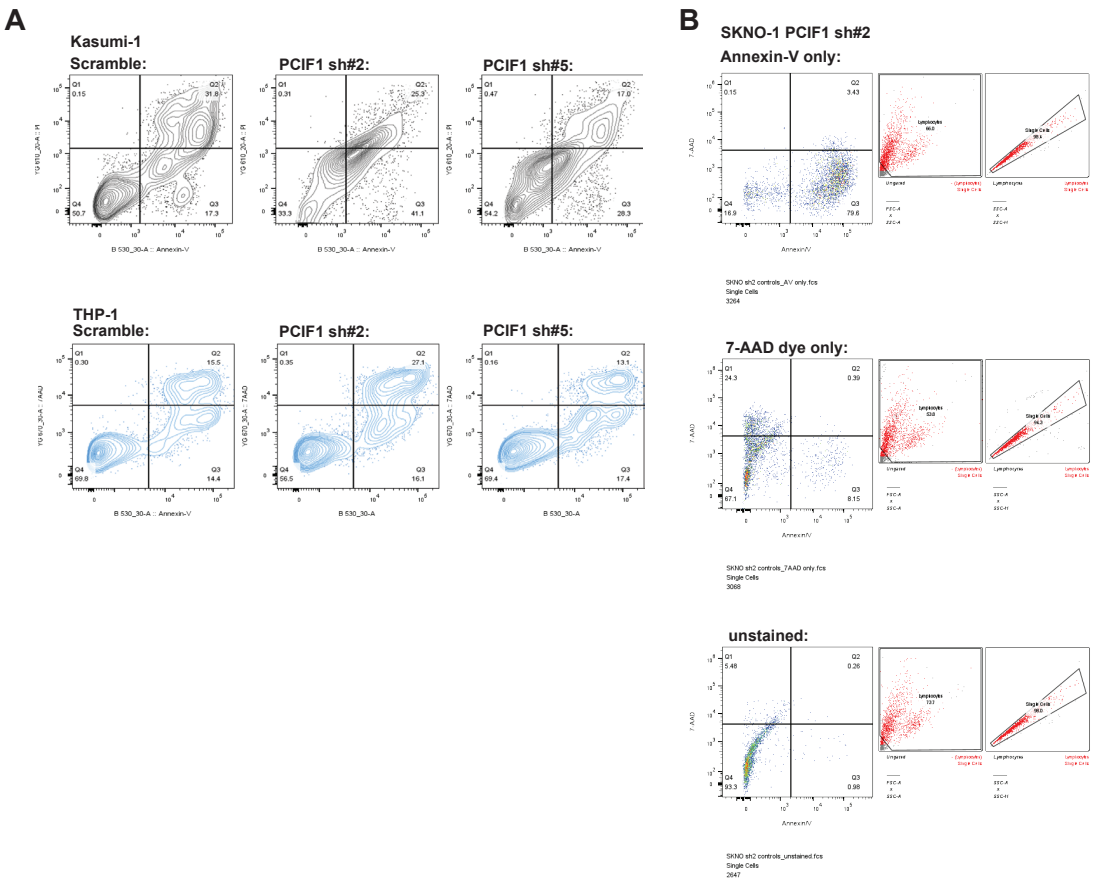

Figure A.9. Resistant THP-1 and Kasumi-1 apoptosis staining gates and SKNO-1 single stained controls. **A.** Resistant cell lines gating, continuation from Figure 4.10. **B.** Gating strategy and ancestry gating of SKNO-1 single and unstained controls. SKNO-1 PCIF1 sh2 (positive apoptosis) were either stained with only annexin-V, 7-AAD, or FACS buffer alone. Gates for the experiment were set up according to the single-stained controls, in a way that false positive signal was < 1%

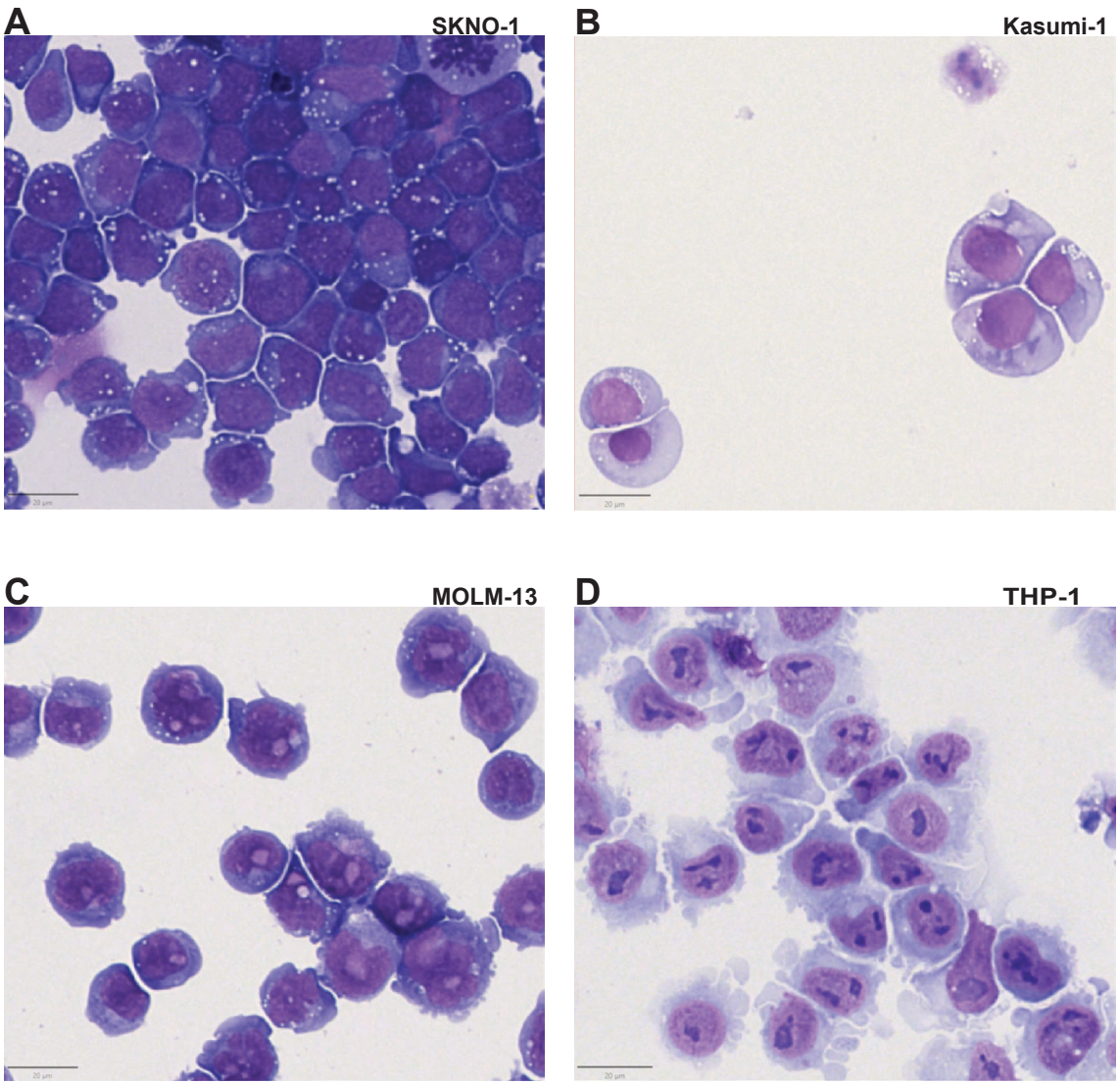

Figure A.10. Representative snapshots from MGG staining of wildtype AML cell line cultures. **A.** Wildtype SKNO-1, **B.** Wildtype Kasumi-1, **C.** Wildtype MOLM-13, **D.** Wildtype THP-1. Scalebar 20 µm. Images taken with a digital slide scanner (Hammamatsu NanoZoomer) and in Quantstudio.

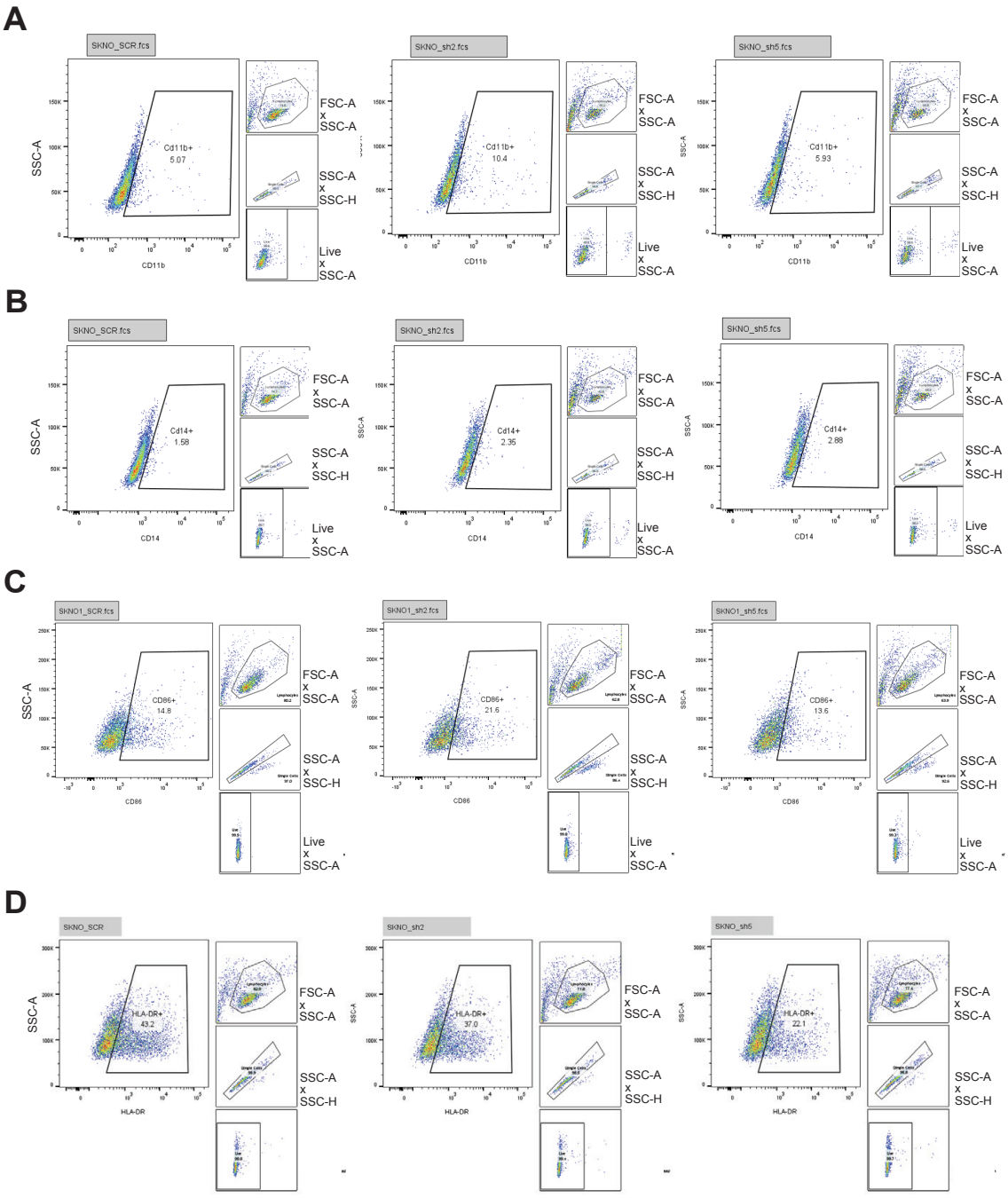

Figure A.11. Gating strategy and representative plots for SKNO-1 cell line of flow cytometry measurements of monocytic differentiation markers. **B.** CD14, **C.** CD86, **D.** HLA-DR)

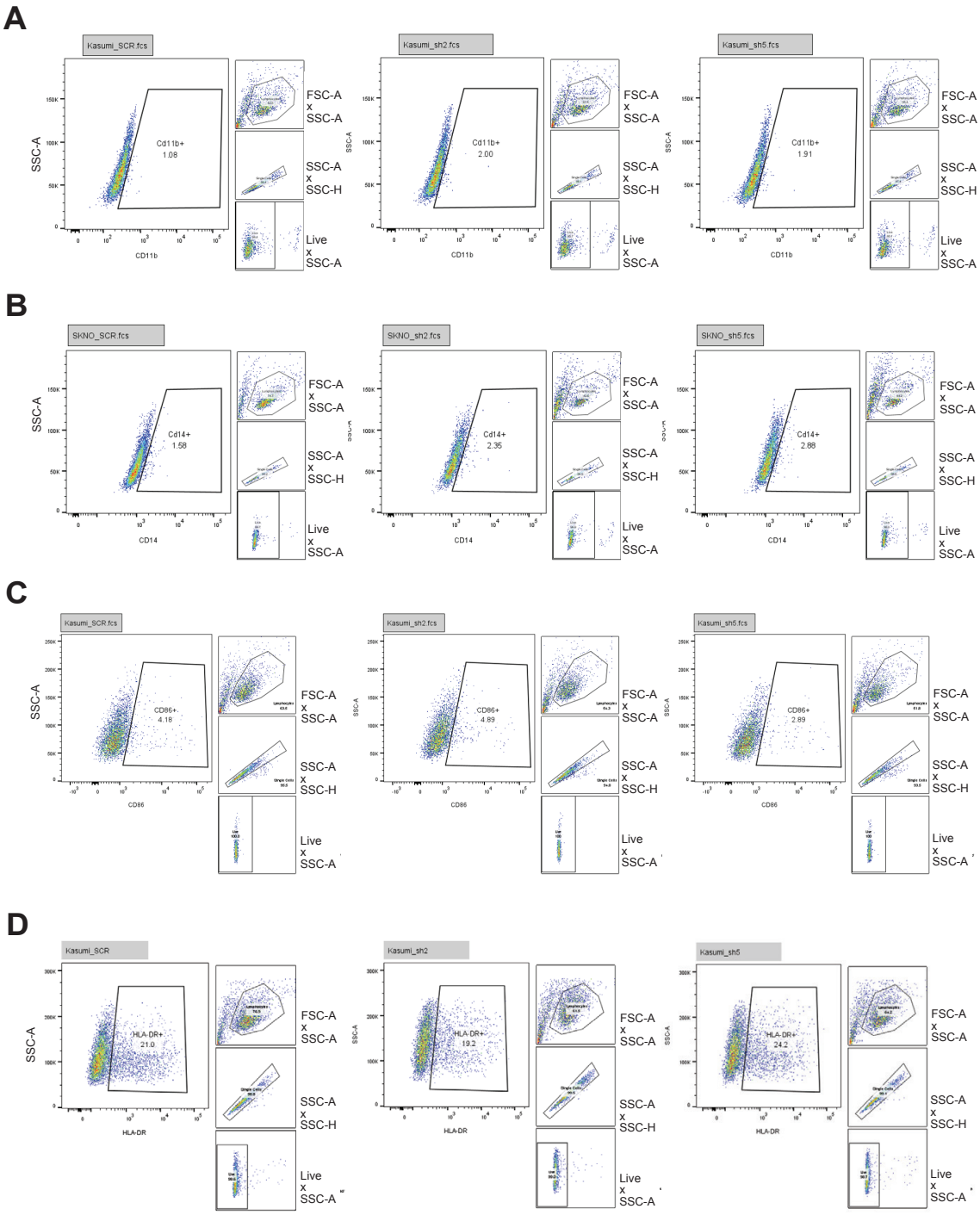

Figure A.12. Gating strategy and representative plots for Kasumi-1 cell line of flow cytometry measurements of monocytic differentiation markers. **A.** CD11b. **B.** CD14, **C.** CD86, **D.** HLA-DR.

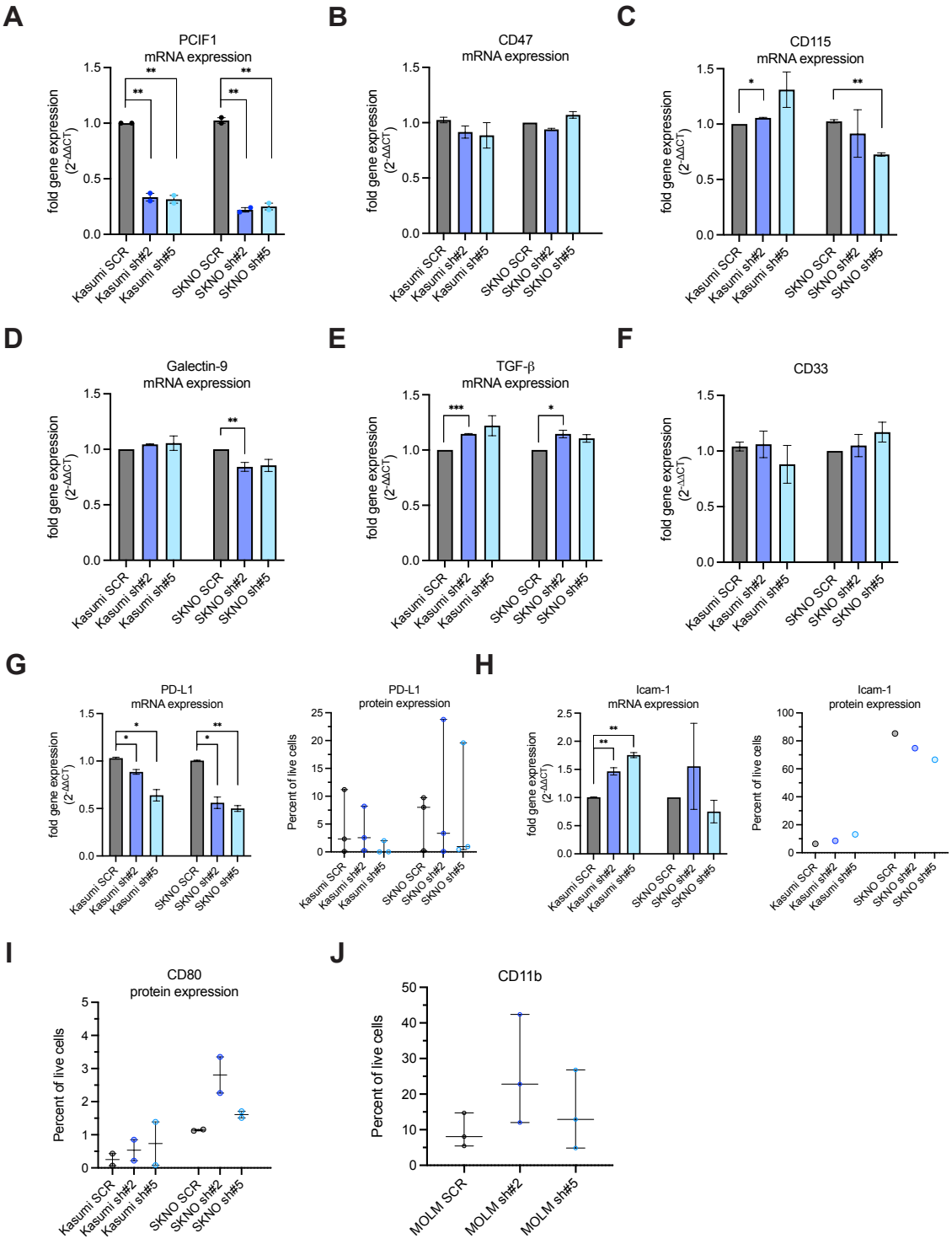

Figure A.13. qpCR and flow cytometry based measurement of monocytic differentiation markers and therapeutic resistant markers. **A.** PCIF1 levels of the replicates used for these measurements. **B.** CD47 mRNA expression,

Figure A.13. (continued) **C.** CD115 mRNA expression, **D.** Galectin-9 mRNA expression, **E.** TGF-b mRNA expression, **F.** CD33 mRNA expression **G.** PD-L1 mRNA and protein expression, **H.** Icam-1 mRNA and protein expression, **I.** CD80 was measured in protein only **J.** MOLM13 CD11b protein expression. Data depicted as means ± SEM of n=2-5 independent replicates, analyzed by two-tailed unpaired t-test: *P < 0.05; **P < 0.01; ***P < 0.001.

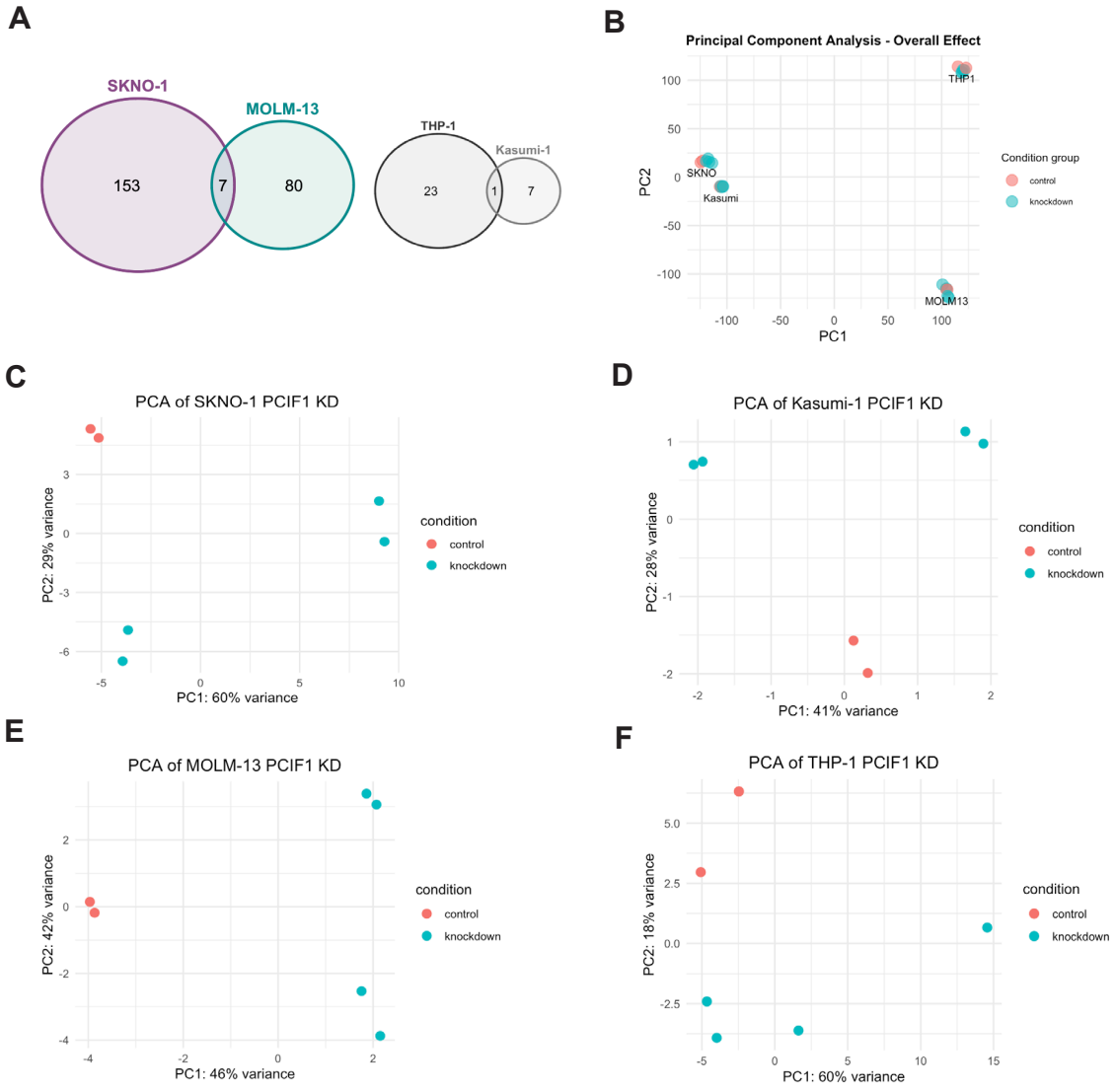

Figure A.14. Appendix: Principle Component Analysis (PCA) of RNA-seq samples. **A.** PCA of all four cell lines. **B-F.** PCA of different shRNAs within SKNO-1, MOLM-13, THP-1 and Kasumi-1 cell lines.

A

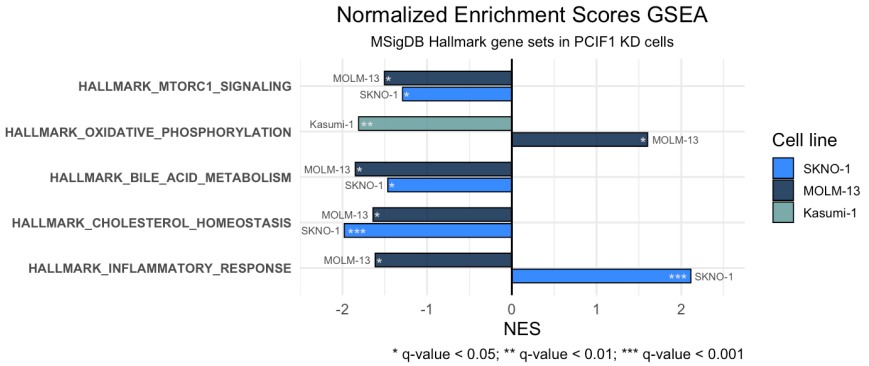

B

SKNO-1				**MOLM-13**			
ID	**NES**	**p.adjust**	**qvalue**	**ID**	**NES**	**p.adjust**	**qvalue**
HALLMARK_INTERFERON_GAMMA_RESPONSE	2,21	1,8E-10	8,9E-11	HALLMARK_BILE_ACID_METABOLISM	-1,85	0,01987	0,01631
HALLMARK_INFLAMMATORY_RESPONSE	2,10	1,3E-07	6,2E-08	HALLMARK_PANCREAS_BETA_CELLS	1,71	0,01987	0,01631
HALLMARK_TNFA_SIGNALING_VIA_NFKB	2,05	2,1E-07	1,0E-07	HALLMARK_OXIDATIVE_PHOSPHORYLATION	1,60	0,01987	0,01631
HALLMARK_MYC_TARGETS_V1	-1,88	2,5E-06	1,2E-06	HALLMARK_INFLAMMATORY_RESPONSE	-1,61	0,05234	0,04298
HALLMARK_INTERFERON_ALPHA_RESPONSE	2,02	4,6E-06	2,2E-06	HALLMARK_MTORC1_SIGNALING	-1,50	0,05234	0,04298
HALLMARK_APOPTOSIS	1,95	1,1E-05	5,3E-06	HALLMARK_CHOLESTEROL_HOMEOSTASIS	-1,64	0,05683	0,04666
HALLMARK_KRAS_SIGNALING_UP	1,88	9,1E-05	4,4E-05	HALLMARK_IL6_JAK_STAT3_SIGNALING	1,58	0,06815	0,05596
HALLMARK_CHOLESTEROL_HOMEOSTASIS	-1,97	0,0002	7,7E-05	HALLMARK_HYPOXIA	1,48	0,07934	0,06514
HALLMARK_IL6_JAK_STAT3_SIGNALING	1,92	0,0003	0,00016	HALLMARK_MITOTIC_SPINDLE	-1,44	0,07934	0,06514
HALLMARK_P53_PATHWAY	1,74	0,0008	0,00037	HALLMARK_HEME_METABOLISM	1,39	0,11315	0,09291
Kasumi-1				**THP-1**			
ID	**NES**	**p.adjust**	**qvalue**	**ID**	**NES**	**p.adjust**	**qvalue**
HALLMARK_OXIDATIVE_PHOSPHORYLATION	-1,81	0,0140	0,0093	HALLMARK_TGF_BETA_SIGNALING	2,28	0,87449	0,87449
HALLMARK_KRAS_SIGNALING_UP	1,81	0,0799	0,0532	HALLMARK_PANCREAS_BETA_CELLS	2,18	0,87449	0,87449
HALLMARK_IL6_JAK_STAT3_SIGNALING	1,71	0,0799	0,0532	HALLMARK_ANDROGEN_RESPONSE	2,13	0,87449	0,87449
HALLMARK_TNFA_SIGNALING_VIA_NFKB	1,70	0,0799	0,0532	HALLMARK_P53_PATHWAY	1,79	0,87449	0,87449
HALLMARK_MYC_TARGETS_V2	-1,67	0,0799	0,0532	HALLMARK_NOTCH_SIGNALING	-1,72	0,87449	0,87449
HALLMARK_BILE_ACID_METABOLISM	-1,64	0,0799	0,0532	HALLMARK_GLYCOLYSIS	1,49	0,87449	0,87449
HALLMARK_UV_RESPONSE_DN	1,63	0,0799	0,0532	HALLMARK_IL6_JAK_STAT3_SIGNALING	-1,44	0,87449	0,87449
HALLMARK_REACTIVE_OXYGEN_SPECIES_PATHWAY	-1,63	0,0799	0,0532	HALLMARK_KRAS_SIGNALING_DN	1,43	0,87449	0,87449
HALLMARK_MYC_TARGETS_V1	-1,61	0,0799	0,0532	HALLMARK_UV_RESPONSE_UP	1,39	0,87449	0,87449
HALLMARK_PEROXISOME	-1,59	0,0799	0,0532	HALLMARK_BILE_ACID_METABOLISM	-1,35	0,87449	0,87449

Figure A.15. Gene Set Enrichment Analysis (GSEA) extended. **A.** NES scores for common enriched gene sets in sensitive cell lines and one significant enrichment in Kasumi-1 resistant cell lines. **B.** Top 10 enriched GSEA terms with statistics for every cell line. p.adj = nominal p-value corrected for multiple comparisons using FDR.

A

SKNO-1

Transcript_name	Transcript_stable_ID	log2FoldChange	padj	Transcript_type	RefSeq	Transcription_start_site_TSS	Transcription_Start_Nucleotide_TSN
uncharacterized transcript	ENST00000691540	3,21418	0,002927858	protein_coding		131432759	A
STK39-201	ENST00000355999	-0,53145	0,000836875	protein_coding	NM_013233.3	168247595	G
PCIF1-201	ENST00000372409	-2,00397	2,70657E-35	protein_coding	NM_022104.4	45934683	G
MPO-201	ENST00000225275	-0,60446	0,067560709	protein_coding	NM_000250.2	58280935	G
LIMK1-208	ENST00000538333	0,01259	0,959698093	protein_coding		74093079	A
LIMK1-201	ENST00000336180	0,97552	0,003841412	protein_coding	NM_002314.4	74083804	G
IGFBP2-204	ENST00000456764	-0,75567	2,95516E-25	protein_coding		216659618	G
IGFBP2-201	ENST00000233809	-0,53557	0,008813201	protein_coding	NM_000597.3	216633420	G
IFITM1-229	ENST00000681938	0,01985	0,986598457	protein_coding		314040	G
IFITM1-218	ENST00000680870	-0,01266	0,992488254	protein_coding		311840	G
IFITM1-214	ENST00000680696	-0,00353	0,998568463	protein_coding		314040	G
IFITM1-210	ENST00000680310	-0,01266	0,992488254	protein_coding		310944	C
IFITM1-202	ENST00000408968	-0,79748	2,29207E-29	protein_coding	NM_003641.5	314040	G
IFITM1-201	ENST00000328221	-0,10286	0,373824526	protein_coding		313527	C
FUCA1-201	ENST00000374479	1,90088	0,0049167	protein_coding	NM_000147.5	23868290	A
FADS2-210	ENST00000522056	-0,00347	0,99090044	protein_coding		61816404	G
FADS2-209	ENST00000521849	-0,63107	0,107722586	protein_coding		61828280	A
FADS2-204	ENST00000517312	-0,03623	0,816303005	protein_coding		61828179	A
FADS2-202	ENST00000278840	-1,17137	3,83289E-07	protein_coding	NM_004265.4	61828300	T
FADS2-201	ENST00000257261	-0,01518	0,935132051	protein_coding		61816256	A
FADS1-206	ENST00000460649	-0,09552	0,429671928	protein_coding		61804680	G
FADS1-201	ENST00000350997	-0,65315	0,000117146	protein_coding	NM_013402.7	61817003	G
ELOVL6-202	ENST00000394607	-0,07995	0,587680734	protein_coding		110198653	G
ELOVL6-201	ENST00000302274	-0,98551	0,013346901	protein_coding	NM_024090.3	110198615	A
CTSG-201	ENST00000216336	-1,25533	1,7178E-05	protein_coding	NM_001911.3	24576250	A
COX7C-207	ENST00000515763	0,67123	0,01221819	protein_coding		86617973	C
COX7C-203	ENST00000509578	0,00796	0,995909946	protein_coding		86617956	G
COX7C-201	ENST00000247655	0,47962	8,5695E-05	protein_coding	NM_001867.3	86617941	C
CAMK1-201	ENST00000256460	0,07175	0,099803122	protein_coding	NM_003656.5	9769947	A
BTG2-202	ENST00000475157	5,37826	0,009957844	nonsense_mediated_decay		203305491	A
BTG2-201	ENST00000290551	1,22105	0,002298989	protein_coding	NM_006763.3	203305519	A
AXL-201	ENST00000301178	1,62151	7,25625E-06	protein_coding	NM_021913.5	41219223	G
ARPC3-202	ENST00000426440	0,03618	0,625085776	protein_coding		110450311	C
ARPC3-201	ENST00000228825	0,34673	0,002274464	protein_coding	NM_001278556.2	110450337	G
AHNAK-202	ENST00000378024	1,65694	7,87642E-05	protein_coding	NM_001620.3	62546806	G

B

MOLM-13

Transcript_name	Transcript_stable_ID	log2FoldChange	padj	Transcript_type	RefSeq	Transcription_start_site_TSS	Transcription_Start_Nucleotide_TSN
uncharacterized transcript	ENST00000691540	0,006	0,206292	protein_coding		131432759	A
STK39-201	ENST00000355999	-1,234	0,008292	protein_coding	NM_013233.3	168247595	G
PCIF1-201	ENST00000372409	-1,346	0,000458	protein_coding	NM_022104.4	45934683	G
MPO-201	ENST00000225275	1,291	1,29E-06	protein_coding	NM_000250.2	58280935	G
LIMK1-201	ENST00000336180	0,542	0,000253	protein_coding	NM_002314.4	74083804	G
IGFBP2-204	ENST00000456764	-0,586	0,090827	protein_coding		216659618	G
IGFBP2-201	ENST00000233809	-0,787	0,028872	protein_coding	NM_000597.3	216633420	G
IFITM1-202	ENST00000408968	-1,037	0,009844	protein_coding	NM_003641.5	314040	G
FUCA1-201	ENST00000374479	-0,840	3,84E-13	protein_coding	NM_000147.5	23868290	A
FADS2-209	ENST00000521849	-0,063	0,009494	protein_coding		61828280	A
FADS2-202	ENST00000278840	-3,329	2,09E-44	protein_coding	NM_004265.4	61828300	T
FADS1-201	ENST00000350997	-2,058	1,69E-21	protein_coding	NM_013402.7	61817003	G
ELOVL6-202	ENST00000394607	-0,016	0,669136	protein_coding		110198653	G
ELOVL6-201	ENST00000302274	0,006	0,240098	protein_coding	NM_024090.3	110198615	A
CTSG-201	ENST00000216336	-0,350	0,042270	protein_coding	NM_001911.3	24576250	A
COX7C-207	ENST00000515763	1,230	5,73E-13	protein_coding		86617973	C
COX7C-203	ENST00000509578	0,019	0,988668	protein_coding		86617956	G
COX7C-201	ENST00000247655	1,281	4,91E-74	protein_coding	NM_001867.3	86617941	C
CAMK1-202	ENST00000397277	-0,009	0,889311	nonsense_mediated_decay		9769961	C
CAMK1-201	ENST00000256460	-0,084	0,241631	protein_coding	NM_003656.5	9769947	A
BTG2-201	ENST00000290551	0,442	0,021415	protein_coding	NM_006763.3	203305519	A
AXL-202	ENST00000359092	-0,028	0,921213	protein_coding		41219235	G
AXL-201	ENST00000301178	-1,226	0,002375	protein_coding	NM_021913.5	41219223	G
ARPC3-201	ENST00000228825	1,054	0,000000	protein_coding	NM_001278556.2	110450337	G
AHNAK-202	ENST00000378024	0,372	6,10E-15	protein_coding	NM_001620.3	62546806	G

Figure A.16. TSN analysis: TSN for significantly differentially regulated transcript isoforms in **A.** SKNO-1 PCIF1 KD cells **B.** MOLM-13 PCIF1 KD cells.

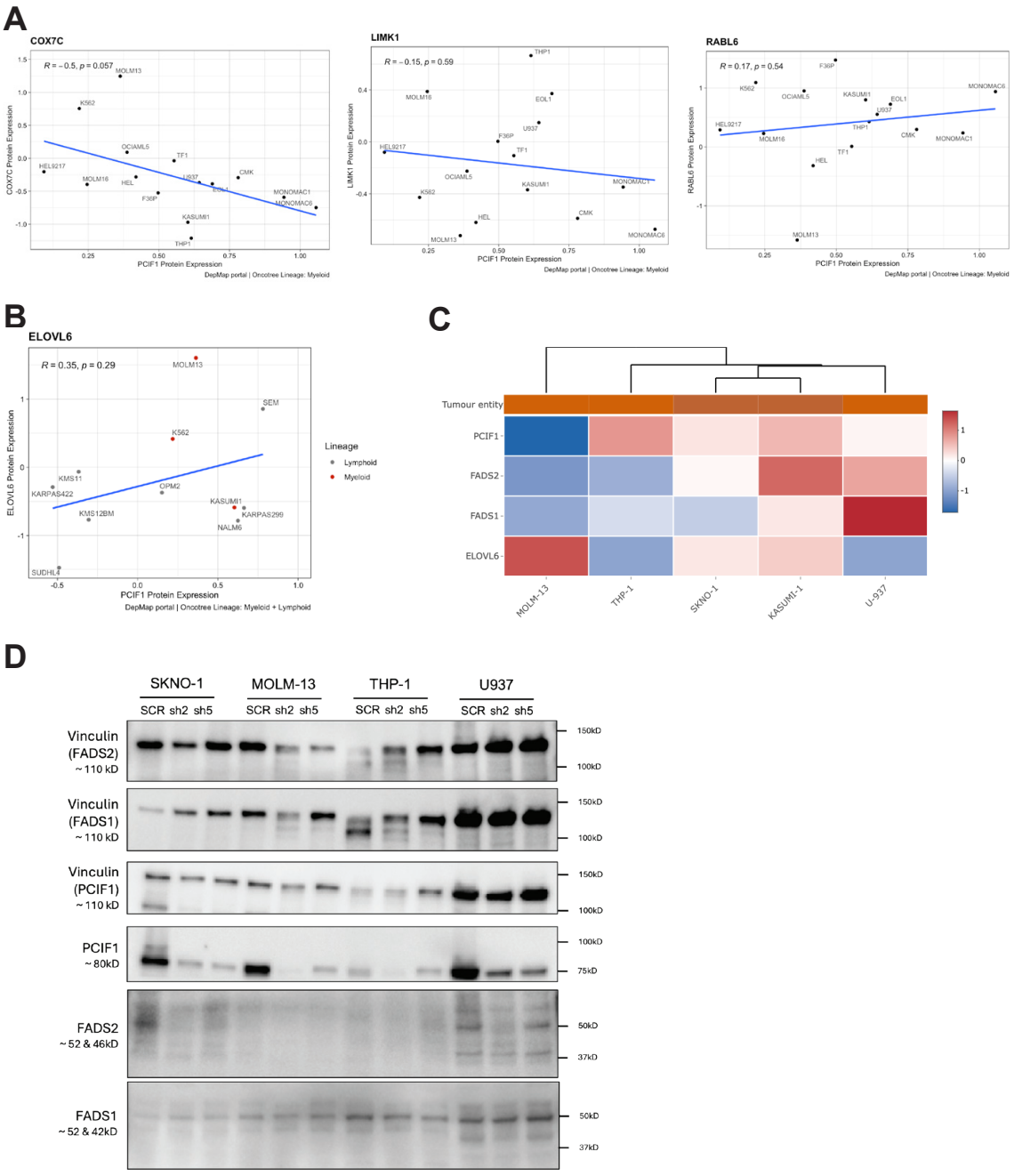

Figure A.17. DEG expression association with PCIF1 expression in WT AML and blood lineage cells. **A.** Scatter plot with linear regression plotting PCIF1 expression vs LIMK1, COX7C or RABL6 (common sensitive DEGs) in AML cells from the DepMap portal. **B.** ELOVL6 DEG required querying in myeloid and lymphoid lineage to get big enough group size for linear regression. **C.** Extended heatmap showing PCIF1, FADS2, FADS1 and ELOVL6 transcript expression in cell lines used in this study. Data queried and downloaded from DSMZ CellDive. **D.** Western blot of *PCIF1* KD cell lines using vinculin as a loading control, and PCIF1, *FADS2* and *FADS1* antibodies on separate blots.

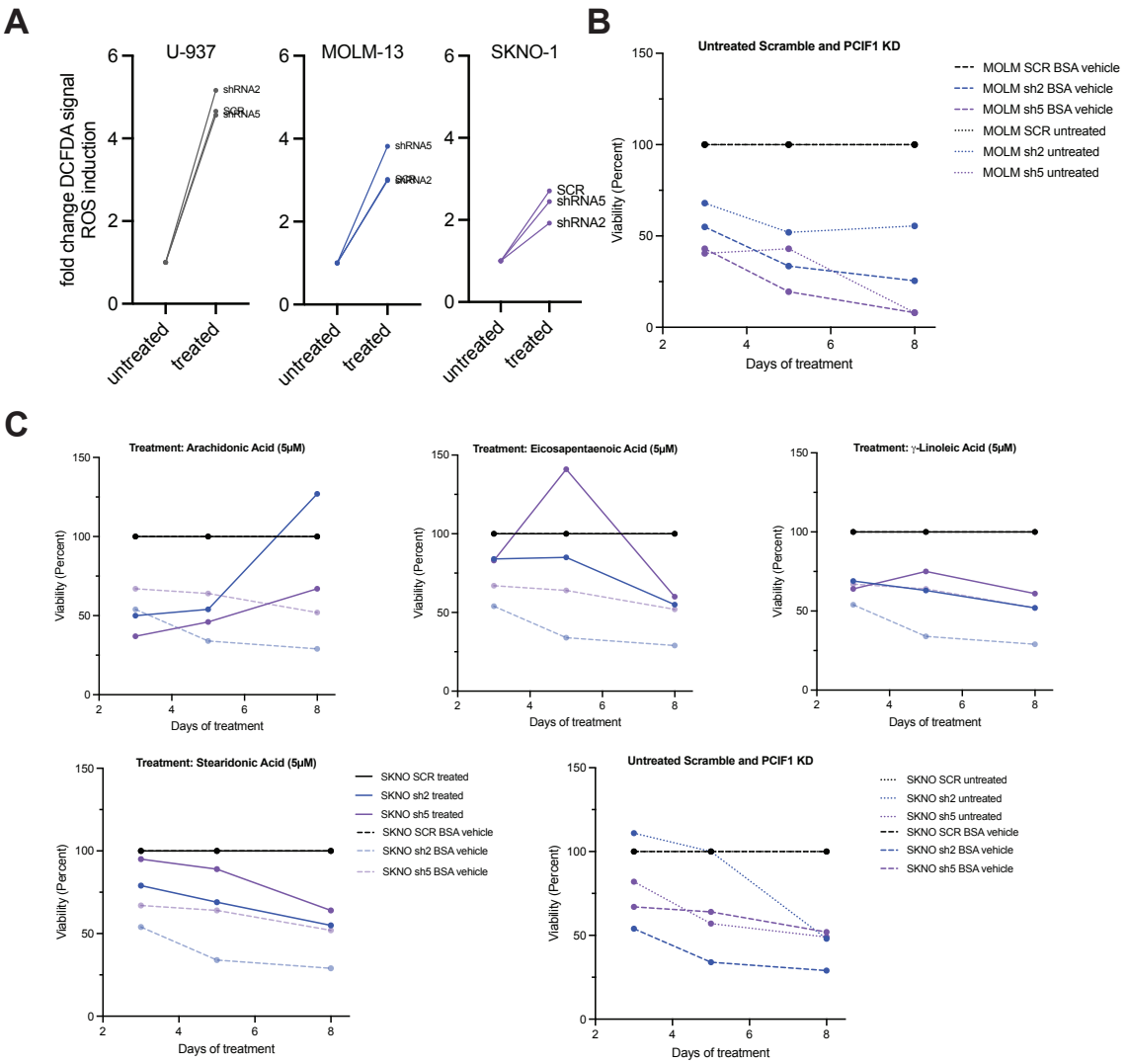

Figure A.18. ROS and Fatty acid supplementation experiment appendix. **A.** U937, MOLM-13 and SKNO-1 DCFDA induction of ROS signal in pos. control treated group relative to untreated vs treated group. **B.** MOLM-13 scramble and PCIF1 KD viability in the BSA vehicle and untreated conditions. Dashed = BSA vehicle, Dotted = untreated. **C.** THP-1 scramble and PCIF1 KD viability during treatment with FA metabolites, normalized to SCR of same treatment.